PUBLISHER :

Address of Publisher & Editor's Office :

GDAŃSK UNIVERSITY
OF TECHNOLOGY
Faculty
of Ocean Engineering
& Ship Technology

ul. Narutowicza 11/12
80-952 Gdańsk, POLAND
tel.: +48 58 347 13 66
fax : +48 58 341 13 66
e-mail : office.pmr@pg.gda.pl

Account number :
BANK ZACHODNI WBK S.A.
I Oddział w Gdańsku
41 1090 1098 0000 0000 0901 5569

Editorial Staff :
Kazimierz Kempa Editor in Chief
e-mail : kkempa@pg.gda.pl
Przemysław Wierzchowski Scientific Editor
e-mail : e.wierzchowski@chello.pl
Jan Michalski Editor for review matters
e-mail : janmi@pg.gda.pl
Tadeusz Borzęcki Editor for international relations
e-mail : tadbor@pg.gda.pl
Piotr Bzura Managing Editor
e-mail : pbzura@pg.gda.pl
Cezary Spigarski Computer Design
e-mail : biuro@oficynamorska.pl

Domestic price :
single issue : 20 zł

Prices for abroad :
single issue :
- in Europe EURO 15
- overseas US$ 20

ISSN 1233-2585

POLISH MARITIME RESEARCH
in internet
www.bg.pg.gda.pl/pmr.html

POLISH MARITIME RESEARCH

No 1(55) 2008 Vol 15

CONTENTS

The papers published in this issue have been reviewed by :
Prof. A. Brandowski ; Prof. J. Girtler ; Prof. J. Lisowski
Prof. K. Rosochowicz ; Prof. Z. Starczewski
Prof. T. Szelangiewicz

Editorial

POLISH MARITIME RESEARCH is a scientific journal of worldwide circulation. The journal appears as a quarterly four times a year. The first issue of it was published in September 1994. Its main aim is to present original, innovative scientific ideas and Research & Development achievements in the field of :

Engineering, **Computing & Technology**, **Mechanical Engineering**,

which could find applications in the broad domain of maritime economy. Hence there are published papers which concern methods of the designing, manufacturing and operating processes of such technical objects and devices as : ships, port equipment, ocean engineering units, underwater vehicles and equipment as well as harbour facilities, with accounting for marine environment protection.
The Editors of POLISH MARITIME RESEARCH make also efforts to present problems dealing with education of engineers and scientific and teaching personnel. As a rule, the basic papers are supplemented by information on conferences , important scientific events as well as cooperation in carrying out international scientific research projects.

Scientific Board

POLISH MARITIME RESEARCH 1(55) 2008 Vol 15; pp. 3-10
DOI: 10.2478/v10012-007-0045-6

A parametric method for evaluation of resistance of swath ships

Jan P. Michalski,
Gdańsk University of Technology
Polish Naval University

ABSTRACT

This paper contains formulation of a parametric method for evaluation of SWATH ship's hull resistance. The method was elaborated on the basis of numerical calculation results obtained by using structural methods based on ship hydrodynamic theory and performed for sufficiently large series of body forms with systematically changing ship form parameters. Also, results of verifying investigations dealing with features of the method in question are presented by comparing the obtained resistance characteristics with those achieved by other authors as well as with ship model experimental test results. The obtained results of the verification indicate that the elaborated method can be useful in preliminary designing the SWATH ships.

Keywords: SWATH ships design method, SWATH ships resistance evaluation method.

INTRODUCTION

The problem of ship hull resistance evaluation by using structural models based on ship hydrodynamic theory belongs to the specially difficult application tasks in shipbuilding, that results from highly complex mathematical relations describing the interaction mechanism of moving ship and surrounding water. Such calculations are performed with the use of computer methods such as e.g. the commercial software SHIPFLOW [1, 2] or those elaborated on the basis of own numerical algorithms, e.g. [3, 4, 5, 6], which require a large outlay of numerical calculations [7], and whose results are loaded by a low numerical stability and reliability [8]. Moreover the methods require a large labour outlay for preparation of an appropriate set of input data for realization of the calculations, mainly the data describing ship body form geometry and water region surrounding the hull.

Predictions of hull resistance characteristics obtained from structural methods are still less reliable and accurate than those resulting from experimental tests of geometrically similar hull models. The theoretical methods find their application in research and study projects to get ship resistance predictions in preliminary design stage, whose results are then verified by means of model tests in further design stage.

The acronym SWATH (Small Water-plane Area Twin Hull) stands for an innovative concept of ship of a specific configuration: its hull consists of two parts distant to each other and formed in such a way as to obtain the ratio of design water-plane area and hull volumetric displacement much smaller than that in the case of single hull ships or classical catamarans. The SWATH ship hull consists of two slender lower hulls (submerged floats) of an elongated spindle-like form, which support deck's box platform by means of one or two slim upper hulls (columns) on each side of ship plane of symmetry, as shown in Fig. 1. On the upper deck a superstructure of a size and arrangement suitable to a given ship operational function, is usually provided. Value of design ship draught should ensure an appropriate draught of floats, low design water-plane area and appropriate clearance between water level and lower deck plating.

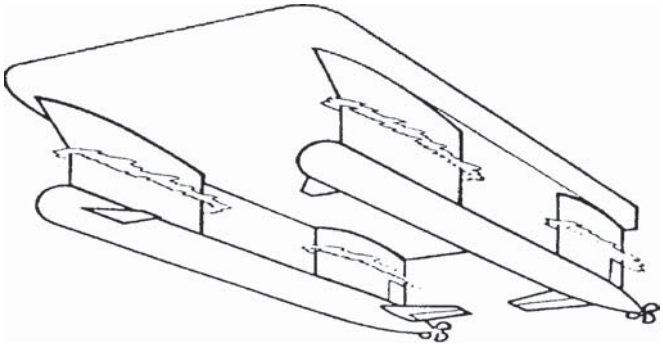

Fig. 1. *Draft configuration of underwater part of SWATH ship hull.*

Both the ratios of main dimensions and body form configuration of SWATH ships much differ from corresponding parameters of single-hull ships, that results in many consequences in the form of various technical features, hydrodynamic, strength and functional qualities. It concerns e.g. relations between ship main dimensions and its resistance characteristics or seakeeping qualities. Today knowledge on the

relations is rather modest. Any extrapolation of the gathered knowledge on classical single-hull ships to SWATH ships is not reasonable as it leads to erroneous estimations rather not useful in design practice.

From practical experience has been gained so far it results that in the case when realization of ship operational function requires such its features as:

- ✦ good seakeeping qualities
- ✦ good resistance characteristics at high speed
- ✦ good stability and unsinkability qualities
- ✦ large loading space on broad deck

– then twin hull ships of small water plane area can be an interesting alternative, competitive to ships of classical body form.

In this paper is presented a parametric method for preliminary evaluation of hull resistance of SWATH ships on the basis of limited set of main design parameters of body form configuration, which is useful especially in early design stages or for carrying out design research and study work aimed at optimization of ship design solutions in a given sense. Detail results of the research on formulation of the method in question together with results of accuracy estimation of the obtained approximating relationships and description of detail assumptions of the method are published in [9].

The presented parametric method is characterized by a simpler structure of its mathematical model and is much simpler in use than the structural methods having computational algorithms based on ship hydrodynamic theory. Also, results of verifying investigations dealing with prediction features of the method in question are presented by comparing the obtained resistance characteristics with those achieved by other authors as well as with ship model experimental test results. The results show that the method in question can be deemed a useful tool in preliminary design stage of SWATH ships.

AIM AND RANGE OF APPLICABILITY OF THE METHOD

The method in question has to serve for predicting hull resistance characteristics of SWATH ships. Its mathematical model, applicability range and results of research on its predicting features are presented by comparing them with results obtained both from structural methods and experimental model tests.

The set of 1215 discrete values of wave and viscosity resistance was determined by means of structural methods for the elaborated series of 243 ship body forms of systematically changing parameters and 5 values of Froude number. For elaboration of the parametric method in question a non linear approximation of the set of discrete values obtained from computer simulations of resistance for the designed body form series, was performed.

The range of applicability of the method covers the hulls and speeds determined by the set of allowable values of the design parameters $\overline{x}(x1, x2, x3, x4, x5, x6)$, where:

- $x_1 = L_p/D_p \in (8 \div 16)$ - lower hull slenderness
- $x_2 = L_k/L_p \in (0.7 \div 0.9)$ - upper hull length
- $x_3 = B_k/D_p \in (0.4 \div 0.6)$ - breadth of columns
- $x_4 = L_p/Y_p \in (2 \div 4)$ - dimensionless spacing of the hulls
- $x_5 = \varphi \in (0.8 \div 0.9)$ - block coefficient of lower hulls (floats)
- $x_6 = Fn \in (0.3 \div 0.5)$ - Froude number related to float length.

The cylindrical coefficient φ stands for the ratio of the float volume V_p and the volume of equivalent circular cylinder circumscribed on it:

$$\varphi = \frac{V_p}{L_p \frac{\pi \cdot D_p^2}{4}} \tag{1}$$

The symbols of important form parameters of underwater part of ship hull are shown in Fig. 2.

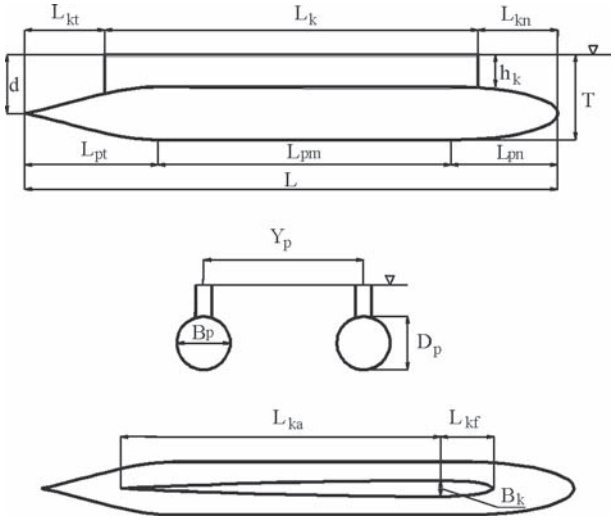

Fig. 2. *Identification of form parameter s of single-column configuration of underwater part of hull of SWATH ship*

The remaining parameters of the computational model such as the water density ρ, gravity acceleration g, dynamic viscosity coefficient μ, constitute components of the vector of constant values, $\overline{c}$.

DESCRIPTION OF THE METHOD

The main element of the method are the analytical mathematical relations obtained by means of approximation procedure, which associate predicted value of hull resistance with the ship design parameters $\overline{x}$, i.e.: its geometrical dimensions, speed as well as important parameters included in the vector of constants, $\overline{c}$.

In the method the superposition principle was applied – the total hull resistance R_t was expressed as the sum of the wave resistance R_w and the viscosity resistance R_v (the remaining components of hull resistance, presented in [9] were omitted in this work as being less important). Therefore the initial relation is expressed in the classical structure form as follows:

$$\begin{aligned} R_t(\overline{x},\overline{c}) &= R_w(\overline{x},\overline{c}) + R_v(\overline{x},\overline{c}) = \\ &= \frac{1}{2}\left[c_w(\overline{x},\overline{c}) + c_v(\overline{x},\overline{c})\right] \cdot \rho \cdot v^2 \cdot \Omega(\overline{x}) \end{aligned} \tag{2}$$

The characteristics of resistance coefficients are related to the wetted surface area of underwater part of ship hull, $\Omega(\overline{x})$, which is consisted of the surfaces of upper hull sides, Ω_k, and the surfaces of lower hulls (floats), Ω_p, lessened by the area of contact (penetration) surfaces of lower and upper hulls:

$$\begin{aligned} \Omega(\overline{x}) &= \Omega_p(L_p, D_p, \varphi, \alpha_k) + \Omega_k(L_k, B_k, T_k) = \\ &= 2 \cdot (\pi \cdot L_p \cdot D_p \cdot \varphi^{c0} - L_k \cdot B_k \cdot \alpha_k^{c1}) + 2 \cdot L_k \cdot T_k \cdot B_k^{c2} \end{aligned} \tag{3}$$

The parameter α_k which appears in the term correcting the surface area of the floats stands for the column water-plane coefficient whose value can be preliminarily assumed to be $\alpha_k = 2/3$. The determined structural constants in the formula expressing the wetted hull surface area are given in Tab. 1.

Tab. 1. The structural constants in the formula (3) for wetted surface area of SWATH ship hull

i =	0	1	2
C_i	0.66666	1.50	0.002

Viscosity resistance characteristics

As values of Reynolds numbers concerning flow around upper and lower hulls (floats) are very different the total viscosity resistance is given as the sum of the viscosity resistance of upper and lower hulls:

$$R_v(\bar{x},\bar{c}) = R_{vp}(\bar{x},\bar{c}) + R_{vk}(\bar{x},\bar{c}) = \frac{1}{2}\rho \cdot v^2 \cdot \left[c_{vp}(\bar{x},\bar{c}) \cdot \Omega_p(\bar{x}) + c_{vk}(\bar{x},\bar{c}) \cdot \Omega_k(\bar{x}) \right] \tag{4}$$

Value of the viscosity resistance coefficient $c_v(\bar{x},\bar{c})$ related to the total wetted surface area, depends on contribution of particular configuration elements of underwater part of ship's hull in generating the viscosity resistance, i.e.: on Reynolds number values, coefficients of form and wetted surface area of lower and upper hulls. The total effective hull's viscosity resistance coefficient related to the total wetted surface area, is expressed as follows:

$$R_v(\bar{x},\bar{c}) = \frac{1}{2}\rho \cdot v^2 \cdot \Omega(\bar{x}) \cdot c_v(\bar{x},\bar{c}) = \frac{1}{2}\rho \cdot v^2 \cdot \Omega(\bar{x}) \cdot \left[c_{vp}(\bar{x},\bar{c}) \cdot \frac{\Omega_p(\bar{x})}{\Omega(\bar{x})} + c_{vk}(\bar{x},\bar{c}) \cdot \frac{\Omega_k(\bar{x})}{\Omega(\bar{x})} \right] \tag{5}$$

The resistance coefficients which appear in the formula were determined in [9] by means of the following parametric approximating formulae.

The viscosity resistance coefficient of lower hulls:

$$c_{vp}(\bar{x},\bar{c}) = c_{fp}(\bar{x},\bar{c}) \cdot \left[1 + k_p(\bar{x}) \right] = c_{fp}(\bar{x},\bar{c}) \cdot \left[1 + k_p(L_p, D_p) \right] = \frac{0.075}{\left(\log \frac{v \cdot L_p}{\mu/\rho} - 2 \right)^2} \cdot \left[1 + \left(\frac{D_p}{L_p} \right)^{c_1} \right] \tag{6}$$

where c_{fp} concerns the lower hull and stands for the friction resistance coefficient (that of equivalent flat plate) and k_p – for the form factor.

The viscosity resistance coefficient of columns is expressed by the formula:

$$c_{vk}(\bar{x},\bar{c}) = c_{fk}(\bar{x},\bar{c}) \cdot \left[1 + k_k(\bar{x}) \right] = c_{fk}(\bar{x},\bar{c}) \cdot \left[1 + k_k(L_k, B_k, \alpha_k) \right] = \frac{0.075}{\left(\log \frac{v \cdot L_k}{\mu/\rho} - 2 \right)^2} \cdot \left(\frac{3.2 \cdot \sqrt{2 \cdot B_k \cdot T_k}}{L_k} \right)^{1.43} \tag{7}$$

where c_{fk} deals with the upper hull and stands for the friction resistance coefficient (that of equivalent flat plate) and k_k – for the form factor whose value was determined with the use of the formula applied in [10].

The total viscosity resistance coefficient is determined in the form which makes it possible to sum it directly with the wave resistance coefficient:

$$C_v(\bar{x},\bar{c}) = C_{vp}(\bar{x},\bar{c}) + C_{vk}(\bar{x},\bar{c}) = \frac{0.075}{\left(\log \frac{v \cdot L_p}{\mu/\rho} - 2 \right)^2} \cdot \left\{ \left[1 + \left(\frac{D_p}{L_p} \right)^{c_1} \right] \cdot \frac{2 \cdot (\pi \cdot L_p \cdot D_p \cdot \varphi^{c_2} - L_k \cdot B_k \cdot {\alpha_k}^{c_3})}{2 \cdot (\pi \cdot L_p \cdot D_p \cdot \varphi^{c_2} - L_k \cdot B_k \cdot {\alpha_k}^{c_3}) + (4 \cdot L_k \cdot T_k \cdot {B_k}^{c_4})} + \left[1 + \left(\frac{3.2\sqrt{2 \cdot B_k \cdot T_k}}{L_k} \right)^{1.43} \right] \frac{(4 \cdot L_k \cdot T_k \cdot {B_k}^{c_4})}{2 \cdot (\pi \cdot L_p \cdot D_p \cdot \varphi^{c_2} - L_k \cdot B_k \cdot {\alpha_k}^{c_3}) + (4 \cdot L_k \cdot T_k \cdot {B_k}^{c_4})} \right\} \tag{8}$$

The structural constants in the formula, determined in [9], are presented in Tab. 2.

Tab. 2. *The structural constants in the formula (8) for viscosity resistance characteristics of SWATH ship hull*

i =	1	2	3	4
$\mathbf{C_i}$	1.250	0.6666	1.50	0.002

Wave resistance characteristics

The parametric relation which expresses generated wave resistance, covers simultaneous interaction of all hull elements:

$$R_W(\overline{x}) = \frac{1}{2} C_W(\overline{x}) \cdot \rho \cdot v^2 \cdot \Omega(\overline{x}) \tag{9}$$

The analytical relation determined in [9], which approximates characteristics of the wave resistance coefficient $Cw(\overline{x})$, is also related to the wetted hull surface area, $\Omega(\overline{x})$, defined by the formula. The relation most accurately approximated – in the sense of the method of minimization of sum of squares of deviations – the set of discrete values to be approximated, determined by using structural methods.

The best approximating relation expressed by a combination of elementary functions was achieved by applying the formula of the following structure:

$$Cw\left(\frac{D_p}{L_p}, \frac{B_k}{D_p}, \frac{L_k}{L_p}, \frac{Y_p}{L_p}, \varphi, Fn\right) =$$

$$= C_{0,0} + C_{0,1}\cdot\frac{D_p}{L_p} + C_{0,2}\cdot\left(\frac{D_p}{L_p}\right)^2 + C_{0,3}\cdot\varphi + C_{0,4}\cdot\varphi^2 + C_{0,5}\cdot\frac{B_k}{D_p} + C_{0,6}\cdot\left(\frac{B_k}{D_p}\right)^2 + C_{0,7}\cdot\frac{Y_p}{L_p} +$$

$$C_{0,8}\cdot\left(\frac{Y_p}{L_p}\right)^2 + C_{0,9}\cdot\frac{L_k}{L_p} + C_{0,10}\cdot\left(\frac{L_k}{L_p}\right)^2 + C_{0,11}\cdot\frac{D_p}{L_p}\cdot\frac{B_k}{D_p}\cdot\frac{L_k}{L_p} + C_{0,12}\cdot\left(\frac{D_p}{L_p}\right)^2\cdot\left(\frac{B_k}{D_p}\right)\cdot\left(\frac{L_k}{L_p}\right) +$$

$$+\left[C_{1,0} + C_{1,1}\cdot\frac{D_p}{L_p} + C_{1,2}\cdot\left(\frac{D_p}{L_p}\right)^2 + C_{1,3}\cdot\varphi + C_{1,4}\cdot\varphi^2 + C_{1,5}\cdot\frac{B_k}{D_p} + C_{1,6}\cdot\left(\frac{B_k}{D_p}\right)^2 + C_{1,7}\cdot\frac{Y_p}{L_p} +\right.$$

$$\left. C_{1,8}\cdot\left(\frac{Y_p}{L_p}\right)^2 + C_{1,9}\cdot\frac{L_k}{L_p} + C_{1,10}\cdot\left(\frac{L_k}{L_p}\right)^2 + C_{1,11}\cdot\frac{D_p}{L_p}\cdot\frac{B_k}{D_p}\cdot\frac{L_k}{L_p} + C_{1,12}\cdot\left(\frac{D_p}{L_p}\right)\cdot\left(\frac{B_k}{D_p}\right)^2\cdot\left(\frac{L_k}{L_p}\right)\right]\cdot Fn + \tag{10}$$

$$\left[C_{2,0} + C_{2,1}\cdot\frac{D_p}{L_p} + C_{2,2}\cdot\left(\frac{D_p}{L_p}\right)^2 + C_{2,3}\cdot\varphi + C_{2,4}\cdot\varphi^2 + C_{2,5}\cdot\frac{B_k}{D_p} + C_{2,6}\cdot\left(\frac{B_k}{D_p}\right)^2 + C_{2,7}\cdot\frac{Y_p}{L_p} +\right.$$

$$\left. C_{2,8}\cdot\left(\frac{Y_p}{L_p}\right)^2 + C_{2,9}\cdot\frac{L_k}{L_p} + C_{2,10}\cdot\left(\frac{L_k}{L_p}\right)^2 + C_{2,11}\cdot\frac{D_p}{L_p}\frac{B_k}{D_p}\frac{L_k}{L_p} + C_{2,12}\cdot\left(\frac{D_p}{L_p}\right)\cdot\left(\frac{B_k}{D_p}\right)\cdot\left(\frac{L_k}{L_p}\right)^2\right]\cdot Fn^2 +$$

$$\left[C_{3,0} + C_{3,1}\cdot\frac{D_p}{L_p} + C_{3,2}\cdot\left(\frac{D_p}{L_p}\right)^2 + C_{3,3}\cdot\varphi + C_{3,4}\cdot\varphi^2 + C_{3,5}\cdot\frac{B_k}{D_p} + C_{3,6}\cdot\left(\frac{B_k}{D_p}\right)^2 + C_{3,7}\cdot\frac{Y_p}{L_p} +\right.$$

$$\left. C_{3,8}\cdot\left(\frac{Y_p}{L_p}\right)^2 + C_{3,9}\cdot\frac{L_k}{L_p} + C_{3,10}\cdot\left(\frac{L_k}{L_p}\right)^2 + C_{3,11}\cdot\frac{D_p}{L_p}\cdot\frac{B_k}{D_p}\cdot\frac{L_k}{L_p} + C_{3,12}\cdot\left(\frac{D_p}{L_p}\right)^2\cdot\left(\frac{B_k}{D_p}\right)^2\cdot\left(\frac{L_k}{L_p}\right)^2\right]\cdot Fn^3$$

The structural constants which appear in the relation describing the hull wave resistance characteristics are presented in Tab. 3.

Tab. 3. *The structural constants in the formula (10) for wave resistance coefficient characteristics of SWATH ship hull*

		i = 0	i = 1	I = 2	i = 3
$C_{i,0}$	j = 0	−12.1397304	92.9980695	−233.111006	191.37337
$C_{i,1}$	j = 1	−1.04586444	6.80487275	−18.1580215	15.9779735
$C_{i,2}$	j = 2	3.55241531	−29.5798224	88.3886875	−77.6752057
$C_{i,3}$	j = 3	31.0710348	−238.120645	598.284408	−492.059972
$C_{i,4}$	j = 4	−19.1679792	147.631585	−372.719428	307.847798
$C_{i,5}$	j = 5	−1.06797869	7.76205472	−19.4101477	15.9798061
$C_{i,6}$	j = 6	0.380383693	−2.99449204	8.25988137	−7.33575198
$C_{i,7}$	j = 7	−1.43530796	10.0595466	−22.915595	16.9069877
$C_{i,8}$	j = 8	0.853411164	−5.32492704	10.4095064	−6.21579753
$C_{i,9}$	j = 9	0.83038227	−6.91822075	18.3849983	−16.0594273
$C_{i,10}$	j = 10	−0.72083999	5.99518048	−16.053947	14.1285268
$C_{i,11}$	j = 11	20.2259023	−147.264231	371.04320	−301.57430
$C_{i,12}$	j = 12	−2.51608454	−1.20224482	−4.0574586	37.0598212

VERIFICATION OF PREDICTING FEATURES OF THE METHOD

A necessary condition of usefulness of the presented method for preliminary designing the SWATH ships should be positive assessment of its predicting features. The presented results of comparative analyses serve both for preliminary assessment of predicting merits of the elaborated structural methods and the simplified parametric method based on results obtained by using them. The verification consists in comparing the obtained results of wave resistance coefficient characteristics dealing with various body forms with theoretical results presented by other authors as well as those achieved experimentally from model tests.

The limited range of the performed comparative analyses as well as legitimacy of usefulness assessment of the verified methods are conditioned both by limited access to experimental results of model tests of SWATH ships and by lack of detail geometrical descriptions of the tested body forms given in available subject-matter literature sources.

The comparative analysis was performed by applying forms of resistance coefficients identical to those used in the publications from which the compared hull resistance characteristics were taken out. Therefore different forms of the resistance coefficient appear in the below presented diagrams. The axis of abscissae is scaled by means of Froude number related to lower hull length.

The wave resistance coefficient Cw is a dimensionless quantity defined in different ways, Rw stands for hull wave resistance, r_o – water density, v – ship speed, S – wetted surface area of hull underwater part, and V – volumetric displacement of hull underwater part. The resistance characteristics marked Cw on the diagram stand for the structural method results, and the curve marked CwA presents the characteristics obtained by means of the parametric method in question. And, the curve marked EXPER. shows the residuary resistance coefficient characteristics obtained experimentally.

Comparison of hull resistance characteristics – Model 5287

Description of selected body form parameters of SWATH ship *Model 5287* as well as results of experimental model tests of resistance and results of theoretical calculation of wave resistance were published independently by Huang [11, 12], Lin [13] and Chun [14]. On the basis of the data the following body form parameters were identified:

xr = 0.375; relative run length of the float
xw = 0.375; relative middle (cylindrical) body length of the float
xd = 0.25; relative entrance length of the float
L_p = 87.78 m; length of the float
D^p = 5.49 m; diameter of an equivalent axially cylindrical float
Y^p_p = 22.88 m; spacing of axes of the floats
L_k = 69.19 m; aft column length
L_{kf} = 0.5; relative entrance length of the aft column
B_k = 2.44 m; breadth of the aft column
T = 8.53 m; design draught of the ship
D = 3906 t; displacement.

The wave resistance characteristics of the hull of *Model 5287* form, shown in Fig. 3, graphically illustrate the results of the verifying calculations of the method in question.

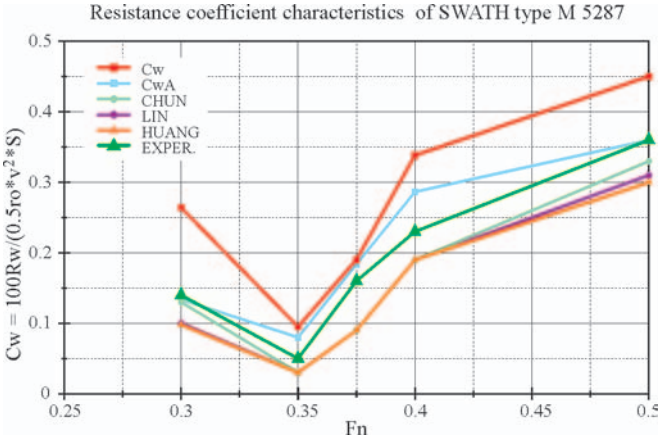

Fig. 3. *Comparison of wave resistance coefficient characteristics of the hull of Model 5287 form.*

The presented diagrams of the resistance coefficient characteristics make it justified to state that the results obtained by means of the structural method provide a better approximation of residuary resistance than those taken from the subject-matter literature sources [11, 12, 13, 14]. For the extreme values of the considered speed range the results achieved from the parametric method are somewhat worse than those obtained from the remaining methods.

The small spacing of the floats, r = 0.26, is characteristic for *M-5287* body form, that significantly contributes to an interferential character of generated wave system. Moreover the geometrical description of the body form was prepared on the basis of scanty data given in [12]. Hence possible inaccuracy of geometrical representation of the body form may cause the mentioned discrepancies of the results obtained from the parametric method.

Comparison of hull resistance characteristics – Model T-AGOS

The selected body form parameters of *T-AGOS* ship together with the experimental results of model tests of its resistance and the results of theoretical calculations of its wave resistance are contained in the publications of Chun [14] and Salvesen [15]. The following main parameters of the body form were determined:

xr = 0.291; relative run length of the float
xw = 0.274; relative length of float's middle (cylindrical) part
xd = 0.434; relative entrance length of the float
L_p = 74.34 m; length of the float
D_p = 5.36 m; diameter of the float if axially cylindrical
Y_p = 23.47 m; spacing of axes of the floats
L_k = 60.80 m; length of aft column
x_k = 8.51; abscissa of trailing edge of aft column
L_{kf} = 0.774; relative entrance length of aft column edge of attack
B_k = 2.133 m; breadth of aft column
T = 7.42 m; design draught of the ship
PZw = 2743m^2; wetted surface area
D = 2968 t; displacement.

The body form *T-AGOS* is characteristic of elliptic frame cross-sections of floats. The wave resistance coefficient characteristics of the *T-AGOS* form hull, shown in Fig. 4, graphically illustrate the performed verifying calculations of the method.

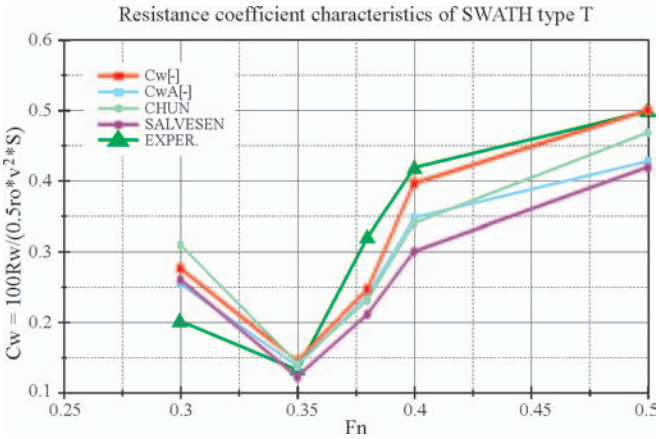

Fig. 4. *Comparison of the wave resistance coefficient characteristics for the T-AGOS form hull*

The comparison of the obtained results makes it justified to state that the best approximation of experimental results was achieved by means of the parametric method. The results concerning the structural method are only somewhat worse. Both the methods give better approximation of the experimental resistance characteristics than those obtained from the methods of other authors. Just this test had to constitute verification of the hypothesis that the form of the float of elliptic frame cross-sections can be approximated by a distribution of hydrodynamic singularities which model an equivalent axially symmetrical float. The obtained results suggest to accept such hypothesis.

Comparison of hull resistance characteristics – Model 8501

The body form of the passenger ship *M-8501* was investigated by Huang [11, 12]. The publications contains some main dimensions and the distribution diagram of frame cross-section areas of body form, that made it possible to approximately reconstruct the investigated body form geometry.

The following main parameters of the body form were determined:

xr = 0.25; relative run length of the float
xw = 0.6; relative length of the float's middle (cylindrical) part
xd = 0.15; relative entrance length of the float
L_p = 28.8 m; length of the float
D_p = 2.4 m; diameter of the float if axially cylindrical
Y_p = 9.6 m; spacing of axes of the floats
L_k = 23.04 m; length of aft column
x_k = 2.8; abscissa of trailing edge of aft column
z_k = 0.3; relative entrance length of aft column edge of attack
B_k = 1.2 m; breadth of aft column
T = 3.60 m; design draught of the ship
PZw = 477.0m^2; wetted surface area
D = 276.9 t; displacement.

The wave resistance coefficient characteristics of the *Model-8501* form hull, shown in Fig. 5, graphically illustrate the performed verifying calculations of the method.

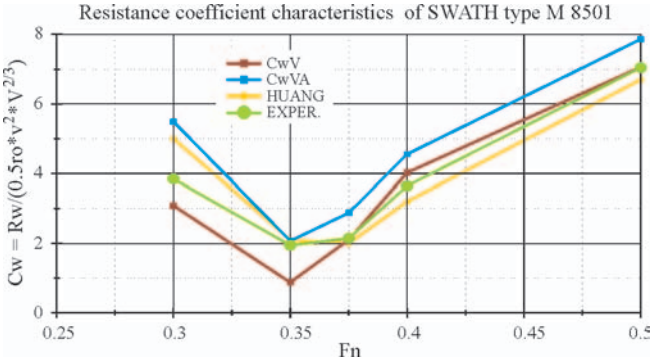

Fig. 5. *Comparison of the wave resistance coefficient characteristics for the Model 8501 form hull*

The resistance coefficient used on the diagram is related to the volumetric displacement of the hull underwater part, V, in 2/3 power, i.e. in the same way as defined in the referred to publications. Assessing the obtained results one can state that the elaborated structural methods as well as the parametric method for the hull resistance predicting of SWATH ships may serve as a useful tool in the preliminary design stage as this way predicted resistance correctly approximates experimental values.

Comparison of hull resistance characteristics of body form series– HSVA *models*

An important verifying information is obtained from comparison of the achieved theoretical results with those obtained from experimental tests of resistance of body form series performed for body forms of systematically changing parameters. Such verification makes it possible both to follow relations of values and trends of changes of resistance characteristics resulting from changes of body form geometrical parameters.

For the verification were used the results of model resistance tests of series of SWATH body forms performed in *HSVA* model basin, whose selected fragments were published by Schenzle [16]. On the basis of the available data the approximate parameters of the body form series were determined, that

made it possible to perform appropriate verifying calculations. The tests of body form series, carried out in *HSVA*, covered about 150 configurations of SWATH hull of simplified form characterized by the following features:

- ★ Hulls of single-column configuration
- ★ Length of floats equal to length of columns – displaced aft by 6% against floats
- ★ Axially symmetrical floats
- ★ Column entrance and run lengths equal to 25% length of column
- ★ Float entrance length equal to 80% of its run length.

The body form series which model the original *HSVA* forms, were obtained by systematic changing the following body form parameters:

- ☆ Cylindrical coefficient of floats – by changing their entrance length
- ☆ diameter / length ratio of floats
- ☆ breadth/length ratio of columns
- ☆ spacing/length ratio of floats (hulls)
- ☆ ratio of float axis draught and float diameter.

The approximated *HSVA* body form series were elaborated on the basis of the available data [16] by generating the series of body forms having geometrical parameters possibly well approximating the original parameters of the *HSVA* body form series. The following body form series were obtained:

- ➢ of similar concept of hull configuration except of that the original forms have columns shifted aft outside region of floats, that could be only approximately taken into account in the frame of the elaborated software
- ➢ of identical relative entrance and run lengths of columns and floats
- ➢ of identical slenderness of floats – expressed by their diameter/length ratios
- ➢ of identical maximum values of column breadth/ float diameter ratios.

The verifying calculations were performed for one determined value of draught/ diameter ratio of floats and one constant value of their spacing/length ratio. The range of investigated speeds was limited to that corresponding with Froude number values from 0.30 to 0.50. Results of the experiments [16] are presented in the form of the residuary resistance coefficients related to displacement.

Information on form of aft and bow zones of column water-planes, important for adequacy of comparisons, is not given in [16]. Therefore the column water-planes were arbitrarily assumed of elliptical form fore and of sharp trailing edge aft. The possible form discrepancy close to actual water-plane results in a doubt as to geometrical similarity of the compared series. The other comment associated with justification of the comparisons deals with that the experimental results were achieved by using instrumentation which made sinking the models without any trim, possible.

The results of the verifying investigations lead to the following comments:

- ➲ the *HSVA* body form series are characteristic by a relatively large column length/float length ratio $L_k/L_p = 1$ which exceeds the assumed range of application of the parametric method, hence it was used only within the range of its possible extrapolation
- ➲ a characteristic feature of the *HSVA* body form series is that the columns extend aft beyond the floats, that places them outside the assumed class of allowable body forms. Therefore the *HSVA* body forms were so corrected as to obtain spread of the columns over the length of the floats only. The performed calculations demonstrated that – in the case of the *HSVA* series – small displacements of columns against floats introduced only small changes of hull resistance ; hence the applied simplification seems to be acceptable.

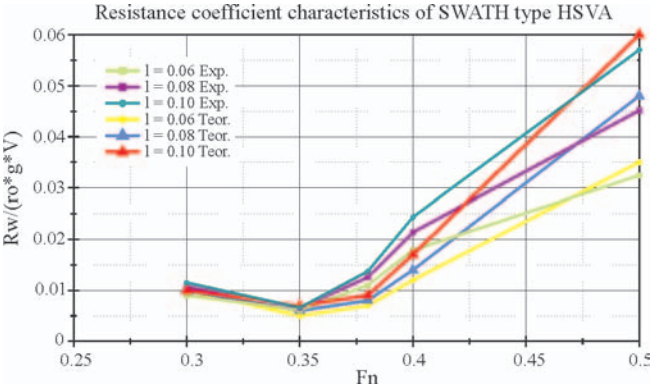

Fig. 6. *Wave resistance coefficient characteristics for HSVA series – changeable ratio l = Dp/Lp*

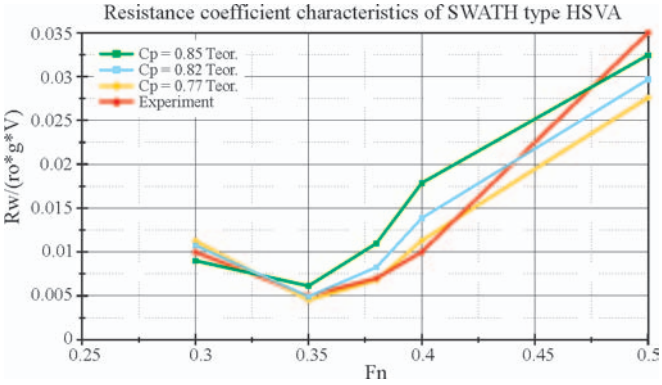

Fig. 7. *Wave resistance coefficient characteristics for HSVA series – changeable coefficient Cp.*

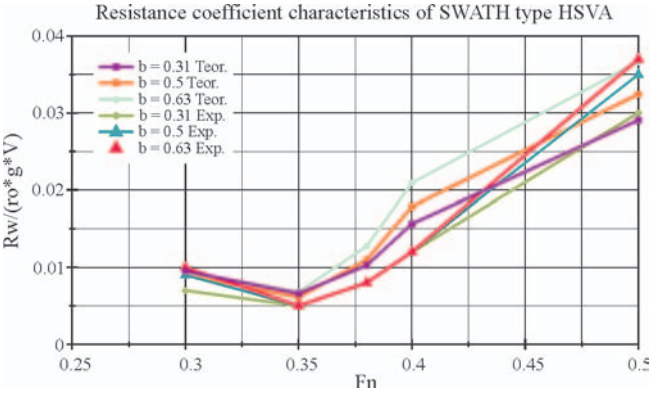

Fig. 8. *Wave resistance coefficient characteristics for HSVA series – changeable ratio b = B_k/D_p*

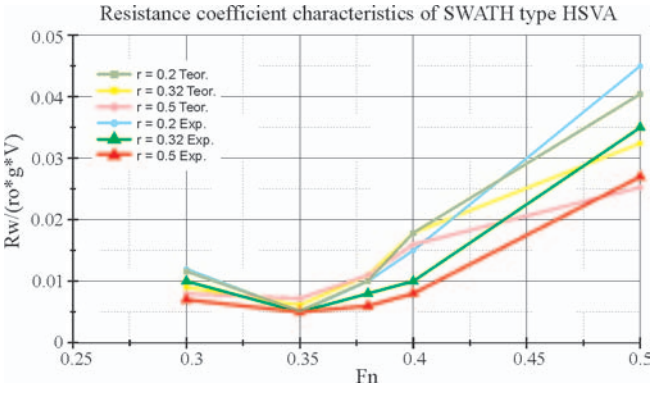

Fig. 9. *Wave resistance coefficient characteristics for HSVA series – changeable ratio r = Y_r/L_p*

CONCLUSIONS

- The obtained results of verifying investigations make it possible to preliminarily state that both the elaborated structural methods and parametric ones dealing with hull resistance prediction of SWATH ships may serve as a useful tool in the preliminary design stage as the predicted resistance characteristics correctly approximate values of the characteristics obtained experimentally.

- The thesis drawn from the preliminary investigations consists in that the elaborated parametric method – in the case of the SWATH ship hulls – provides resistance predictions of a reliability similar to that of results obtained by means of sophisticated structural methods based directly on theoretical formulations. Therefore the method may serve as a useful tool in the preliminary designing of SWATH ships.

BIBLIOGRAPHY

1. *SHIPFLOW Training course*. FLOWTECH International AB., Göteborg 1995
2. Larsson L.A. et al.: *SHIPFLOW Theoretical Manual.* FLOWTECH Int AB, Gothenburg 1994
3. Michalski J.P.: *Investigation of the fitness of chosen quadratures to the calculation of wave resistance of ship.* Scientific Bulletins of Gdańsk University of Technology *(*Zeszyty Naukowe Politechniki Gdańskiej) no. 212, Gdańsk 1974
4. Michalski J.P, Pramila A., Virtanen S.: *Computer algorithm for approximate evaluation of ship body forms with minimum resistance*. Nionde Nordiska Dagarna I Hallfastheslar, Oulu 1987
5. Michalski J.P., Pramila A., Virtanen S: *Creation of ship body form with minimum resistance using finite element method*. Proceedings of the International Conference on Numerical Methods in Engineering, NUMETA 87, Martinus Nijhoff Publ. Vol.1, Swansea 1987
6. Michalski J.P., Kozłowski K.: *Elaboration of computer procedures for approximate determination of resistance of SWATH ships and assessment of their usefulness in preliminary designing* (in Polish). Research Reports (Prace Badawcze) no. 618. Gdańsk University of Technology (Politechnika Gdańska), Faculty of Ocean Engineering and Ship Technology (Wydział Oceanotechniki i Okrętownictwa), Gdańsk 1995
7. Nowacki H., Michalski J., Oleksiewicz B., Bloor M., Dekanski C., Wilson M.: *Computational geometry for ships.* World Scientific, London 1995
8. *Proceedings of the Workshop on Ship Wave Resistance Computation.* Volume I. David W. Taylor Naval Ship Research and Development Center. Bethesda 1979
9. Michalski J.P.: *Methods of determining resistance and generalized mass in the preliminary design stage of small water-plane area twin hull ships* (in Polish). Publishing House of Gdańsk University of Technology (Wydawnictwo Politechniki Gdańskiej), Monographs 24. Gdańsk 2002
10. Min K.S.,Lee Y.W.: *Design of a High−Speed 300 Passenger SWATH Ship*. FAST'95: Third International Conference on Fast Sea Transportation,Travemünde 1995
11. Huang D.L., Cai Y.J.: *An optimization method for form design of SWATH ships*. International Shipbuilding Progress, No 414, 1991
12. Huang D.L.:*A modified method for calculating the wave resistance of SWATH Ships*. International Shipbuilding Progress, No 392, 1987
13. Lin W.C., Day W.G.: *The still−water resistance and propulsion characteristics of small−water-plane−twin−hull (SWATH) ships*. AIAA/Transactions of the Society of Naval
14. Chun H.H.: *A new approach to determine the wave resistance of SWATH ships.* University of Glasgow, Department of Naval Architecture and Ocean Engineering, Report no 87/46, 1987
15. Salvesen N. et al.: *Hydro−numeric design of SWATH ships.* Transactions SNAME, Vol.93, 1985
16. Schenzle P.: *The HSVA systematic SWATH model series*. FAST'95: Proceedings of the Third International Conference on Fast Sea Transportation, Lübeck − Travemünde 1995

NOMENCLATURE

B_k	− breadth of columns
B_p	− breadth of floats
$\overline{c}$	– vector of model constants
C_f	− friction resistance coefficient
C_{fk}	− friction resistance coefficient of column
C_{fp}	− friction resistance coefficient of float
C_p	– cylindrical coefficient of floats
C_v	− viscosity resistance coefficient
C_{vk}	− viscosity resistance coefficient of column
C_{vp}	− wave resistance coefficient
D	– ship displacement
D_p	– diameter of equivalent axially-symmetric cylindrical float
Fn	− Froude number
g	– gravity acceleration
k_k	– column form factor
k_p	– float form factor
L_k	− length of columns
L_p	− length of floats
PZw	− hull wetted surface area
Rn	− Reynolds number
R_t	– total resistance of hull
R_v	− viscosity resistance of hull
R_w	– wave resistance of hull
T_k	– draught of columns
v	− ship speed
V	− volumetric displacement of hull underwater part
xd	− relative entrance length of floats
xr	− relative run length of floats
xw	− relative length of middle (cylindrical) part of float
Y_p	− spacing of axes of floats
$\overline{x}$	− vector of main ship design parameters
$x_1 = L_p/D_p$	– slenderness of lower hulls
$x_2 = L_k/L_p$	– length of upper hulls
$x_3 = B_k/D_p$	– breadth of columns
$x_4 = L_p/Y_p$	– dimensionless spacing of hulls
$x_5 = \varphi$	– block coefficient of lower hulls
x_6 = Fn	– Froude number related to float length
α_k	− water-plane coefficient of column
φ	− cylindrical coefficient of floats
ρ	− water density
μ	− dynamic viscosity coefficient of water
Ω	− area of reference surface
Ω_k	– area of wetted surface of upper hulls
Ω_p	– area of wetted surface of lower hulls.

CONTACT WITH THE AUTHOR

Assoc. Prof. Jan P. Michalski
Faculty of Ocean Engineering
and Ship Technology
Gdansk University of Technology
Narutowicza 11/12
80-952 Gdansk, POLAND
e-mail : janmi@pg.gda.pl

POLISH MARITIME RESEARCH 1(55) 2008 Vol 15; pp. 11-18
DOI: 10.2478/v10012-007-0046-5

Hydrodynamic Analysis of Trimaran Vessels

M.R. Javanmardi, **E. Jahanbakhsh**,
M.S. Seif, **H.Sayyaadi**,
Sharif University of Technology

ABSTRACT

Trimaran vessels are developed for different applications and hydrodynamic behavior of such vessels is different than usual mono-hulls. In this paper hydrodynamic resistance and maneuvering of a trimaran with Wigley body form are investigated. The effects of outriggers position in four different longitudinal and two transverse locations are studied. For hydrodynamic simulations a CFD code has been developed and used. This code is capable for simulating three dimensional, time dependent, two phases, viscous flow coupled with rigid body motion. Formulation and solution algorithm are described in detail. Different case studies have been performance and numerical results have shown good agreement with experimental data. Based on resistance and maneuvering simulation of the trimaran vessels different conclusion are made. The results show that positions of outriggers have great effect on resistance and maneuverability of trimaran. The present method can be further employed to investigate other hydrodynamic qualities of trimaran vessels.

Keywords: trimaran; resistance; maneuvering; computational fluid dynamic

INTRODUCTION

Wave making resistance is an important component of ship resistance. It is very effective at high speeds and will require more attention in designing of high speed ships. Normally large slenderness ratio is necessary to decrease the wave making resistance. Therefore the ship hull should be as slender as possible for attaining higher speeds. But the main drawback of the slenderness is that the transverse stability decreases. Hence to overcome this challenge, the single body must be changed to multi-hull with proper separation distance. It means that a trimaran vessel which is composed of a main slender body and two outriggers can be an appropriate solution to improve vessel transverse stability, while the efficient wave interaction, created by main body and outriggers is able to compensate for wetted surface increase and guaranties slender bodies with good stability at high Froude numbers. Trimarans share most of the characteristics of catamarans, but in few aspects, trimarans are more efficient than catamarans. Lyakhovitsky compared a trimaran with a mono-hull and a catamaran of same characteristics and showed that the trimaran is better in hydrodynamic performances compared to other alternatives [1]. In addition trimarans have some other privileges such as: extended deck, lower draft and better transverse stability compared with single body vessels [2]. In order to study the effect of outriggers position on trimaran resistance, some experimental tests are done and results show that the outriggers location has considerable effect in hydrodynamic performance of the vessel [3], but in vessel design, some cases such as maneuverability must be consider.

Optimization procedures demand the performance of a ship to be assessed in its early design stage. This leads to a prediction tool independent of experimental results, although model tests will still be indispensable. CFD modeling based on numerical solution of the governing equations is a good choice. It must be remembered that, such a problem combines the complexity of free surface flow with rigid body motions. NUMEL[1] code [4], [15] which is used for present study provides an effective numerical tool for hydrodynamic simulation. Trimaran maneuvering simulation is a complex hydrodynamic problem that should be divided into minor sub-problems.

The motion of a floating body is a direct consequence of the flow-induced forces acting on it while at the same time these forces are functions of the body movement itself. Therefore, the prediction of flow-induced body motion in viscous fluid is a challenging task and requires coupled solution of fluid flow and body motions. In recent two decades, with the changes in computer hardware, ship motion simulation is the subject of many numerical hydrodynamic researches. These researches were started from the restricted motions such as trim or sinkage by Miyata [5], Hochbaum [6] Alessandrini [7] and Kinoshita [8] and continued to the evaluation of 6-DoF motions by Miyake [9], Azcueta [10], Vogt [12], Xing [12] and Jahanbakhsh et. al [13]. In this paper fully nonlinear motion of Trimaran is simulated based on 6-DOF motions and hydrodynamic interaction.

[1] Numerical Marine Engineering Laboratory

GOVERNING EQUATIONS

There is an approach in simulation of two-phase flow where different fluids are modeled as a *single fluid* obeying the same set of governing equations, with the different local identified volume fraction values α. Incompressible Navier-Stokes and continuity equations are well-known and given by the equations:

$$\frac{\partial u_i}{\partial t}+u_j\frac{\partial u_i}{\partial x_j}=-\frac{1}{\rho}\frac{\partial P}{\partial x_i}+\nu\frac{\partial^2 u_i}{\partial x_j\partial x_j}+g_i \tag{1}$$

$$\frac{\partial u_i}{\partial x_i}=0 \tag{2}$$

where:
u_i – velocity
P – pressure
ν – kinematic viscosity.

Local density ρ and viscosity ν of the single fluid are defined as:

$$\begin{aligned}\rho_{cell} &= \alpha\rho_1+(1-\alpha)\rho_2\\ \nu_{cell} &= \alpha\nu_1+(1-\alpha)\nu_2\end{aligned} \tag{3}$$

Subscripts 1 and 2 indicate two fluids (e.g. water and air), where α (volume fraction) is the percentage of fluid 1 (e.g. water) available in cell and defined as follow:

$$\alpha=\begin{cases}1 & \text{for cells inside fluid 1}\\ 0 & \text{for cells inside fluid 2}\\ 0<\alpha_0<1 & \text{for transitional area}\end{cases} \tag{4}$$

Reformulating the continuity equation (Eq.2) and using the definition of the single fluid density, results in extracting a scalar transport equation for volume fraction α (Spalding, 1974):

$$\frac{\partial\alpha}{\partial t}+\vec{\nabla}\cdot(\alpha\vec{u})=0 \tag{5}$$

Discretisation of the governing equations is considered by integration of the momentum equation over a control volume it becomes as below:

$$\begin{aligned}&\frac{d}{dt}\int_V\vec{u}\,dV+\int_A\vec{u}(\vec{u}\cdot\vec{n})dA=\\ &=\int_A\nu\vec{\nabla}\vec{u}\cdot\vec{n}dA-\frac{1}{\rho}\int_A P\vec{n}dA+\int_V\vec{g}dV\end{aligned} \tag{6}$$

Where: $\vec{u}$ is the velocity vector, ν is the cell volume and A is the area around it.

The diffusion term (the first term in r.h.s. of Eq.6) is discretised using the over-relaxed interpolation for velocity component u_i (Jasak, 1996):

$$\int_A\nu\vec{\nabla}\vec{u}_i\cdot\vec{n}dA=\sum_{f=1}^{n}\nu_f\vec{A}_f\cdot(\vec{\nabla}\vec{u}_i)_f \tag{7}$$

Where: $\vec{A}_f$ is the CV face area vector.

Discretisation of the convection term (the second term in l.h.s. of Eq.6) needs to the fluid velocity component on CV face u_{i-f} as shown in Eq.8:

$$\int_A u_i(\vec{u}\cdot\vec{n})dA=\sum_{f=1}^{n}u_{i-f}F_f \tag{8}$$

Where: $F_f=\vec{A}_f\cdot\vec{U}_f$ is the volumetric flux. The fluid velocity on CV face $\vec{U}_f$ must be calculated separately in the co-located arrangement to avoid checkerboard pressure and will be discussed later in the solution algorithm. Here, u_{i-f} is approximated using Gamma interpolation scheme (Jasak, 1996) based on NVD (Normalized Variable Diagram) (Leonard, 1991) concept:

$$u_{i-f}=\begin{cases}u_{i-D} & \text{for } \tilde{u}_{i-D}\le 0 \text{ or } \tilde{u}_{i-D}\ge 1\\ \frac{1}{2}(u_{i-D}+u_{i-A}) & \text{for } k\le\tilde{u}_{i-D}<1\\ \left(1-\frac{\tilde{u}_{i-D}}{2k}\right)u_D+\frac{\tilde{u}_{i-D}}{2k}u_{i-A} & \text{for } 0\le\tilde{u}_{i-D}<k\end{cases} \tag{9}$$

Subscripts D and A stand for donor and acceptor cells determined for each CV's face according to the direction of flow as shown in Fig. 1. In addition, $\tilde{\phi}_D$ and $\tilde{\phi}_f$ are defined based on NVD as Eqs.10 and 11.

$$\tilde{\phi}_D=\frac{\phi_D-\phi_U}{\phi_A-\phi_U} \tag{10}$$

$$\tilde{\phi}_f=\frac{\phi_f-\phi_U}{\phi_A-\phi_U} \tag{11}$$

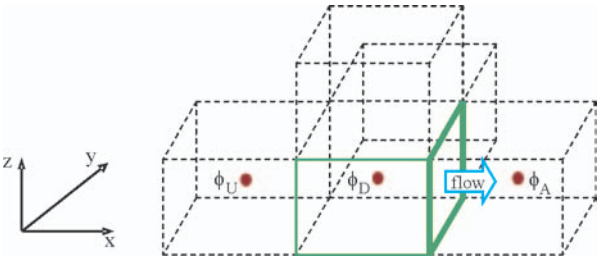

***Fig. 1**. Flow direction (arrow) determines doner, acceptor and upwind cells for each CV's face*

It must be mentioned that the Crank-Nicholson scheme is used for time discretisation of diffusion and convection terms in momentum equation (Eq.6). The pressure term (second term in r.h.s. of Eq.6) is discretised as Eq.12:

$$\int_A P\vec{n}dA=\sum_{f=1}^{n}P_f\vec{A}_f \tag{12}$$

Using the common Linear Interpolations (LI) for calculation of face pressure P_f, results in severe oscillations in velocity field. This is of great importance, especially when there are two fluids with high density ratio e.g. water and air. Here a Piecewise Linear Interpolation (PLI) shown in Fig. 2 is introduced and used for P_f estimation. It is based on a constraint for lines L_{Af} and L_{Bf} which connect pressure values at CVs' center P_A and P_B to P_f as Eq.13:

$$\frac{\text{Slope of } L_{Af}}{\text{Slope of } L_{Bf}}=\frac{\rho_A}{\rho_B} \tag{13}$$

Where ρ_A and ρ_B are the densities of CVs A and B, respectively. Therefore P_f can be estimated by using the pressure value at CVs' center P_A and P_B as well as Eq.14:

$$P_f=P_A\kappa+P_B(1-\kappa) \tag{14}$$

κ is the weighting factor and can be calculated as Eq.15:

$$\kappa=\frac{\rho_B\delta_B}{\rho_A\delta_A+\rho_B\delta_B} \tag{15}$$

Where δ_A and δ_B are distance from face center f to CVs' center A and B, respectively (Fig. 2). Finite volume discretisation of volume fraction transport equation (Eq.5) is based on the integration over CV and time step:

$$\int_t^{t+\delta t}\left(\int_V \frac{\partial \alpha}{\partial t} dV\right) dt + \int_t^{t+\delta t}\left(\int_V \vec{\nabla}\cdot(\alpha \vec{u})\, dV\right) dt = 0 \qquad (16)$$

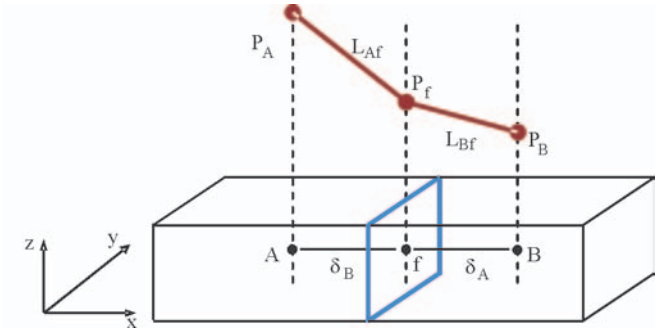

Fig. 2. *PLI for CV's face pressure calculation*

The first term in Eq.16 is a common integral form and applying the Gauss theorem on the second term results in:

$$(\alpha_P^{t+\delta t} - \alpha_P^t)\frac{V}{\delta t} + \frac{1}{2}\left(\sum_{f=1}^{n} \alpha_f^{t+\delta t} F_f^{t+\delta t} + \sum_{f=1}^{n} \alpha_f^t F_f^t\right) = 0 \qquad (17)$$

The time integral of the second term is discretised using Crank-Nicholson scheme. Assuming a linear and small variation of F_f in small time step, results in using the most recent value of it. Taking this into account, and rearranging of Eq.17 yield to:

$$\alpha_P^{t+\delta t}\frac{V}{\delta t} + \sum_{f=1}^{n}\frac{1}{2}\alpha_f^{t+\delta t} F_f = S_{\alpha_P} \qquad (18)$$

Where the source term is:

$$S_{\alpha_P} = \alpha_P^t \frac{V}{\delta t} - \sum_{f=1}^{n}\frac{1}{2}\alpha_f^t F_f \qquad (19)$$

One can see the face values α_f which must be approximated using an interpolation. As aforementioned, simple interpolations leads to non-physical or too diffusive volume fraction values. This leads to use a high order composite one. Most of composite methods, typically switch between two high and low order interpolations to use their advantages. Here, the main distinctions are how and when they switch between these schemes according to flow information.

CICSAM uses CBC (Convection Boundedness Criteria) (Gaskell and Lau, 1988) and UQ (ULTIMATE-QUICKEST) (Leonard, 1991) by introducing a weighting factor γ_f (Eq.20) which takes into account the slope of the free surface relative to the direction of motion. CBC is the most compressive scheme that stipulates robust local bounds on $\tilde{\alpha}_f$ nevertheless does not actually preserve the shape of interface. Here UQ uses for its ability to better preserving of interface shape. Based on NVD, normal face value is obtained as follows:

$$\tilde{\alpha}_f = \gamma_f \tilde{\alpha}_{f_{CBC}} + (1-\gamma_f)\tilde{\alpha}_{f_{UQ}} \qquad (20)$$

Using the definition of Eq.11 in Eq.20, results in estimation of α_f, shown in Eq.18. This value contains all the information regarding to the fluid distribution in the donor, acceptor and upwind cells as well as the interface orientation relative to flow direction. To avoid non-physical α in highly skewed meshes, a correction step is added to volume fraction calculation procedure and used in the developed software which can be found in Ubbink and Issa (1999) by details. Fig. 3 shows the solution algorithm in the developed numerical tool.

NUMERICAL RESULTS

Trimaran Resistance

Although many simulations have been done to investigate the accuracy of this software and all of the results were in good agreement with experimental data [4, 15], but still in present study, the accuracy of the code is validated by simulating a trimaran vessel and comparing the numerical result with experimental result.

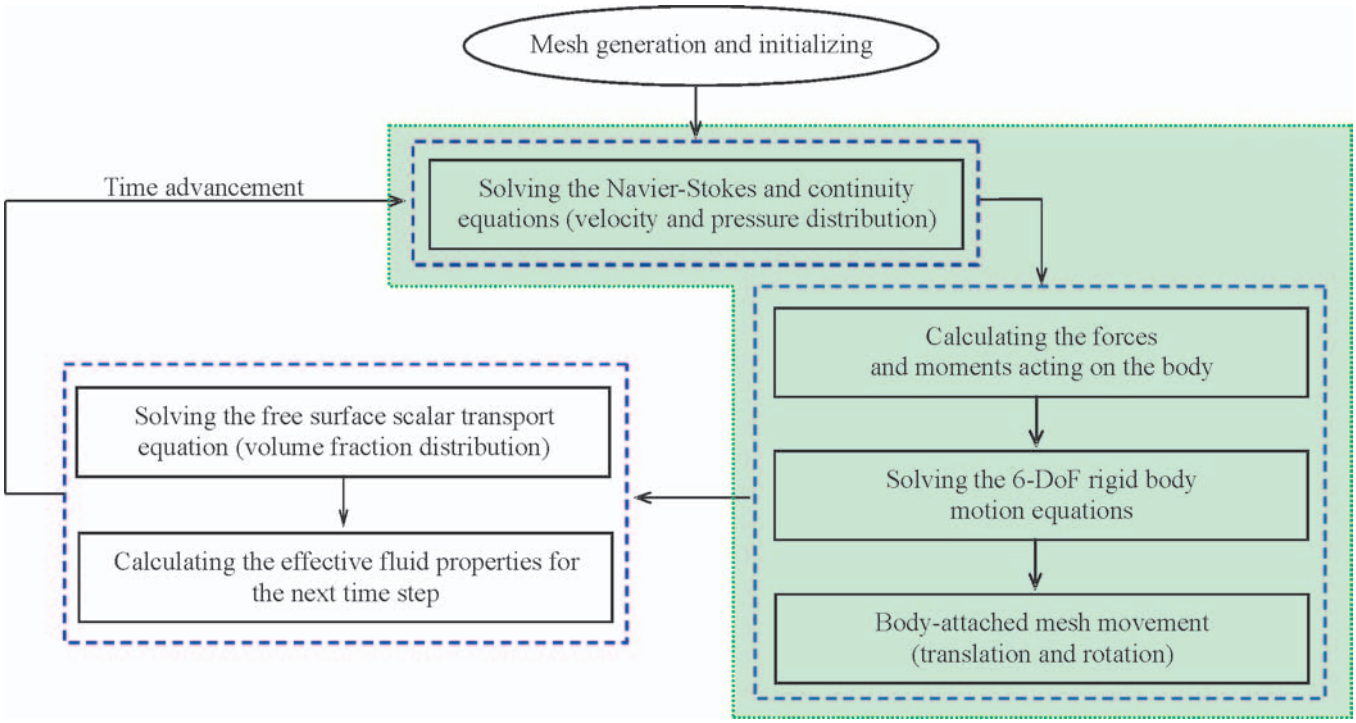

Fig. 3. *Solution algorithm in the developed numerical tool*

The trimaran with wigley form has been chosen; the main geometric characteristics of trimaran are given in Table 1. These characteristics are similar to that used in the experimental tests at Naples and Trieste Universities [14]. The computational domain dimensions are 28x14x3 meters (7 meters in front of vessel, 13.3 in behind of the vessel, 1 meter upside the water line and 2 meters under the keel line). In this software, the hexagonal meshes are used. For resistance simulation, since trimaran is an axis-symmetric body, because of symmetric shape of the hull, only half of the domain is used to reduce calculation as shown in Fig. 4. The numbers of cells in this domain are about 120000. This vessel has been simulated for speed range of 4~6 m/s. Since longitudinal location (the direction of motion) has more influence on the resistance than transverse location, the effect of four longitudinal and two transverse locations of outriggers have been studied as shown in Table 2. The parameters are defined in Tables 1 and 2, and illustrated in Fig. 5. The trimaran configuration is defined by the ratios d/L_M and s/L_M , where d is the longitudinal distance between the bows of the main hull and the outriggers, and s is the transverse distance between the centerline of outriggers. In Table 2 and Fig. 5, the under notes M and O are pointed to main hull and outriggers respectively. In order to validate simulation results, initially a simulation similar to the one studied in reference [16] is performed and then the results are compared, Fig. 6.

Table 1. *Trimaran particulars*

	Main Hull	Side Hull
Length waterline (m)	4.694	2.347
Draught (m)	0.166	0.0463
Wetted surface (m^2)	1.948	0.252
Displacement (kg)	120.489	4.259
Beam waterline (m)	0.332	0.109

Table 2. *Trimaran configurations*

d/Lm / s/Lm	-0.25	0.0	+0.5	+0.75
0.2	A	B	C	D
	-	E	F	-

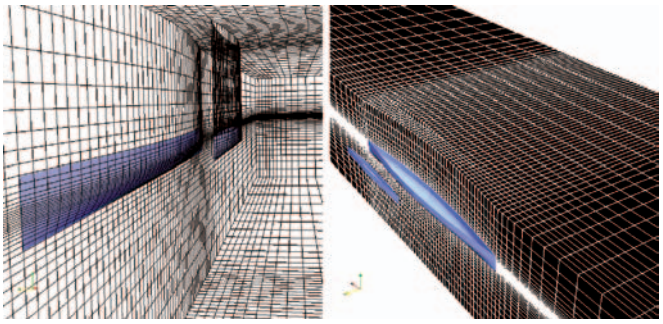

Fig. 4. *Computational domain*

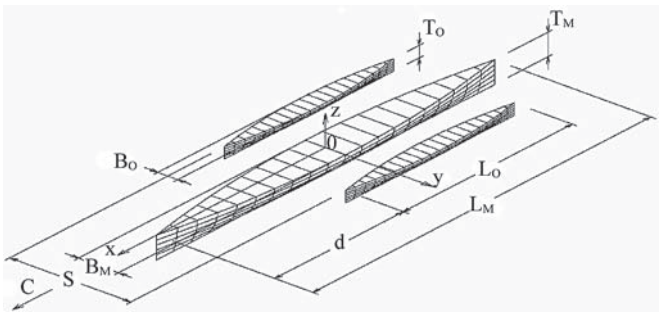

Fig. 5. *trimaran configuration with main particulars and relative position of outriggers*

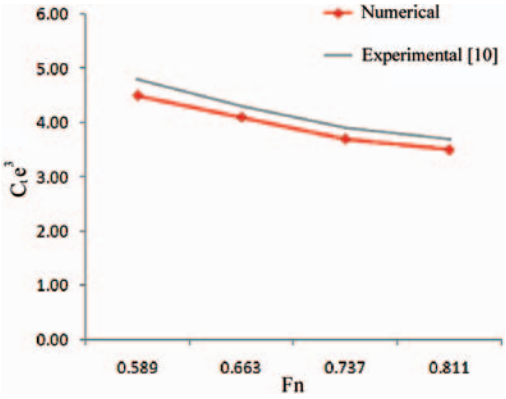

Fig. 6. *Comparison between numerical results and experimental data for case C*

Fig. 7 represents pressure drag relative to vessel speed for four cases with same clearance. For speed less than about 4.3 m/s, case A has the least pressure drag and for speed more than approximately 4.3, case D has the least pressure drag. The case B has the largest pressure drag for speed less than 5 m/s and at speeds more than 5 m/s, the case C has the largest pressure drag. Viscous drag versus speed is shown in Fig. 8 and also shows that case A has the least viscous drag. The case B has highest viscous drag for speed less than 5.1 m/s and for speed more than 5.5 m/s it is close to configuration A, but as the speed increases, the case C has the most viscous drag. Generally, the optimal viscous and pressure drag depend on vessel speed. In other words, the vessel speed must be considered in order to obtain the appropriate trimaran configuration which has the least pressure or viscous drag. It can be seen from Fig. 9 that trimaran with configuration A has the least of total drag (Sum of viscous and pressure drag). In this configuration, the waves created by main body do not interact with side bodies. This phenomenon can be accounted as a reason drag reduction. Fig. 10 represents trimaran with A configuration at speed 4 m/s. So it is seen that at higher speeds, because of decreasing of wave propagation angle, the wave created by main body do not interact with side bodies.

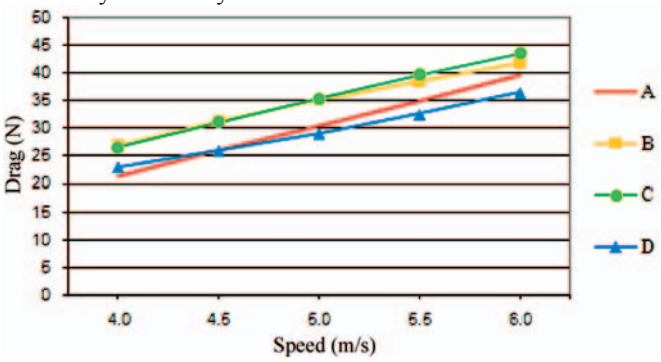

Fig. 7. *Pressure drag for various configurations*

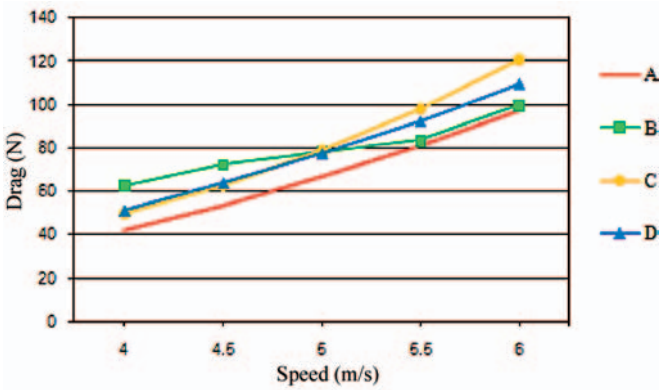

Fig. 8. *Viscous drag for various configurations*

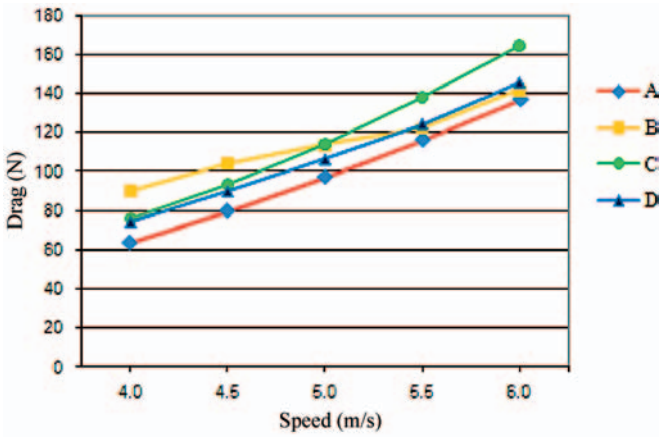

Fig. 9. Total drag for various configurations

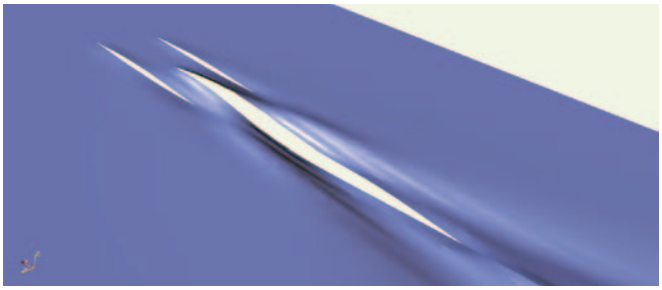

Fig. 10. Free surface for case A at speed 4 m/s

At higher speeds, the rate of increasing total drag in configuration B decreases. As the speed increases, the wave propagation angle decreases, so the interaction length between waves created by main body with the side bodies decrease. It is seen from Fig 11-A and 11-B, that at speed of 4 m/s, waves created by main body interacts with about ¾ length of side bodies, whereas at speed 5.5 m/s, they affected only the transom of side bodies. In order to validate the above statement, trimaran with configurations E and F are simulated. Fig. 12 shows pressure drag. It is observed that with increasing transverse distance, pressure drag decreases. Comparison of configuration B and E, showed that viscous drag in configuration E is less than configuration B, but increase in transverse distance has inverse effect when stern of bodies are aligned (compare configurations C and F). Fig. 13 shows viscous drag. In Fig. 14 it is observed that for configuration E, even at speed of 4 m/s main hull waves do not interact with outriggers but with increasing separation when stern of bodies are aligned, more waves pass through the tunnel between bodies, as a result the wave interaction increases, and consequently, as a result of increase in wet surface, viscous drag increases in configuration F with respect to configuration C. Finally, increase in transverse distance causes drag reduction when three hulls bow are aligned, but does not affect when three hulls stern are aligned (see Fig. 15).

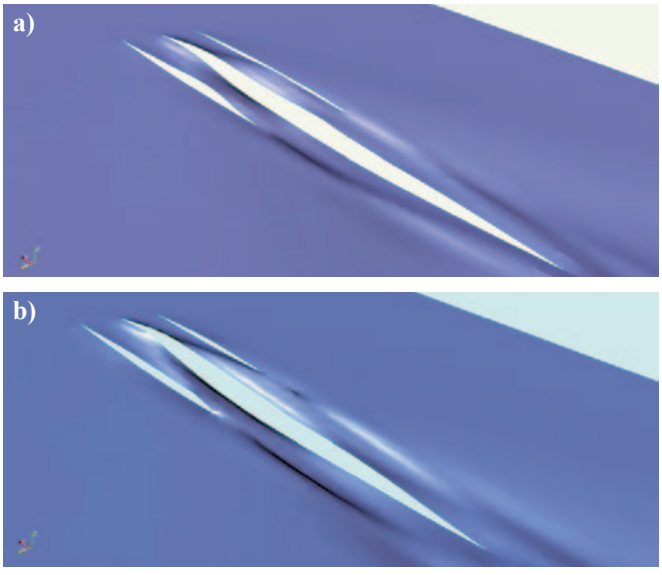

Fig. 11. *Free surface for configuration B.*
a) *at speed 4 m/s,* ***b)*** *at speed 5.5 m/s*

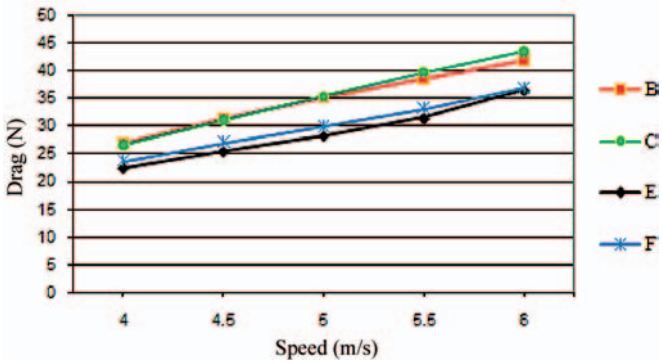

Fig. 12. Pressure drag for various configurations

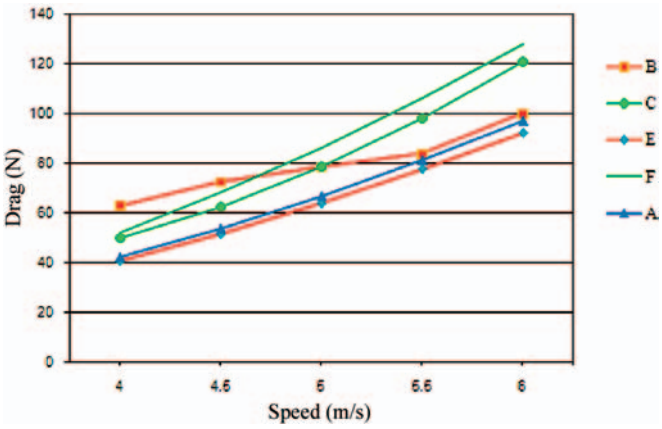

Fig. 13. Viscous drag for various configurations

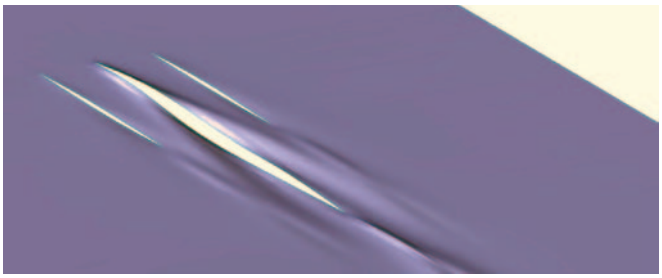

Fig. 14. Free surface for configuration E at speed 4 m/s

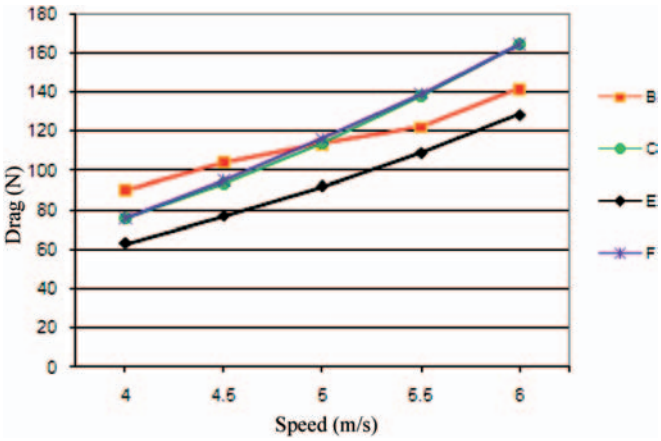

Fig. 15. Total drag for various configurations

Trimaran Maneuvering

For study of outriggers position on trimaran maneuvering, the effects of three longitudinal positions of outriggers are investigated. Since motions in maneuvering are not symmetric, it is not possible to use half domain for simulating, so in maneuvering simulation used wigley trimaran that is smaller than that used for resistance study to reduce the calculation. Table 3 and Table 4 present the characteristics and configurations of this trimaran. Applying forces and moments of maneuvering is performed by rotation of thrusters. So there is no rudder here and whole of propulsion system assumed to be rotated. Angle of rotation which applied on the trimaran's propulsion systems is 30 degrees. It should be noted that propulsion system assemble on the main hull and turning starts just after 10 seconds from the beginning of simulation. This permits the ship to reach a nearly steady forward motion due to thrusters' force. At first, various trimaran configurations are simulated at 4 m/s speed and required force to reach this speed is calculated which is shown in Table 5. It is clear that for each configuration the thruster force is equal to its corresponding total resistance forces.

Table 3. *Trimaran characteristics*

	Main Hull	Side Hull
Length L(m)	2.4	1.2
Breadth B(m)	0.24	0.12
Draft T(m)	0.15	0.075
Displacement (kg)	40.0	5.0
Wetted surface (m^2)	0.88	0.44

Table 4. *Trimaran configurations*

d/Lm	0	0.25	0.5
0.2	A	B	C

Table 5. *Total drag at 4 m/s speed for different configuration*

Configuration	A	B	C
Total drag (N)	43.92	55.00	48.24

Fig. 16 shows the time history of ship speed for different configurations. It can be seen that for A configuration decreasing speed at turning is more than other configurations. Path of ship's center of gravity is shown in Fig. 17. In the turning circle, the diameter of rotation circle for A configuration is most magnitude and for B and C configuration is close together. In Fig. 18 trim angle of the vessel are shown. It is obvious that when the side bodies stem are aligned with main hull stem, the vessel trim is more than B and C configuration and when the three bodies stern of vessel are aligned (C configuration), trimaran has least trim angle. Therefore when the outriggers are in front of vessel (A configuration), it leads to a large trim angle which causes some section of side hulls come out of water and therefore stability decreases. In Fig. 19, heel angle of various trimaran configurations is plotted. It can be seen that A configuration has least heel angle and its magnitude is near 1.5 degree, but oscillation magnitude is more than other configurations. Drift angle of three different configurations is also plotted in Fig. 20. It is clear that trimaran with A configuration has not stable drift angle. Fig. 21 shows Time history of yaw speed. It can be seen that A configuration has lowest yaw speed. Least yaw speed and unstable drift angle for A configuration can be reason of largest diameter of turning circle relate to other configurations. Figs 22~24 includes few snapshots of trimaran and free surface around it during turning maneuver. The unsymmetrical waves generated during turning can be seen in this figure.

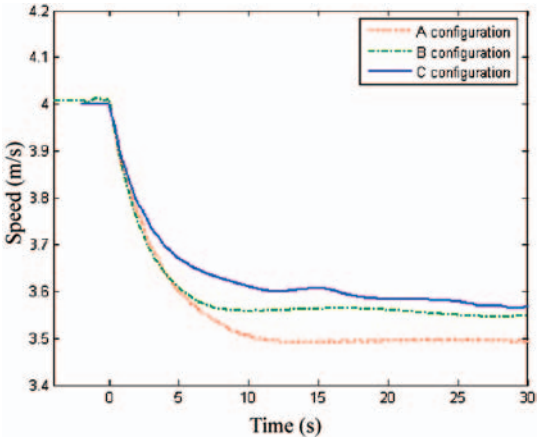

Fig. 16. *Speed time history for different configurations*

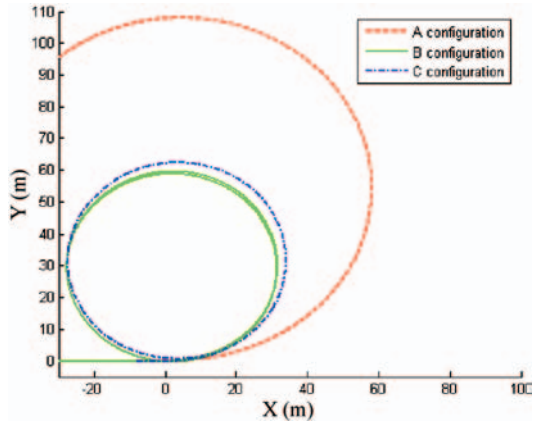

Fig. 17. *Ship mass center path*

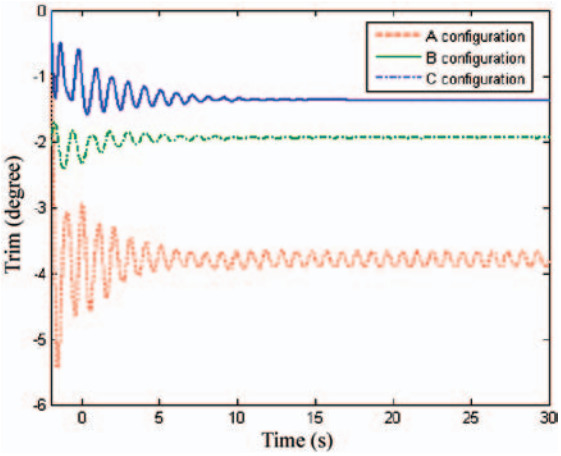

Fig. 18. *Trim angle time history for different configuration*

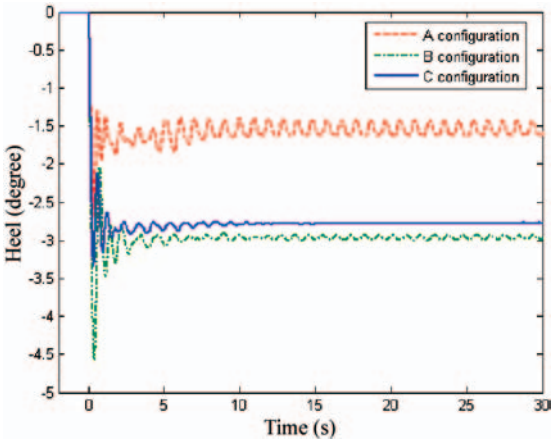

Fig. 19. *Heel angle time history for different configurations*

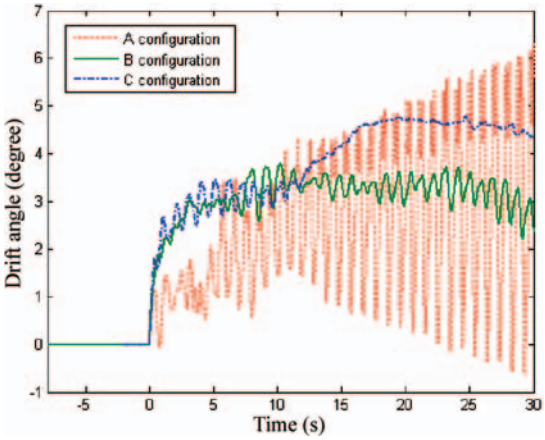

Fig. 20. Drift angle time history for different configuration

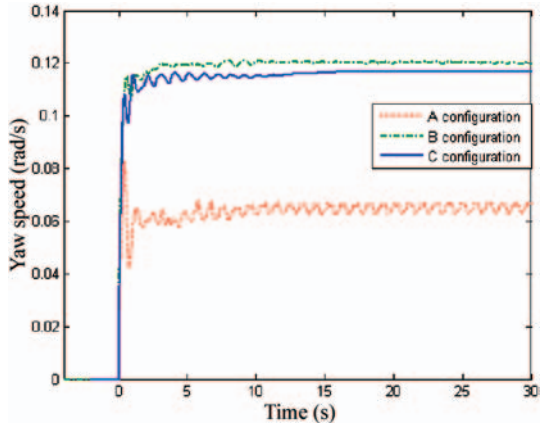

Fig. 21. Yaw speed time history for different configuration

Fig. 22. Free surface for A configuration

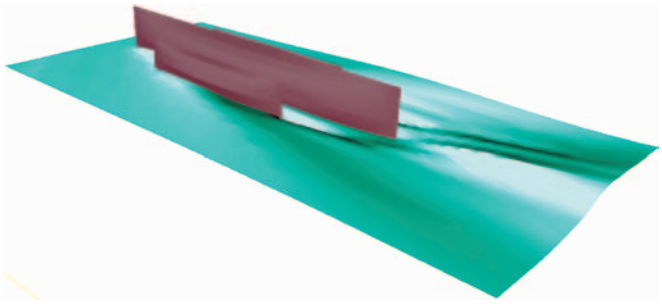

Fig. 23. Free surface for B configuration

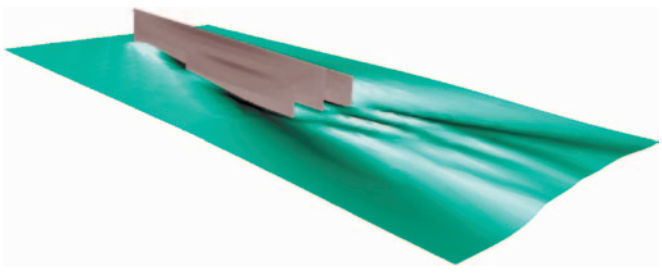

Fig. 24. Free surface for C configuration

CONCLUSION

- In this paper, the effects of outriggers location on trimaran hydrodynamic resistance and maneuverability are studied. Vessel body form is considered as standard wigley series and it is analyzed by numerical simulation scheme. In order to generalize the results, simulations for wide speed range are necessary, but based on the simulations performed the following conclusions can be drawn.

- For trimaran configuration when the three bow hulls are aligned, as the speed increases, the rate of total drag growth will decrease, because the length of interaction between the waves created by the main hull with outriggers decreases. Resistance decreases with increasing transverse distance where three hulls bow are aligned, but increasing transverse distance does not affect where three bodies stern are aligned.

- Finally, it should be taken into account that hydrodynamic resistance is an important factor for trimaran design, but factors such as maneuverability and seakeeping are also considerable. Maneuvering of a trimaran vessel has been also investigated in present paper taking into account 6-DoF rigid body motion. Numerical results show that outriggers position has great effect on trimaran maneuverability. Based on these results, it can be seen that when the bow of three bodies are aligned, the maneuvering quality is not good, because in this case, vessel trim causes outriggers to come out from water. Therefore motion stability decreases. Other configurations have almost the same turning circles diameter. But from resistance point of view, when the stern of three hulls are aligned, less thrust force is necessary, so it is more effective than other configurations.

BIBLIOGRAPHY

1. V. Dubrovsky & A. Lyakhovitsky, *Mullty Hull Ships*, Backbone Publishing,USA, (2001)
2. N. Degiuli, A. Werner, I. Zotti, *an experimental investigation into the resistance components of Trimaran configurations*, FAST (2005)
3. K. Kang , C. Lee , D. Kim , *Hull form development and powering performance characteristics for a 2500ton class Trimaran*, Practical Design of ships and Other Floating Structures, (2001)
4. E. Jahanbakhsh, R. Panahi and M.S. Seif, *Numerical Simulation of Three-Dimensional Interfacial Flows*, International Journal of Numerical Methods for Heat & Fluid Flow, Vol. 17, Issue 4, (2007)
5. H. Miyata, T. Sato and N. Babo, *Difference solution of a viscous flow with free-surface wave about an advancing ship*, J. Comput. Phys., Vol.72, p.393-421, (1987)
6. C. Hochbaum, *A finite volume method for turbulent ship flows*, Ship Technology Research Schiffstechnik, Hamburg, Germany, (1994)
7. B. Alessandrini and G. Delhommeau, *Simulation of three-dimensional unsteady viscous free surface flow around a ship model*, Int. J. of Numerical Math. Fluids, Vol.19, p.321-342, (1994)
8. T. Kinoshita, H. Kagemoto and M. Fujino, *A CFD application to wave-induced floating-body dynamics*, 7th Int. Conference on Numerical Ship Hydrodynamics, Nantes, France, (1999)
9. R. Miyake, T. Kinoshita and H. Kagemoto, *Ship Motions and loads in large waves*, 23rd ONR Symp. On Naval Hydrodynamics, Val de Reuil, France, (2000)
10. R. Azcueta, *Computation of turbulent free surface flow around ships and floating bodies*, PhD Thesis, Teschnichen Universitat Hamburg-Harburg, (2001)

11. M. Vogt and C. Hochbaum, *Numerical simulation of ship motions in head waves with a RANSE method*, HSVA Report 1649, Hamburg, Germany, (2002)
12. Y. Xing-Kaeding, *Unified approach to ship seakeeping and maneuvering by a RANSE method*, PhD Thesis, Teschnichen Universitat Hamburg-Harburg, (2004)
13. E. Jahanbakhsh, R. Panahi and M.S. Seif, *Ship dynamic simulation, based on a three-dimensional viscous free surface flow solver*, 9th Numerical Towing Tank Symposium (NuTTs'06), Le Croisic, (2006)
14. J.C. Park, H. Miyata, *Numerical simulation of fully-nonlinear wave motions around arctic and offshore structures*, J. Society of Naval Architects Japan, 2001, Vol.189, p. 13-19
15. R. Panahi, E. Jahanbakhsh and M.S. Seif, *Development of a VoF-fractional step solver for floating body motion simulation*, Applied Ocean Research, Volume 28, Issue 3, (2006)
16. C. Bertorello, D. Bruzzone, P. Cassella and I. Zotti, *Trimaran model test results and comparison different high speed craft*, Practical Design of Ships and Floating Structures, (2001)

CONTACT WITH THE AUTHOR

M.R. Javanmardi, E. Jahanbakhsh,
M.S. Seif, H.Sayyaadi
Mechanical Engineering Department,
Sharif University of Technology
Tehran, IRAN
e-mail : seif@sharif.edu

Photo: C. Spigarski

POLISH MARITIME RESEARCH 1(55) 2008 Vol 15; pp. 19-28
DOI: 10.2478/v10012-007-0047-4

Dissipation energy in viscoelastic solids under multiaxial loads

Janusz Kolenda,
Naval Academy of Gdynia

ABSTRACT

On the basis of the three-dimensional constitutive equations for strains resulting from the Kelvin-Voigt's model and modified Hooke's law for multiaxial stress in viscoelastic solids, the formulae for the energy dissipated in a given time per unit volume have been derived. It is shown that after application or removal of triaxial static load there is no difference in the time functions governing the dissipation of strain energy of volume change and the dissipation of strain energy of distortion. Harmonic in-phase stress and harmonic out-of-phase stress as well as multiaxial periodic stress are also considered. It is demonstrated that in the process of energy dissipation due to normal and shear stress components the role of the latter is dominant.

Keywords: viscoelastic material, multiaxial stress, energy dissipation, static load, vibratory load

INTRODUCTION

Engineering materials are not perfectly elastic and their service time periods may be relatively long. Therefore, at the design stage the energy dissipated through damping mechanisms in the material and, consequently, the rise of temperature of the parts loaded by time-varying forces, as well as the conditions of heat dissipation, are frequently taken into account. However, in practice such considerations are rarely followed by the estimation of amount of the energy dissipated in such parts in a given time. This situation may be avoided if an adequate damping model of the material and load history are known. As an example, in the present paper the Kelvin-Voigt's model of the material is used and the dissipation energy per unit volume as well as in a given volume is calculated in selected load cases. To simplify the calculations, the modified Hooke's law for multiaxial stress in viscoelastic solids [1] and the relevant three-dimensional constitutive equations for strains [2] are applied which requires that the material is homogeneous, isotropic and loaded below the yield point.

For the sake of clarity, our presentation of the problem solutions will start with some important relationships given in the literature.

ENERGY DISSIPATED AFTER REMOVAL AND APPLICATION OF MULTIAXIAL STATIC LOAD

If a viscoelastic rod is loaded for a long time by an axial force P = const, in its cross-section a uniformly distributed normal stress

$$\sigma_{x0} = \frac{P}{A} \tag{1}$$

is present, which corresponds to the normal strain:

$$\varepsilon_{x0} = \frac{\sigma_{x_0}}{E} \tag{2}$$

where:
A – area of the cross-section
E – Young modulus.

Removal of the load at the time t = 0 results in a creep recovery [2-4]:

$$\varepsilon_x(t) = \varepsilon_{x0} e^{-\frac{E}{\eta}t} \tag{3}$$

where:
η – coefficient of viscous damping of normal strain.

According to the Kelvin-Voigt's model of a viscoelastic material [3-5], the internal restoring force, F, and the counteracting resistance force, R, can be expressed by:

$$\begin{aligned} F &= -AE\varepsilon_x \\ R &= A\eta\dot{\varepsilon}_x \end{aligned} \tag{4}$$

where the dot denotes differentiation with respect to t. Consequently, the dissipation energy can be calculated as the work, W, of the restoring force. If at the time t the rod length is l + Δl, where l is its length prior to load, then:

$$\varepsilon_x = \frac{\Delta l}{l} \tag{5}$$

and the elementary work of the restoring force is equal to

$$dW = Fd(\Delta l) = Fld\varepsilon_x = Fl\dot{\varepsilon}_x dt = -AEl\varepsilon_x\dot{\varepsilon}_x dt \quad (6)$$

Denoting φ the dissipation energy per unit volume, one obtains:

$$d\phi = \frac{dW}{Al} = -E\varepsilon_x\dot{\varepsilon}_x dt \quad (7)$$

so that

$$\phi(t) = -E\int_0^t \varepsilon_x\dot{\varepsilon}_x dt = \frac{E^2}{\eta}\varepsilon_{x_0}^2\int_0^t e^{-\frac{2E}{\eta}t} dt \quad (8)$$

Hence:

$$\phi(t) = \frac{1}{2}E\varepsilon_{x_0}^2\left(1-e^{-\frac{2E}{\eta}t}\right) = \frac{1}{2}\sigma_{x0}\varepsilon_{x0}\left(1-e^{-\frac{2E}{\eta}t}\right) \quad (9)$$

and

$$\lim_{t\to\infty}\phi(t) = \frac{1}{2}\sigma_{x0}\varepsilon_{x0} \quad (10)$$

Now let us consider what happens to a cubic element with fixed bottom side (Fig. 1) and subjected for a long time to the shear stress τ_{zy0} on its upper side, if at t = 0 the load is removed.

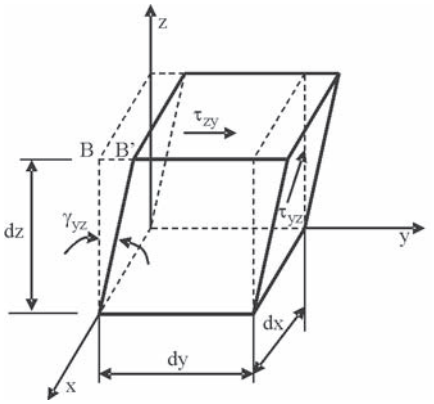

Fig. 1. *Shear strain γ_{yz} of infinitesimal cubic element*

The restoring force and its elementary work on the line segment:

$$\beta\beta' = \gamma_{yz}\,dz \quad (11)$$

are as follows:

$$F = -G\gamma_{yz}\,dxdy$$
$$dW = Fd\gamma_{yz}\,dz = F\dot{\gamma}_{yz}\,dzdt = -G\gamma_{yz}\dot{\gamma}_{yz}\,dxdydzdt \quad (12)$$

where: γ_{yz} is the shear strain and

$$G = \frac{E}{2(1+\upsilon)} \quad (13)$$

is the shear modulus. Here υ is the Poisson's ratio. Thus:

$$d\phi = \frac{dW}{dxdydz} = -G\gamma_{yz}\dot{\gamma}_{yz}dt \quad (14)$$

Knowing that removal of the shear load at t = 0 is followed by the creep recovery [2]:

$$\gamma_{yz}(t) = \gamma_{yz0}e^{-\frac{E}{\eta}t} = \gamma_{yz0}e^{-\frac{G}{\lambda}t} \quad (15)$$

where: $\gamma_{yz0} = \tau_{yz0}/G$ is the shear strain corresponding to the shear stress $\tau_{zy0} = \tau_{yz0}$, the dissipation energy per unit volume can be in this case expressed as:

$$\phi(t) = -G\int_0^t \gamma_{yz}\dot{\gamma}_{yz}dt = \frac{G^2}{\lambda}\gamma_{yz0}^2\int_0^t e^{-\frac{2G}{\lambda}t}dt \quad (16)$$

In Eqs (15) and (16), λ is the coefficient of viscous damping of shear strain given by [2]:

$$\lambda = \frac{\eta}{2(1+\upsilon)} \quad (17)$$

Hence:

$$\phi(t) = \frac{1}{2}G\gamma_{yz0}^2\left(1-e^{-\frac{2G}{\lambda}t}\right) = \frac{1}{2}\tau_{yz0}\gamma_{yz0}\left(1-e^{-\frac{2E}{\eta}t}\right) \quad (18)$$

and

$$\lim_{t\to\infty}\phi(t) = \frac{1}{2}\tau_{yz0}\gamma_{yz0} \quad (19)$$

It is noteworthy that the time function of energy dissipation by normal and shear stress components is the same.

Similar equations can be obtained for the dissipation energy in viscoelastic solids caused by the stress components σ_{y0}, σ_{z0}, τ_{xy0}, and τ_{zx0} if at t = 0 a three-dimensional load has been removed. After summation of the resulting dissipation energies one gets:

$$\phi(t) = \psi_0\left(1-e^{-\frac{2E}{\eta}t}\right) \quad (20)$$

where:

$$\psi_0 = \frac{1}{2}\left(\sigma_{x0}\varepsilon_{x0}+\sigma_{y0}\varepsilon_{y0}+\sigma_{z0}\varepsilon_{z0}+\right.$$
$$\left.+\tau_{xy0}\gamma_{xy0}+\tau_{yz0}\gamma_{yz0}+\tau_{zx0}\gamma_{zx0}\right) \quad (21)$$

is the elastic strain energy per unit volume before removal of the load, and [6, 7]:

$$\varepsilon_{x0} = \frac{1}{E}\left[\sigma_{x0}-\upsilon(\sigma_{y0}+\sigma_{z0})\right]$$
$$\varepsilon_{y0} = \frac{1}{E}\left[\sigma_{y0}-\upsilon(\sigma_{x0}+\sigma_{z0})\right]$$
$$\varepsilon_{z0} = \frac{1}{E}\left[\sigma_{z0}-\upsilon(\sigma_{x0}+\sigma_{y0})\right] \quad (22)$$
$$\gamma_{k0} = \frac{1}{G}\tau_{k0}\,;\ k = xy, yz, zx$$

are the strain components at t < 0.

With Eqs (22), ψ_0 can be expressed in terms of the stress components. It can be also divided into the strain energy of volume change, ψ_{v0}, and strain energy of distortion, ψ_{d0}, that is:

$$\psi_0 = \psi_{v0} + \psi_{d0} \quad (23)$$

where [6]:

$$\psi_{v0} = \frac{1-2\upsilon}{6E}(\sigma_{x0}+\sigma_{y0}+\sigma_{z0})^2$$
$$\psi_{d0} = \frac{1+\upsilon}{6E}\left[(\sigma_{x0}-\sigma_{y0})^2+(\sigma_{y0}-\sigma_{z0})^2+\right. \quad (24)$$
$$\left.+(\sigma_{z0}-\sigma_{x0})^2+6(\tau_{xy0}^2+\tau_{yz0}^2+\tau_{zx0}^2)\right]$$

Eqs (20) and (23) lead to:

$$\phi(t) = (\psi_{v0} + \psi_{d0})\left(1 - e^{-\frac{2E}{\eta}t}\right) \tag{25}$$

Hence it is clear that the time functions governing the dissipation of strain energy of volume change and the dissipation of strain energy of distortion are identical.

The problem of energy dissipation in viscoelastic materials after application of static loads can be solved analogously. For example, if an axial load is applied at t = 0 to a viscoelastic rod and the resulting stress σ_{x0} is maintained constant, then a time-dependent strain response will occur [2-4]

$$\varepsilon_x(t) = \varepsilon_{x0}\left(1 - e^{-\frac{E}{\eta}t}\right) \tag{26}$$

where: ε_{x0} is given by Eq. (2). The dissipation energy in this case can be calculated as the work of this part of the external load which is overcoming the resistance force R.

The elementary work is then:

$$dW = R\,d(\Delta l) = R\,l\,d\varepsilon_x = R\,l\,\dot{\varepsilon}_x dt = A\,l\,\eta\dot{\varepsilon}_x^2 dt \tag{27a}$$

With Eqs (26) and (27a) one obtains:

$$d\phi = \frac{dW}{Al} = \eta\dot{\varepsilon}_x^2 dt \tag{28a}$$

and

$$\phi(t) = \frac{E^2}{\eta}\varepsilon_{x0}^2\int_0^t e^{-\frac{2E}{\eta}t}\,dt \tag{29}$$

Hence the relationship for the dissipation energy per unit volume of the rod reads:

$$\phi(t) = \frac{1}{2}E\varepsilon_{x0}^2\left(1 - e^{-\frac{2E}{\eta}t}\right) = \frac{1}{2}\sigma_{x0}\varepsilon_{x0}\left(1 - e^{-\frac{2E}{\eta}t}\right) \tag{30}$$

Of course,

$$\lim_{t\to\infty}\phi(t) = \frac{1}{2}\sigma_{x0}\varepsilon_{x0} \tag{31}$$

Note that the other part of the external constant load executes the work of elastic deformation of the rod which per unit volume is finally also equal to $\frac{1}{2}\sigma_{x0}\varepsilon_{x0}$ [6]. As a stored elastic strain energy, it will be dissipated after removal of the load [see Eq. (10)].

Similar equations can be written for the energy dissipated after application of the other stress components so that in the general case of static load applied at t = 0 the summary dissipation energy per unit volume becomes again:

$$\phi(t) = \psi_0\left(1 - e^{-\frac{2E}{\eta}t}\right) \tag{32}$$

According to the Kelvin-Voigt's model,

$$E\varepsilon_x + \eta\dot{\varepsilon}_x = \sigma_x$$

so that the resistance force can be also expressed by

$$R = A\eta\dot{\varepsilon}_x = A(\sigma_x - E\varepsilon_x)$$

Consequently, Eqs (27a) and (28a) can be rewritten as

$$dW = A(\sigma_x - E\varepsilon_x)d(\Delta l) = Al(\sigma_x - E\varepsilon_x)\dot{\varepsilon}_x dt \tag{27b}$$

$$d\phi = (\sigma_x - E\varepsilon_x)\dot{\varepsilon}_x dt \tag{28b}$$

In what follows, Eq. (28b) and analogous relationships for the elementary dissipation energy due to the stress components σ_y, σ_z, τ_{xy}, τ_{yz}, and τ_{zx} will be applied.

THE CASE OF HARMONIC IN-PHASE STRESS

Suppose that a vibratory load is producing in a viscoelastic solid the stress of components:

$$\begin{aligned}\sigma_j &= \sigma_{ja}\sin\omega t \quad ; \quad j = x, y, z\\ \tau_k &= \tau_{ka}\sin\omega t \quad ; \quad k = xy, yz, zx\end{aligned} \tag{33}$$

where: σ_{ja} and τ_{ka} are the amplitudes of the stress components and ω is their circular frequency. The relevant constitutive equation for strains reads [2]:

$$\boldsymbol{\varepsilon} = \mathbf{H}\boldsymbol{\sigma}_a\sin(\omega t - \alpha)\varepsilon \tag{34}$$

where $\boldsymbol{\varepsilon}$ is the vector of strain components. $\mathbf{H}$ is the matrix of dynamical flexibility of the material at the load circular frequency ω, $\boldsymbol{\sigma}_a$ is the vector of amplitudes of the stress components and α is the phase shift between stress and strain components as follows:

$$\boldsymbol{\varepsilon} = \left[\varepsilon_x\ \varepsilon_y\ \varepsilon_z\ \gamma_{xy}\ \gamma_{yz}\ \gamma_{zx}\right]^T$$

$$\boldsymbol{\sigma}_a = \left[\sigma_{xa}\ \sigma_{ya}\ \sigma_{za}\ \tau_{xya}\ \tau_{yza}\ \tau_{zxa}\right]^T$$

$$\boldsymbol{H} = \frac{1}{\sqrt{E^2 + \eta^2\omega^2}}\begin{bmatrix} 1 & -\upsilon & -\upsilon & 0 & 0 & 0\\ -\upsilon & 1 & -\upsilon & 0 & 0 & 0\\ -\upsilon & -\upsilon & 1 & 0 & 0 & 0\\ 0 & 0 & 0 & 2(1+\upsilon) & 0 & 0\\ 0 & 0 & 0 & 0 & 2(1+\upsilon) & 0\\ 0 & 0 & 0 & 0 & 0 & 2(1+\upsilon)\end{bmatrix} \tag{35}$$

$$\alpha = \operatorname{arctg}\frac{\eta\omega}{E}$$

Starting with Eqs (28b), (34) and (35), for a viscoelastic cubic element under uniaxial stress:

$$\sigma_z = \sigma_{za} \sin\omega t \tag{36}$$

we write:

$$d\phi = (\sigma_z - E\varepsilon_z)\dot{\varepsilon}_z dt$$
$$\varepsilon_z = \frac{1}{\sqrt{E^2 + \eta^2\omega^2}} \sigma_{za} \sin(\omega t - \alpha) \tag{37}$$

Thus, during the stress period $T = 2\pi/\omega$ the amount of dissipated energy per unit volume, $\varphi(T)$, becomes:

$$\phi(T) = \int_0^T (\sigma_z - E\varepsilon_z)\dot{\varepsilon}_z dt \tag{38}$$

Obviously,

$$\int_0^T \varepsilon_z \dot{\varepsilon}_z dt = 0 \tag{39}$$

which leads to:

$$\phi(T) = \int_0^T \sigma_z \dot{\varepsilon}_z dt = \frac{1}{2} \frac{\omega T \sin\alpha}{\sqrt{E^2 + \eta^2\omega^2}} \sigma_{za}^2 \tag{40}$$

In the case of harmonic shear stress:

$$\tau_{yz} = \tau_{yza} \sin\omega t \tag{41}$$

in place of Eq. (28b) we have:

$$d\phi = (\tau_{yz} - G\gamma_{yz})\dot{\gamma}_{yz} dt \tag{42}$$

Eqs (34) and (35) yield:

$$\gamma_{yz} = \frac{2(1+\upsilon)}{\sqrt{E^2 + \eta^2\omega^2}} \tau_{yza} \sin(\omega t - \alpha) \tag{43}$$

Accordingly,

$$\phi(T) = \int_0^T \tau_{yz} \dot{\gamma}_{yz} dt = \frac{(1+\upsilon)\omega T \sin\alpha}{\sqrt{E^2 + \eta^2\omega^2}} \tau_{yza}^2 \tag{44}$$

If the viscoelastic element is simultaneously subjected to the stress components (36) and (41), then:

$$\phi(T) = \frac{1}{2} \frac{\omega T \sin\alpha}{\sqrt{E^2 + \eta^2\omega^2}} \left[\sigma_{za}^2 + 2(1+\upsilon)\tau_{yza}^2\right] \tag{45}$$

Summarizing, the following formula for the dissipation energy per unit volume during the period T can be written:

$$\phi(T) = \int_0^T (\sigma_x \dot{\varepsilon}_x + \sigma_y \dot{\varepsilon}_y + \sigma_z \dot{\varepsilon}_z + \tau_{xy} \dot{\gamma}_{xy} + \tau_{yz} \dot{\gamma}_{yz} + \tau_{zx} \dot{\gamma}_{zx}) dt \tag{46}$$

With Eqs (33) through (35), one obtains from Eq. (46).

$$\phi(T) = \frac{1}{2} \frac{\omega T \sin\alpha}{\sqrt{E^2 + \eta^2\omega^2}} \left[\sigma_{xa}^2 + \sigma_{ya}^2 + \sigma_{za}^2 - 2\upsilon(\sigma_{xa}\sigma_{ya} + \sigma_{ya}\sigma_{za} + \sigma_{za}\sigma_{xa}) + \right.$$
$$\left. + 2(1+\upsilon)(\tau_{xya}^2 + \tau_{yza}^2 + \tau_{zxa}^2)\right] \tag{47}$$

Eqs (45) and (47) show that the shares of normal and shear stress components in the summary dissipation energy may be different. In order to prove the role of individual stress components in energy dissipation, let us assume that:

$$\sigma_{xa} = \sigma_{ya} = \sigma_{za} = \sigma \;\; ; \;\; \tau_{xya} = \tau_{yza} = \tau_{zxa} = \tau \;\; ; \;\; \upsilon = 0.3 \tag{i}$$

Eqs (45) and (47) become then:

$$\phi(T) = \frac{1}{2} \frac{\omega T \sin\alpha}{\sqrt{E^2 + \eta^2\omega^2}} (\sigma^2 + 2.6\tau^2) \tag{ii}$$

$$\phi(T)=\frac{1}{2}\frac{\omega T\sin\alpha}{\sqrt{E^2+\eta^2\omega^2}}\left(1.2\sigma^2+7.8\tau^2\right) \tag{iii}$$

These results suggest to check the following ratios, ρ_{sn} and ρ_{dv}, of dissipated energies per unit volume:

$$\rho_{sn}=\frac{\phi_s(T)}{\phi_n(T)}\ ,\quad \rho_{dv}=\frac{\phi_d(T)}{\phi_v(T)} \tag{48}$$

where:
$\varphi_s(T)$ – dissipation energy associated with shear stress components
$\varphi_n(T)$ – dissipation energy associated with normal stress components
$\varphi_d(T)$ – dissipation energy associated with distortions
$\varphi_v(T)$ – dissipation energy associated with volume changes.

At the stress (33), these quantities are given by:

$$\begin{aligned}
\phi_s(T)&=\frac{(1+\upsilon)\omega T\sin\alpha}{\sqrt{E^2+\eta^2\omega^2}}\left(\tau_{xya}^2+\tau_{yza}^2+\tau_{zxa}^2\right)\\
\phi_n(T)&=\frac{\omega T\sin\alpha}{2\sqrt{E^2+\eta^2\omega^2}}\left[\sigma_{xa}^2+\sigma_{ya}^2+\sigma_{za}^2-2\upsilon\left(\sigma_{xa}\sigma_{ya}+\sigma_{ya}\sigma_{za}+\sigma_{za}\sigma_{xa}\right)\right]\\
\phi_d(T)&=\frac{(1+\upsilon)\omega T\sin\alpha}{6\sqrt{E^2+\eta^2\omega^2}}\left[\left(\sigma_{xa}-\sigma_{ya}\right)^2+\left(\sigma_{ya}-\sigma_{za}\right)^2+\left(\sigma_{za}-\sigma_{xa}\right)^2+6\left(\tau_{xya}^2+\tau_{yza}^2+\tau_{zxa}^2\right)\right]\\
\phi_v(T)&=\frac{(1-2\upsilon)\omega T\sin\alpha}{6\sqrt{E^2+\eta^2\omega^2}}\left(\sigma_{xa}+\sigma_{ya}+\sigma_{za}\right)^2
\end{aligned} \tag{49}$$

The values of ρ_{sn} and ρ_{dv} vary from:

$$\rho_{sn}=2.6\left(\frac{\tau}{\sigma}\right)^2\ ,\quad \rho_{dv}=6.5+19.5\left(\frac{\tau}{\sigma}\right)^2 \tag{iv}$$

in the case (ii), to:

$$\rho_{sn}=\rho_{dv}=6.5\left(\frac{\tau}{\sigma}\right)^2 \tag{v}$$

in the case (i). From comparison of Eqs (iv) and (v) if follows that the role of shear stress components and distortions in energy dissipation is dominant.

THE CASE OF HARMONIC OUT-OF-PHASE STRESS

Let the stress components in a viscoelastic solid under triaxial harmonic load be:

$$\sigma_j=\sigma_{ja}\sin\left(\omega t+\varphi_j\right)\ ;\ \tau_k=\tau_{ka}\sin\left(\omega t+\varphi_k\right) \tag{50}$$

where: φ_j(j = x, y, z) and φ_k(k = xy, yz, zx) are the phase angles. Introducing the vector of complex amplitudes of the stress components:

$$\overline{\boldsymbol{\sigma}}_a=\left[\overline{\sigma}_{xa}\,\overline{\sigma}_{ya}\,\overline{\sigma}_{za}\,\overline{\tau}_{xya}\,\overline{\tau}_{yza}\,\overline{\tau}_{zxa}\right]^T \tag{51}$$

the vector of the strain components can be written as [2]:

$$\boldsymbol{\varepsilon}=\mathbf{H}\,\mathbf{Im}\left[\overline{\boldsymbol{\sigma}}_a e^{i(\omega t-\alpha)}\right] \tag{52}$$

Here **i** is the imaginary unity, Im denotes the imaginary part, and

$$\begin{aligned}
&\overline{\sigma}_{ja}=\sigma_{ja}e^{i\varphi_j}\ ;\quad \overline{\tau}_{ka}=\tau_{ka}e^{i\varphi_k}\ ;\quad \alpha=\operatorname{arctg}\frac{\eta\omega}{E}\\
&\boldsymbol{\varepsilon}=\left[\varepsilon_x\,\varepsilon_y\,\varepsilon_z\,\gamma_{xy}\,\gamma_{yz}\,\gamma_{zx}\right]^T
\end{aligned} \tag{53}$$

If time-varying stress components act on a viscoelastic solid, the knowledge of resulting strain components enables us to evaluate their combined effect in terms of dissipation energy by means of Eq. (46). In accordance with Eqs (51) through (53), the constitutive equations for strains under the stress state (50) read:

$$\varepsilon_x = \frac{1}{\sqrt{E^2+\eta^2\omega^2}}\left[\sigma_{xa}\sin(\omega t+\varphi_x-\alpha)-\upsilon\sigma_{ya}\sin(\omega t+\varphi_y-\alpha)-\upsilon\sigma_{za}\sin(\omega t+\varphi_z-\alpha)\right]$$
$$\varepsilon_y = \frac{1}{\sqrt{E^2+\eta^2\omega^2}}\left[\sigma_{ya}\sin(\omega t+\varphi_y-\alpha)-\upsilon\sigma_{xa}\sin(\omega t+\varphi_x-\alpha)-\upsilon\sigma_{za}\sin(\omega t+\varphi_z-\alpha)\right] \quad (54)$$
$$\varepsilon_z = \frac{1}{\sqrt{E^2+\eta^2\omega^2}}\left[\sigma_{za}\sin(\omega t+\varphi_z-\alpha)-\upsilon\sigma_{xa}\sin(\omega t+\varphi_x-\alpha)-\upsilon\sigma_{ya}\sin(\omega t+\varphi_y-\alpha)\right]$$

and

$$\gamma_k = \frac{2(1+\upsilon)}{\sqrt{E^2+\eta^2\omega^2}}\tau_{ka}\sin(\omega t+\varphi_k-\alpha) \quad (55)$$

In the present case, Eq. (46) becomes:

$$\begin{aligned}\phi(T) = \frac{\omega}{\sqrt{E^2+\eta^2\omega^2}}\int_0^T\{&\sigma_{xa}\sin(\omega t+\varphi_x)[\sigma_{xa}\cos(\omega t+\varphi_x-\alpha)-\upsilon\sigma_{ya}\cos(\omega t+\varphi_y-\alpha)+\\ &-\upsilon\sigma_{za}\cos(\omega t+\varphi_z-\alpha)]+\sigma_{ya}\sin(\omega t+\varphi_y)[\sigma_{ya}\cos(\omega t+\varphi_y-\alpha)-\upsilon\sigma_{xa}\cos(\omega t+\varphi_x-\alpha)+\\ &-\upsilon\sigma_{za}\cos(\omega t+\varphi_z-\alpha)]+\sigma_{za}\sin(\omega t+\varphi_z)[\sigma_{za}\cos(\omega t+\varphi_z-\alpha)-\upsilon\sigma_{xa}\cos(\omega t+\varphi_x-\alpha)+\\ &-\upsilon\sigma_{ya}\cos(\omega t+\varphi_y-\alpha)]+2(1+\upsilon)\sum_k\tau_{ka}^2\sin(\omega t+\varphi_k)\cos(\omega t+\varphi_k-\alpha)\}dt\end{aligned} \quad (56)$$

Hence:

$$\begin{aligned}\phi(T) = \frac{1}{2}\frac{\omega T\sin\alpha}{\sqrt{E^2+\eta^2\omega^2}}\{&\sigma_{xa}^2+\sigma_{ya}^2+\sigma_{za}^2-2\upsilon[\sigma_{xa}\sigma_{ya}\cos(\varphi_x-\varphi_y)+\\ &+\sigma_{ya}\sigma_{za}\cos(\varphi_y-\varphi_z)+\sigma_{za}\sigma_{xa}\cos(\varphi_z-\varphi_x)]+2(1+\upsilon)(\tau_{xya}^2+\tau_{yza}^2+\tau_{zxa}^2)\}\end{aligned} \quad (57)$$

It is evident that the phase angles of shear stress components do not affect the process of energy dissipation in viscoelastic solids under multiaxial harmonic loads whereas the phase shifts between normal stress components increase the amount of aforementioned energy in comparison with that under in-phase stress. Of course, the amount of dissipated energy depends also on the amplitudes of the stress components and their number, on the load duration and frequency as well as on two parameters of the Kelvin-Voigt's model and Poisson's ratio. The Reader interested in application of three-parameter models of viscoelastic materials is referred, e.g., to [4,8].

DISSIPATION ENERGY IN VISCOELASTIC SOLIDS UNDER MULTIAXIAL PERIODIC LOADS

In engineering calculations referring to stationary operating conditions, the history of vibratory loads is frequently confined to periodic excitations. In such cases the stress state at a given point can be described by Fourier series representing the normal and shear stress components:

$$\begin{aligned}\sigma_j &= \sigma_{j0}+\sum_n\sigma_{jn}\sin(n\omega t+\varphi_{jn}) \quad ; \quad j=x,y,z\\ \tau_k &= \tau_{k0}+\sum_n\tau_{kn}\sin(n\omega t+\varphi_{kn}) \quad ; \quad k=xy,yz,zx\end{aligned} \quad (58)$$

where:
σ_{j0}, τ_{k0} – mean values of the stress components
σ_{jn}, τ_{kn} – amplitudes of n-th terms in Fourier expansion of the stress components
φ_{jn}, φ_{kn} – phase angles of n-th terms in Fourier expansion of the stress components
ω – fundamental circular frequency.

The associated constitutive equation for strains reads [2]:

$$\boldsymbol{\varepsilon} = \boldsymbol{\varepsilon}_0+\sum_n\mathbf{H}_n\,\mathrm{Im}\left[\overline{\boldsymbol{\sigma}}_n e^{i(n\omega t-\alpha_n)}\right] \quad (59)$$

where $\boldsymbol{\varepsilon}$ is given in Eqs (35), $\mathbf{H}_n=\mathbf{H}(n\omega)$ is obtained from the matrix $\mathbf{H}$ defined in Eqs (35) by inserting $n\omega$ in place of ω, and

$$\overline{\boldsymbol{\sigma}}_n = \left[\overline{\sigma}_{xn}\overline{\sigma}_{yn}\overline{\sigma}_{zn}\overline{\tau}_{xyn}\overline{\tau}_{yzn}\overline{\tau}_{zxn}\right]^T;\ \overline{\sigma}_{jn}=\sigma_{jn}e^{i\varphi_{jn}};\ \overline{\tau}_{kn}=\tau_{kn}e^{i\varphi_{kn}};\ \alpha_n=\mathrm{arctg}\frac{\eta n\omega}{E};\ \boldsymbol{\varepsilon}_0=\left[\varepsilon_{x0}\varepsilon_{y0}\varepsilon_{z0}\gamma_{xy0}\gamma_{yz0}\gamma_{zx0}\right]^T \quad (60)$$

The elements of the vector $\boldsymbol{\varepsilon}_0$ are given in Eqs (22). Eq. (46) makes it possible to determine the energy dissipation due to the stress components (58) or to any of them. For instance, if a viscoelastic rod is acted upon by the stress:

$$\sigma_x = \sigma_{x0} + \sum_n \sigma_{xn} \sin\left(n\omega t + \varphi_{xn}\right) \tag{61}$$

from Eqs (59) and (60) one gets:

$$\varepsilon_x = \varepsilon_{x0} + \sum_n \frac{\sigma_{xn}}{\sqrt{E^2 + \left(\eta n\omega^2\right)}} \sin\left(n\omega t + \varphi_{xn} - \alpha_n\right) \tag{62}$$

so that:

$$\dot{\varepsilon}_x = \sum_n \frac{n\omega\sigma_{xn}}{\sqrt{E^2 + \left(\eta n\omega\right)^2}} \cos\left(n\omega t + \varphi_{xn} - \alpha_n\right) \tag{63}$$

For the time period:

$$T = \frac{2\pi}{\omega} \tag{64}$$

the dissipation energy per unit volume can be calculated as:

$$\phi(T) = \int_0^T \sigma_x \dot{\varepsilon}_x dt = \int_0^T \left[\sigma_{x0} + \sum_n \sigma_{xn} \sin\left(n\omega t + \varphi_{xn}\right)\right]\left[\sum_n \frac{n\omega\sigma_{xn}}{\sqrt{E^2 + \left(\eta n\omega\right)^2}} \cos\left(n\omega t + \varphi_{xn} - \alpha_n\right)\right] dt \tag{65}$$

Hence:

$$\phi(T) = \frac{1}{2}\omega T \sum_n \frac{n \sin\alpha_n}{\sqrt{E^2 + \left(\eta n\omega\right)^2}} \sigma_{xn}^2 \tag{66}$$

Similarly, if a viscoelastic solid is subjected to a periodic shear stress:

$$\tau_{xy} = \tau_{xy0} + \sum_n \tau_{xyn} \sin\left(n\omega t + \varphi_{xyn}\right) \tag{67}$$

in conformity with Eqs (59) and (60) the strain response is:

$$\gamma_{xy} = \gamma_{xy0} + 2(1+\upsilon)\sum_n \frac{\tau_{xyn}}{\sqrt{E^2 + \left(\eta n\omega\right)^2}} \sin\left(n\omega t + \varphi_{xyn} - \alpha_n\right) \tag{68}$$

Eqs (44), (67) and (68) imply that:

$$\phi(T) = \int_0^T \tau_{xy}\dot{\gamma}_{xy} dt = \tag{69}$$
$$= \int_0^T \left[\tau_{xy0} + \sum_n \tau_{xyn} \sin\left(n\omega t + \varphi_{xyn}\right)\right]\left[2(1+\upsilon)\sum_n \frac{n\omega\,\tau_{xyn}}{\sqrt{E^2 + \left(\eta n\,\omega\right)^2}} \cos\left(n\omega t + \varphi_{xyn} - \alpha_n\right)\right] dt$$

Eq. (69) yields:

$$\phi(T) = (1+\upsilon)\omega T \sum_n \frac{n \sin\alpha_n}{\sqrt{E^2 + \left(\eta n\omega\right)^2}} \tau_{xyn}^2 \tag{70}$$

We now turn to the general state of periodic stress (58). On the basis of Eqs (59) and (60), the following time derivatives of the strain components are obtained:

$$\begin{aligned}
\dot{\varepsilon}_x &= \sum_n \frac{n\omega}{\sqrt{E^2 + \left(\eta n\omega\right)^2}}\left[\sigma_{xn} \cos\left(n\omega t + \varphi_{xn} - \alpha_n\right) - \upsilon\sigma_{yn} \cos\left(n\omega t + \varphi_{yn} - \alpha_n\right) - \upsilon\sigma_{zn} \cos\left(n\omega t + \varphi_{zn} - \alpha_n\right)\right] \\
\dot{\varepsilon}_y &= \sum_n \frac{n\omega}{\sqrt{E^2 + \left(\eta n\omega\right)^2}}\left[\sigma_{yn} \cos\left(n\omega t + \varphi_{yn} - \alpha_n\right) - \upsilon\sigma_{xn} \cos\left(n\omega t + \varphi_{xn} - \alpha_n\right) - \upsilon\sigma_{zn} \cos\left(n\omega t + \varphi_{zn} - \alpha_n\right)\right] \\
\dot{\varepsilon}_z &= \sum_n \frac{n\omega}{\sqrt{E^2 + \left(\eta n\omega\right)^2}}\left[\sigma_{zn} \cos\left(n\omega t + \varphi_{zn} - \alpha_n\right) - \upsilon\sigma_{xn} \cos\left(n\omega t + \varphi_{xn} - \alpha_n\right) - \upsilon\sigma_{yn} \cos\left(n\omega t + \varphi_{yn} - \alpha_n\right)\right] \\
\dot{\gamma}_k &= 2(1+\upsilon)\sum_n \frac{n\omega}{\sqrt{E^2 + \left(\eta n\,\omega\right)^2}} \tau_{kn} \cos\left(n\omega t + \varphi_{kn} - \alpha_n\right)
\end{aligned} \tag{71}$$

$$\phi(T)=\frac{1}{2}\omega T\sum_{n}\frac{n\sin\alpha_n}{\sqrt{E^2+(\eta n\omega)^2}}\{\sigma_{xn}^2+\sigma_{yn}^2+\sigma_{zn}^2-2\upsilon[\sigma_{xn}\sigma_{yn}\cos(\varphi_{xn}-\varphi_{yn})+$$
$$+\sigma_{yn}\sigma_{zn}\cos(\varphi_{yn}-\varphi_{zn})+\sigma_{zn}\sigma_{xn}\cos(\varphi_{zn}-\varphi_{xn})]+2(1+\upsilon)(\tau_{xyn}^2+\tau_{yzn}^2+\tau_{zxn}^2)\} \tag{72}$$

Eq. (72), as well as other formulae for the amount of energy dissipated in unit volume, may be directly applied to the whole volume if the stress distribution is uniform. Otherwise, in order to determine the total amount of energy dissipated in a given part of the viscoelastic solid, additional calculations are necessary. The example below was chosen not only as an illustration for this problem, but also to gain more information on the influence of shear stress and distortions on energy dissipation in viscoelastic materials.

EXAMPLE

Compare the total energy dissipated in a viscoelastic rod of constant diameter $2r_0$ and length l by its purely axial twisting with that due to its axial tension-compression. Consider the energies dissipated in the rod by its distortions and volume changes.

Solution. In twisting, the shear stress at the radius r is (Fig. 2):

$$\tau=\frac{r}{r_0}\tau_0 \tag{i_0}$$

where: τ_0 is the shear stress at the outer radius r_0 .

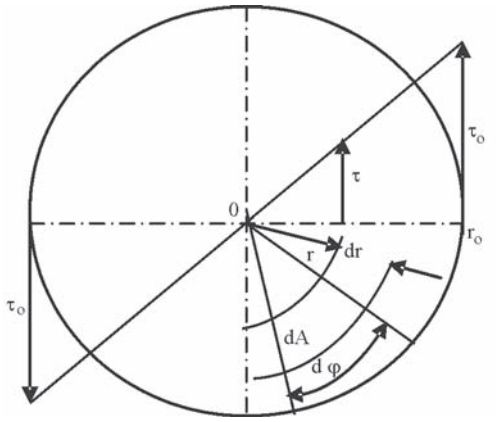

Fig. 2. *Distribution of shear stress in the cross-section of a twisted rod*

Suppose τ_0 is given as:

$$\tau_0=\tau_{0a}\sin\omega t \tag{ii_0}$$

where: τ_{0a} and ω are its amplitude and circular frequency. Then:

$$\tau=\tau_a\sin\omega t \tag{iii_0}$$

where:

$$\tau_a=\frac{r}{r_0}\tau_{0a} \tag{iv_0}$$

is the stress amplitude at the radius r. For the unit volume:

$$dV=dAdl=rd\varphi drdl \tag{v_0}$$

we write:

$$\phi(T)=\phi_r(T)=\int_0^T\tau\dot{\gamma}\,dt \tag{vi_0}$$

where:

$$\gamma=\frac{2(1+\upsilon)}{\sqrt{E^2+\eta^2\omega^2}}\tau_a\sin(\omega t-\alpha) \tag{vii_0}$$

is the shear strain at the radius r. Thus:

$$\phi_r(T)=\frac{r^2(1+\upsilon)\omega T\sin\alpha}{r_0^2\sqrt{E^2+\eta^2\omega^2}}\tau_{0a}^2 \tag{$viii_0$}$$

For the whole rod, the total energy dissipated by twisting in the time period $T=2\pi/\omega$, $W_s(T)$, is:

$$W_s(T)=\iiint_V \phi_r(T)dV=\int_0^{2\pi r_0}\int_0^{1}\int_0^{1}\phi_r(T)r\,d\varphi\,dr\,dl=$$
$$=\frac{(1+\upsilon)\omega T\sin\alpha}{2\sqrt{E^2+\eta^2\omega^2}}\tau_{oa}^2\pi r_0^2 l$$

i.e.,

$$W_s(T)=\frac{(1+\upsilon)\omega T\sin\alpha}{2\sqrt{E^2+\eta^2\omega^2}}\tau_{0a}^2 V \tag{73}$$

where: V is the volume of the rod. On the other hand, the total energy dissipated in the rod during one cycle of tension-compression in the case of uniformly distributed harmonic stress of the amplitude σ_a and circular frequency ω amounts to:

$$W_n(T)=\frac{\omega T\sin\alpha}{2\sqrt{E^2+\eta^2\omega^2}}\sigma_a^2 V \tag{74}$$

Through Eqs (73) and (74), the ratio, μ_{sn} , of dissipated energies in these load cases:

$$\mu_{sn}=\frac{W_s(T)}{W_n(T)} \tag{75}$$

equals:

$$\mu_{sn}=(1+\upsilon)\left(\frac{\tau_{0a}}{\sigma_a}\right)^2 \tag{76}$$

It means that despite decreasing shear stress towards the rod axis, twisting creates relatively more heat than tension-compression. Note also that the considered ratio does not depend on the rod dimensions and load frequency.

In the case of unequal frequencies of twisting and tension-compression, $\omega_s \neq \omega_n$, the ratio μ_{sn} depends also on their values and parameters of the Kelvin-Voigt's model. For instance, if:

$$\frac{\omega_s}{\omega_n}=\frac{m}{p} \tag{77}$$

where: m and p are natural numbers, the ratio of energies dissipated in the rod during the time period:

$$T_c=\frac{2\pi m}{\omega_s}=\frac{2\pi p}{\omega_n} \tag{78}$$

becomes:

$$\mu_{sn}=\frac{W_s(T_c)}{W_n(T_c)}=(1+\upsilon)\frac{\omega_s}{\omega_n}\sqrt{\frac{E^2+\eta^2\omega_n^2}{E^2+\eta^2\omega_s^2}}\left(\frac{\tau_{0a}}{\sigma_a}\right)^2 \tag{79}$$

Now let us assume that the rod is simultaneously subjected to harmonic twisting and tension-compression of the same frequency. Then, the dissipation energies associated with distortions and volume changes are given per unit volume by Eqs (49) as:

$$\phi_d(T)=\frac{(1+\upsilon)\omega T\sin\alpha}{6\sqrt{E^2+\eta^2\omega^2}}\left(2\sigma_a^2+6\tau_a^2\right) \tag{ix$_0$}$$

$$\phi_v(T)=\frac{(1-2\upsilon)\omega T\sin\alpha}{6\sqrt{E^2+\eta^2\omega^2}}\sigma_a^2 \tag{x$_0$}$$

Calculation of the total energy dissipated in the rod by distortions in the time period T results in:

$$W_d(T)=\frac{(1+\upsilon)\omega T\sin\alpha}{6\sqrt{E^2+\eta^2\omega^2}}\left(2\sigma_a^2+3\tau_{0a}^2\right)V \tag{80}$$

For the total energy dissipated in the rod due to volume changes one has:

$$W_v(T)=\frac{(1-2\upsilon)\omega T\sin\alpha}{6\sqrt{E^2+\eta^2\omega^2}}\sigma_a^2 V \tag{81}$$

Their ratio, μ_{dv} is:

$$\mu_{dv}=\frac{W_d(T)}{W_v(T)}=\frac{2(1+\upsilon)}{1-2\upsilon}+\frac{3(1+\upsilon)}{1-2\upsilon}\left(\frac{\tau_{0a}}{\sigma_a}\right)^2 \tag{82}$$

which again indicates the significance of distortions in energy dissipation.

As far as the elastic strain energy in twisting is concerned, its total maximum value in the rod, W_{se}, is expressed by:

$$W_{se}=\frac{1}{2G}\iiint_V \tau_a^2 dV=\frac{1+\upsilon}{E}\int_0^{2\pi r_0}\int_0^{1}\int_0^{1}\left(\frac{r}{r_0}\tau_{0a}\right)^2 r\,d\varphi\,dr\,dl \tag{xi$_0$}$$

which gives:

$$W_{se}=\frac{1+\upsilon}{2E}\tau_{0a}^2 V \tag{83}$$

The counterpart of this quantity in tension-compression reads:

$$W_{ne}=\frac{1}{2E}\sigma_a^2 V \tag{84}$$

Thus:

$$\frac{W_{se}}{W_{ne}}=(1+\upsilon)\left(\frac{\tau_{0a}}{\sigma_a}\right)^2 \tag{85}$$

which corresponds to Eq. (76).

With Eqs (9) and (18), it is easy to prove that the ratio of energy dissipated in the rod after removal of torsional static load to the energy dissipated after removal of axial static load, as well as the ratio of energies dissipated after application of these loads, is also equal to the value of μ_{sn} given in Eq. (76).

CONCLUSIONS

- On the basis of three-dimensional constitutive equations for strains in viscoelastic solids [2], the dissipation energy in selected load cases has been determined.
- The dissipation energy in viscoelastic materials is a quadratic form of stress components.
- The time function governing the energy dissipation in homogeneous, isotropic viscoelastic material by normal and shear stress components is the same. Consequently, there is no difference in the time functions governing the dissipation of strain energy of volume changes and the dissipation of strain energy of distortions.
- Under vibratory loads, the dissipation energy rises linearly in course of time and non-linearly with increasing values of the coefficient of viscous damping of the material and load frequency.
- The dissipation energy does not depend on the phase angles of shear stress components but rises with increasing phase shifts between normal stress components of the same frequency.

- In the process of energy dissipation due to normal and shear stress components the role of the latter is dominant.
- Comparing the amount of energy dissipated due to distortions with that caused by volume changes it is seen that the influence of distortions on the dissipation effect is much more significant.

BIBLIOGRAPHY

1. Kolenda J.: *Modification of Hooke's law for multiaxial stress in viscoelastic solids*. Polish Maritime Research, 2, 2007
2. Kolenda J.: *On the behaviour of viscoelastic solids under multiaxial loads*. Polish Maritime Research, 3, 2007
3. Lubahn J.D., Felgar R.P.: *Plasticity and Creep of Metals*. J. Wiley & Sons, New York, 1961
4. Blake A. (Ed.): *Handbook of Mechanics, Materials, and Structures*. J. Wiley & Sons, New York, 1985
5. Nashif A.D., Johnes D.I.G., Henderson J.P.: *Vibration Damping*. J. Wiley & Sons, New York, 1985
6. Jakubowicz A., Orłoś Z.: *Strength of Materials* (in Polish). WNT, Warszawa, 1996.
7. Haslach H.W., Jr., Armstrong R.W.: *Deformable Bodies and Their Material Behaviour*. J. Wiley & Sons, 2004
8. Pisarenko G.S., Lebedev A.A.: *Resistance of Materials to Deformation and Failure in Complex Stress State* (in Russian). Izd. Naukova Dumka, Kiev, 1969

NOMENCLATURE

- A – area of the cross-section of the rod
- E – Young modulus
- F – internal restoring force
- G – shear modulus
- $\mathbf{H}$ – matrix of dynamical flexibility of the viscoelastic material at the load circular frequency ω
- $\mathbf{H}_n$ – matrix of dynamical flexibility of the viscoelastic material at the load circular frequency $n\omega$
- I – imaginary unity
- Im – imaginary part
- l – length of the rod prior to load
- m, n, p – natural numbers
- R – internal resistance force
- t – time
- T – stress period
- T_c – common period of normal and shear stress components
- V – volume
- W – dissipated work, energy dissipated in a given volume and time
- α – phase angle of the strain components
- α_n – phase angle of n-th terms of the strain components
- γ_k – k-th shear strain component (k = xy, yz, zx)
- γ_{k0} – k-th strain component at the static load, mean value of k-th strain component
- $\boldsymbol{\varepsilon}$ – vector of the strain components
- ε_j – j-th normal strain component (j = x, y, z)
- ε_{j0} – j-th strain component at the static load, mean value of j-th strain component
- $\boldsymbol{\varepsilon}_0$ – vector of mean values of the strain components
- η – coefficient of viscous damping of normal strain
- λ – coefficient of viscous damping of shear strain
- μ_{dv} – ratio of total dissipation energies due to distortions and due to volume changes
- μ_{sn} – ratio of total dissipation energies due to shear and due to normal stress components
- υ – Poisson's ratio
- ρ_{dv} – ratio of dissipation energies per unit volume due to distortions and due to volume changes
- ρ_{sn} – ratio of dissipation energies per unit volume due to shear and due to normal stress components
- $\boldsymbol{\sigma}_a$ – vector of the amplitudes of stress components
- σ_j – j-th stress component
- σ_{ja} – amplitude of j-th stress component
- σ_{jn} – amplitude of n-th term in Fourier expansion of σ_j
- σ_{j0} – j-th stress component at the static load, mean value of j-th stress component
- σ_n – vector of complex amplitudes of n-th terms in Fourier expansions of the stress components
- τ_k – k-th stress component
- τ_{ka} – amplitude of k-th stress component
- τ_{kn} – amplitude of n-th term in Fourier expansion of τ_k
- τ_{k0} – k-th stress component at the static load, mean value of k-th stress component
- φ_j – phase angle of j-th stress component
- φ_{jn} – phase angle of n-th term in Fourier expansion of σ_j
- φ_k – phase angle of k-th stress component
- φ_{kn} – phase angle of n-th term in Fourier expansion of τ_k
- φ – dissipation energy per unit volume
- φ_d – dissipation energy associated with distortions
- φ_n – dissipation energy associated with normal stress components
- φ_s – dissipation energy associated with shear stress components
- φ_v – dissipation energy associated with volume changes
- ψ_0 – elastic strain energy per unit volume under static load
- ω – circular frequency, fundamental circular frequency of periodic stress
- ω_s – circular frequency of twisting
- ω_n – circular frequency of tension-compression
- $(\overline{*})$ – complex quantity

CONTACT WITH THE AUTHOR
Prof. Janusz Kolenda
Mechanic-Electric Faculty,
Polish Naval Academy
Śmidowicza 69
81-103 Gdynia POLAND
phone : +48 58 626 27 89

POLISH MARITIME RESEARCH 1(55) 2008 Vol 15; pp. 29-36
DOI: 10.2478/v10012-007-0048-3

Research on preliminary concept of ship intended for mining poly-metallic concretions from sea bed

Monika Bortnowska,
Szczecin University of Technology

ABSTRACT

Necessity to design and build a ship for winning Fe-Mn concretions from sea bed, and put it into operation, results mainly from decreasing land resources of mineral rough materials and increasing prices of metals. Main dimensions and parameters of such mining ship were determined by elaborating its main design assumptions and making use of suitable data on drilling ships considered similar from the point of view of attributed functions and spatial arrangement. In this paper a design study on preliminary concept of dimensions and spatial arrangement of a ship for winning poly-metallic concretions from sea bed, is presented. The study has been aimed at elaboration of an appropriate mathematical model to be applied for optimization of ship's winning system.

Keywords: deposits of Fe-Mn concretions, design assumptions, concept of mining ship, main parameters and dimensions of mining ship.

INTRODUCTION

Sea-bed concretions are poly-metallic minerals which can be found in deep water regions of seas and oceans. They usually are spread over sea – bed in the form of a single layer of irregular oval solids of 3-10 cm diameter, usually. Density of the concretions depending on their chemical composition amounts to about 2-3 g/cm^3 on average. Water content of the concretions reaches 40 % of their dry weight and their average chemical composition usually assumed to economic analyses is as follows : manganese – 25%, iron – 15%, nickel – 1.25%, copper – 1.25%, cobalt – 0.25%. Also, small amounts of lead, molybdenum, vanadium, titanium and other metals can be present [4].

Fe-Mn concretions have not been so far mined on industrial scale firstly because of lack of legal regulations dealing with sea and ocean bed areas outside state jurisdiction zones, secondly because of high investment costs associated with mining process and thirdly because of lack of a feasible industrial technology for winning the concretions from ocean bed.

Presently, Poland – being a member of *Interoceanmetal* Common Organization, one of international consortia - has a chance to get access to sea-bed deposits of Fe-Mn concretions occurring at a water depth of over 4000 m in Clarion-Clipperton field of the Pacific Ocean. The field is of a special value characterized by a high specific concentration of concretions amounting to over 10kg/m^2 and simultaneously by the highest concentration of metals in the concretions [7].

The mining of the valuable rough materials is one of the most promising ways of winning metal ores from sea bed; their exploitation can result in important changes on the world market of metals in the future. Taking into account possible present applications of automated mining complexes (on development of which intensive work is carried out in the most developed countries of the world) and possible applications of modern techniques of processing the concretions, one can deem continuation of work on development of resources of concretions to be an important task in prospect of the year 2020 [7].

TECHNIQUE AND SYSTEM OF MINING FE-MN CONCRETIONS

For realization of mining process of the concretions from sea bed it will be necessary to design and build a large technical system of high reliability and possibly low cost of operation. The complete designed system for industrial mining and transport of Fe-Mn concretions will contain:

1. mining and transport system:
   - mining ship
   - winning installation
   - bottom gathering vehicle
   - floating pipe line for reloading the concretions from mining ship to transport ship,
2. transport and supply ships
3. ships for technical support and rescue actions at sea, and, the operational process will be considered as that of a complete system consisted of mining, storing, transporting and processing devices.

In the case if industrial exploitation of concretions resources of and a large depth of their winning is considered the mining system is to be adjusted to realization of multi-year operation process difficult from the point of view of engineering and organization of work.

The winning process of the Fe-Mn concretions from deep water - being the main task of the mining system- will be realized by the conventional single-hull ship (1) fitted with the hydraulic winning pipe line (2) and the bottom self-propelled gathering vehicle (3), Fig. 1. This is one of the most often proposed concepts of rough material mining, which can be aplied for elaboration and possible modification of a concept of mining system and ship. The mining ship plays main role in the whole mining system as it makes correct functioning – by keeping at position and supplying electric power both to the bottom gathering vehicle and winning pipe line, possible.

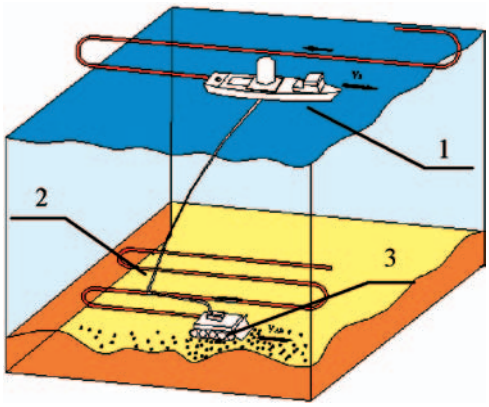

Fig. 1. *Schematic diagram of mining system for Fe-Mn concretions*

The main function of the mining ship is to win the concretions from sea bed by making use of a suitable winning system and then after collecting appropriate amount of the concretions in its holds to reload the win to transport ships by means of a transport pipe line floating on water surface.

Bottom gathering vehicle (self-propelled) will make it possible to gather concretions from sea bed. Moving over sea bed along a given route it will be able to change its speed and direction of motion depending on sea bed shape and encountered obstacles (large boulders, cracks etc). Though the vehicle will be connected with the buffer of the winning vertical pipe with the use of elastic zero-buoyancy transport piping, motions of the mining ship with lowered winning installation must be correlated with those of the gathering vehicle.

For transporting the concretions from sea bed will serve the **vertical winning pipe line** hung to ship hull and connected with bottom gathering vehicle. The so long pipe will be exposed to permanent changes of its position and deformations in sea depth due to motions of the mining ship and gathering vehicle as well as sea current action. During winning the concretions the winning pipe line cannot disturb motion of bottom gathering vehicle.

Out of all winning methods the greatest chance of application is attributed to hydraulic or pneumatic-hydraulic ones (hoisting the concretions by means of a working medium contained in piping installation) because of high operational capacity and reliability required for industrial exploitation of concretions resources. And, it may be a single-pipe or twin-pipe installation depending on location of water pumps (if single-pipe one then deep-well pumps are used, if twin-pipe one then water pumps are installed inside ship hull). The above presented concepts influence design of mining ship and in consequence the whole designed model (at least from the point of view of the system's resistance to motion).

PRELIMINARY DESIGN PROCESS OF MINING SHIP

Problem of determination of main design parameters of mining ship confronts its designer to much more difficult task than that in the case of designing typical transport ships such as: containerships, bulk carriers, tankers etc because of lack of population of existing mining ships, as well as of information on size and amount of special equipment and devices which greatly influence ship's dimensions.

Formulae and algorithms used in the traditional design methods have been implemented to shipbuilding practice as a result of collecting experience, drawing conclusions or observations on technical and operational features of existing ships. In consequence there are in use various methods of theoretical, statistical or empirical nature, for instance calculation algorithms containing formulae, equations, coefficients and diagrams which express relations between ship parameters and its technical features, which can not be used in the considered case.

Because of lack of existing ships or even only designed ones intended for industrial exploitation of Fe-Mn concretions and resulting from it large number of unknowns concerning a.o. design dimensions and masses, ship body geometry, it was necessary to make use (for designing purposes) of population of drilling ships deemed similar to the above mentioned from the point of view of their geometry and dimensions, spatial arrangement, amount of special equipment etc.

Requirements for elaboration of a general concept of mining ship

The mining ship constitutes a crucial element of the whole mining system whose mission is to win a given amount of wet concretions per year from sea-bed.

Spatial arrangement of mining ship is strictly depending on its function. Its casing containing a stabilized hoist tower which supports winning pipe line, is located amidships. Systems of a special functional unit and that maintaining the winning operations are placed in the neighbourhood of the hoist tower. Near the casing a compartment for preliminary cleansing the concretions and system of internal transport devices is located. The ship's holds should be so designed as to make it possible to uniformly load and reload concretions by means of an appropriate system. Capacity of holds results from winning effectiveness and storing time interval of concretions in the holds. And, the storing time interval is directly depending on : number and size of transport ships (their load capacity), their service speed as well as a distance from port of destination.

Design of mining ship should - as far as its size and spatial arrangement is concerned – ensure the following quantities:

- an appropriate loading space for temporary storing the concretions
- an appropriate volume of space amidships to install winning pipe line system
- in the vicinity of the winning system - an appropriate compartment to locate devices for initial cleansing and transporting the concretions to ship holds
- an appropriate area amidships to spread and store pipes of winning system
- a sufficiently large space to accommodate ship power plant (which results from large power demand for numerous power consumers, mainly drives of propellers applied in motion control system, and devices for winning, processing and transporting the concretions etc)

- an appropriate area or space for location a large number of various ship systems and auxiliary devices (preferably in compartments sheltered against atmospheric exposure, in which the devices would be grouped depending on a kind of their work)
- an appropriate capacity of tanks and stores to accommodate various supplies resulting from an assumed autonomy of the ship
- an appropriate space for living and social accommodations sufficiently distant from sources of noise and vibration.

Hence for mining ship the main design problem is to determine size and on board location of the devices which have to ensure realization of the winning process of concretions at fulfilled design assumptions and in assumed weather conditions. Knowledge of quantities which characterize the devices would make it possible to determine deadweight of a designed mining ship and consequently its dimensions.

Main design assumptions for mining system

To elaborate the mining ship design concept the following main design parameters were formulated :

- the yearly rate of winning the wet concretions, Q_{MK}
- the time interval of storing the concretions in mining ship holds T_{SK} (the ship's load capacity P_L will result from both the above given parameters, T_{SK} and Q_{MK})
- the average concentration per unit area of the concretions in sea bed deposit
- the water depth from which the concretions have to be won
- the maximum design sea conditions in which the winning process has to be continued.

Both the time interval of storing the concretions in ship holds and sea conditions in mining field region decisively influence ship's size, and the winning depth and the unit area concentration of the concretions in their deposit influence mainly rate of gathering the concretions from sea bed, which also influences the ship's speed of motion over the mining field.

On the basis of the performed economic analyses and the published results and data dealing with the deposit of poly-metallic concretions [5] the following design assumptions were selected for further considerations:

- Values of the yearly rate of winning the concretions:

Rate of winning the dry concretions Q_{SK} [t/year]	1.000.000	1.250.000	1.500.000
Rate of winning the wet concretions Q_{MK} [t/year]	1.400.000	1.750.000	2.100.000
Theoretical rate of winning the concretions Q_{teor} [t/h]	200	250	300

- The time interval of storing the concretions in ship's holds T_{SK}, from which ship's load capacity results (volume of the holds)
- The average unit area concentration of the concretions $\rho_k = 10$ kg/m^2
- The water depth of winning $h_w = 4600$ m.

The effective operation time interval T_e was determined by means of the following relation:

$$T_e = 365 - t_r - t_p \text{ [days]} \quad (1)$$

where:

t_r – yearly down-time interval resulting from technological causes

t_p – yearly down-time interval resulting from bad weather conditions.

For t_r and t_p 20% of yearly time resources was assumed according to [5].

To determine ship's load carrying capacity it is assumed that the concretions (at their average wet density $\rho_{mk} = 2$ t/m^3) will be stored in ship's holds during the assumed time interval (assuming that ship's holds are filled up in 96 % and some capacity margin is maintained for possible delays in reloading the concretions to transport ship without any break of the winning process).

ELABORATION OF SIMPLIFIED VARIANTS OF MINING SHIP

The first estimation of main parameters of mining ship

For the first estimation of main dimensions of mining ship were used the statistical data on drilling ships – assumed similar regarding their functions and spatial arrangement. Moreover the drilling ships are usually equipped with a dynamic positioning system (*DSP*) which makes it possible to maintain a set ship's position over a bore-hole. In the case of mining ship the above mentioned system will be one of those necessary for carrying out mining operations as it allows for - apart from maintaining a set ship's position and course - also moving the ship with controlled speed along a set trajectory within a given corridor. The *DSP* system is of importance as its power demand is crucial for size of ship, and its areas first of all. Hence to estimate the main dimensions of mining ship it was necessary to take into account *DSP* system's power output and sea conditions for which the ships had to be designed. The ship main dimensions and *DSP* system's power output are mutually related. Increasing the ship's main dimensions or displacement is associated with simultaneous increasing the power demand, that makes initial and operational costs of ship increasing and - in consequence - adversely influences profitability of the whole mining process. Therefore it is very important to so elaborate design of the mining ship as to make its size and power demand optimum.

From economic point of view it is equally important to set the maximum permissible sea conditions (in which the designed ship has to operate) on a reasonable level so as to obtain operational costs acceptable. In this connection a compromise between down-time interval, ship's effectiveness and financial reasons is searched for. Hence the range of design weather conditions should be taken into account during realization of the ship's design.

On the basis of the collected data on drilling ships (Tab. 1 and 2) a regression analysis was performed (by using *Statistica* software) between the main dimensions and characteristics of the drilling ships, that crucially influence *DSP* system's power output. Their results in the form of regression relationships were used to elaborate a preliminary concept of mining ship dimensions.

In Fig. 2 ÷ 4 of this paper are graphically illustrated only a few statistical analyses selected from [2, 3], which made it possible to estimate - in the first approximation – the main dimensions of the designed mining ship.

Tab. 1. Main dimensions and parameters of drilling ships

No.	Drilling ships	h_{wr} [m]	L_{bp} [m]	B [m]	H [m]	T [m]	P_N [t]	Δ [t]	S_y [m²]	S_x [m²]	F_y [m²]	C_B [-]
1	Pelican	6000	137.0	21.35	12.5	7.32	7700	15500	2000	400	975	0.740
2	Gusto 5000	7000	140.0	28.0	13.3	9.8	14800	31500	2350	650	1400	0.795
3	Glomar Jack Ryan	10668	210.0	36.0	17.7	11.0	37697	65000	4880	1150	2300	0.810
4	Deepwater Pathfinder	11650	213.0	42.0	20	13.0	72700	103000	4950	1480	270	0.850
5	Gusto 10000	9600	194.4	30.0	19.1	11.0	26200	47200	3250	870	2200	0.800
6	Gusto P 10000	9600	211.0	35.8	17.8	12.0	51000	75000	3800	1210	2340	0.780
7	Navis Explorer I	11278	185.7	40.0	19.5	12.2	-	70131	3950	1290	2250	0.800
8	Discoverer 534	7620	157.0	24.4	10.0	8.0	4200	21150	2350	480	1200	0.800
9	Glomar Eksplorer	9144	180.0	35.4	15.5	10.4	27700	51300	2900	1100	1760	0.820
10	Discoverer Spirit	10688	243.2	38.0	19.0	13.0	67000	105000	5100	1250	3100	0.850
11	Saipem 1000	9140	214	41.7	19.0	12	-	97000	5150	1400	2670	-

Tab. 2. Sea conditions and DSP system's power output for drilling ships

No.	Drilling ships	Wind speed V_A [m/s]	Wave height H_s [m]	Sea current speed V_C [m/s]	Power output of DSP system's propellers [kW]
1	Pelican	23.0	4.9	1.0	5500
2	Gusto 5000	20.0	4.5	0.7	13800
3	Glomar Jack Ryan	21.0	5.8	-	29600
4	Deepwater Pathfinder	26.0	5.79	1.02	24000
5	Gusto 10000	25.0	6.0	1.1	24000
6	Gusto P 10000	25.0	6.0	1.1	26000
7	Navis Explorer I	27.0	7.0	-	20000
8	Discoverer 534	25.7	7.6	0.77	11190
9	Glomar Eksplorer	18.0	8.8	-	17200
10	Discoverer Spirit	25.0	6.0	1.13	30100
11	Saipem 1000	25.7	5.8	-	24600

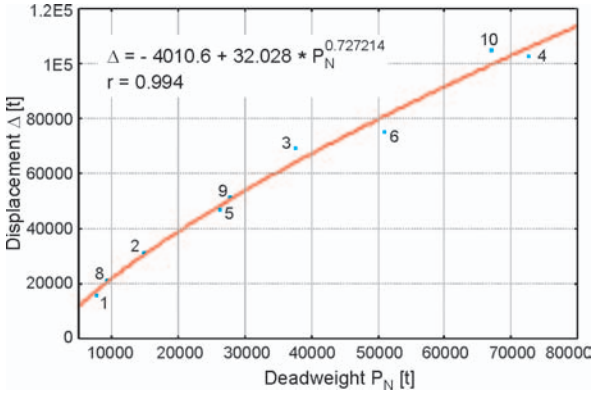

Fig. 2. Ship displacement Δ versus ship deadweight P_N for drilling ships

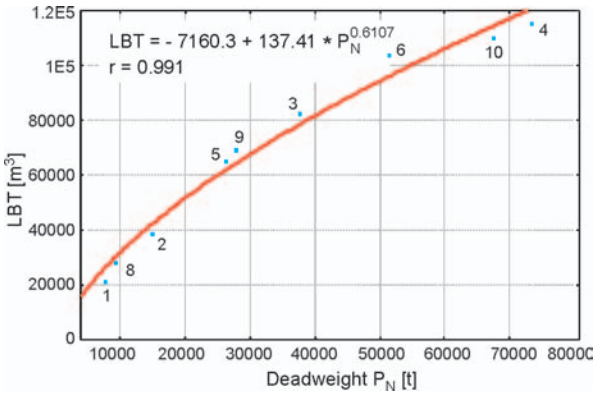

Fig. 3. LBT module of ship versus its deadweight P_N for drilling ships

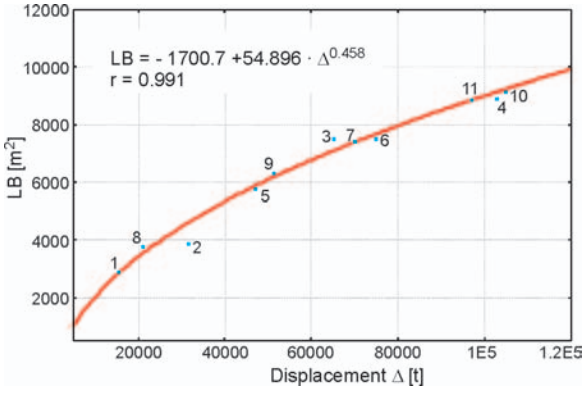

Fig. 4. LB product versus ship displacement Δ for drilling ships

The sets of all the functional relations together with the complete list of data on the group of the drilling ships taken into account in the analyses in question, are included in the publications [2] and [3].

The diagrams given below show the form of the searched-for regression function which best represents course of the investigated parameters, as well as values of the correlation coefficient *r*.

For the mining ship the main initial parameter is the rate of winning the wet concretions Q_{MK} from which the ship load carrying capacity P_L results (assuming values of the time interval of storing the concretions in holds, T_{SK}, and the operation time interval T_e). To determine a size of the mining ship, first was determined a value of the load carrying capacity

parameter on the basis of which the elaborated functional relations for drilling ships could be used.

The schematic diagram of determination first of mining ship deadweight and then its main dimensions and surface areas – with taking into account the design assumptions – is presented in Fig. 5.

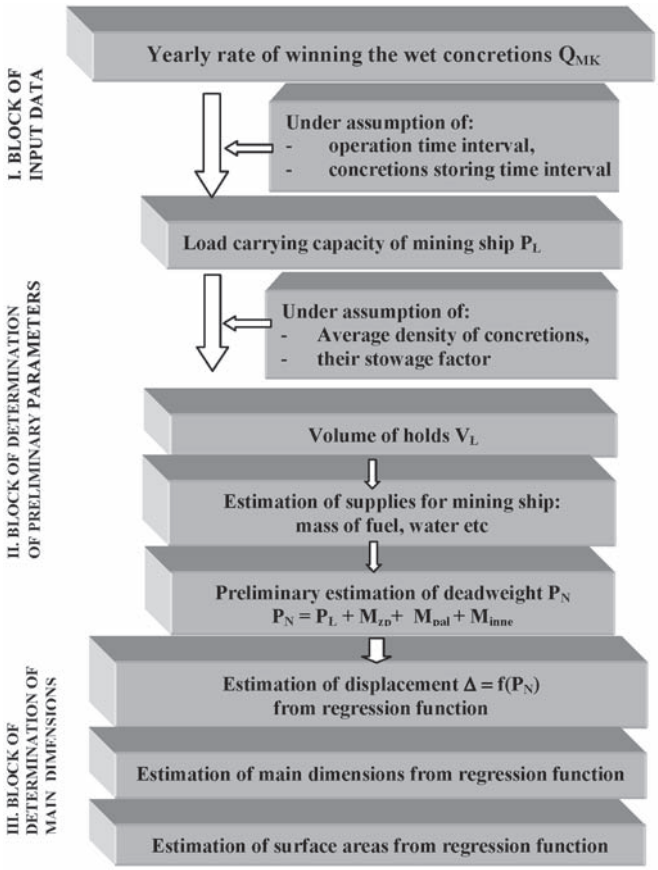

Fig.5. *Schematic diagram of determination of main parameters and dimensions of mining ship in preliminary design stage*

In order to determine the total deadweight of mining ship, P_N, additional supplies such as : fuel, water, mining process equipment etc were also determined by making use of the data on drilling ships [3]. The statement of values of particular supplies is presented in Tab. 3.

Tab. 3. *Statement of supplies, load carrying capacity and deadweight of mining ships for T_{SK} = 10 [days]*

Rate of winning the wet concretions Q_{MK} [t/year]	1.400.000	1.750.000	2.100.000
Number of crew members n_z [persons]	155	160	165
Mass of water and food supplies M_{wp} [t]	1465	1512	1559
Mass of fuel supplies M_{pal} [t]	5382	5718	6073
Mass of various supplies M_{inne} [t] wg [6]	110	110	110
Load carrying capacity $P_Ł$ [t]	48904	61130	73356
Deadweight P_N [t]	55861	68470	80988

The detail schematic diagram of determination process of mining ship parameters and main dimensions (expanded Block III of Fig. 5) together with the nonlinear regression functions of the largest values of correlation coefficient is presented in Fig. 6.

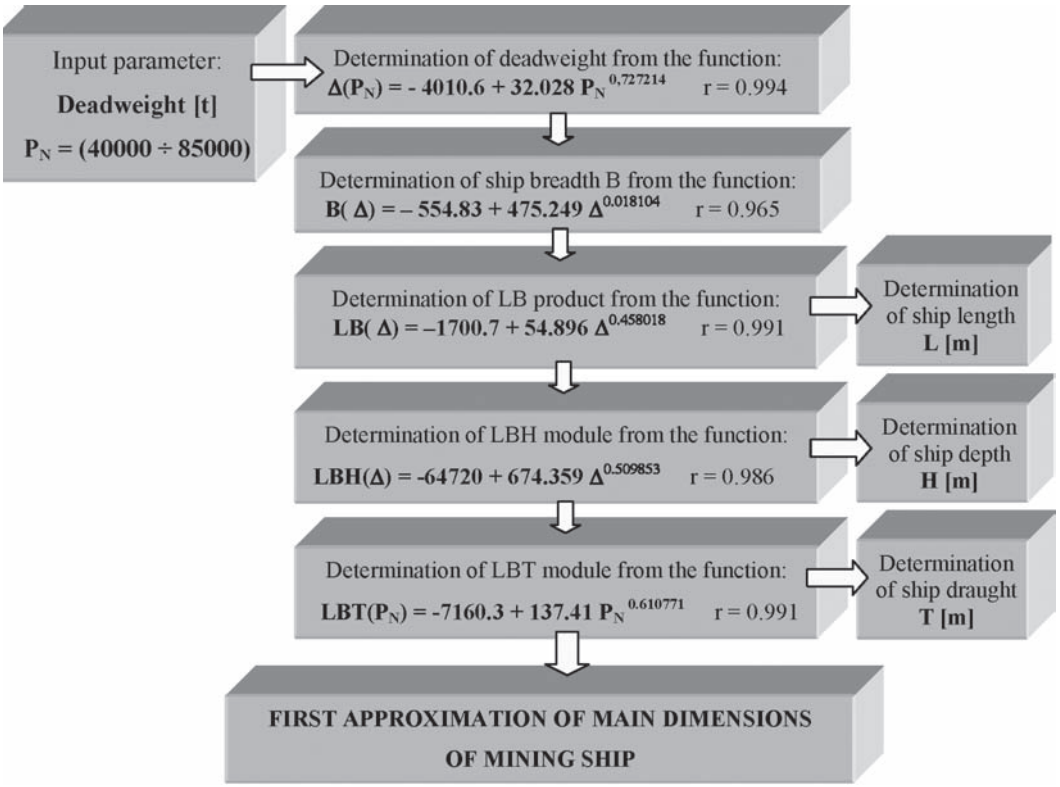

Fig.6. *Schematic diagram of determination of main dimensions of mining ship*

The first results of determination of main dimensions of three variants of mining ship are presented in Tab. 4.

Tab. 4. *Statement of the preliminarily estimated main parameters of mining ship (for T_{SK} = 10 days)*

	Variant of mining ship	Variant 1	Variant 2	Variant 3
Operational assumptions	Rate of winning the wet concretions Q_s [t/year]	1.400.000	1.750.000	2.100.000
	Operation time interval [days/year]	292	292	292
	Theoretical rate of winning [t/day]	4795	5993	7192
	Average density of concretions [t/m^3]	2	2	2
	Time interval of storing the concretions [days]	10	10	10
Main parameters of ship	Ship load carrying capacity $P_Ł$ [t]	48904	61130	73356
	Loading volume $V_Ł$ [m^3]	22961	28684	34441
	Deadweight P_N [t]	55861	68470	80988
	Displacement Δ [t]	86710	101200	114480
	Empty ship mass M_{SP} [t]	30849	32730	33492
	Length b.p. L_{pp} [m]	213.3	222.8	230.94
	Breadth B [m]	39.05	40.68	42.02
	Depth H [m]	18.9	19.37	19.74
	Draught T [m]	12.23	12.83	13.36

Verification of main parameters of mining ship

Lack of information on quantity, weight and gabarites of special equipment as well as data on weights of particular technological – constructional classes of the elements was the reason that the ship's size (especially its length) was determined with a view of:

- ☆ demanded volume of the holds for temporary storing the concretions
- ☆ size of the engine room, which was determined on the basis of the relation $LB_{sił.} = f(\Delta)$ given in [1]
- ☆ value of superstructure surface area which was determined on the basis of the relation $LB_{nadb.} = f(n_z)$ and $L_{nad} = f(n_z)$ given in [1]
- ☆ dimensions of the winning casing (dependent on dimensions of bottom gathering vehicle)
- ☆ value of surface area for storing the pipes (dependent on winning operation water depth)
- ☆ volume of the compartment for preliminary cleansing the concretions (resulting from winning rate of winning devices).

For approximate verification of the determined parameters of mining ship the data on the ships converted - in the 1970s - to the function of mining the concretions [1], [6], were used. The used data dealt with the displacement usage factor η_N and that of load carrying capacity, $\eta_Ł$, as well as indices of the dependencies of the LBH and LBT volumetric modules, and that of LB area versus the ship displacement Δ and its deadweight P_N. Knowledge of the factors made it possible to introduce corrections to the dimensions of the designed variants of mining ship. First of all the ship's length, deadweight, displacement and main dimensions modules were corrected.

Additionally, after determination of the main dimensions the ship displacement was corrected on the basis of the displacement equation expressed in function of main dimensions:

$$\Delta = \rho_w k_p L\, B\, T\, C_B \qquad (2)$$

where:
k_p =1.005 ÷1.01 – allowance coefficient for ship's outer plating and appendages

The statement of the corrected main parameters and dimensions of the mining ships is presented in Tab. 5. Their operational assumptions dealing with winning rate and winning time interval, average density of the concretions are kept unchanged.

Spatial arrangement of mining ships of simplified design concept

The designed mining ship is of single hull. Compartments of its power plant, electric power plant together with auxiliary devices are located aft, and wheel house and living accommodations fore. Also in the bow part all the systems and devices associated with functioning the superstructure are located. The midship part is used to accommodate the following :

- ✪ the stabilized hoist tower and winning casing fitted with winning pipe line,
- ✪ the compartment containing the devices for preliminary cleansing the concretions and transporting them to holds,
- ✪ the hold compartments (on aft and fore side of the cleansing compartment),
- ✪ the supplies of winning pipes (stored on the platform over the aft holds and in the pipe store room fore).

The ship is fitted with double bottom extending fore and aft as well as double side structure along the working space. The double bottom spreads from the after-peak bulkhead to the collision bulkhead. The double bottom height was assumed equal to 3000 mm (on the basis of drilling ships) over its full length, and the breadth of double sides equal to 2500 mm. The inner bottom is assumed flat over the whole breadth of hull, and the upper deck is of no sheer and camber.

If the breadth of double sides and double bottom height as well as the hold structure is taken into account, values

Tab. 5. The statement of the corrected main parameters and dimensions of three mining ship design variants (for T_{SK} = 10 days)

	Variant of mining ship	Variant 1	Variant 2	Variant 3
Mass parameters	Number of crew members n_z [persons]	190	195	200
	Mass of water and food supplies M_{wp} [t]	2713	2790	2856
	Mass of fuel supplies M_{pal} [t]	9403	10439	12136
	Mass of various supplies M_{inne} [t]	110	110	110
	Load carrying capacity $P_Ł$ [t]	48904	61130	73356
	Deadweight P_N [t]	61130	75469	89458
Parameters and main dimensions of ship	Length b.p. L_{pp} [m]	203.5	215.6	230.1
	Breadth B [m]	39.05	40.68	42.02
	Depth H [m]	18.9	19.37	19.74
	Draught T [m]	12.23	12.83	13.36
	Hull block coefficient C_B	0.83	0.83	0.83
	Displacement Δ [t]	83100	96250	110500
	Volume of holds $V_Ł$ [m^3]	22961	28684	34441

of the length of the crucial compartments of the ship are as follows:

Variant of mining ship	Variant 1	Variant 2	Variant 3
Length of hold compartment $L_{ład}$ [m]	48.4	55.6	62.5
Length of engine room $l_{sił}$ [m]	37.0	39.0	41.0
Length of superstructure l_{nad} [m]	29.0	30.0	30.7
Length of winning casing [m]	20	20	20
Length of pipe storing compartment [m]	On the basis of drilling ships 15		

The research work [6] was used to prepare the general arrangement plan of the mining ship. In Fig. 7 the concept of general arrangement of one of the variants of the mining ship is presented.

CONCLUSIONS

- Design of mining ship should be realized with a view of its effectiveness which consists a.o. in minimization of down - time interval (the time during which carrying out winning operations is not possible due to bad weather conditions) as well as minimization of unit winning cost (e.g. per 1 t of concretions).
- The effectiveness is mainly influenced by the main parameters of ship, and consequently by power output of its motion control system, whose values depend a.o. on weather condition parameters. Therefore it is important to design a mining ship which constitutes an optimum from the point

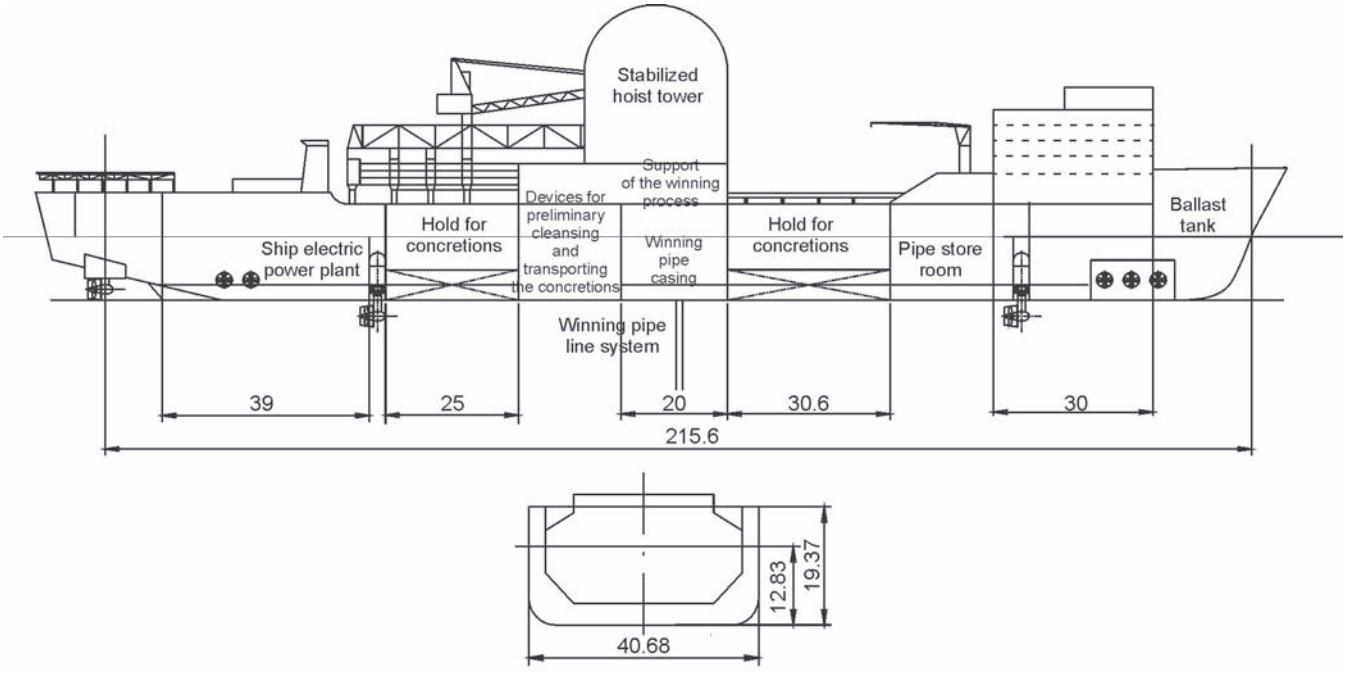

Fig.7. *A concept of general arrangement of mining ship (based on the dimensions of Variant II ship)*

of view of its initial and operational costs as it will have prevailing impact on success of the entire undertaking.

- In this paper were formulated the main design assumptions crucial for a size of ship for winning Fe-Mn concretions.
- On the basis of the main design assumptions, namely : the yearly rate of winning Q_{MK}, the time interval of storing the concretions in ship holds, T_{SK}, as well as parameters of concretions deposit, the necessary load space of the mining ship was estimated. By making use of the data on drilling ships (deemed similar regarding their functions and space arrangement) and the functional relations between the main parameters and dimensions, the first preliminary concept of mining ship dimensions was elaborated. This way were determined the ship parameters which have not been so far fully defined and elaborated.
- The task was especially difficult because it concerned the mining system which contains many unknowns in the range of geometry and mass of the ship. Therefore the presented concept of mining ship's main parameters should be considered only as a preliminary source of information even if because the ship's displacement and its dimensions have not been verified by applying real values of weight and size of devices for winning and cleansing the concretions as well as of special equipment.
- The elaborated preliminary design of the mining ship was already used a.o. for performing approximate analyses of power demand for such ship and mainly for estimation of electric plant power output including necessary power demand for the ship's motion control system.

NOMENCLATURE

B – ship breadth
C_B – hull block coefficient
D_{rz} – outer diameter of winning pipe line
F_y – projection area of hull underwater part surface to ship's plane of symmetry
H – ship depth
h_{wr} – drilling depth
l_r – length of winning pipe line
L_{pp} – ship length b.p.
M_{pal} – mass of fuel supplies
M_{SP} – mass of empty ship
M_{wp} – mass of water and food supplies
M_{ZP} – mass of supplies
n_Z – number of crew members
$P_Ł$ – ship load carrying capacity
P_N – ship deadweight
S_x, S_y – projections of windage areas (to midship plane and symmetry plane, respectively)
t_p – yearly down-time interval due to bad weather conditions
t_r – yearly down-time interval due to technological reasons
T – ship draught
T_e – effective operation time interval
T_{SK} – time interval of storing concretions in holds
$V_Ł$ – load volume
V_s – ship speed
Q_{MK} – yearly rate of winning the wet concretions
Q_{SK} – rate of winning the dry concretions
ρ_w – sea water density
Δ – ship displacement.

BIBLIOGRAPHY

1. Бакуров Г.И.: Суда для глубоководных горнотехнологических исследованний, Судостроение, № 3, 1988
2. Bortnowska M., Szelangiewicz T.: *Approximate method of determining power output of dynamic positionig system of drilling ships useful at preliminary design*, Polish Academy of Sciences, Marine Technology Transactions,Vol. 16, 2005
3. Bortnowska M.: *A method of determining power output of motion control system of floating unit during the winning of Fe-Mn concretions, useful at preliminary design* (in Polish), Doctoral dissertation, Szczecin University of Technology, 2006
4. Depowski S., Kotliński R., Ruhle E., Szamałek K.: *Mineral rough materials of seas and oceans* (in Polish), *Scholar* Scientific Publishers (Wydawnictwo Naukowe *Scholar*), Warszawa 1998
5. Sobota J.: *Estimation of power demand for the systems of winning the concretions from sea bed* (in Polish), *Interoceanmetal* Common Organization (Wspólna Organizacja *Interoceanmetal)*, Szczecin 2003
6. Szelangiewicz T.: C*oncept design of the ship for winning Fe-Mn concretions* (in Polish), Theme D5, Ship Design Office (Biuro Projektowo-Konstrukcyjne), Szczecin Shipyard, Szczecin 1978
7. Szelangiewicz T.: *Research on dynamics of the winning complex for exploitation of deep-sea- bed concretions* (in Polish), Research project report, Szczecin University of Technology, Faculty of Maritime Technology, Szczecin 2006

CONTACT WITH THE AUTHOR

Monika Bortnowska, Ph. D.
Faculty of Marine Technology,
Szczecin University of Technology
Al. Piastów 41
71-065 Szczecin, POLAND
e-mail : mwojciechowska@ps.pl
tel.: (091) 449 47 20


Photo: C. Spigarski

POLISH MARITIME RESEARCH 1(55) 2008 Vol 15; pp. 37-41
DOI: 10.2478/v10012-007-0049-2

Research on a control system based on stepping motor for ship's controllable pitch propellers

Czesław Dymarski, Prof.
Gdansk University of Technology

ABSTRACT

This paper presents description of a laboratory stand for testing servo-mechanisms of ship low-power CP propellers, as well as a remote control system for such propellers, based on electric stepping motor. Also, are presented results of the first series of tests of the control system, carried out on non-loaded CP propeller by applying stepped values of propeller pitch at two values of rotational speed of the stepping motor.

Keywords: ship controllable pitch (CP) propellers, hydraulic drive and control, control systems

INTRODUCTION

Ship's CP propellers have experienced their dynamic development and their applications on new built ships have systematically increased for a few dozen years. They are the most frequently applied type of propellers on ships required to have high manoeuvrability. The increasing popularity of the CPPs results from many crucial advantages they show. As compared with fixed screw propellers they are characterized by the following favourable features:

a) possible use of full power output in every, even entirely different service conditions;
b) better satisfying different demands expected from towing vessels (e.g. tugs, fish trawlers, minesweepers), namely:
   - as large as possible towing power available during towing operations,
   - as large as possible speed available in free-floating conditions;
c) possible maintaining the rotational speed of driving engine at changeable ship's speed and in various service conditions, constant, that is very important for ships equipped with shaft generators and pumps;
d) possible fast changing direction of thrust action without necessity of changing direction of propeller's shaft rotation, which is associated with a few additional advantages, namely:
   - it makes it possible to apply simpler, less expensive and more reliable non-reversible driving engines;
   - it significantly lowers the time necessary for propeller reverse from „ full ahead" to „ full astern" as compared with that of reversible driving engine;
   - it makes it possible to shorten twice ship stopping distance and time;
   - it makes service life-time of engine longer by elimination of significant number of stopping and starting operations during manoeuvres, e.g. in ports; such manoeuvres may be executed at very low ship speed of the order of 0.5 ÷ 1 m/s, whereas in the drives with fixed propeller the stable ship speed amounts to 2 ÷ 3 m/s due to engine rotational speed limited from below;
   - possible automation and remote control of CPP systems and of the entire propulsion system and in consequence - possible lowering number of crew members (unattended mode of power plant operation), better protection of engine against overloading, improved safety at sea, lower fuel oil consumption.
e) lower torsion stresses in shafting, experienced during changing direction of rotations as compared with those in propulsion systems with fixed propeller.
f) simpler driving system of steam turbine power plant due to lack of astern-drive turbine.

The CPPs show also some disadvantages out of which the following are the most important :

a) greater design complexity and in effect lower reliability of such system,
b) greater investment and operational costs and higher qualifications demanded from operators,
c) greater susceptibility to cavitation at the root of blades (at boss) because of their limited breadth and in consequence greater thickness in this zone.
d) rather lower hydrodynamic efficiency of the CPP by about 3% as compared with that of fixed propeller, which mainly results from a greater boss diameter, however that does not lead to a lower ship propulsion efficiency in a given service time at variable operational conditions.

Already since the beginning of the 1970s The Faculty of Ocean Engineering and Ship Technology, Gdańsk University of Technology has been engaged with the above described topics, by realizing important R&D investigations at first for the Mechanical Works Zamech, Elbląg, and next also for Polish Navy and private owners of fishing vessels. In 1991 at the Faculty a CP propeller was manufacture and a laboratory stand for its testing was built. The propeller, though of a low power, was fitted with a hydraulic pitch control servomechanism. In it a slide

timing gear of negative-lap, located in stationary system, was used. Stability and accuracy of operation of the servomechanism was the subject of the research carried out in a broad range of external load simulations, results of which was published in [1, 2]. And, the servomechanism was equipped only with a local system of propeller pitch setting.

The gained experience was used for the designing, manufacturing and testing of two CP propellers intended for small fishing vessels. In Fig. 1 is shown the photograph of one of the propellers during the tests at the Faculty's laboratory. Principle of operation, load calculations and results of the laboratory and service tests of the servomechanism applied to the propeller were presented in [3 ÷ 7]. In the servomechanism a slide positive-lap timing gear different from that used for the laboratory test stand, was applied, that required to elaborate an appropriate remote control system activated from the ship's bridge.

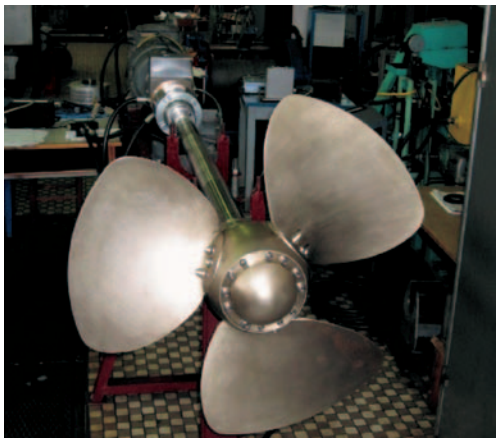

Fig. 1. *Low-power CP propeller placed at the Faculty's laboratory test stand*

DESCRIPTION OF THE LABORATORY TEST STAND

The existing CP propeller and laboratory test stand was supplemented with the remote control system in order to satisfy current needs. Taking into account present demand for the CPPs in Poland, mainly from the side of small-ship owners, one decided to choose a relatively simple and cheap system of the kind, fitted with an electric stepping motor. The design of such system was presented in detail in [8].

Realization of the above mentioned research task required to do many preparatory operations on the existing laboratory test stand. For the reason that the CPP's servomechanism in question is intended for its using not only in research and education but also for installing onboard small fishing boats mainly, it was decided to fit it with the remote control system capable of making it possible to automate the whole propulsion system easily. Schematic diagram of the servomechanism together with hydraulic and measuring systems is presented in Fig. 2. Two-lever pitch setting unit with possibility of switching the

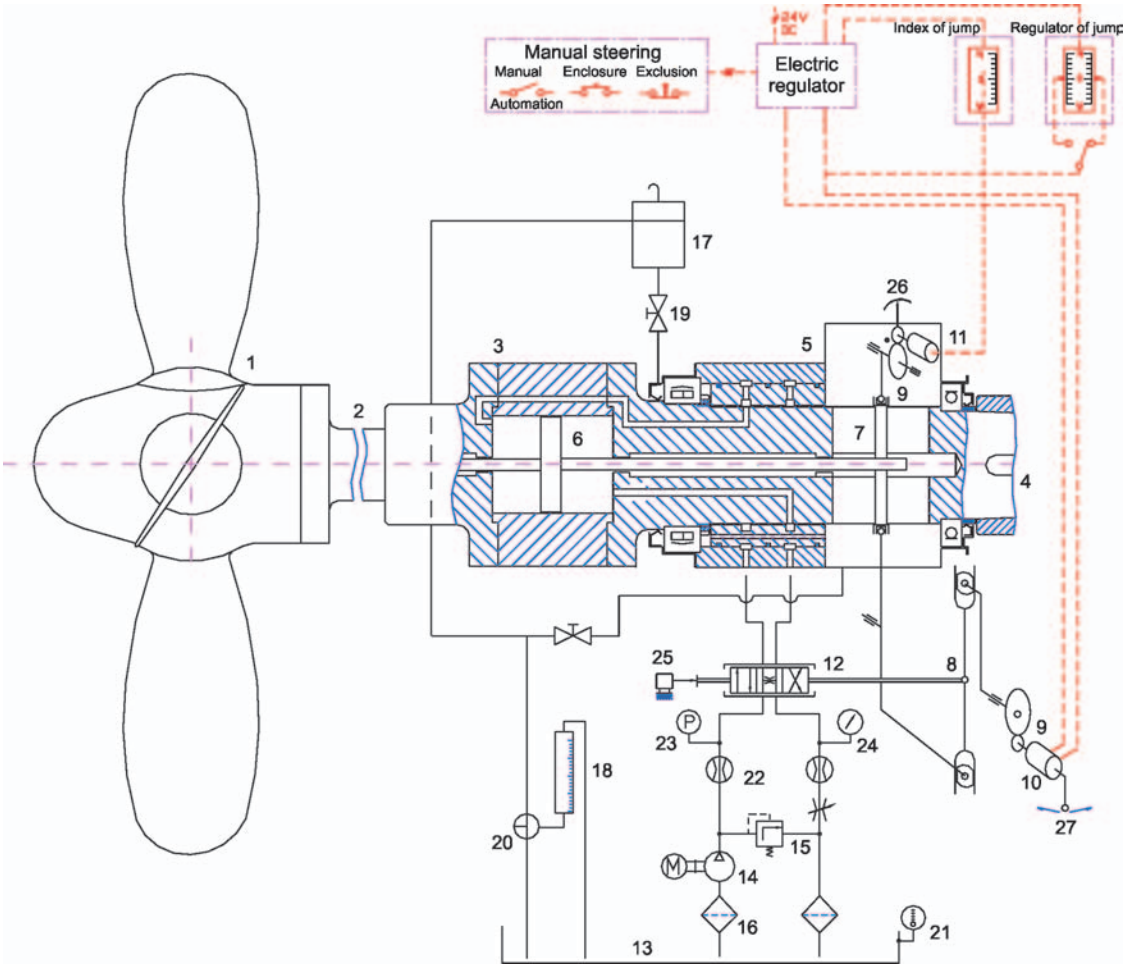

Fig. 2. *Schematic diagram of the laboratory test stand for controllable pitch propellers.*
Notation*: **1** – CPP; **2** – propeller shaft; **3** – flange coupling; **4** – intermediate shaft; **5** – oil timing box; **6** – hydraulic cylinder of propeller pitch control mechanism; **7** – real pitch signal input system; **8** – feedback lever system; **9** – toothed transmission gear; **10** – stepping motor; **11** – rotation angle indicator; **12** – three-position four-way distributor of negative laps; **13** –oil tank; 14 constant capacity oil pump; **15** – overflow valve; **16** – oil filter; **17** – gravitational oil tank; **18** – measuring tank; **19** – cut-off valve; **20** – three-way valve; **21** – temperature gauge; **22** – flow-meter; **23** – pressure gauge; **24** – manometer; **25** – linear displacement gauge; **26** – real pitch indicator; **27** – propeller pitch local setting lever*

set values, is applied to it, that makes it possible to examine the system's response to stepped changes of the input values.

Two photographs of the tested servomechanism together with the control desk and measurement recording equipment are shown in Fig. 3, and the photograph of the remote control desk – in Fig. 4.

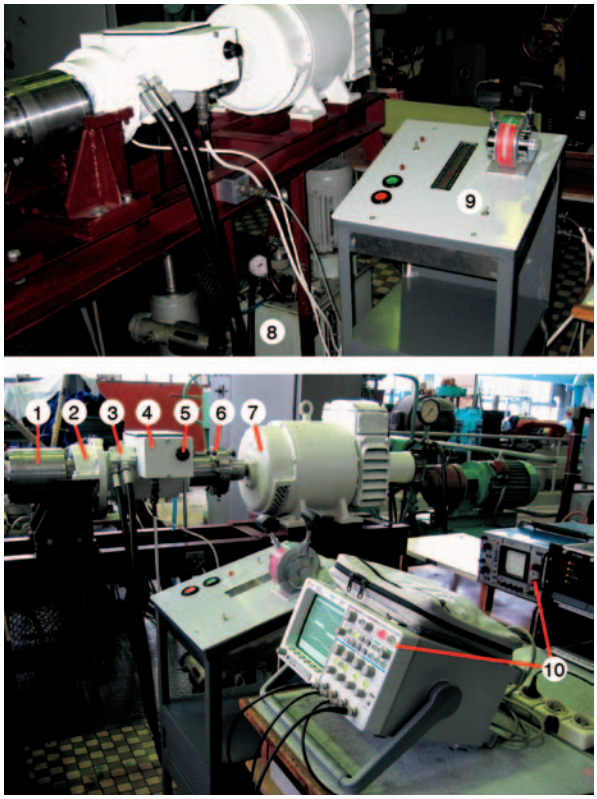

Fig. 3. *The laboratory stand for testing the CP propeller servomechanism.* ***Notation****: **1** – hydraulic pitch control cylinder placed between flanges of propeller shaft and intermediate shaft; **2** – angular bearing; **3** – hydraulic distributor; **4** – oil timing box with internal control unit; **5** – hand wheel for propeller pitch local setting; **6** – clutch; **7** – shaft driving DC motor; **8** – hydraulic supply unit; **9** – remote control desk; **10** – measurement recording equipment*

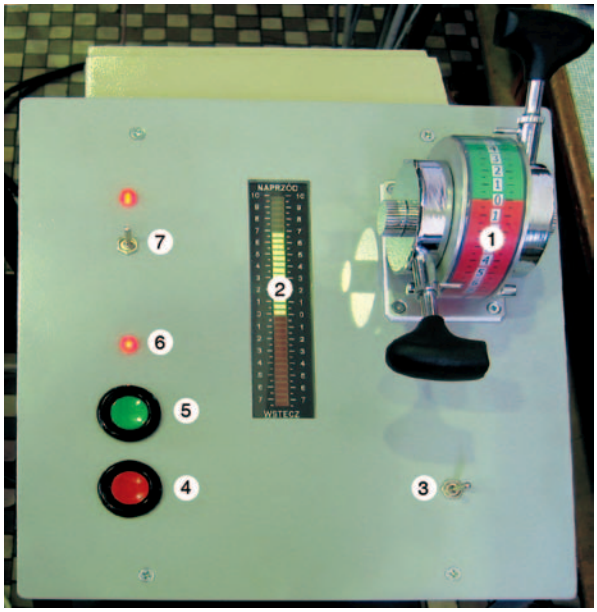

Fig. 4. *The control desk of the tested CP propeller.* ***Notation****: **1** – two-lever handle for propeller pitch setting; **2** –electronic indicator of real propeller pitch; **3** – change-over switch of setting handle; **4** – cut-out; **5** – switch-in; **6** – control lamp; **7** – change-over switch for remote or local control*

LABORATORY TESTS

The performed tests were aimed at the checking of correctness of operation of the built remote control system in cooperation with the existing servomechanism, as well as of stability and accuracy of the whole propeller pitch control system without any external load. The only acting load was that due to friction forces and very small inertia forces of moving elements of the servomechanism. The greatest share in the load was associated with friction forces of the piston sealing rings and - to a little smaller extent – the piston rods of the hydraulic cylinder.

Influence was also checked of one of the adjustable quantities, namely rotational speed of stepping motor, on dynamics of motion of the system's elements and pitch setting accuracy.

Step change of the propeller blade-angle setting from α = 0 to α = 9°, and next back to α = 0°

The recorded runs of:

- ⇨ the electronic control operation state $u_{z,}$
- ⇨ the axial displacements of the hydraulic distributor slide, x,
- ⇨ values of the blade-angle setting $\alpha_{z,}$ and
- ⇨ real values of the angle α

are presented in Fig. 5. The measurements were performed at the pulse generator frequency ν = 7.5 [Hz] which - for the stepping motor executing 200 steps per revolution - ensures its shaft's rotational speed n = 2.25 [rpm]. Hence the duration time of one working cycle of the system, t_c, was equal to 133.3 [ms] (milliseconds).

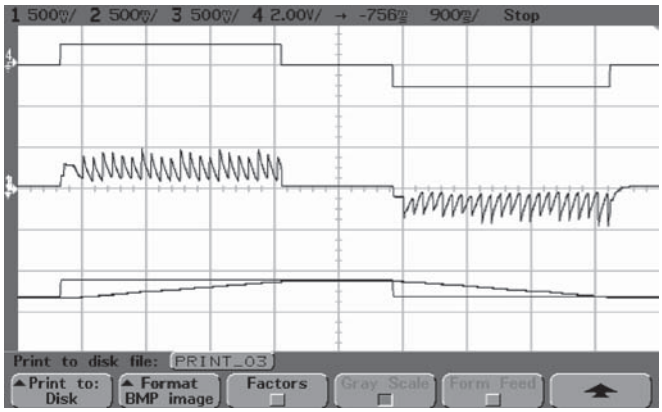

Fig. 5. *The oscilloscope screen's photograph which shows the recorded runs of : the control signal $u_{z,}$ displacements of hydraulic distributor slide, x, values of the set propeller blade angle $\alpha_{z,}$ and the real one α*

When only the propeller pitch setting handle is inclined (at the test stand the step action switch is activated) a constant voltage signal is generated which triggers the stepping motor working and maintains constant until the value of the real blade angle α is equal (within the set accuracy limits) to that of the set angle $\alpha_{z,}$ Then the feed-back system switches off the control signal. The inclination of the propeller pitch setting handle in the opposite direction to its initial position will trigger again analogous process of propeller pitch changing until its new set value it attained, then the entire process is stopped.

The run of the hydraulic distributor slide displacements is worth attention. Every "step" rotation angle of the stepping motor shaft makes initially the distributor slide displacements violent and in effect starts delivery of oil under compression to one of the cylinder chambers, piston motion and propeller pitch

change. With a view of the very small value of the set „step" equal to 1.8°, realization of such real pitch change makes the deviation relatively fast decreasing and, due to operation of the feed-back system, the slide gradual coming-back towards its initial position. In the meantime the successive „step" of motor shaft rotation, successive stepwise slide displacement as well as propeller pitch change occur, and the above described cycle of operations is repeated until a set pitch change value executed this way is finally attained.

It is worth noting a little smaller displacement of the slide during the first step just after starting the pitch changing process both forward and aft. In the opinion of this author it is caused by a relatively greater drag of the slide due to a somewhat thicker and colder oil layer adhering to surfaces of small pistons and cylinder before starting than that observed during fast cyclic displacements.

Values of the slide displacements x and frequency of their occurrence depend on the stepping motor rotational speed and flow rate of oil delivered to the distributor.

Step change of the propeller blade-angle setting from α = 0 to $α_{max}$ = 34°, and next back to α = 0°

The runs of u_z, x, $α_z$ and α recorded during this test are presented in Fig. 6. The recording of the measurements was computer-aided. Number of the measurements is marked on the horizontal axis of the diagram.

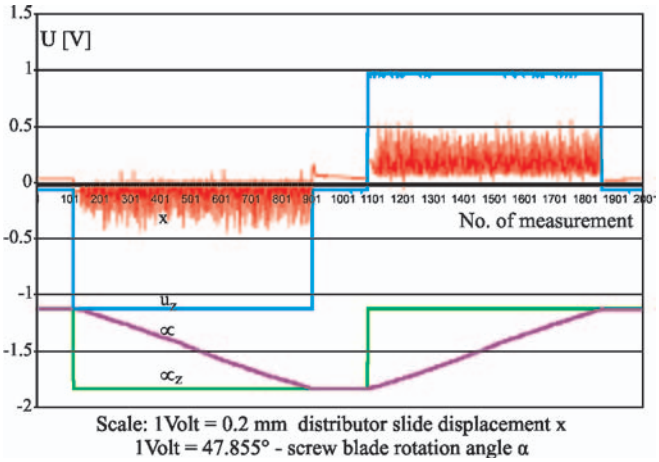

Fig. 6. *Measured runs of : u_z – control signal, **x** – hydraulic distributor slide displacement, $α_z$ and **α** - set and real values of propeller pitch during its step setting change from α = 0 to $α_{max}$ = 34°, a then back to α = 0°*

On the vertical axis are given values of voltage signals of particular measured quantities, and their scale – below the diagram. The zero-point of the axis does not correspond with zero value of measured quantity.

The character of the recorded runs is similar to those discussed in the preceding chapter with one exception, namely: the slide's movement in the instant of termination of the returning control process. In this case fast return of the slide from a working position causes its instantaneous displacement behind the middle one. This can be supposed to be caused first of all due inertia forces of the fast moving slide, as well as a greater accuracy of the computer-aided measurements.

Analyzing the run of propeller blade-angle setting changes one should state that it is stable despite the non-uniform velocity of motion and that the achieved setting accuracy is sufficiently correct. The diagrams of the measured values of α and $α_z$, after realization of the task, practically coincide.

The test of influence of change of stepping motor speed on operation of the system

The test was performed in such a way that the step change of propeller pitch from „full astern" to „full ahead" was set from $α_{min}$ = - 24° to $α_{max}$ = 34°, and during realization of the process at the same velocity as in the first described test the stepping motor rotational speed was temporarily increased more than twofold (the pulse generator frequency ν = 15.6 [Hz], the motor rotational speed n = 4.68 [rpm] and cycle period t_c = 64.1 [ms]). The computer-recorded results made it possible to elaborate the runs of the measured quantities u_z, x, $α_z$ and α, shown in Fig. 7.

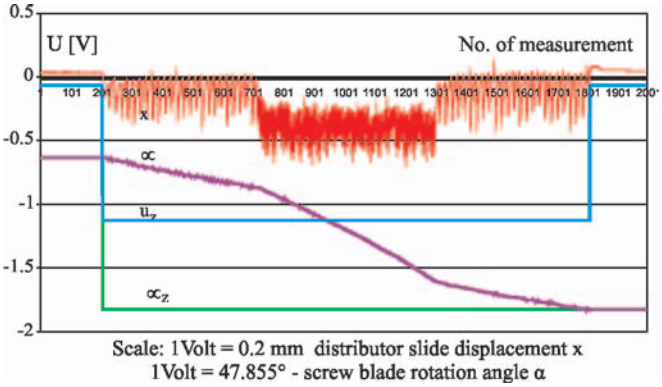

Fig. 7. *Measured runs of : u_z – control signal, **x** – hydraulic distributor slide displacement, $α_z$ and **α** - set and real values of propeller pitch during its step setting change from $α_{min}$ = -24° to $α_{max}$ = 34° together with changing the rotational speed of stepping motor from n_1 = 2.25 [rpm] (Generator frequency ν = 7.5[Hz]; cycle period t_c = 133.3[ms]) to n_2 = 4.68 [rpm] (ν = 15.6[Hz]; t_c = 64.1[ms])*

The run of the distributor slide motion should be discussed here. When only the rotational speed of the stepping motor increased and the single cycle period decreased twofold, the average value of the displacements x increased almost twofold too. It can be explained is such a way that after the motor speed increasing and the working cycle period shortening the closing slide had been earlier displaced further than at the lower speed and in effect its successive displacement had been commenced in the instant when it had been much more distant from the middle position than in the preceding step. Consequently, successive displacements of the slide occurred at a more and more greater value of the average displacement. This way the oil flow rate and cylinder piston speed were increasing. After several cycles, value of the average displacements of the slide became fixed on a new, higher level. When only the motor rotational speed decreased the slide displacement cycles went consequently on a lower level.

CONCLUSIONS

- The presented tests of the CP propeller servomechanism together with the remote control system are only the first, but very important phase of the necessary research on devices of the kind. They were aimed at the checking of quality and accuracy of realization of the system's main tasks during its operation without any load. The achieved results which showed the correct and sufficiently accurate operation of the servomechanism justify purposefulness of continuation of such research.

- The research should be carried out in the conditions which simulate possibly exactly real service conditions especial-

ly in the range of values and character of external loads applied to the servomechanism. However to this end it is necessary to design and manufacture a special device for setting a given value and direction of the loading exerted to the pitch control mechanism. It is assumed to locate the device in a rotating system, in the rear part of propeller boss, instead of the propeller cap. The similar device was already used in testing the CP propeller for KR10 fishing cutter [3].

- Moreover it is planned to investigate the influence of increasing the gear ratio of the toothed transmission gear (9) placed between the stepping motor (10) and the lever (8), (see Fig. 2), on dynamic behaviour of the system under operation.

- To sum up, positive results of the planned research would make it possible to offer the relatively simple and inexpensive solution mainly for application to small modern floating units, especially fishing ones.

BIBLIOGRAPHY

1. Dymarski C.: *Laboratory tests of a hydraulic servomechanism of low-power controllable pitch propeller* (in Polish). Marine Technology Transaction, Polish Academy of Sciences - Branch in Gdańsk, Marine Technology Committee. Vol. 8. 1997.
2. Dymarski C.: *Laboratory investigations of the stern tube bearings and pitch control mechanism of the low – power CP propeller with screw-toothed gear*. Polish Maritime Research No 3 September 1998, Vol. 5.
3. Dymarski Cz.: *Pitch Control Servomechanism for a Low Power Rate CP Propeller*. Marine Technology Transaction, Polish Academy of Sciences-Branch in Gdańsk, Marine Technology Committee. Vol. 12, 2001.
4. Dymarski P., Dymarski Cz.: *Curvilinear Panels and Higher Order Dipole Distribution Method for Ducted Propeller Flow Calculations*. Marine Technology Transaction, Polish Academy of Sciences-Branch in Gdańsk, Marine Technology Committee. Vol. 12, 2001.
5. Dymarski Cz.: *The hydraulic drive and control of the equipment of the small fishing cutter*. Marine Technology Transaction, Polish Academy of Sciences - Branch in Gdańsk, Marine Technology Committee. Vol. 13, 2002.
6. Dymarski Cz.: *A ship CP propeller servomechanism* (in Polish). Proceedings of 4th Conference „Shipbuilding and Ocean Engineering": Reliability and Safety of Transport Systems. Międzyzdroje, June 2002. Publishing House of Szczecin University of Technology.
7. Dymarski Cz.: *A propulsion system for small fishing vessel* (in Polish). Proceedings of 3rd International Scientific – Technical Conference EXPLO – DIESEL & GAS TURBINE'03. Gdańsk – Miedzyzdroje – Lund (Sweden), May 5 ÷ 9, 2003.
8. Dymarski Cz., Blekiewicz T.: *Elaboration of a remote control system based on stepping motor, intended for CP propeller, and a mechanical transmission gear of negative feedback ensuring stability of a set position* (in Polish). Research reports, Faculty of Ocean Engineering and Ship Technology, Gdańsk University of Technology, Gdańsk 2005.

CONTACT WITH THE AUTHOR

Assoc. Prof. Czesław Dymarski
Faculty of Ocean Engineering
and Ship Technology,
Gdańsk University of Technology
Narutowicza 11/12
80-952 Gdańsk, POLAND
e-mail : cpdymars@pg.gda.pl

POLISH MARITIME RESEARCH 1(55) 2008 Vol 15; pp. 42-51
DOI: 10.2478/v10012-007-0050-9

Management of assignment of operational tasks realized in ship power plant

Piotr Kamiński
Wiesław Tarełko
Gdynia Maritime Academy

ABSTRACT

The frequent cause of ships' detentions by port authorities are abnormalities of ship power plant functioning. Each extended ship lay time in port results in waste of ship operating time thus costs rise to shipowners. This is connected with improper ship power plant management. In order to avoid this, a ship engineer should have at his disposal computer aided system supporting him in managing of ship power plant. Such a system can be worked out on condition that mathematical formula which represents the decision – making process of an engineer has been built. The present work shows approache to the problem according to the situation in which the engineer is made to take certain decisions. In formulation of the most substantial operating states of a ship like lay time in harbour and sea voyage the ,knapsack algorithm' was applied. For both approaches objective function was formulated.

Keywords: ship power plant, management

INTRODUCTION

According to many experts to reach correct management of ship power plant involves great difficulties to decision-making persons, i.e. ship chief engineers. This is caused a.o. by:

- ⇨ increasing number of automated ship systems
- ⇨ multiple number of operational processes executed in parallel
- ⇨ lack of appropriate information making it possible to quickly master systems and task planning
- ⇨ frequent changes of staff members
- ⇨ increasing number of requirements for safety of persons, ship and environment.

Moreover changing international maritime law imposes many additional tasks dealing not only with new procedures connected with safety at sea but also with their detail documentation.

Such state leads to a situation in which decision-making is more and more difficult and knowledge and experience of ship engineers may appear insufficient. In such conditions making a decision dealing with power plant management may be incorrect or irrational and in consequence causing various losses, e.g. loss of ship service time leading this way to increasing overall cost of ship operation. In order to eliminate such situations ship engineers should have at his disposal a software which could be a „tool" aiding him in organizing ship power plant management process. Such system would collect information concerning realization of all operations in power plant or make use of data bases of already functioning information systems, analyze any limitations associated with their realization and finally advising ship engineer on which tasks and in which sequence they have to be realized.

In ship power plant a team often consisted of several persons performs operations resulting from realization of many tasks of different time horizons, realized in parallel.

This requires, from chief engineer, to make rational decisions concerning a.o. determination of a kind, range, sequence and executors of operations. To make such decisions it is necessary to collect and process suitable information. Among other, the following can serve as their sources:

- ➡ technical and operational documentation of machines and installations, requirements associated with safety at sea and marine environment protection (conventions, codes, rules of classification societies, rules of maritime administrations, ship owner's regulations etc)
- ➡ data bases of information systems used in ship power plant
- ➡ assessment of technical state of ship power plant machines and systems
- ➡ assessment of state of provisions (fuels, lubricants, spare parts etc)
- ➡ occurrence of a destructive event, e. g. machine failure
- ➡ assessment of feasibility of appropriate actions, e.g. expected time of port staying, deadline of subsequent shipyard's repair etc
- ➡ assessment of accessibility of an external service in a given shipping region
- ➡ assessment of capability of crew to realize planned operations
- ➡ assessment of crew experience associated with carrying out given kinds of operations [4].

All the information may appear or be used during decision making process in various service states of ship. Generally ship's service process can be represented by a sequence of three main states:

- staying in port (loading – reloading)
- manoeuvres (in ports, channels etc)
- sea voyage.

In the above presented states disturbances may appear as a result of e.g. changes of ship motion parameters (or ship stopping) or a longer time of ship staying in port.

The main problem to be solved by ship chief engineer within the scope of ship power plant management can be formulated as follows:

„Knowing a set of tasks to be realized as well as taking into account available means (technical, personnel and time resources),operational requirements concerning ship, as well as limitations of different kind, one should make choice of appropriate operations and integrate them into one ordered set of actions".

In other words the thing is that a decision should be taken as to such above mentioned operations whose realization would be most effective from the point of view of ship service.

FORMULATION OF DECISION-MAKING PROBLEM OF SHIP ENGINEER

From the operational point of view the best (optimum) plan of the tasks which are necessary to be realized in a given operational situation constitutes the solution of the decision problem faced by ship engineer.

Analyzing situations in which ship engineer may be forced to solve the presented decision problem one can distinguish several, different to each other ways of its formulation. For instance, the first situation of the kind is that in which a ship continues a long sea voyage. In such situation there are no strict time limitations as to realization of ship power plant operation process as well as to particular operational tasks. So, the decision problem can be formulated as a planning process without any time limitations. However the tasks should be effectively planned with the use of available personnel and material resources as well as with taking into account the instant of realization of a given task, imposed by external factors such as: requirements resulting from regulations given by producers of ship machines and devices, classification societies, port control (*PSC*) etc.

The other situation is that in which strict time limitations are present such as e.g.: during ship staying in a port where the ship's strict departure time is known and number of the tasks to be realized is usually much greater than that possible for crew of power plant. In such situation the chief engineer must make decision regarding which of the operational tasks should be made during the time being at his disposal and which could be postponed to another time as well as who should be assigned to execute particular tasks. In such moment, making incorrect decisions can cause non-fulfilment of the tasks, that consequently may result e.g.: in stopping the ship by port control (*PSC, FSC*) or subsequently in breaking the normal process of ship power plant operation (e.g. *black-out*). The decision problem in such situation can be formulated as the choice of the crucial tasks from the point of view of ship power plant operation and planning them in such a way as to make use of the available time most effectively.

Another situation is that in which both the strict time limitations are present and one aims at the best making use of the available resources, where the features of the first above described situation and the other one are combined in a sense. Such formulation of the decision problem may concern the situation when a ship undergoes repair in a shipyard.

In ship operation many other situations (ship service states) can also happen such as e.g.: lying at anchor, manoeuvres, canal passing etc, in which the chief engineer may be forced to take decisions dealing with planning the operational tasks. However such states constitute a very small part of overall operational time of ship as they appear very rarely during its service process, or a situation requires to promptly make decision regarding a way of action to be undertaken (e.g. manoeuvres in port) where possible making use of a computer system is not rational.

In this connection for further considerations only two - out of the presented service states - namely: sea voyage and staying in port, are taken into account.

In the general theory of decision making the decision problem is such situation in which decision maker faces necessity of choosing one – out at least two possible – variants of acting. In ship power plant the chief engineer must take decision on which of the acting variants (sets of sequenced operations) would be the best from the point of view of ship service. According to the definition of the problem faced by ship engineer, he must, out of all operations to be executed, select and sequence as well as assign (to respective members of machinery crew) the most important ones in a given operational situation taking into account all relevant conditions and limitations.

On the basis of the general, formal theory of decision making the overall form of the management problem of operations in ship power plant, can be presented as follows:

$$PD_{ZSO}=(Z_Z, Z_O, r) \tag{1}$$

where:

PD_{ZSO} – Decision making problem of ship power plant management
Z_Z – set of operational tasks
Z_O – set of operators
r – relations appearing between elements, operators, tasks etc.

The decision problem of technical management of ship power plant, (PD_{ZSO}), is defined as the following triple: the set of decision variables, Z_Z, (i.e. the set of all operations to be executed), the set of operators to which appropriate operations should be assigned, Z_O, as well as that of the relations r understood as the relationships between elements of the sets Z_Z and Z_O and also containing some features of the elements.

In the process of decision making by ship engineer dealing with assigning the operational tasks to power plant crew members the following three main phases should be distinguished:

- collecting and processing all available and necessary data (those earlier mentioned and those presented in [4])
- selecting the tasks whose realization is constrained by all possible operational limitations as well as ambient conditions in which a given decision is made [3]
- assigning the earlier selected tasks to power plant crew members, in compliance with their competences so as to obtain the best schedule from the operational point of view [1, 2].

In this work only the latter presented stage is considered, i.e. the assigning of the operational tasks to ship power plant operators with imposing the additional time limitation T_S in

which the tasks have to be realized (e.g. short stay in port, short sea voyage etc). In the situation, strategy of task assigning can be based on two aims: maximization of sum of values of the tasks included into the schedule or the most effective use of the available time T_S.

The problem of planning the operational tasks in ship power plant in the case of both the aims, can be presented, like many problems, as the problem of packing (in other words: knapsack problem or loading problem) being a special cause of zero-one problems of linear programming [6, 7]. The zero-one character consists in that one of the task parameters takes value of one if the task is included to the schedule or value of zero if the task is omitted during elaboration of the schedule.

FORMULATION OF THE CONSIDERED PROBLEM AS A KNAPSACK PROBLEM

General problem of packing

In the literature on task scheduling there are many papers describing different methods and algorithms for planning various particular kinds of problems, e.g. [5, 8]. However the models are as a rule excessively general as compared with real problems and they do not take into account different practical conditions.

The standard knapsack problem consists in filling the "knapsack" of a given limited volume by using elements (blocks) of various dimensions and values in such a way as to fill the knapsack so as to make its value the greatest.

In the same way can be formulated the problem faced by ship chief engineer in some specific situations (e.g. short stay in port or short sea voyage), who must assign operational tasks to power plant crew members so as to make the best use of available time and simultaneously to realize the most important tasks out of the set of the tasks whose realization cannot be performed during the available time interval.

Scheduling the operational tasks, considered as a packing problem

Problem of planning the operational tasks, i.e. assigning them to particular members of power plant crew, can be considered as a multi-knapsack problem (shortly: 0-1 MKP) [7]. The operators o_j, i.e. power plant crew members are considered to be "knapsacks" of equal height which represents the time available for realization of tasks, T_S (e.g. time of staying in port, sea voyage time). They have the suitable competences k_j graphically represented by knapsack's breadth. To the operators are assigned the operational tasks z_i considered as the things packed to the knapsacks (Fig. 1). Every task, like the things placed in the knapsacks, has some parameters:

- the competences necessary for execution of a given task are represented by block's breadth ($k_i=o_i$)
- the time t_i necessary for realization of a given task – by block's height
- the importance of task, w_{gi}, i.e. that of a given operational task from the operational point of view – by block's value.

Such schedule of operational tasks which should be realized within a given time and in a given service situation, elaborated for each of the operators available in power plant, constitutes the solution of the presented problem. Such schedule has the form of a list of appropriately sequenced tasks which satisfy all limitations present in the problem.

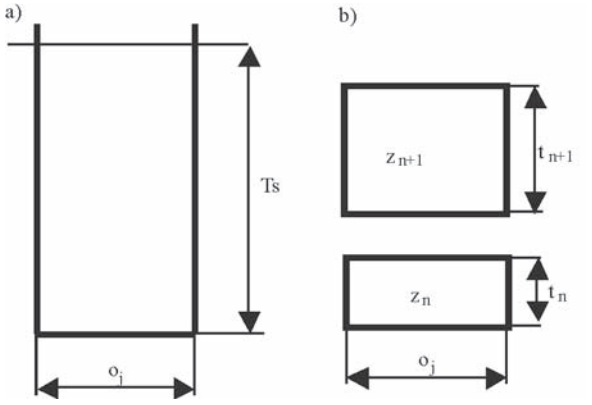

Fig. 1. *Graphical representation of elements of knapsack problem*

Mathematical model

The main elements of the decision problem of chief engineer, considered as a packing problem are as follows:

- tasks of given parameters (the importance index wg_i, realization time t_i etc)
- operators of determined capability of realizing the tasks [having the suitable competences $k_i(o_i)$]
- time being at disposal, t_s.

The operational task constitutes a sequence of actions performed by an operator or a team of operators in power plant in compliance with a procedure valid in a given situation, to ensure continuous operation of all systems, machines and devices as well as installations. An example operational task - fuel bunkering covers a.o. the following actions (operations): opening or closing appropriate valves of fuel installation, connecting the fuel installation with a fuel source from which it will be delivered, starting the fuel transport pump, and also appropriate reverse operations after ending the fuel bunkering.

All operational tasks realized in power plant are characterized by certain important parameters, i.e.: the realization time of each of them, t_i, as well as the assignment of each of the tasks to concrete operators, resulting from proffesional obligations assigned to them. The tasks out of which the schedule is directly prepared, are those selected, fulfilling operational limitations, as well as being hierarchized regarding their realization importance, that is described in [1, 2].

The operators constitute all persons working in ship power plant and realizing necessary operational tasks, i.e. those to whom the scheduled tasks will be assigned. Number of persons working day after day in power plant is usually constant, however it may be sometimes changed depending on a given operational situation. For instance, a member of permanent power plant crew may be disable to work (that will make number of operators lower) or other persons not being members of the permanent crew, e.g. external service, shipyard pesonnel, may work in the power plant (that can increase number of operators). Consequently, it is not possible to unambigously and in advance determine the number of available operators, j; it will be changeable and individually determined for each considered situation:

$$Z_O = \{o : (o_1, \ldots, o_j)\} \tag{2}$$

where:
Z – set of operators
o – available operators.

Every day each member of power plant crew realizes his tasks in compliance with his obligations assigned to him depending on a held post. In some situations, with a view of necessity to maintain continuous work of power plant systems and devices, certain operational tasks can be performed by other members of power plant crew than those to whom the obligations were assigned. The tasks should be however assigned with satisfying all requirements (according to knowledge, experience and capabilities of operators), hence a given task can be performed by the operator o_p (to whom it was assigned in the frame of his obligations) or by an operator who has the higher competences $k(o_j)$, i.e. that being higher ranked within professional hierarchy of power plant crew members (3):

$$k(o_p) \leq k(o_j) \;;\; \forall x_{ij} \in H \tag{3}$$

where:
- $k(o_p)$ – competences of the operator to whom i-th task was assigned in the frame of his obligations
- $k(o_j)$ – competences of the operator to whom the task x_{ij} was assigned in the schedule **H**
- x_{ij} – a factor which determines the assignement of i-th task to j-th operator.

During ship power plant operation one has to do with the situations in which the time allocated for realization of necessary tasks is limited, e.g.: staying in port, staying in shipyard. Therefore, the taking into account of the available time allocated for realization of tasks is necessary (4):

$$\sum_{i=1}^{n} t_i x_{ij} \leq T_S \;;\; \forall i, \forall j : i \in Z_Z,\ j \in Z_O \tag{4}$$

where:
- t_i – realization time of i-th task
- x_{ij} – a factor which determines the assignement of i-th task to j-th operator
- Z_Z – set of operational tasks
- Z_O – set of available operators
- T_S – termination time of i-th task realization, imposed from outside (e.g. by PSC, etc).

It should be stressed that in the presented approach to scheduling the operational tasks in ship power plant, certain general assumptions and simplifications were made. It was namely assumed that:
- every operator is able to realize only one task within a given time interval
- every task is realized only by one operator
- number of tasks to be realized in ship power plant greatly exceeds that possible to be realized by the operators
- every task is characterized by a few parameters saved in a data base or determined in advance during preceding stages (elimination of tasks impossible to be realized in given conditions, hierarchization of tasks) [1, 2]
- assignement of tasks to particular operators will be performed in accordance with the above described proffesional relationships (3).

The searched schedule expressed in a graphical form, will be hence a set of knapsacks (boxes) of an equal height corresponding to the available time Ts within which the tasks must be fulfilled (Fig. 1a). The operators o_j are graphically represented by knapsacks whose number corresponds to a number of operators available in power plant in a given time instant. To them are packed the operational tasks represented by blocks whose height corresponds to the realization time t_i of each of them, and whose breadth of base – to competences of the operator to whom the task is assigned in the frame of his obligations (Fig. 1b).

According to the presented definition of the problem in question one aims at filling the "knapsacks" to a maximum degree by using the blocks of maximum validity (i.e. importance from operational point of view in a given situation) or to a maximum degree of packing.

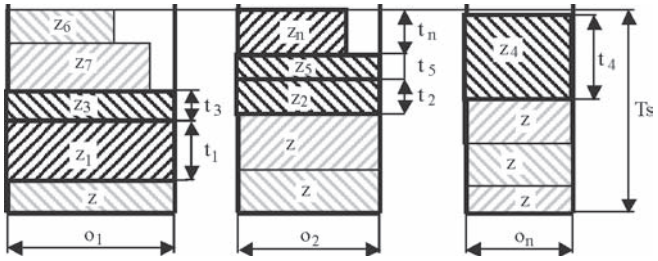

Fig. 2. *The example showing the assignement of operational tasks to three operators, i.e. packing three different knapsacks*

In Fig. 2 the example of possible solution of the problem in question is graphically presented.

Objective function

Large number of operational tasks of which their schedule is prepared, makes that the problem has many allowable solutions satisfying all appearing requirements and limitations. To find the best solution (optimum schedule) from the operational point of view, it is necessary to determine quality of each of the obtained solutions - i.e. the objective function Fj of optimization problem.

In the problem in question two following assessment criteria have to be applied:
- the most important tasks fj_1 (5) should be realized, i.e. the schedule should consist of the lists of the tasks assigned to every operator, and having the importance index wg_i of the possible largest value
- the time of realization of the tasks should be close to the available time for their realization, fj_2, (6), in other words to obtain the best use of the available time.

$$fj_1 = wg_1 x_{1j} + wg_2 x_{2j} + \ldots + wg_n x_{nj} = \sum_{i=1} wg_i x_{ij} \tag{5}$$

$$fj_2 = x_{1j}\frac{t_1}{T_S} + x_{2j}\frac{t_2}{T_S} + x_{3j}\frac{t_3}{T_S} + \ldots + x_{nj}\frac{t_n}{T_S} = \frac{\sum_{i=1}^{n} t_i x_{ij}}{T_S} \tag{6}$$

In accordance with the way of formulation of optimization function, described in [9], in the presented problem such function can be assumed to be a combination of assessment criteria of scalar form, generally defined as a weighed sum of: task importance indices and time intervals for their realization.

In the case of the so formulated objective function one has to do with two-criterion optimization. By introducing to it the coefficients ρ_1, ρ_2 called the criterion weighing factors, a choice on which criterion would be more important, becomes possible. Such choice is made by the decision maker, i.e. chief engineer, depending on needs appearing in a given instant. The coefficients ρ_1, ρ_2 can take values from the interval <0, 1>, and their sum should be always equal to 1. Hence it is usually assumed that: $\rho_2 = (1 - \rho_1)$.

Therefore the best schedule, out of all allowable solutions, is that for which the sum of the weighed sums of two presented

criteria, fj_1 and fj_2, for all considered operators, reaches a maximum (7).

$$Fj = \max \sum_{j=1}^{o} \sum_{i=1}^{2} sk \cdot \rho_i \cdot fj_i(o_j) = \sum_{j=1}^{o} \left(sk \cdot \rho_1 \cdot \sum_{i=1}^{n} wg_i x_{ij} + (1-\rho_1) \frac{\sum_{i=1}^{n} t_i x_{ij}}{T_S} \right) \quad (7)$$

where:
- $i = 1,2,3,....,n$ – number of tasks
- $j = 1,2,3,....,o$ – number of operators
- ρ_1 – weighing factor of the criterion fj_1
- x_{ij} – factor which determines the assignement of i-th task to j-th operator
- sk – scale (a coefficient so selected as to obtain balanced values of sum components)
- wg_i – task importance index.

However such form of objective function suffers a deffect consisting in that the schedule consisted of many tasks of a low importance index (i.e. rather non-important) and short realization time, can show a greater value of such function than that consisted of the tasks of a high importance index and a longer time of realization of particular tasks.

In this connection a modified form of it is here proposed. The change consists in supplementing the first criterion with the relative task importance factor kw_i (8) which is the product of the relative realization time of a given task and the relative competences necessary to its realization. In compliance with the notation used in the knapsack problem the product in question represents a relative size of the rectangle (height x breadth) with regard to the knapsack in which a given object is placed.

$$kw_i = t_{wzgl} \cdot k_{wzgl} = \frac{t_i}{T_S} \cdot \frac{k_i}{k_o} \quad (8)$$

where:
- kw_i – relative importance factor of i-th task
- k_i – competences necessary for realization of a given task
- k_o – competences of operator to whom a given task is assigned in the schedule.

In such situation the objective function will be of the following form:

$$Fj = \max \sum_{j=1}^{o} \left(sk \cdot \rho_1 \cdot \sum_{i=1}^{n} wg_i kw_i x_{ij} + (1-\rho_1) \frac{\sum_{i=1}^{n} t_i x_{ij}}{T_S} \right) \quad (9)$$

Such form of the objective function eliminates the above mention deffect consisting in possible elaboration of an optimum schedule which contains many tasks of a low importance.

Decision variables

In the so formulated problem the decision variables are as follows: the event whether a given task will be included into the considered schedule or not, determined by value of the parameter x_{ij} which can take one of the two values: 1 or 0, (10), as well as by the time instants of beginning the realization of particular operational tasks, tr_i. The decision maker decides which of the tasks will be included into the schedule under elaboration, as well as in which sequence they should be realized.

$$x_{ij} = \begin{cases} 1 & \text{If the task is in the schedule} \\ 0 & \text{If the task is beyond the schedule} \end{cases} \quad (10)$$

The time instant of task beginning, tr_i,will depend on the position a given task takes in the schedule. Hence for each of the tasks the variable will be directly dependent on the sum of values of the realization time, t_i, of the tasks preceding in the schedule. Values of tr_i (time instant of beginning the realization of i-th task) are not direct decision variables because they are not taken into account directly in the process of scheduling (such value does not appear in the objective function equation).

The quantity tr_i can take only certain limited values. They cannot be smaller than zero (as it is not possible to determine time of realization of a given task in the past – its minimum is the beginning of the considered schedule). And, its maximum cannot be greater than the time interval covered by the schedule in question, T_S, (11).

Moreover, with a view of that realization time of particular tasks is given by ship engineers as well as producers of machines only in an approximate way, the decision variables can be given values with the accuracy of 5 min. Such accuracy of the decision values seems to be rationally justified; it will be discrete values, that will definitely make number of allowable solutions of the optimization problem of scheduling the operational tasks in ship power plant, lower. For the decision variables tr_i the following range of their variability can be provisionally determined:

$$0 \le tr_i < T_S \;\; , \;\; tr_i = 0,5,10,... \;\; ; \;\; i = 1,...,n \quad (11)$$

where:
- tr_i – time instant of the begining of i-th task realization
- T_S – time interval covered by the schedule in question.

Constraints

In such approach to the considered problem two main constraints (limitations) appear:
- the total realization time of the tasks assigned to each of the operators cannot be greater than the available time interval t_s provided for their realization (3)
- a given task can be assigned only once in the schedule, (12):

$$\sum_{i=1}^{m} x_{ij} \in H \le 1 \quad \forall i \in Z_Z \quad (12)$$

where:
- $x_{ij} \in H$ – tasks placed in the schedule H,

The remaining constraints of the problem are the following:
- the way of assigning the tasks to particular operators, determined by (2)
- every task is realized by one of the operators only:

$$\sum_{i=1}^{m} o_n(x_{ij}) \le 1 \quad \forall n \in Z_O \quad (13)$$

SELECTION OF CALCULATION METHOD FOR SOLVING THE PROBLEM

Method of searching the space of general problem solutions

From the point of view of calculations the knapsack problems are deemed difficult. Like in the case of other optimization problems, many different calculation methods for solving the problems of the kind have been elaborated. In

the subject-matter literature can be found both approximate methods (reduction and approximation ones) and exact ones such as: network approach, dynamic programming or searching methods. For solving the problem of optimization of the schedule of operational tasks in ship power plant the last of the presented method, i.e. the method of indirect searching, called also the searching with reversals. The method was selected due to its simplicity, as it contains basic steps of almost all searching methods and simultaneously is one of the quickest among them [7].

Algorithm of the method of searching with reversals finds a solution of a given problem by applying the systematic searching its whole space of solutions. It makes use of the space represenation in the form of the tree in which problem variables correspond to successive levels of the tree and each of the tree nodes has at last two branches corresponding to 0-1values (Fig.3). The method of searching the space of solutions consists in forming first the left branch, and as soon as the searching process on the left side is terminated the right branch (of the tree) is formed and the searching is moved to this side. Such method of forming the tree nodes is very economical, and despite this, no three which could lead to a better solution, is ommited.

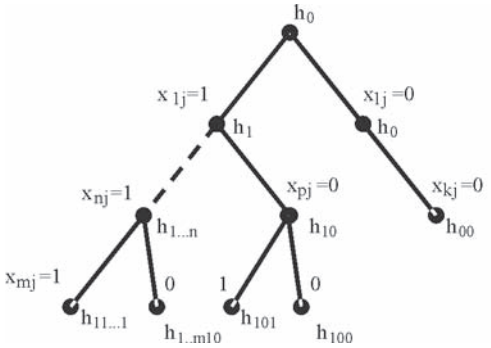

Fig. 3. *Way of elaborating the solution tree for the knapsack problem by means of searching method with reversals. Numbers given at nodes correspond to values of the coefficient which determines the assignment of i-th task to j-th operator in the considered schedule harmonogramie $h_{n...n}$.*

Method of searching the solution space of the problem of assigning the tasks to several operators in ship power plant

The above presented algorithm of searching the space of allowable solutions of optimization problem deals with the one-knapsack problem. However in ship power plant the situation occurs in which the tasks must be assigned to a greater number of operators; hence the presented algorithm requires some modifications to be introduced. For further considerations is selected the following situation usually met in merchant fleet, i.e.: four operators to whom operational tasks are assigned. They are: chief engineer – I, second (first assistant) engineer – II, third engineer – III, fourth engineer – IV.

The use of the greater number of operators (four) makes that every task, provided the imposed constraints do not hold off, can be assigned to any of the four operators. Therefore in the state in which to a given task the value of the parameter x_{ij} equal to 1 is attributed (Fig.3), four additional solution variants appear (Fig.4a). However the principle of searching the space of solutions remains the same as in the case of the one-knapsack problem, hence the solutions on the left-hand side of the solution tree are searched (Fig.4b). The checking of possibility of assigning a given task is started from the operator whose proffessional competences are the lowest. If any of the constraints does not allow to assign it to this operator the task is tried to be assigned to that whose competences are the lowest among the remaining operators available in a given moment.

The assignement of the task to one of the operators creates the new allowable solution in which value of the objective function is checked („sum of weighing factors" of each of the operators) and compared with the best solution has been obtained so far. If the calculated value of the objective function is greater than that has been obtained so far, its new value and the new entire solution are saved.

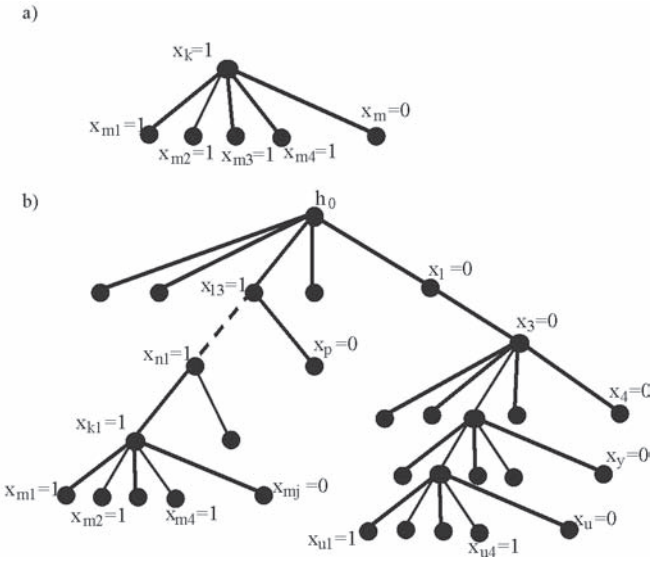

Fig. 4. *Modified way of forming three solutions for the multi-knapsack problem by means of the method of searching with reversals*

In the case of scheduling the operational tasks in ship power plant, the successive solutions h_n would be created by adding or omitting (the factor x_i in Fig. 4) one by one successive tasks taken from the hierarchized list of tasks, to each of the operators, with simultaneous checking all constraints and value of the objective function for each solution in each case. The process will be continued up to the moment when adding a successive task makes the available time Ts exceeded by the sum of realization time values of the tasks included in the schedule for a given operator or no task which would improve the schedule by increasing the value of the solution objective function, is found.

The graphical representation of the algorithm for searching the solution space for the problem of assigning the operational tasks, considered as a knapsack problem, is shown in Fig. 5.

COMPUTER SYSTEM FOR PLANNING THE OPERATIONAL TASKS, BASED ON THE PRESENTED MULTI-KNAPSACK PROBLEM

In order to check the above presented mathemetical model as well as the method of solving of the decision problem usually faced by ship chief engineers, a prototype computer software for aiding the chief engineer in planning the operational tasks in ship power plant in some definite conditions, was elaborated.

The presented graphical interface of the software consists of two main parts. The first of them, shown on the right-hand side of Fig. 6, is characteristic for computer systems applied in ship power plants and it represents structure of ship power plant design solution.

The second part of the interface (on the right-hand side of the screen), i.e. working one, consists of two bookmarks:

- ⇨ TASKS (Fig.6) in which the operational task parameters are defined for particular elements of ship power plant structure
- ⇨ SCHEDULE (Fig.7) in which the functions triggering the searching process of allowable solution space for the

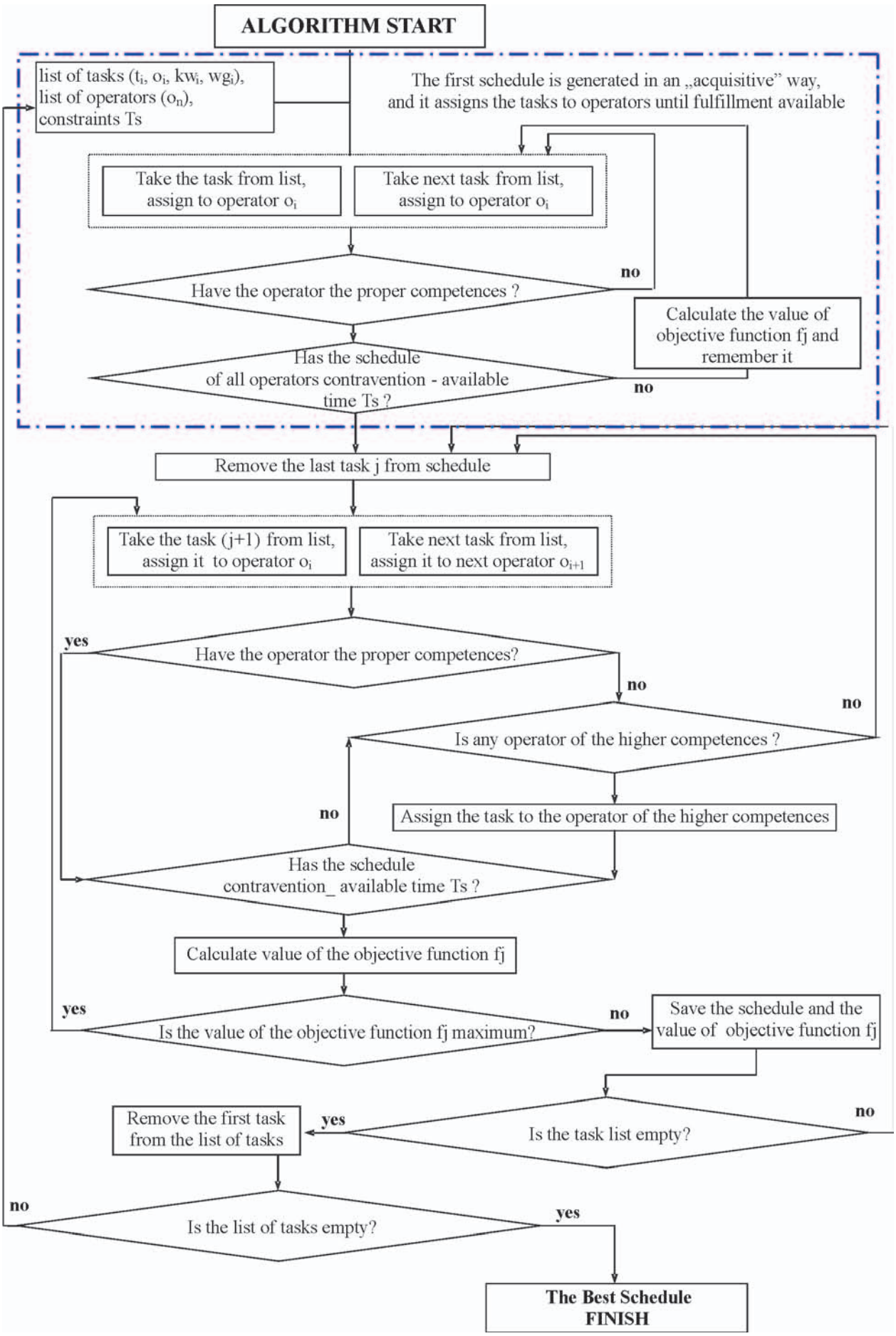

Fig. 5. *Algorithm of searching the solution space for multi-knapsack problem*

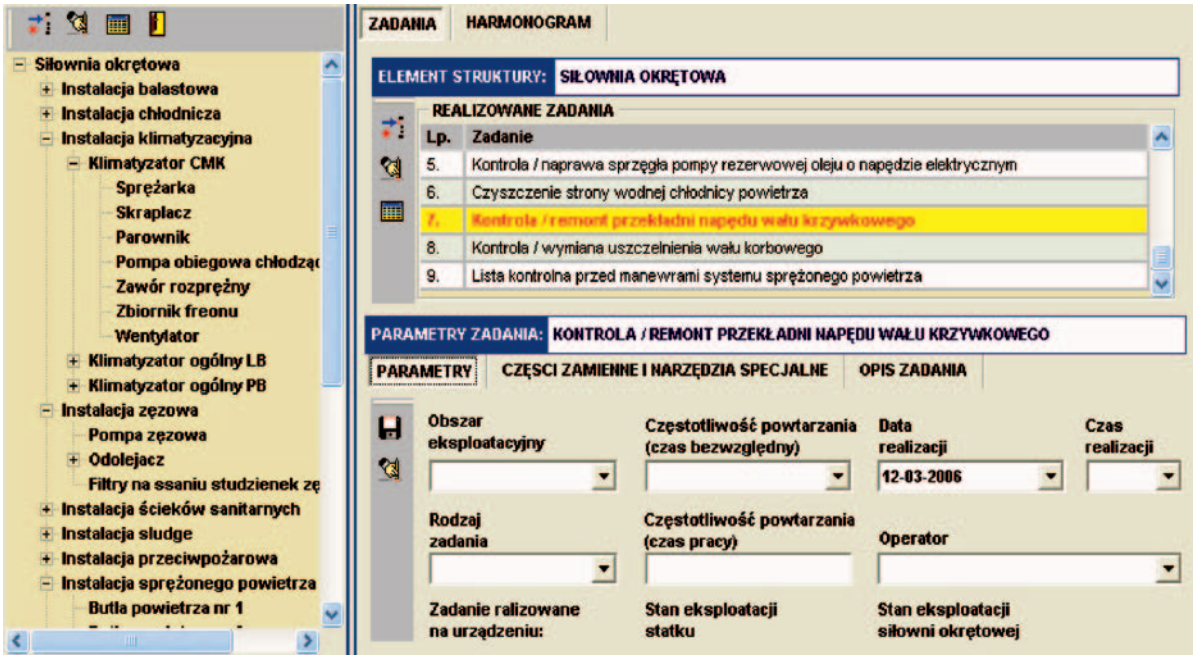

Fig. 6. *An example screen of the graphical interface of the computer software for assigning the operational tasks in ship power plant. Ship power plant structure (on left hand side), task operational parameters (on rightrighthand sideright hand side)*

Notation displayed on:
Left hand side area : Siłownia okrętowa – Ship power plant, Instalacja balastowa – Ballast system, Instalacja chłodnicza – Cooling system, Instalacja klimatyzacyjna – Air conditioning system, Sprężarka – Compressor, Skraplacz – Condenser, Parownik – Evaporator, Pompa obiegowa chłodząca – Cooling circulation pump, Zawór rozprężny – Expansion valve, Zbiornik freonu – Freon tank, Wentylator – Fan, Klimatyzator ogólny LB – General air conditioner – Portside, Klimatyzator ogólny PB – General air conditioner – Starboard side, Instalacja zęzowa – Bilge system, Pompa zęzowa – Bilge pump, Odolejacz – Oil separator, Filtry na ssaniu studzienek zęzowych – Filters at bilge well suction, Instalacja ścieków sanitarnych – Sanitary sewage system, Instalacja sludge – Sludge system, Instalacja przeciwpożarowa – Fire extinguishing system, Instalacja sprężonego powietrza – Compressed air system, Butla sprężonego powietrza nr.1 – Starting air receiver no.1, ….
Right hand side area: Zadania – Tasks, Harmonogram – Schedule, Element struktury: Siłownia okrętowa – Structure element: Ship power plant, Realizowane zadania – Realized tasks, Lp. .. Zadanie – No...Task, 5. Kontrola/naprawa sprzęgła pompy rezerwowej oleju o napedzie elektrycznym – Control/ repair of coupling of electrically driven stand–by pump, 6. Czyszczenie strony wodnej chłodnicy powietrza – Cleansing of air cooler water side, 7. Kontrola/remont przekładni napędu wału krzywkowego – Control/repair of reduction gear of camshaft drive, 8. Kontrola/wymiana uszczelnienia wały korbowego – Control/ replacement of crankshaft packing, 9. Lista kontrolna przed manewrami systemu sprężonego powietrza – Check list before manoeuvers of air compression system, Parametry zadania: Kontrola/remont przekładni napędu wału krzywkowego – Task's parameters : Control/repair of reduction gear of camshaft drive, Parametry..Części zamienne i narzędzia specjalne..Opis zadania – Parameters..Spare parts and special tools.. Task's description, Obszar exploatacyjny.. Częstotliwość powtarzania (czas bezwzględny)..Data realizacji..Czas realizacji… – Operational area.. Repeating frequency (absolute time).. Realization date… Realization time.., Rodzaj zadania…Częstotliwość powtarzania (czas pracy)..Operator..– Type of task..Reapeating frequency (time of operation).. Operator.., Zadanie realizowane na urządzeniu:…Stan eksploatacji statku..Stan eksploatacji siłowni okrętowej.. – Task realized on the device : …Ship's operation stage.. Ship power plant's operation stage...

operational task assigning problem are contained. Its user unaided defines two main parameters of the optimization process:

- → „Maximum time", i.e. the time interval for which the schedule is considered (e.g. port staying time, sea voyage time etc)
- → „Criterion weighing factor" (the parameter ρ in Eqs. 7 and 9), i.e. that determining which choice is of a greater importance: that of the most important tasks or that of the most effective use of the available time.

The main area of the interface screen is divided into two parts in the first of which the obtained results on " Schedule variants" are displayed, and in the other, i.e. „Gantt's Diagrams", graphical presentation of the obtained results for each of the operators is shown in the form of Gantt's diagrams. Each of the operators is assigned by an area in which the "rectangulars" representing the assigned operational tasks are drawn. The area is shown as a white rectangular whose dimensions stand for:

- the time interval available for task realization (length of the rectangular)
- the competences attributed to a given operator (height of the rectangular).

In the area „Schedule variants " the following data are displayed:

- ✦ the tasks assigned to each of the considered operators; only identification numbers of assigned tasks are displayed to make control of the software's operation correctness, possible
- ✦ sum of values of the task realization time intervals
- ✦ sum of values of the task weighing factors
- ✦ sum of values of the weighing factors for the whole schedule, which simultaneously stands for the quality index of a given solution.

In the other part of the interface screen are placed also two keys whose switching-on leads to display and visualization of all solutions determined in the course of optimization process.

In the status bar placed at the lower edge of the interface screen (Fig. 7) are displayed three aditional information data important in analyzing the obtained results:

- ✧ number of the analyzed solutions
- ✧ number of the tasks taken into account
- ✧ calculation time consumed for finding the best solution.

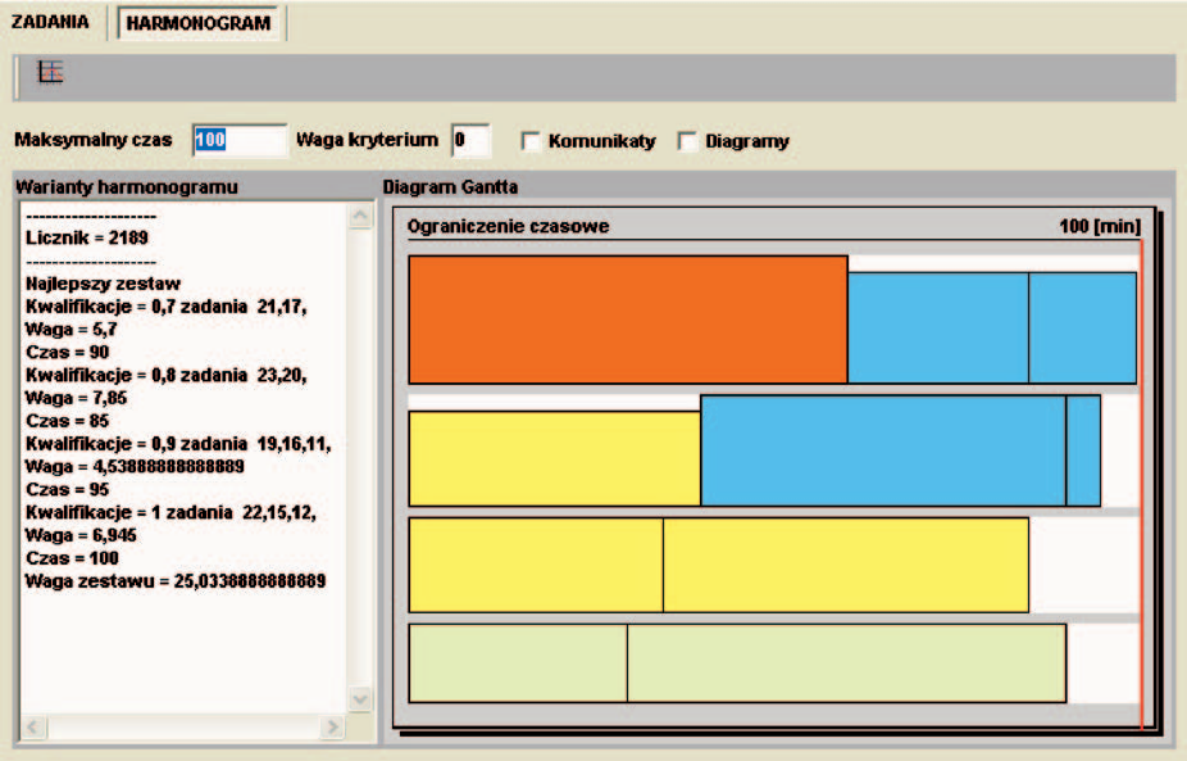

Fig. 7. *An example fragment of the graphical interface of the computer software, which displays results of optimization process of assigning the operational tasks in ship power plant*

Notation displayed on:
Upper horizontal bar : Zadania -Tasks, Harmonogram – Schedule
Upper area : Maksymalny czas – Maximum time, Waga kryterium-Criterion weighing factor, Komunikaty – Messages, Diagramy – Diagrams
Left hand side area : Warianty harmonogramu – Schedule variants, Licznik – Counter, Najlepszy zestaw – The best set, Kwalifikacje... zadania.. – Competences... tasks no., Waga – Weighing factor, Czas – Time, Kwalifikacje ...zadania – Competences...tasks no., Waga – Weighing factor, Time – Czas, Kwalifikacje… zadania – Competences... tasks no., Kwalifikacje… zadania – Competences... tasks no. , Waga – Weighing factor, Czas – Time, Set's weighing factor..
Right hand side area : Wykresy Gantta – Gantt's diagrams, Ograniczenie czasowe – Time limitation,
Lower horizontal bar : Akademia – Gdynia Maritime University, Liczba rozwiązań – Number of solutions, Liczba zadań – Number of tasks, Czas obliczeń – Calculation time.

RECAPITULATION AND CONCLUSIONS

In this paper has been presented an approach to solving the decision problem associated with attribution of operational tasks realized by relevant operators in ship power plant, with taking into account different conditions. The problem has been presented as a packing (knapsack) problem often used for scheduling the tasks in industry.

The paper covers only one, the last stage of the considered decision problem, out of its several stages such as the collecting and analyzing of information concerning operational tasks, their selection, generating the schedules being single allowable solutions of the problem in question.

A mathematical model of two-criterion optimization process of scheduling the operational tasks in ship power plant, i.e. finding the best solution out of the set of allowable ones, has been presented, and within its frame the following has been done in particular:

- The objective function which takes into account the crucial elements considered by chief engineer in scheduling the operational tasks in ship power plant: i.e. importance of a given task, competences of each of the operators, time available for realization of necessary tasks, has been elaborated.
- The most important limitations (constraints) occurring in scheduling the tasks in ship power plant have been defined.
- The method of searching the solution space, i.e. the searching algorithm with reversals, has been selected and modified for its application in the problem in which four operators are considered.
- The prototype computer software for assigning the operational tasks in ship power plant, based on the presented mathematical model, has been elaborated.

Several assumptions and limitations have been made, among which the following are the most important:

- Every task can be realized by one of the operators only.
- Every operator is able to realize only one task in a given time.

Further investigations are aimed at checking whether the assumed objective function as well as the constraints are sufficient for solving the problem in question, as well as whether the assumed method of thorough searching would be fast enough for application to ship power plant problems.

BIBLIOGRAPHY

1. Kamiński P.: *Formulation of objective function of the decision - making problem in ship power plant*. Proceedings of 4th Conference on Engineering Design in Integrated Product Development, Zielona Góra 2006
2. Kamiński P.: *Identification of elements of decision problem of ship power plant management* (in Polish), Proceedings of

Polyoptimization & CAD Conference (Materiały Konferencyjne Polioptymalizacja i CAD), Mielno 2006
3. Kamiński P.: *Selected problems associated with ship power plant operation* (in Polish). Proceedings of the Conference on Design and Management of Realization of Production (Materiały Konferencyjne – Projektowanie i zarządzanie realizacją produkcji), Zielona Góra 2005
4. Kamiński P, Tarełko W., Podsiadło A.: *Information sources used in the aiding system for ship power plant management* (in Polish). 25th International Symposium on Ship Power Plants (XXV Międzynarodowe Sympozjum Siłowni Okrętowych), Gdańsk 2004
5. McDiarmid C.J.H.: *The Solution of a Timetabling Problem*. Journal of Institute of Mathematics Applications, 9, pp. 23-34, 1972
6. Smutnicki C.: *Algorithms of sequencing* (in Polish), Exit, Warszawa 2002.
7. Sysło M.M., Doite N., Kowalik J.S.: *Algorithms of discrete optimization* (in Polish), PWN, Warszawa 1995
8. Szwed C., Toczyłowski E.: *Optimization of compartment resources in conditions of elastic studying* (in Polish), Proceedings of Polyoptimization & CAD Conference (Materiały Konferencyjne Polioptymalizacja i CAD), Mielno 2000
9. Tarnowski W.:*Simulation and optimization in MATLAB software* (in Polish), WSM Publishing House -Wydawnictwo WSM, Gdynia 2001

CONTACT WITH THE AUTHORS

Piotr Kamiński, M.Sc., Eng.
Wiesław Tarełko, Assoc.Prof., Eng.
Faculty of Marine Engineering
Gdynia Maritime University
Morska 81-87
81-225 Gdynia,POLAND
e-mail : pkam@am.gdynia.pl

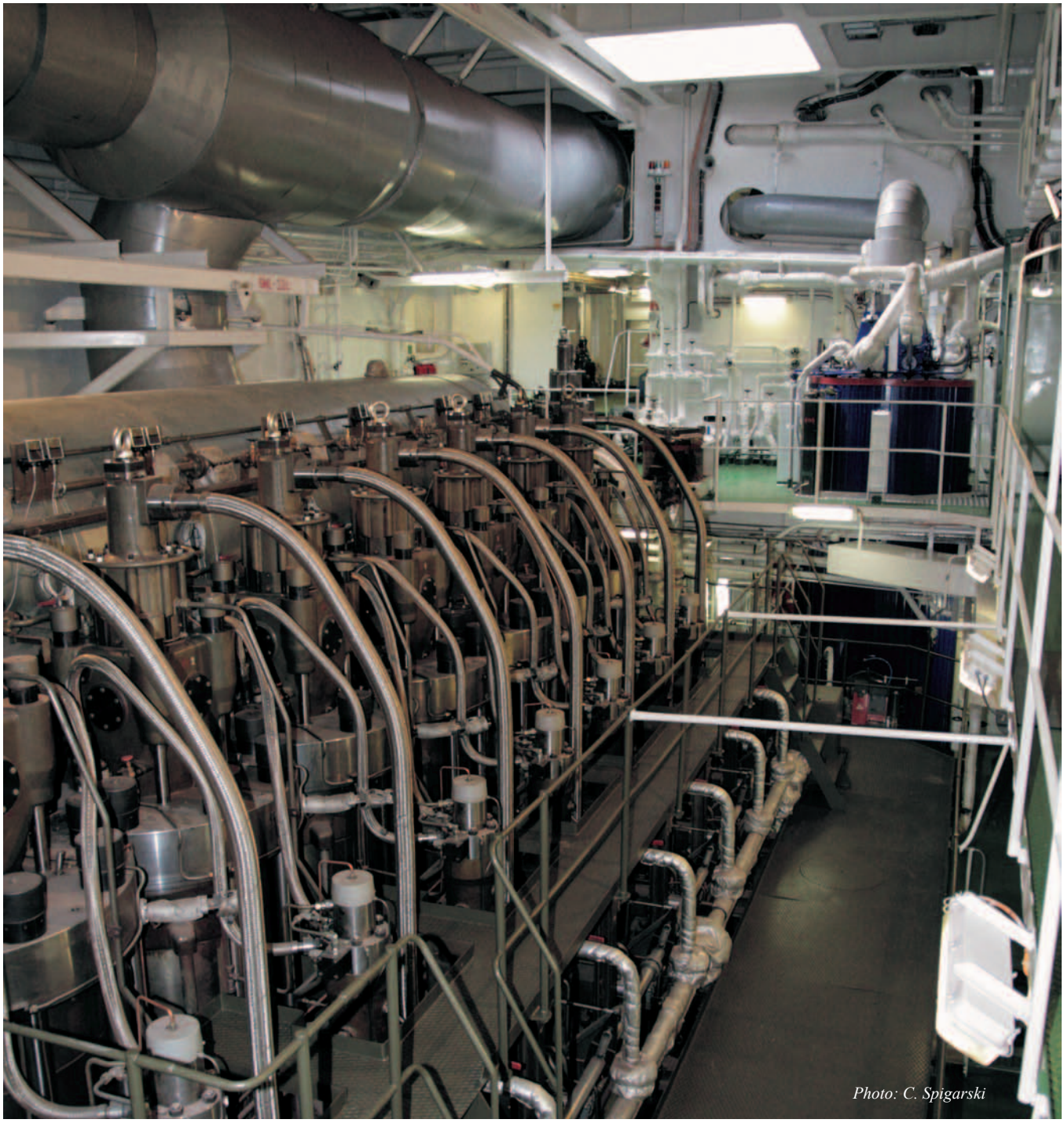

Photo: C. Spigarski

POLISH MARITIME RESEARCH 1(55) 2008 Vol 15; pp. 52-55
DOI: 10.2478/v10012-007-0051-8

Statistical analysis of sea accidents and breakdowns in the Polish Navy

Zbigniew Korczewski,
Polish Naval University

ABSTRACT

This paper presents the results of systematic, statistical approach to naval accidents and breakdowns which occurred in the Polish Navy between years 1985 – 2004. Additionally, the author of this work has made an initial assessment of the human factor. Human errors, which appeared on considered warships in the examined period of time, have been analyzed in the overall number of accidents and breakdowns.

Keywords: naval accidents and breakdowns, statistical analysis, human factor

INTRODUCTION

A warship stands for a complex technical system, which comprises a lot of technical equipment, that operational reliability has a serious impact on her warfare ability [2, 4, 6, 12, 13]. During warfare there may happen partial or total loss in functioning mechanisms and installations, in a word - the occurrence of breakdowns.

Breakdowns of ship's technical equipment can be classified according to the occurrence of the following causes: the impact of enemies warfare agents, materials' defects and defects within the production process, constructional defects, technological defects in the process of renovation, excessive natural process of material's wear and tear, not fulfilling the requirements for operation and service of equipment, not taking security measures while storing dangerous cargoes e.g. explosive materials, petroleum products and other chemical components of serious fire hazard.

Failures which are caused by navigational mistakes or maneuverability represent the next group of possible reasons for ship accidents and breakdowns. But taking into consideration safety of a warship during combat missions as well as during daily operation it goes without saying that fires represent the greatest threat [2, 4, 5, 6, 11]. Despite the fact that fire very rarely leads the ship to sink, the destruction is usually very serious and always depends on the crew's training perfection in a damage control.

STATISTICAL APPROACH TO NAVAL ACCIDENTS AND BREAKDOWNS

Naval experiences show that even highly organized fleets struggle against accidents and technical breakdowns which couldn't be completely eliminated. This paper presents analysis of accidents and technical breakdowns which took place on warships of the Polish Navy between years 1985 – 2004.

The considered accidents and technical breakdowns were divided into three time periods: years 1985 – 1990, years 1991 – 1998 and years 1999 – 2004.

This division has been accepted taking into consideration geopolitical changes which had happened in Europe in the late 80's, and the fact of joining Poland to NATO on March 12, 1999 which was related to them. These transformations have been reflected in the Polish Navy forces developmental plans spanning years up to 2012, whose main goal is to increase the operational potential within strict financial limits [1]. In these plans it was assumed that the increase of the operational potential would be based on replacement or modernization of presently possessed warships. As a consequence, the warships of outdated construction and the ones of which operation was not included in plans of state's strategic defense had been withdrawn from operation (among them landing crafts 770 and 771 type, submarines 641 type, destroyer 61MP type, some of cutters 205 type, submarine chaser 912M type), and replaced by, for instance, submarines "Kobben" type, guided missile frigates "Oliver Hazard Perry" type, logistic support ship "Kontradmirał Xavery Czernicki" or modernized warships such as rescue ship 570 type, minesweeper 206F and 207D type, mine transport - landing warship 767 type, guided missile warships 660 type, frigate 620D type. Moreover, building multi-purpose corvette 621 type has been started.

While analyzing consequences of these alterations it should be taken into consideration that a warship is a complex technical system, and if so, then everything should be done in order to interpret and modify regulations aiming at keeping its safety of floating in combat operation and daily action at the highest level.

Statistical data prepared by the Polish Navy Commission of Warship Accidents and Breakdowns reveal that between years 1985 – 2004 there have been recorded 159 warship accidents and breakdowns and their overall structure examined in certain periods, taking into account the annual mean, is presented in Fig. 1.

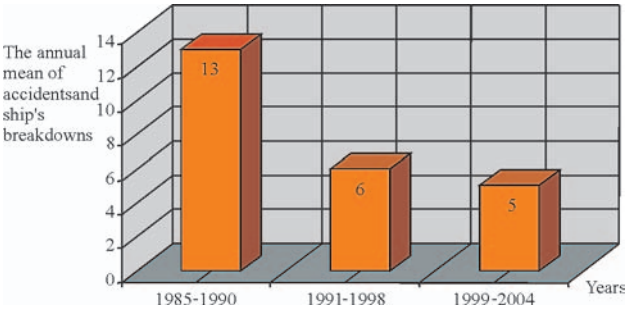

Fig. 1. *The overall structure of accidents and ship's breakdowns between 1985 - 2004*

The structure of accidents and technical breakdowns shown in Fig. 2 indicates that the most numerous are technical causes [4, 6]. They constitute 65% of the whole number of accidents and breakdowns being the greatest losses in our Navy and they have increasing tendency.

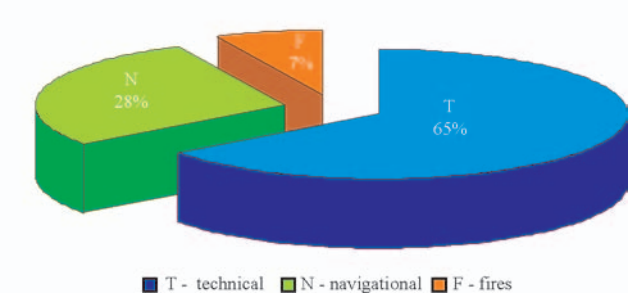

Fig. 2. *The structure of accidents and breakdowns of ships between 1985 - 2004 expressed in percentage terms*

Data shown by numbers [4, 6] given in Fig. 3 tell, that between 1985 – 2004 there have been recorded different mean annual technical accidents and breakdowns.

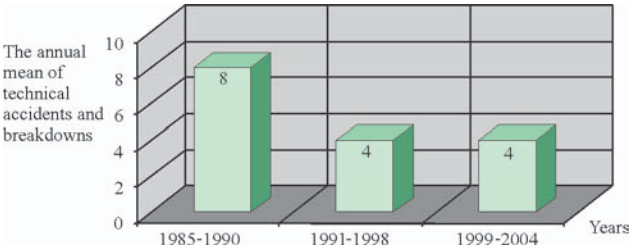

Fig. 3. *The total number of the annual mean of technical accidents and breakdowns in years 1985 - 2004*

Fig. 4 presents numerical data concerning causes of accidents and technical breakdowns between 1985 -2004, whereas figure 5 – their structure expressed in percentage terms.

By analyzing these data of breakdowns with relation to real causes, it should be stated, that the greatest number of breakdowns is observed due to defects of materials and technological production and defects during technological renovation. However, in the examined time period 1991–1998 initial decrease in number of accidents and technical breakdowns resulting from constructional defects was followed by their increase in the years 1999 – 2004 and they account for the highest number of the total number of accidents and technical breakdowns in the analyzed period of time.

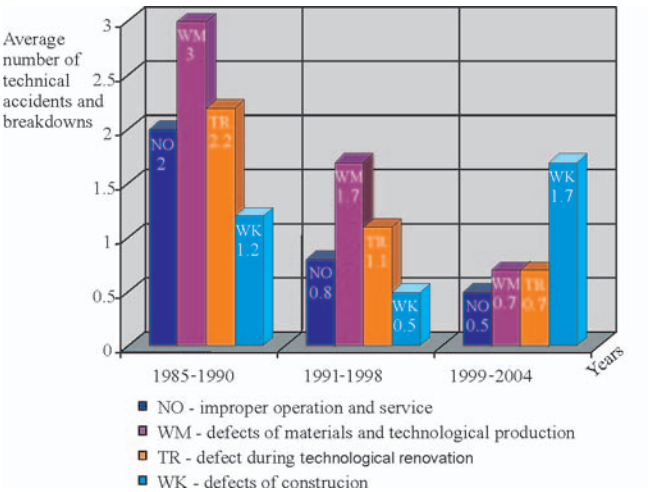

Fig. 4. *The causes of technical accidents and breakdowns in years 1985 - 2004*

In the examined period of time spanning years 1985 – 2004, 103 accidents and technical breakdowns happened. From this analysis, concerning the percentage of particular causes of accidents and breakdowns, we should infer that still the highest number of breakdowns are recorded due to defects of materials and technological production which equal 34% of the total number of technical accidents and breakdowns. Considerable amount of breakdowns results from defects of technological renovation, which constitute 25%, although the number of technical accidents and breakdowns caused by improper operation and service still reach relatively high level, which amounts to 20% of total number of technical accidents and breakdowns and it is here where we can see the great considerable scope for action of the persons responsible for the safety of floating.

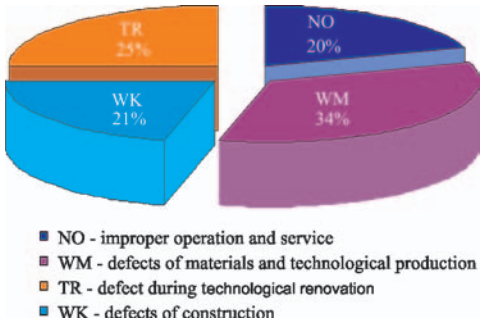

Fig. 5. *The structure of technical accidents and breakdowns in years 1985 - 2004 in percentage terms*

Failures of ship's technical equipment also occur due to mistakes in navigation and maneuvering warships. Numerical data shown in Fig. 6 indicate that the most frequent causes of those breakdowns between 1985 -1990 were strikes on a quay and obstructions to navigation. The situation has changed between years 1999 – 2004, when grounding prevailed. It was mainly caused by improper maneuvering through main fairways (main navigable channels), taking more precisely, inaccurate assessments of the navigational situation made by the persons responsible for the safety of floating.

Analyzing the structure of accidents and warship failures in technical equipment resulting from navigational mistakes expressed in percentage terms and shown in Fig. 7, it could be observed that strikes on quays and obstructions to navigation constitute 35%, whereas collisions with other ships – 30% of the total number of accidents and navigational breakdowns. Ship collisions and strikes on quays and obstructions to navigation

are the consequence of human errors in maneuvering, failures of the propeller pitch control system and wrong decisions taken by the persons responsible for the safety of floating. The number of grounding grows as well, which equal 23% of the total number of accidents and breakdowns resulting from navigational mistakes and this process has increasing tendency.

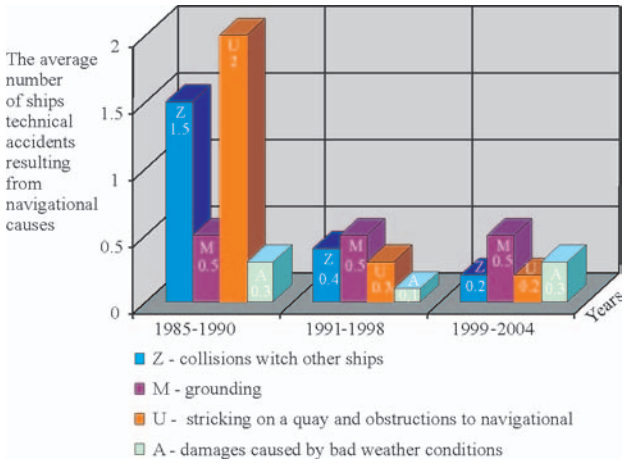

Fig. 6. The overal structure of accidents and ship's technical equipment resulting from navigational causes in years 1985-2004

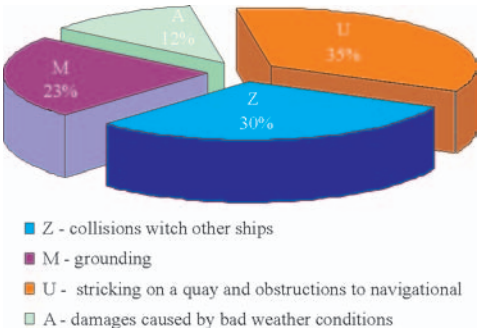

Fig. 7. The structureof accidents and failures in ships technical equipment resulting from navigational mistakes between 1985 - 2004 expressed in percentage terms

Taking into consideration the structure of accidents and breakdowns between 1985 – 2004, it could be observed that fires amounted to 7% of their total number. They occurred primarily due to electrical failures in electrical installations, breakdowns in technical equipment and mechanisms, self ignition of pure oxygen coming into contact with oil – extracted materials (the crew was found partly at fault) and defects in firing. It may be concluded that such a small number of fires is probably related to crews' absolute compliance with fire – fighting regulations and established requirements regarding STCW 95 convention according to which, fire – fighting trainings of crews are carried out. Recently, crews of warships have undergone such trainings as well.

According to the statistical analysis placed in the elaborations as [3,5,9] majority of accidents at sea (about 80%) are caused by operation in which appear Human and Organizational Errors (HOE). Designing and constructing reasons constitute 20% of HOE. The rest of causes are due to operation reasons which depend on such factors as: culture of society, organization, human error and system – where it can be distinguished design standards, operation characteristics, information on operation characteristics for functional persons, weather factors and constructional characteristics of a warship. The potential causes of naval accident of the warship are illustrated in Fig. 8, which was created on the basis of [5].

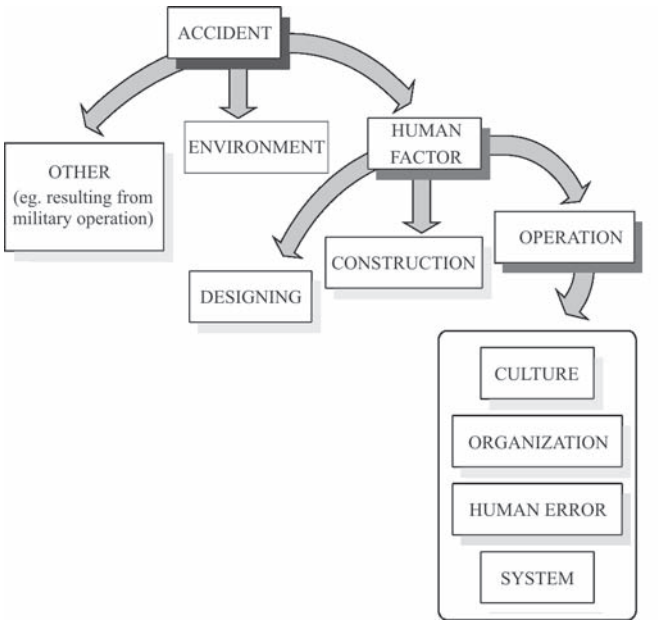

Fig. 8. The causes of naval accidents of a warship at sea

By means of surveys through the accidents and breakdowns occurring on warships of the Polish Navy between years 1985 – 2004, which are shown in figure 9, the author of this work has made initial assessment of human factor.

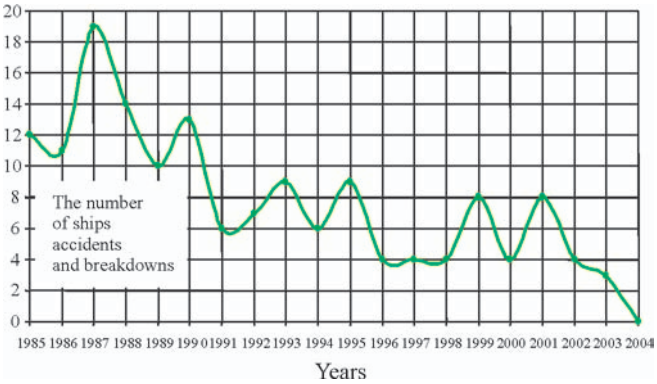

Fig. 9. General number of warships accidents and breakdowns in the time period 1985 - 2004

Human errors, which appeared on warships in the examined period of time, were analyzed in the overall number of breakdowns, as shown in figure 10.

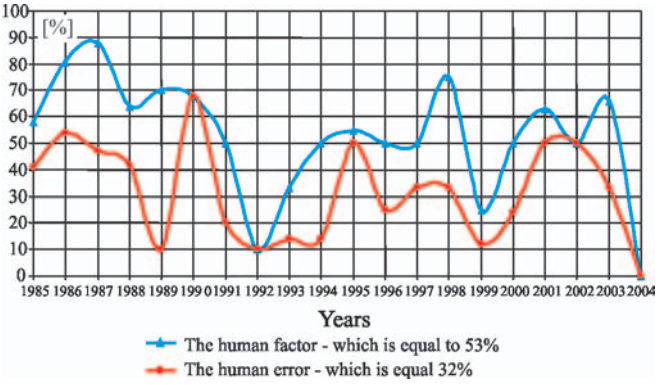

Fig. 10. The human factor and human error in total number of ships accidents and breakdowns in year between years 1985 - 2004

Numerical data presented on the foregoing graph provide information on the total mean of human factor in overall

number of breakdowns on warships of the Polish Navy. The mean amounts to 53% and current values fluctuates between 88% in the year 1987 and 10% in 1992. The cause of the rest of accidents and breakdowns was the widely interpreted marine environment. On average, a human error was the reason for 32% of total number of accidents and breakdowns and current values fluctuated between 68% in 1990 and 10% in 1992. (data for 2004 were collected up to October, 2004 and were equal to 0%).

Accidents and breakdowns of warships, which occurred as a result of human error, were mainly caused by excessive speed not adjusted to the surrounding navigational and maneuvering conditions, inaccurate maneuvering, improper operation and service of machines and warship technical equipment, carelessness, lack of proper assessment of the situation, improperly kept watch, and in some cases - even the bad routine.

It is common knowledge that the best form of schooling are training and exercises on a warship and group of warships at sea, after adequate theoretical and practical preparation of crews in their naval bases.

Taking into account that research carried out in our Navy between 1985 – 2004 it might be initially analyzed from the view of spending moto - hours ascribed to each warship. So called running hours of the main (propulsion) engines on three chosen types of warship in the years 1985 – 2004, are illustrated in Fig. 11. From numerical data presented in this figure, we can infer that in the period of time spanning years 1985 – 2004 the time of real work of the main engines on the considered representatives was reduced by 30% or even 60% in relation to the year 1985.

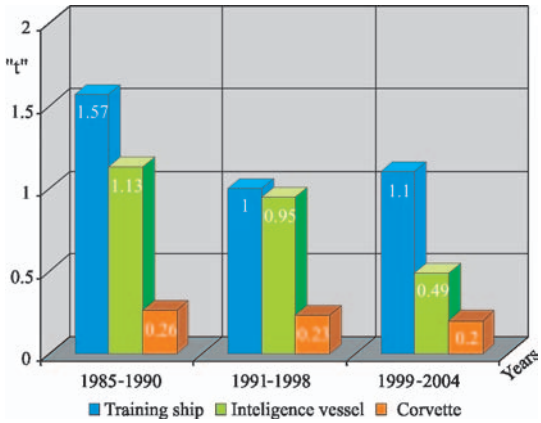

Fig. 11. *Time of work the "t" main engines on the three chosen ship types between 1985 - 2004*

Besides, taking into account that the Polish Navy constitutes a vital element in the structure of state's defense (528 km of the seashore protected), everything should be done in order to keep marine awareness in the country at the highest level for the sake of business in the Polish marine territory.

CONCLUSIONS

- From the carried out analyses of warship accidents and breakdowns between years 1985 – 2004 it can be assumed that the most frequent ones happened due to technical failures (65%). They cause the greatest loss in the Polish Navy, and have an increasing tendency.
- As a consequence of navigational mistakes, including grounding, the percentage of accidents and technical breakdowns is grooving as well. Maybe it would be advisable to use navigational simulator as a very useful aid to train crews more extensively at the Naval University in Gdynia.
- The role of commanders as well as every member of a crew is enduring keeping operational ability at the highest level. It is inherently connected with safety of a warship. Nevertheless, all efforts should be made at every level of command in our Navy, which would aim at reducing human factor in overall number of accidents and technical breakdowns.
- It is undoubtedly associated with training and financial aids, which should be taken into consideration.

BIBLIOGRAPHY

1. Dilling J., Sołkiewicz H.: *Stan oraz zamierzenia w dziedzinie rozwoju wojskowej techniki morskiej w MW RP*. Przegląd Morski nr 2. Gdynia 2000
2. Gawlilienko A.: *Wzrywopożarobjezopasnost korablia: probliemy inżjeniernoj podgotowki.- Morskoj Sbornik*, 1997 nr 8
3. Jacobsen T.: *A potential of reducing the risk of ship casualties by 50%*. Marine Technology V. Szczecin, 2003, pp 171 – 181
4. Jakus B., Korczewski Z., Mironiuk W., Szyszka J., Wróbel R.: *Obrona przeciwawaryjna okrętu, cz.1*, Gdynia 2001
5. Kobyliński L.K.: *Podstawy i filozofia bezpieczeństwa w żegludze*. 1st Summer School Safety at Sea. Technical University of Gdańsk, Gdańsk 2001
6. Korczewski Z., Wróbel R.: *Charakterystyka wypadków i awarii okrętowych środków technicznych*. Przegląd Morski nr 2. Gdynia 2000, str.40-53
7. Miller D.: *Damage control - an „insurance policy" navies neglect at their peril.* International Defence Review. 5/1994
8. Mironiuk W., Pawlędzio A., Wróbel R. *Trenażer do walki z wodą*. Przegląd Morski nr 5. Gdynia 2003, str.14-30
9. Plewiński, L.: *Wypadki na morzu*, Szczecin 2000
10. Polska Norma. 1993. *Słownik terminologiczny elektryki. Niezawodność, jakość obsługi*. PN -93/N-50191
11. *Protokoły z postępowań po awariach Głównej Komisji d.s. Wypadków i Awarii Okrętowych MW RP*. 1985-2004
12. Turner S.C.: The US Navy In Review, Proceedings, may 2001, s. 78-84
13. Wysokiński W.: *Analiza przyczyn awarii i wypadków okrętowych zaistniałych w MW w latach 1985 - 1995*. (praca dyplomowa Akademia Marynarki Wojennej). Gdynia1996

CONTACT WITH THE AUTHOR
Assoc. Prof. Zbigniew Korczewski
Mechanic-Electric Faculty,
Polish Naval University
Śmidowicza 69
81-103 Gdynia POLAND
e-mail: zkorczewski@wp.pl

POLISH MARITIME RESEARCH 1(55) 2008 Vol 15; pp. 56-59
DOI: 10.2478/v10012-007-0052-7

The analysis of research results concerning heat release rates of ship materials with regard to dynamic parameters of the research station

Krzysztof Sychta,
Szczecin University of Technology

ABSTRACT

Based on the results of author's research it was stated that significant differences between heat release rates measured according to ISO 5660-1 and FTP Code Part 5 (Res. A. 653 (16)) are not caused by measurement uncertainties. A basic factor determining the lack of correlation is treating the heat release rate in the category of static measurements in the normalized measurement methods. Taking into account dynamic parameters of the test station allowed the coincidence rate (reproducibility and correlation) of the results of heat release rates measured using different methods to be improved, without changing test stations and procedures. Author's research performed on 42 materials has revealed that the relative dynamic errors of the heat release rate measurements are significant (2%÷120%). The average value of these changes for the tested group of materials was equal to 39%.

Keywords: fire safety, heat release rate, dynamic measurement

INTRODUCTION

Object safety evaluations aim at predicting and preventing possible hazards as early as at the planning stage of object operation. For this purpose databases are created on these hazards, their possible effects, frequencies of their appearance, along with protective measures applied and their efficiency. An object safety evaluation is expected to provide an exhaustive description of the object environment, its complexity and possible changes resulting from the hazard. In particular, evaluating fire safety on marine objects requires the information on heat release rates characteristic for thermal decomposition and combustion of materials. The heat release rate contributes to the rate of fire temperature changes, and to the emission of smoke and toxic products of thermal decomposition and combustion. Fire progress on a ship can be only controlled in the pre-ignition phase [1], when the heat release rate of burning materials does not exceed a critical value. The information on the heat release rate of the materials used in marine object cabins makes it possible to predict the fire progress and, consequently, to take appropriate actions and technical measures in order to evacuate people from the dangerous area and fight the fire during its initial phase.

RESEARCH

Numerous research methods oriented on evaluating heat release rates during thermal decomposition and combustion of materials have been developed. In the shipbuilding industry the heat release rates are determined using the methods defined in the FTP Code Part 5 [Res. A. 653 (16)] [2] and ISO 5660-1 standard [3].

The analyses of heat release rate tests found in the literature [4÷7], along with those done by the author using various methods have revealed no correlation between the obtained results (fig. 1).

Based on the analysis of author's results [8] it was concluded that significant differences between the heat release rates measured according to ISO 5660-1 and FTP Code Part 5 (Res. A. 653 (16)) are not caused by measurement uncertainties.

A decisive factor for the lack of correlation is treating the heat release rate in category of static measurements in the normalized measurement methods.

The basis for making distinction between static and dynamic measurements is the time variation of the measured quantity. Combustion of materials is a process that changes in time. That is why the measurement of the heat release rate should be treated as a dynamic process.

Consequently, the results of dynamic measurements are presented as time functions. Correctness of the presentation depends on factors both related and not to the variations of the measured quantity.

The pulse response functions of all transducers [9], except those of integral type, approach zero when $t \to \infty$ (fig.3).

Time characteristics of a transducer, given in the form of a pulse response k(t), make it possible to calculate the transducer response for any input signal x(t). Here the **Duhamel** integral is used [9].

$$y(t)=\int_0^t k(t-\tau)\cdot x(t)\cdot d\tau \qquad (1)$$

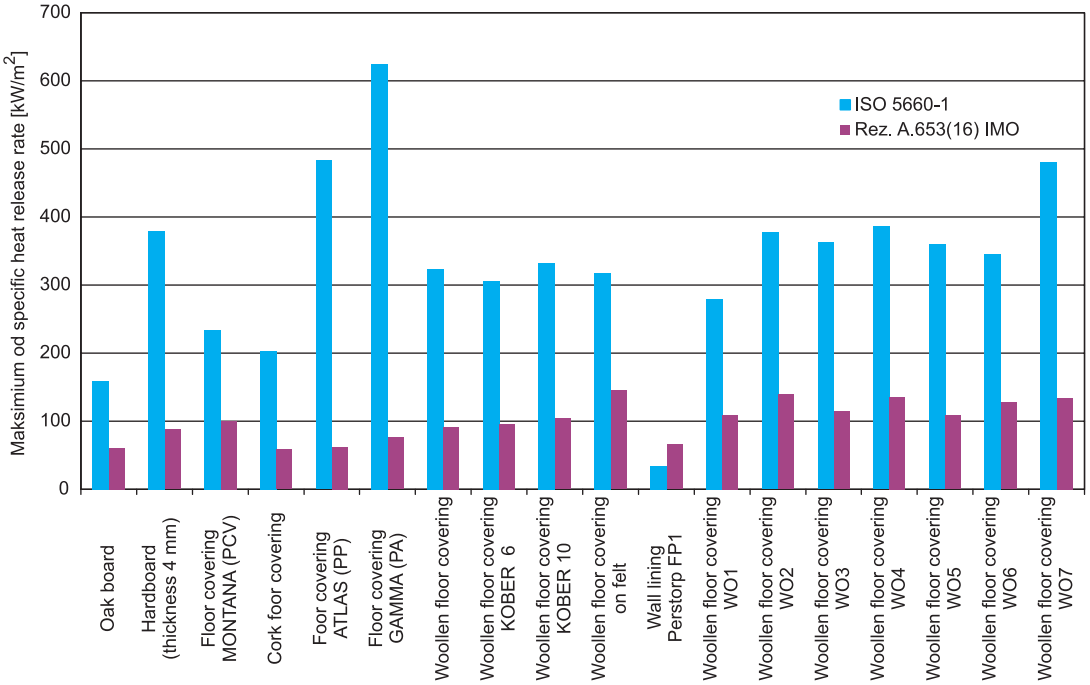

Fig. 1. *Comparison between maximum heat release rates defined using FTP Code Part 5 (Res. A. 653 (16)) and ISO 5660-1 standard, for heat stream rates on sample surface equal to 50 kW ×m^{-2} (author's results related to unit of surface area)*

Fig. 2. *Heat release rates obtained for wool carpet using ISO 5660-1 and FTP Code Part 5 (Res. A. 653 (16)) methods, and taking into account measurement uncertainties ($k \cdot u_c$ – extended uncertainty)*

It can be assumed in practice that k(t) values can be neglected after a finite time period t_o (fig. 3). At any time t_i, the output value y(t) is equal to the integral of a product of a "reversed" characteristic with the starting point shifted to t_i and the input signal x(t).

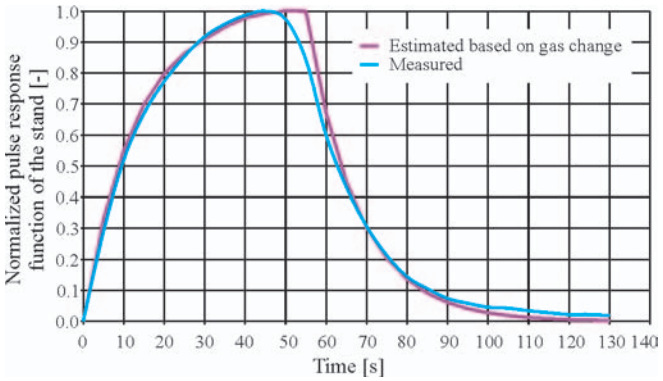

Fig. 3. *Normalized pulse response function of the stand, according to ISO 5660-1*

The above integral is represented by the area marked blue in fig. 4. which is proportional to the value of transducer response at t_i = 215 s. By "shifting" the pulse response function k(t-τ) along the time axis and performing relevant calculations (fig. 5) we can obtain the values of the transducer response y(t) at any time t.

It is clearly visible from figure 4 that the integral has nonzero values only for the time period ranging from t_i - t_o to t_i. Calculating the time-history y(t) can be interpreted as "shifting" the function k(t) along the time axis and performing the operations presented in the figure. Higher t_o values mean greater influence of the time-distant past input signal fragments on the current value of the transducer output. Therefore the pulse response function can be treated as a function which generates the output signal from the past input values. In case of slowly fluctuating signals any measuring transducer usually reacts as a delay transducer. When the rate of input signal variations increases - the input signal delay is observed at the beginning; further increase of the variation rate leads to signal distortion.

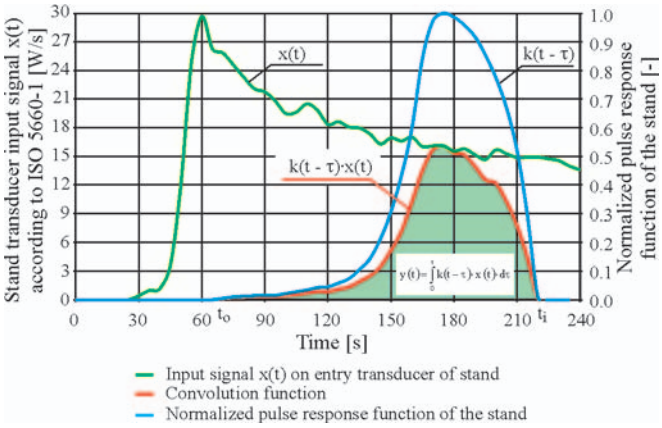

Fig. 4. *Interpretation of the transducer response calculation procedure making use of a convolution function*

To perform calculations the knowledge of the function x(t) is required, which minimizes practical use of those formulas.

The performed identification of the research stations as converters for heat release rate measurements consisted in determining the structure and functional relations that describe dynamic features of their measurement systems. Based on this identification it was determined that [8]:

- the station for testing the heat release rate using ISO 5660 method is a first-order converter with time constant T

- the station for measuring the heat release rate using FTP Code Part 5 (Res. A.653(16)) is a second-order converter described by: time constants T_1 and T_2, suppression factor ζ, and free vibration pulsation ω_o.

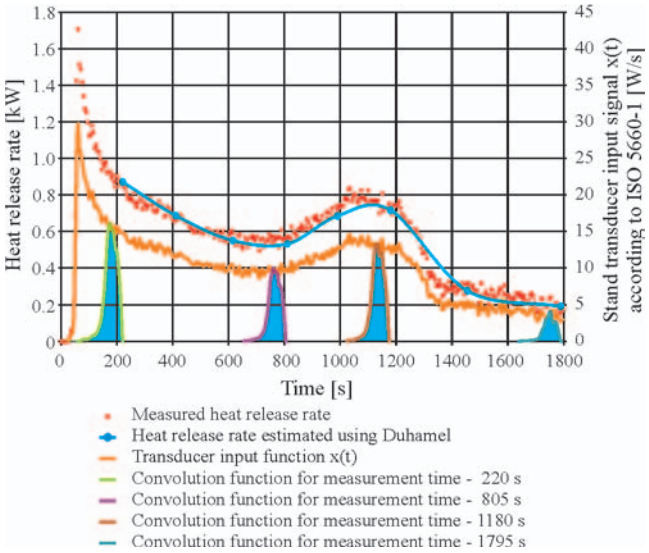

Fig. 5. Interpretation of transducer response at different times using a convolution function

Responses of the heat release rate test stations to linearly increasing inputs were used to correct the dynamic error. It was assumed (Fig. 6 and 7), that within the time interval: $t_i - \Delta t < t_i < t_i + \Delta t$ (where Δt is the measurement period) the measured heat release rate is a linear function with constant speed of changes a_i. The corrected heat release rate for the station making use of the method ISO 5660-1 was defined by the author as:

$$\dot{q}_k(t_i) = \dot{q}(t_i) + a_i T = \dot{q}(t_i) + \frac{\dot{q}(t_{i+1}) - \dot{q}(t_{i-1})}{t_{i+1} - t_{i-1}} T \quad (2)$$

The corrected heat release rate for the station using the FTP Code Part 5 (Res. A.653(16)) method is defined as:

$$\dot{q}_k(t_i) = \dot{q}(t_i) + a_i \frac{2 \cdot \zeta}{\omega_o} = \dot{q}(t_i) + \frac{\dot{q}(t_{i+1}) - \dot{q}(t_{i-1})}{t_{i+1} - t_{i-1}} \frac{2 \cdot \zeta}{\omega_o} \quad (3)$$

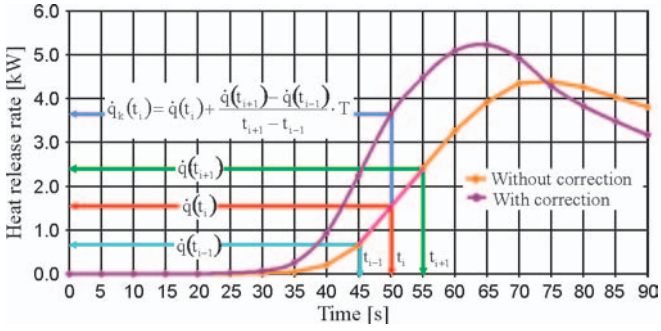

Fig. 6. Principle of determining dynamic correction for heat release rate measurements making use of ISO 5660-1 standard

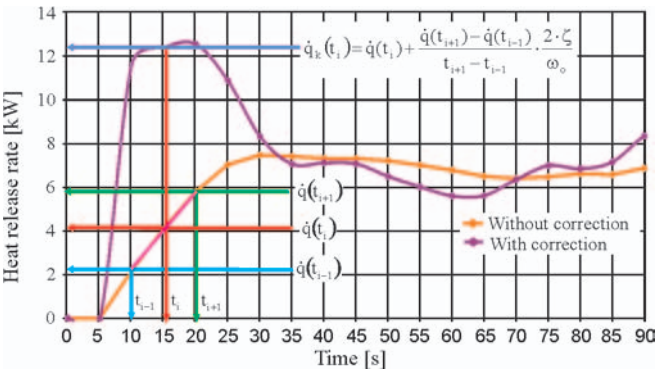

Fig. 7. Principle of determining dynamic correction for heat release rate measurements making use of FTP Code Part 5 (Res. A.653(16))

It is noteworthy that the dynamic error correction for the second-order converter does not depend on time constants T_1 and T_2 (3).

The validation of the dynamic error correction method has confirmed the agreement between the average values of the heat release rate obtained using the FTP Code Part 5 (Res. A.653(16)) and ISO 5660-1 methods.

Taking into account dynamic parameters of the heat release rate test station (Fig. 8) provided opportunities for increasing the coincidence rate (reproducibility and correlation) of the heat release rate results measured using different methods, without changing test stations and procedures.

The effect of the of dynamic error correction on the measured maximum of the heat release rate and on the heat released during material tests performed according to the FTP Code Part 5 (Res. A.653(16)) method is shown in Figs 9, 10, 11, 12 and 13.

As can be seen, the dynamic error of the heat release rate increases in those tests with the increase of the measured value of the heat release rate (Fig. 9).

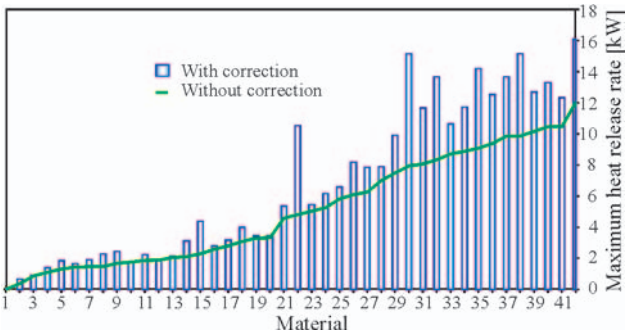

Fig. 9. Comparing results of maximum heat release rate tests, with and without dynamic error correction

Results recorded by the author in the tests performed on 42 materials allow a conclusion to be formulated that the relative dynamic errors of the heat release rate measurement are significant (2%÷120%). An average value of these changes for the tested group of materials equals 39%.

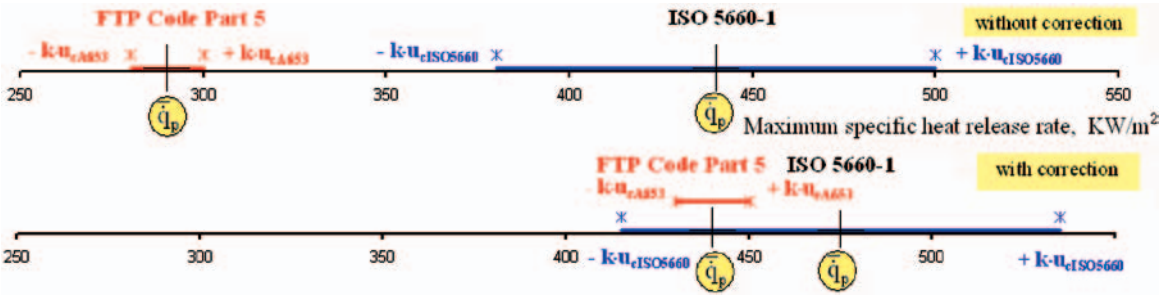

Fig. 8. Heat release rates obtained for WO7 wool carpet using ISO 5660-1 (50 kW × m^{-2}) and FTP Code Part 5 (Res. A.653(16)) methods, and taking into account measurement uncertainty.

The highest dynamic error is recorded for materials that are characterized by low resistance to external ignition sources, and fast acceleration of the thermal decomposition and combustion process (Fig. 10, 11 and 12).

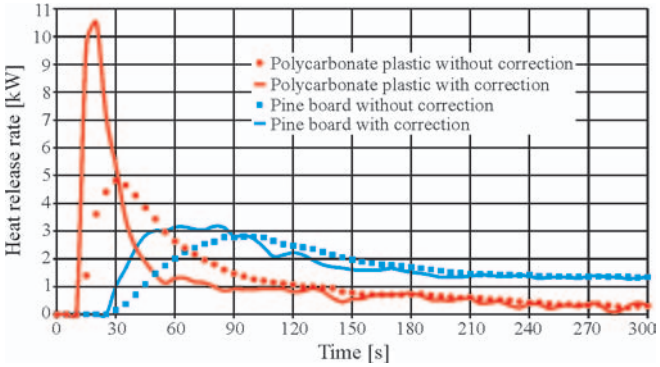

Fig. 10. *Time-history of heat release rate fluctuations taking into account dynamic correction of the station for polycarbonate panel of 2 mm thickness and for pine board of 20 mm thickness, according to FTP Code Part 5 (Res. A.653(16)) method*

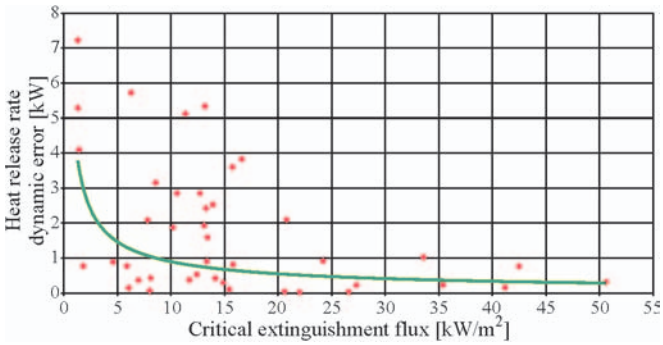

Fig. 11. *Dynamic error for materials of different critical extinguishment flux values defined by FTP Code Part 5 (Res. A.653(16)) method*

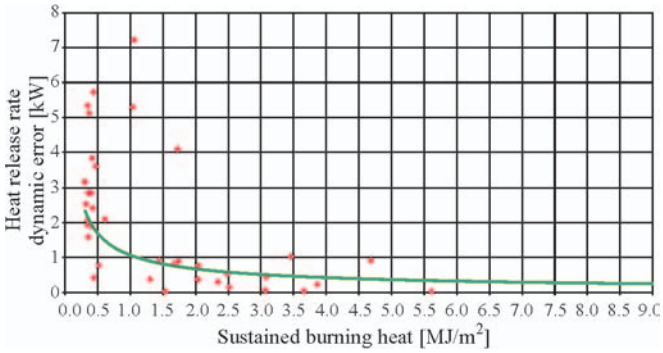

Fig. 12. *Dynamic error for materials of different flame combustion support heat values defined by FTP Code Part 5 (Res. A.653(16)) method*

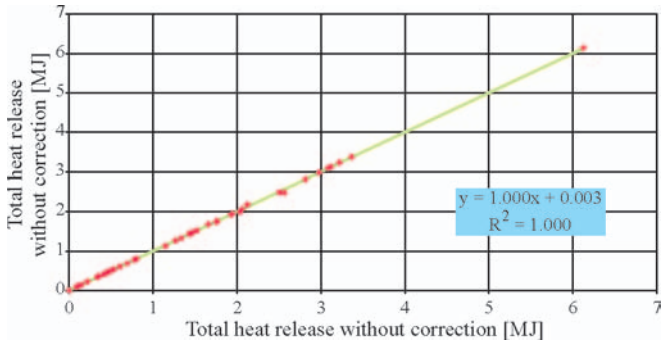

Fig. 13. *Effect of dynamic error correction on the volume of the heat released during the test*

The influence of the dynamic error (fig. 11 and 12) for wall and ceiling materials characterized by slow surface flame propagation (KSP $\geq$ 20 kW·m^{-2}, $Q_{sb} \geq$ 1.5 MJ·m^{-2}), which are used in shipbuilding, is not significant. However, for floor finish materials characterized by slow surface flame propagation (KSP $\geq$ 7.0 kW·m^{-2}, $Q_{sb} \geq$ 0.25 MJ·m^{-2}), also used in shipbuilding, the influence of the dynamic error should be taken into account (fig. 11 and 12).

Comparing the results of author's research performed on 42 materials according to FTP Code Part 5 (Res. A.653(16)) method has revealed (fig. 13) that the proposed method of heat release rate dynamic error correction does not affect the measured value of the released heat (both the inclination ratio and the correlation ratio equal 1.000).

This way the requirement of correct operation of the dynamic error corrector was fulfilled. The areas below the heat release rate time-histories with and without dynamic error correction are equal. The volume of the thermal energy released during the research is strictly defined and it should not depend on procedures used for converting the intermediate results of the measured quantity. This is a basic advantage of the dynamic correction method applied to heat release rate measurements making use of ISO 5660-1 and FTP Code Part 5 (Res. A.653(16)).

The applied method of measurement result correction reduced the differences between the maximum heat release rate values determined using the two methods. At the same time, it did not affect the measured heat value.

The proposed improvement [8] of the heat release rate research method taking into account dynamic parameters of the station according to FTP Code Part 5 (Res. A.653(16)) may be widely used in shipbuilding. Production and repair shipyards make use of significant volumes of materials and articles for ship interior design and furnishings, which, according to the regulations in force, have to reveal slow surface flame propagation. 42 materials and articles typically used on ships were selected to check the usefulness of the proposed modification to the research method defined by FTP Code Part 5 (Res. A.653(16)), and the possible effect of this change on the obtained results.

BIBLIOGRAPHY

1. *Quantification problems of fire-safety level of marine object*. Polish Academy of Sciences, Branch in Gdańsk, Marine Technology Transactions. Vol.16, 2005
2. *International Code for Application of Fire Test Procedures*. International Maritime Organization. London 1998
3. *ISO 5660 Fire tests - Reaction to fire - Rate of heat release rate from building products* (Cone calorimeter method)
4. Lyon R.E.: *Effect of instrument response time on heat release rate measurement*. Fire an materials. vol. 19, 11-17 (1995)
5. Vandevelde P.: *An evaluation of heat release criteria in reaction-to-fire test*. Fire an materials. vol. 4, no. 3. 1980
6. Blume D., Getka R.: *Rate of heat release test – calibration, sensitivity and time constants of ISO RHR apparatus*. NORDTEST PROJECT 115-77, PART 1. National Institute for Testing Materials, Statsproveanstalten 1979
7. Evans D.D., Breden L.H.: *Time delay correction for heat release rate data*. Technology 14 85, 1978
8. Sychta K.: *Comparison analysis of heat release rates from ship materials, and a method for improving measurement accuracy* (in Polish). Ph.D. Thesis. Szczecin University of Technology, Faculty of Maritime Technology, Szczecin, October 10, 2006
9. Hagel R., Zakrzewski J.: *Dynamic measurements* (in Polish). WNT Warszawa 1984

CONTACT WITH THE AUTHOR
Krzysztof Sychta, Ph. D.
Faculty of Marine Technology,
Szczecin University of Technology
Al. Piastów 41
71-065 Szczecin, POLAND
e-mail : krzysztof.sychta@ps.pl

POLISH MARITIME RESEARCH 1(55) 2008 Vol 15; pp. 60-64
DOI: 10.2478/v10012-007-0053-6

Elastic protection coatings for ship tanks to increase environment protection level

Janusz Kozak
Gdansk University of Technology

ABSTRACT

Greater and greater number of cargo ships sailing over small, restricted water areas can endanger the environment - in the case of disaster - by spilling fuel oil, carried in the ship's bottom tanks for its propulsion. In this paper is proposed an alternative solution (against that of double plating) in the form of the second, elastic protective barrier which would be able to decrease risk of spilling in the case of loss of ship's plating tightness due to collision or grounding.

Keywords : elastic protection coatings, ship tanks, environment protection

INTRODUCTION

During the last ten years a dramatic increase of number of cargo ships has been observed in the world fleet. The greater ship traffic has been caused by progressing process of economy globalization. Many sea regions of the world have become more busy and hazardous for navigation, and one of them is the Baltic Sea [1]. On average about 2000 ships every day sail in this waters, Fig. 1.

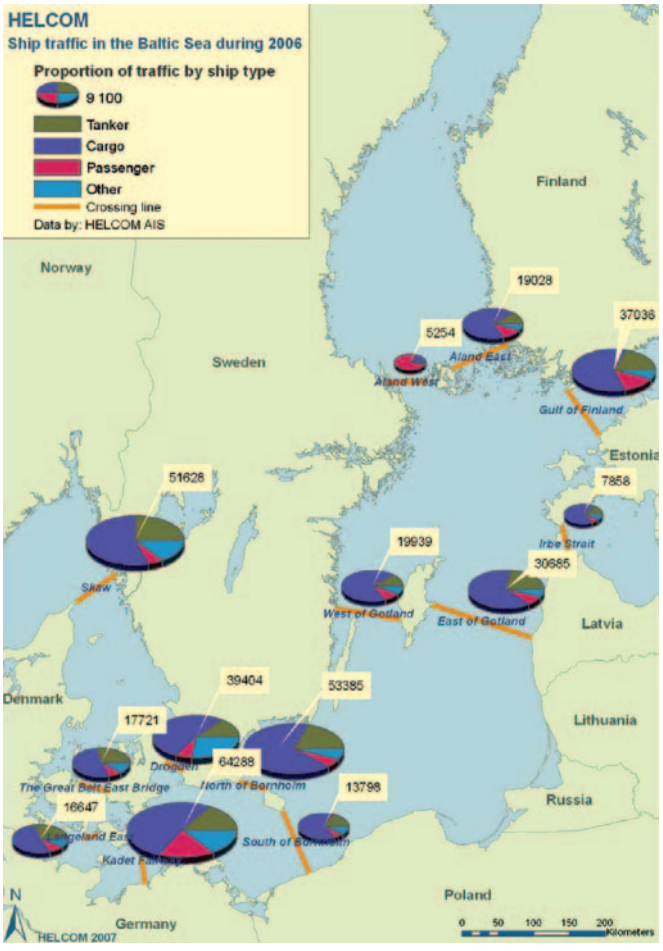

Fig. 1. *Ship traffic in the Baltic Sea [2]*

These are ships of different types; out of the total number of 13600 ships crossing Skagen between July 2005 and October 2005 - 60% of them belonged to dry cargo ships, 25% - tankers, 7% - passenger ships and 8% - other ships [2]. Main shipping routes in the Baltic are presented in Fig. 2.

Fig. 2. *Main shipping routes in the Baltic Sea [3]*

Moreover, a further dynamic increase of number of cargo ships sailing in the Baltic waters is predicted - Fig.3 [2].

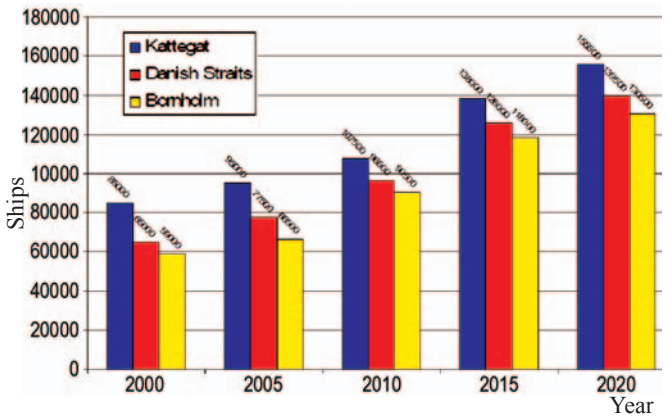

Fig. 3. *Ship traffic intensity (ships/year) in the Baltic [4].*

The Baltic Sea basin is a specific region of the world not only due to the busy shipping routes. It is a sea of a very limited amount of water exchanged with the ocean – the time necessary to completely echange its water with the Atlantic Ocean is estimated to be 25÷30 years, which means that in the case of a greater oil spill in the region its consequences will be severe and long-lasting. According to the performed analyses [3] the probable profit loss resulting from tourism limitation in a spill suffering region would be many times greater than pollution removal cost. Additionally, in the Baltic waters – apart from shipping routes – in coastal zones are also carried out other activities such as fishing, tourism and operation of farms of wind power plants.

The very intensive ship traffic over the restricted area of the Baltic greatly influences occurrence number of sea accidents. The high traffic intensity, difficulty in navigation through the straits leading from the North Sea to the Baltic, often occurring bad weather conditions and other factors make that the Baltic is a sea region where many ship accidents occur year after year. The highest number of 146 sea accidents was recorded in 2005; as many as 13 of which resulted in pollution of the environment.

The map of particular kinds of the accidents together with indication of places of their occurrence is presented in Fig. 4.

In the years 2000-2006 the most frequent cause of ship accidents was grounding (46%), the next one - ship-to-ship collisions (31%). A failure of ship power plant or structure was responsible for disasters in 3% cases, and fire - in 5%. The most severe accidents which caused oil spills in the Baltic are listed in Tab. 1.

Tab. 1. *The most severe pollutions caused by spills of oil product materials from ships in the Baltic waters [6].*

Year	Ship name	Amount of spilled oil	Place
2003	Fu Shan Hai	1200 t	Bornholm (Denmark/Sweden)
2001	Baltic Carrier	2700 t	Kadetrenden (Denmark)
1998	Nunki	100 m^3	Fjord Kalundborg (Denmark)
1995	Hual Trooper	180 t	Sund (Sweden)
1990	Volgoneft	1000 t	Karlskrona (Sweden)

In the connection with the increasing risk of ecological disasters associated with sea transport, in the last years the European Union adopted two packages of legal instruments dealing with safety at sea, the so called principles : *Erika I* and

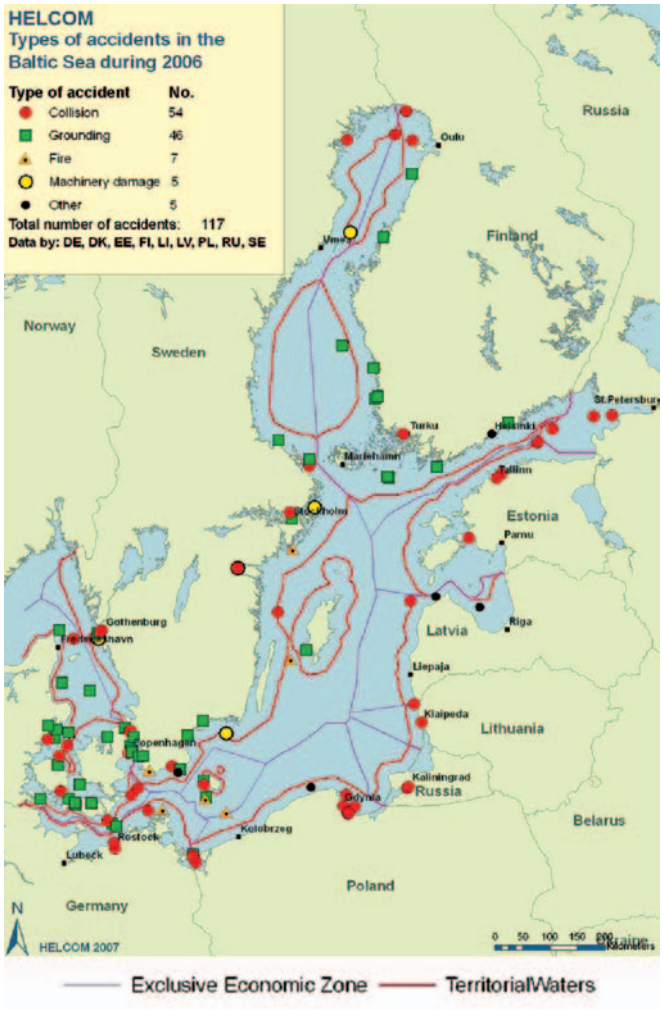

Fig. 4. *Places where ship accidents occurred at the Baltic Sea in 2006 [5]*

Erika II. As a result of their implementation the range of port control of ships was intensified and extended, and single side plating ships were banned from oil shipping; also, the European Maritime Safety Agency (EMSA) was established. In 2005 the European Commission prepared the package *Erika III*.

In the existing and being- in- force requirements for construction and equipment of new ships possible collisions and groundings have not been taken into account. Only basic design regulations concerning stability and floatability of damaged ships or amount of spill of liquid load from damaged hull are commonly accepted. However in 2004 Germanischer Lloyd (GL) introduced to its rules the notation COLL which determines degree of ship hull resistance (strength) against collisions [7]. The resistance is measured by comparing the strength against impact of strengthened ship side structure with that not strengthened of single plating. The only regulations directly concerning collisions are the requirements for ships intended for inland navigation on the Rhine (Switzerland, Germany, the Netherlands), introduced in 2003. The ADNR regulations require to so design structural elements of gas tankers as to make them able to absorb the energy of 22 MJ released during collision against ship side structure [8].

Though for cargo tanks of oil cargo tankers the legal requirements have been recently made much more stringent, similar ones for fuel oil tanks are still lacking, nevertheless amount of fuel oil contained in them is often comparable with that of liquid cargo carried by a small tanker. The hazard becomes greater by the fact that most of such tanks is located in double bottom, i.e. in the zone very susceptible to failure both in the case of ship-to-ship collision and taking the ground or rock.

IDEA OF THE PROGRAMME CORET

The above mentioned premises indicate that grounding or collision of e.g. a container carrier of medium size may lead to environmental pollution of the Baltic by the oil released from unseal single plating bottom tanks and its amount can be significant. In this connection was undertaken a research work aimed at elaboration of a way of lowering the risk of releasing oil spill in the case of collision, by introducing a second protection barrier. The idea of the project consists in adding an internal elastic oil-resisting coating placed inside the tank on a foundation which fills the tank in such a way as to ensure – in the case of tank plating tear occurring as a result of a collision - tightness of the tank by means of the elastic coating able to be displaced to some distance and thus preventing against oil spill in emergency, Fig. 5.

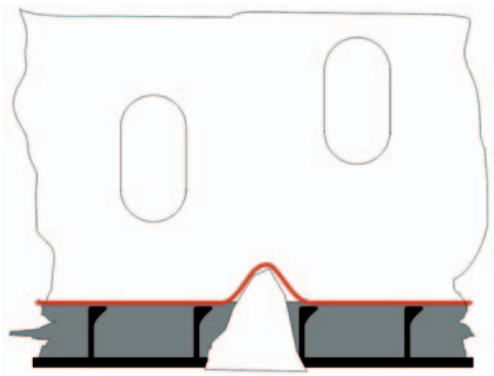

Fig. 5. *Idea of the second elastic barrier for fuel oil bottom tank.*

In order to elaborate such novel solution many problems should be first investigated, including the following:

- ⇨ elaboration of recipe for an oil resistant plastic material, inexpensive and suitable for coating it inside closed spaces in shipyard's conditions.
- ⇨ selection of a material for intermediate filling layer,
- ⇨ elaboration of an engineering process of applying the components of the barrier in industrial conditions with special taking into account difficult places such as corners, bends etc,
- ⇨ selection of the dimensions of the second barrier components: depth of the filling layer and thickness of the protection coating,
- ⇨ influence of the additional coating and filling material on corrosion rate of steel structure,
- ⇨ elaboration of a method for control of state of hidden surfaces,
- ⇨ making agreement with classification societies as to principles of implementation and use of the novel solution.

The mentioned problems constitute the subject of work carried out in the frame of the research project EUREKA E!3614 „CORET": *"Elastic protection coatings for ship tanks to increase environment protection level"*. Below are presented results of a preliminary work associated with developing some of the above mentioned problems.

COLLISION MODELING TO ESTIMATE DISTANCE BETWEEN THE SECOND BARRIER AND SHIP PLATING

In order to compare behaviour of the tank structure having internal protection barrier with that of the classical solution, was performed a numerical analysis of behaviour of such structures during collision with an external rigid object, e.g. a rock. On the basis of technical documentation of double bottom of a medium container carrier (Lo. a. = 120 m) a computational spatial model with introduced minor simplifications (where bulb plates were replaced by equivalent flat bars), was prepared. The model covers a fragment of fuel oil double bottom tank located in the middle part of ship hold. The rock was modeled in the form of a cone of the radius r = 50 mm. The collision process was modeled as a slow (quasi-static) motion of the cone (v =10 mm/s), perpendicular to tangent line of the bilge in the place of contact. The depth of penetration of the cone was assumed equal to 500 mm. The calculations were performed with the use of the LS-DYNA (v 9.71) software.

The computational mesh was formed from 13 500 shell elements. For the cone the rigid body model of the type "20" was applied, and for the double bottom structure - that of the type "24" (of piece-wise linear isotropic plasticity). The elements which exceeded limit elongation values were automatically removed from the model. During numerical calculations of the ship/rock collision, to take into account the coming into contact of various elements of the model is necessary. The standard approach used in such cases consists in application of an automatic algorithm for monitoring and determining which elements of the model are taking part in the contact. The generated model of the hull fragment together with the model of penetrating object is presented in Fig. 6. For the calculations the cone's movement velocity of 10 [mm/s] was assumed with a view of planned verification of numerical modeling results by those from testing real structural models.

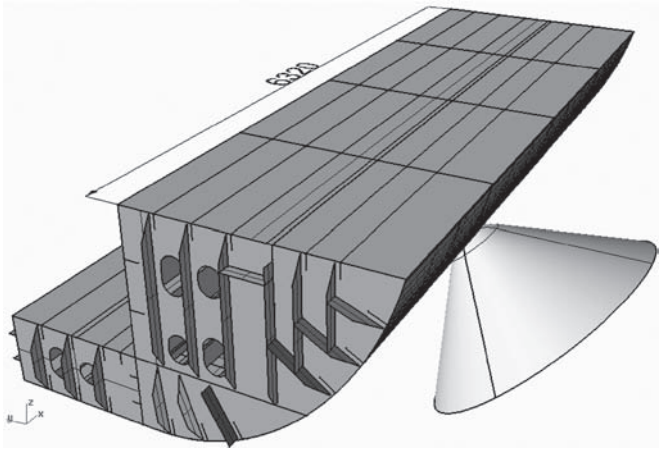

Fig. 6. *Model for numerical simulation of collision*

In Fig. 7 are presented the contours of von - Mises effective stresses in structural elements and outer plating for the selected time instant of simulation, t=62s.

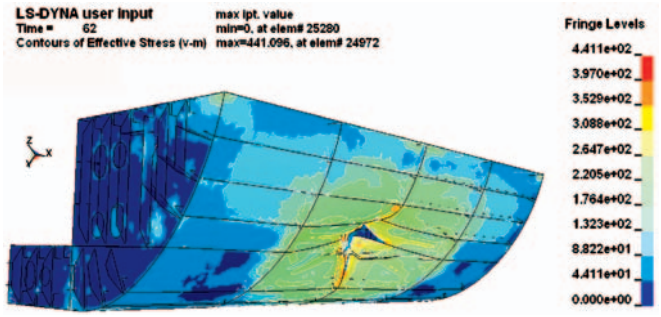

Rys. 7. *The effective stresses in outer plating for the time instant t=62s.*

Fig. 8 shows the run of deformation energy changes in the structure during penetration.

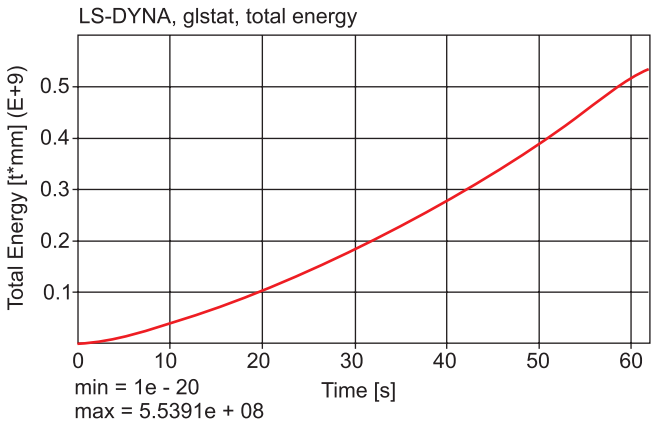

Fig. 8. *Change of deformation energy of the structure during penetration.*

The calculated deformation energy values extended by numerical calculations for the whole ship and verified with the use of the planned laboratory full-scale tests will finally serve for determination of behaviour of the internal elastic coating during the collision resulting in a tear damage of tank outer plating, and for evaluation of degree of effectiveness of the coating in preventing possible oil spill from the damaged tank.

SELECTION OF A FILLING MATERIAL INTENDED FOR SUPPORTING THE SECOND BARRIER

During searching for a filling material for supporting the elastic internal barrier, was performed a comprehensive research study to select the materials which satisfy majority of a dozen or so requirements, often contradictory to each other. Such filling material should be light in weight, non-flammable, non-gassing in an elevated temperature, non-toxic, non-corrosive, easy for implementing in industrial conditions, easily utilized and inexpensive, of course. After reviewing possibly applicable materials it was revealed that lightweight concretes can fulfill most of the postulated features. The concretes are of the volumetric density not greater than 2000 kg/m^3 in dry state. In land structures they are used to significantly lower weight of an element and/or its dimensions. The concretes are made by mixing cement mortar and various natural or artificial aggregates. Application of lightweight aggregates makes it possible to obtain the concretes of the strength exceeding 60 MPa, at simultaneous reduction of structural weight by 25÷30% relative to the common concrete. It leads to a significant reduction of cost of shuttering, scaffolding and reinforcement, as well as to a reduction of dimensions of structural elements, thus - total volume of concrete and reaching a greater freedom of designing. The application of lightweight artificial aggregates to concretes results not only from the need of obtaining more lightweight structures but also from limited resources of rock aggregates and economic necessity of utilization of industrial wastes. This is especially important in the aspect of implementing the balanced development policy recommended by European Union.

A characteristic common feature of all lightweight aggregates is their porous structure and - as a rule - a lower strength than that of hardened cement mortar. Consequently, concretes made of the aggregates differ from common ones not only in their volumetric density but also other features as well as manufacturing process.

During the work on choice of parameters of concrete filling material the laboratory tests of mechanical properties of various combinations of concrete, aggregate and applied way of preparation of steel structure surface were carried out by using full-scale specimens. In Fig. 9 is presented the specimen tested to determine a degree of binding the filling material with the steel structure under tension, depending on a way of preparation of steel surface, and in Fig. 10 – the example record of deformation of the concrete filling material versus deformation of the steel structure.

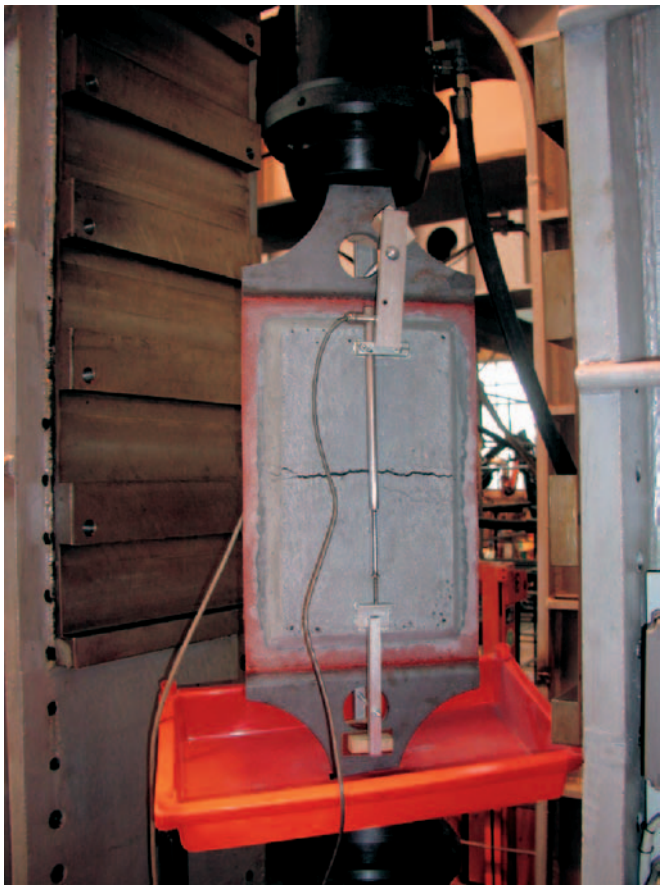

Fig. 9. *Tests of mechanical properties of filling layer*

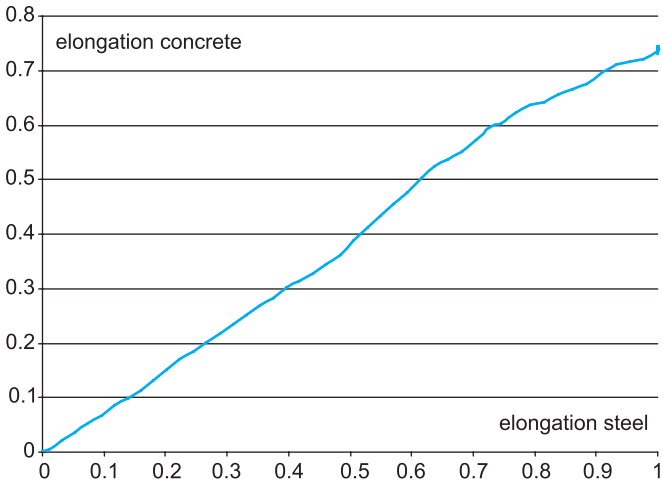

Fig. 10. *Relative elongation of concrete filling material versus elongation of deforming steel structure.*

SUMMARY

- Large number of cargo ships sailing over small, restricted water areas such as the Baltic Sea can endanger - in the case of disaster –the environment by spilling fuel oil carried in the ship's bottom tanks for ship propulsion.

- An alternative solution (against the double plating structure) was proposed consisting in applying the second, elastic protection barrier to decrease risk of oil spill resulting from loss of tightness of ship plating as a consequence of e.g. collision or grounding.

- Implementation of such solution would make it possible to increase safety of existing ships without necessity of their expensive rebuilding.

BIBLIOGRAPHY

1. *Maritime Transport in the Baltic Sea.* Draft HELCOM Thematic Assessment in 2006. HELCOM Stakeholder Conference on the Baltic Sea Action Plan 07.03.2006, Helsinki, Finland
2. Baltic Master: *General Assumptions Of The Ship Safety On Southern And Western Baltic Sea*, Report (M II part 2/4), Maritime University of Szczecin, 2006
3. SSPA Sweden AB : *Socioekonomiska Effekter Av Större Oljepåslag – Scenariostudier För Halland*, Skåne, Blekinge Och Kalmar Län, Rapport till Räddningsverket, September 2006
4. *Report on ship's accidents in the Baltic Sea area for the year 2004.* Issued by HELCOM 2004.
5. *Report on shipping accidents in the Baltic Sea area for the year 2006,* HELSINKI COMMISSION, August 2007
6. Baltic Master : *Statistics on accidents and sea traffic*, August 2006
7. Germanischer Lloyd : *Strengthening against Collisions*, Rules for Classification and Construction, Ship Technology Part 1 - Seagoing Ships, Chapter 1 - Hull Structures, Section 33, Germanischer Lloyd, Hamburg 1992
8. *Rules for the Transport of Dangerous Cargo on the Rhine* (in German, French and Dutch), http://www.ccr-zkr.org, ADNR 2003

CONTACT WITH THE AUTHOR

Assoc. Prof. Janusz Kozak
Faculty of Ocean Engineering
and Ship Technology,
Gdańsk University of Technology
Narutowicza 11/12
80-952 Gdańsk, POLAND
e-mail : kozak@pg.gda.pl

Miscellanea

Solemn session to celebrate 90th birthday of Professor Doerffer

If Prof. Doerffer had not passed away on 9 August 2006 he would have celebrated his 90th birthday on 21 April 2008. Just on the day the solemn session devoted to Prof. Doerffer was held at the Faculty of Ocean Engineering and Ship Technology, Gdańsk University of Technology, to commemorate this anniversary of the Professor, a person of merit for development of Polish shipbuilding industry, respectfully called the Nestor of Polish shipbuilders.In the Session took part a numerous group of persons graduated from this Faculty, educated under supervision of the Professor, managers and chairmen of shipbuilding firms, representatives of present scientific and didactic staff of the Faculty together with Prof. Dzida, Dean of the Faculty, at that very moment elected for second term of this office. Mrs Maria Teresa Doerffer, the wife of the Professor, together with the Professor's daughter Christine, the son Carol and his wife, two granddaughters and grandson were also present.

The session, organized by the Professor Doerffer Foundation established in December 2006, was opened by Mr Dzida, the Faculty's Dean, then Prof. Katulski, the University's vice-Rector for R&D matters passed greetings in the name of the University's authority. The subject-matter part of the Session contained four presentations (papers). Prof. Rosochowicz told the still continued directions of Prof. Doerffer's scientific research and didactic activity over, and reminded that Prof. Doerffer promoted two full professors, five associate professors, ten doctors of science, and that he himself was honoured with six dignity appellations of *honoris causa* doctor. Connections of Prof. Doerffer with shipbuilding industry, especially with shipyards located in Gdańsk, Gdynia and Szczecin were discussed by Mr Skrzypiński, long-standing manager of the Office of FORUM OKRĘTOWE, the Association of Shipbuilding Industry Employers, which was initiated and arranged by Prof. Doerffer in 1993. And, the Professor's son Carol made the audience acquainted with family life of the Professor and illustrated his presentation with many photos projected onto the screen.

Next, Mr Spigarski, editor, performed promotion of the last, fourth volume of the Professor's memoirs titled „Life and Passions", having its subtitle „Retirement", that was also edited - similarly as the third volume - by Mr Spigarski, and published in a very careful graphical form by the Foundation for Promotion of Shipbuilding Industry and Maritime Economy, the Publishing House specialized in publishing the books on shipyard and maritime economy problems. Prof. Mazurkiewicz told about his friendship and cooperation with Prof. Doerffer, especially in the times when both of them took the top positions in the University's authority, of the rank of Rector and vice-Rector. A solemn moment of the Session was the unvailing of the Commemorating Plate devoted to Prof. Doerffer, placed close to the then his office room, which was solemnized by the Professor's wife and Prof. Dzida, the Dean of the Faculty. (**spi**)

Photo: C. Spigarski

From the left side: Karol Doerffer, prof. Bolesław Mazurkiewicz, Sławomir Skrzypiński, prof. Krzysztof Rosochowicz, Jerzy Bunikowski, Marek Dzida

POLISH MARITIME RESEARCH 1(55) 2008 Vol 15; pp. 65-71
DOI: 10.2478/v10012-007-0054-5

Influence of cathodic-protection-induced hydrogenation on mechanical properties of two ship hull plate steels

Marek Jakubowski,
Łukasz Modelski, **Marek Podbereski**,
Gdansk University of Technology

ABSTRACT

Tensile testing and Charpy V impact testing results for two ship hull steels: an ordinary strength steel grade A and a higher strength steel grade AH32 each in both as-received conditions and in hydrogenated by zinc protector in salt water conditions. For both steels the hydrogenation has slightly increased yield stress (R_e) and elongation (A) and has not influenced ultimate tensile strength (R_m), while reduction of area has been unchanged (A steel) or even decreased (AH32 steel) due to the hydrogenation. The effect of the hydrogenation on Charpy tests results has evidently been beneficial: the increase of Charpy energy and of percent fibrosity (ductility) of fracture appearance as well as a shift down of ductile-brittle transition temperatures have been observed. It seems that the present practice to evaluate the mechanical properties of ship steels by testing the specimens without hydrogenation leads to conservative results. The Authors have hypothesized that the beneficial effect of hydrogenation can occur if the deformation rate is fast enough, the notch is sharp enough (although only for specimens hydrogenated in unstressed conditions) and hydrogen concentration is moderate.

Keywords: ship steels, hydrogenation, Charpy-V impact test, tensile testing

INTRODUCTION

A small effluent of cargo occurred during the loading of a small tanker on September 2002. A crack in the bottom plating at the edge of a scallop was detected. Since the buckling of the bottom plating in the considered region of hull was visible, most of experts suggested the crack was an immediate result of the buckling, i.e. deformation-induced stress had been released in the form of the crack. Some analysis and tests made by Jakubowski [1, 2] have shown that the explanation was not very probable. However, sacrificial zinc anode was not far from the crack location and it could cause some degree of hydrogenation of steel in this region. Therefore some preliminary tests [1, 2] have been carried out in order to explain could the cathodic-protection-induced hydrogenation of steel reduce charpy impact toughness energy and a critical value of plastic deformation in static tension, because the buckling could be caused by quasistatic or dynamic grounding of the ship. The specimens were manufactured of the original bottom plating segment cut off from the buckled region of the ship's bottom close to the considered crack. In order to hydrogenation some specimens were submerged in 3.5% water solution of NaCl and coupled to zinc anodes. Both results of tensile testing and Charpy impact tests of hydrogenated and not hydrogenated specimens satisfied requirements of Classification Societies for ship hull steels of ordinary strength. Hydrogenation effect, however, has appeared somehow unexpected.

In tensile testing the values of ultimate tensile strength (UTS) and yield strength (YS) of smooth and notched specimens were practically unaffected by the applied hydrogenation. Values of total elongation after fracture (A) for notched specimens were slightly reduced by hydrogenation (but only one hydrogenated notched specimen was compared to one not hydrogenated specimen), while for smooth specimens hydrogenation caused an increase of A-value from 27% to 31% (2 hydrogenated specimens and 2 not-hydrogenated ones). Charpy-V impact toughness was evaluated at the temperature of 15°C for three as-received and three hydrogenated specimens. Impact toughness energy was 30-48 J (average 38 J) for not hydrogenated specimens and 63-76 J (average 70.3 J). Fracture surface was ductile in 42-71% (average 54%) for not-hydrogenated specimens and in 76-100% (average ca. 95%) for hydrogenated ones. Thus hydrogenation of steel appeared to be insignificant (but rather slightly positive) factor in the standard tensile testing conditions, while it evidently positively influenced charpy V impact toughness of the low carbon steel.

The above mentioned preliminary tensile tests results [1, 2] are not totally unexpected. There is a general opinion, that hydrogenation of steels markedly reduce their plastic properties, i.e. elongation (A) and the reduction of area (Z), but this opinion is mainly based on slow strain rate tests (SSRT) results, e.g. [3-7]. Strain rates in standard (so called static) tensile testing are significantly (2 or 3 orders of magnitude) higher, than those in SSRT. The standard tensile tests usually show also a reduction

of plastic properties of steels after hydrogenation, although the reduction is smaller than in SSRT [8-10]. However, Lunarska [11] stated that; "softening or hardening of low carbon mild steels can be expected according to the kind and amount of impurities and to the conditions during hydrogenation process". Some of her investigations results [11] show significant increase of plastic properties of iron whiskers of different orientation due to hydrogenation (2 or 3-fold increase of elongation A). The above mentioned Charpy V impact tests results, i.e. significant increase of impact fracture energy due to hydrogenation [1, 2] were more unexpected than the tensile testing results.

The Author has formulated a working hypothesis that the influence of hydrogenation of steels on their mechanical properties can change from very negative for very slow strain rates (SSRT), through approximately neutral for medium strain rates (standard tensile testing), up to positive for very high strain rates (impact testing). The hypothesis is based, however, on the Author's preliminary tests on a small population of specimens, and only some of the Archakov's [12] test results corroborated positive effect of hydrogenation on Charpy toughness of steel. Juraszek's *et al* investigations [13] have shown that Charpy V specimens of a ship steel did not fracture when they had been pre-exposed in salt water and they fractured when pre-exposed in laboratory air, and it cannot be attributed to corrosion-induced increase of notch root radius. Fair-sized lamellar cracks perpendicular to main crack direction have been present only in specimens pre-exposed in water, and in the present Authors opinion they could be due dissolution of sulfide inclusions accompanied by local hydrogenation of steel. However, numerous tests showed evident degradation of Charpy impact toughness energy of steels, c.f. Karpenko [9] and a literature survey by Smialowski [8]. The problem of the strain rate effect on hydrogen embrittlement of steels is discussed in literature. Smialowski suggested that the negative influence of hydrogen on impact properties of steels is weaker than on static properties. This is because under impact conditions the time of testing is not sufficient for hydrogen to diffuse into the process zone at the crack tip and a critical concentration of hydrogen cannot be approached. Tensile testing of smooth specimens also showed that the faster the strain rate the weaker the hydrogen-induced degradation of plasticity of steels is, and under dynamic loads and/or cryogenic temperatures hydrogen embrittlement did not occur [5, 9]. Toribio and Kharin [14] have shown that the influence of load dynamics on hydrogen embrittlement is not unique. In the case of stress-controlled microfracture event in the process zone, the applied loading must be slow enough to allow hydrogen concentration to follow the evolution of the stress with negligible delay. However, in case of strain controlled micromechanism of fracture: "approaching in a dynamic manner the crack tip situation when hydrogen-assisted cracking may commence, local fracture event must occur at lower stress intensity factor than obtained in sustained load test. This way, load dynamics may act as promoter of hydrogen assisted cracking, which has been noted in some experiments"[14]. Thus, in the above analysis and experiments, hydrogen appears to be more or less damaging agent, never beneficial for impact propertied of smooth and notched steel specimens.

Previously the Author [1, 2] tested steel prestrained due to the grounding of ship hull bottom and after the repairing of the buckled region of plate. Karpenko [15] has shown that prestraining of steels can reduce their susceptibility to hydrogen embrittlement. This fact can be explained on the base of Zieliński and Domzalicki [6] statement that susceptibility of steels to hydrogen embrittlement is likely to be dependent on the amount of mobile hydrogen rather than trapped hydrogen. Structural defects created by prestraining of the steel act as traps for hydrogen, therefore they can reduce the amount of diffusible hydrogen.

The present tests have been carried out in order to show what the influence of cathodic protection of ship hull structures on their mechanical properties is. Tensile testing and Charpy V impact tests have been chosen as common the acceptance mechanical tests for ship hull steels according to the rules of Classification Societies. The present investigations are continuation of preliminary ones [1, 2] but are based on steels of two different categories, and more numerous population of specimens of each of the steels while the steels were in as-delivered-to-shipyard condition (not pre-strained).

TEST METHOD

Two grades of ship hull plate steels have been testes: A and AH32 (denoted according to the rules of Classification Societies). Two types of specimens have been used for tensile testing: twelve smooth specimens of the diameter (d_0) equal 8 mm and the gage length (L_0) equal 40 mm, and twelve notched specimens with the round notch profile very similar to Charpy V notch profile, but only 1 mm deep. The notched specimens diameter has been equal to 10 mm, but diameter measured at the bottom of the V-groove has been equal to the smooth specimen diameter (8 mm) in order to avoid the scale-effect. Twenty two standard Charpy V specimens, but of reduced thickness equal 7.5 mm, have been tested in different temperatures (room temperature of ca. 20°C, 0°C, -20°C, -40°C). All the specimens have been divided into two groups. For each steel the first group (3 smooth and 3 notched specimens for tensile testing and 11 for Charpy impact testing) had been stored in room temperature air before testing without hydrogenation, while the second (analogous) group had been hydrogenated by cathodic charging before testing. The specimens of the second group had been submerged in 3.5% salt water and coupled to zinc anodes. Such conditions of hydrogenation are similar to conditions created by in-service cathodic protection of ship hull structures, although they are not strong as in numerous laboratory tests focused on hydrogen embrittlement problem.

The time necessary for hydrogen to diffuse from surface to the center of the specimen has been calculated by the following solution of the Second Fick's Law

$$X_{0.5} = 0.954\sqrt{D_H t}$$

where:

$X_{0.5}$ – the distance of diffusion at which the hydrogen concentration C equals $0.5C_0$ (C_0 – hydrogen concentration in the surface layer of steel)
D_H – diffusion coefficient for hydrogen in the steel
t – the time of diffusion

Putting the following values: $X_{0.5}$ = 0.4 mm (half of the Charpy specimen thickness, because half of the tensile testing specimen was smaller), $D_H = 10^{-7}$ cm^2/s, into the above equation, one can obtain t = 1758918 s = 21 days. The specimens were hydrogenated for 60 days therefore real concentration of hydrogen is the specimens' center could be higher than 50% of its concentration in the surface layer of the specimens. Zinc anodes were periodically cleaned in order to remove the surface oxide layer.

Among hydrogenated specimens all the tensile ones and some of the Charpy impact ones have been tested in room temperature directly after they were pulled out of the water and wiped dry. The Charpy impact specimens tested in lowered temperatures have been tested after a cooling period (denatured

alcohol and liquid nitrogen) and wiped dry, but no longer than 20-25 minutes after the end of hydrogenation procedure.

The tests have been carried out according to the Polish Standards PN-EN 10002-1 (tensile testing) and PN-EN 10045-1 (Charpy impact test) and only geometry of the notched specimen for tensile testing was not standard.

TEST RESULTS AND DISCUSSION

Tension diagrams for smooth (unnotched) specimens are shown in Figs. 1 and 2. For hydrogenated specimens of the both steels tested the strength parameters, i.e. ultimate tensile strength UTS (R_m), yield stress YS (R_e) and a plasticity parameter elongation after fracture (A) are slightly higher than for as-received (not hydrogenated) steel specimens. Tension diagrams for notched specimens are not reported in the present paper. The same tendency is evident on the base of averaged data summarized in Table 1, (each value represents an average based on 3 specimens).

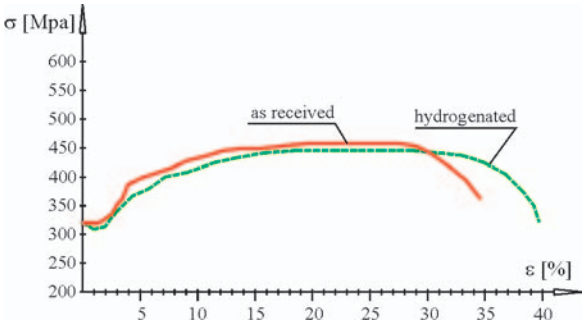

Fig. 1. *Comparison of the tensile diagrams for an as received specimen to a hydrogenated one of ordinary strength steel grade A*

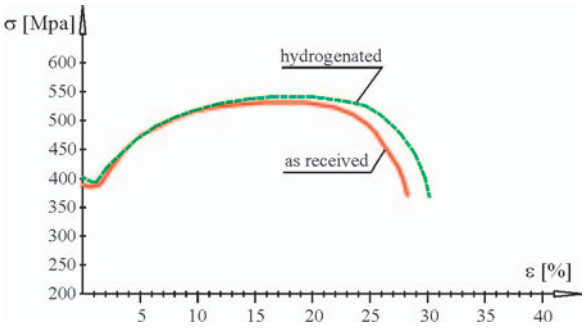

Fig. 2. *Comparison of the tensile diagrams for an as received specimen to a hydrogenated one of higher strength steel grade AH32*

Table 1. *Averaged results of tensile testing*

steel	specimen type	hydrogenation	A_5 %	Z %	R_e MPa	R_m MPa	% brittle fracture
A	plain	no	36.8	68.3	309.2	449.2	0
		yes	38.9	68.3	327.1	446.5	0
	notched	no	8.9	-	463.8	625.0	25
		yes	10.3	-	-	621.0	15
AH32	plain	no	33.0	79.3	392.8	533.4	0
		yes	32.6	70.4	408.7	535.4	0
	notched	no	6.7	-	612.4	747.1	0
		yes	8.3	-	-	735.8	0

For smooth specimens the following effects of cathodic hydrogenation have been observed:

- it has increased yield stress (R_e) 6% for A steel and 4% for AH32 steel
- It has practically not changed ultimate tensile strength (R_m) for the both steels
- it has 6% increased elongation (A) for A steel and has not changed for AH32 steel
- it has not changed the reduction of area (Z) for A steel and decreased for AH32 steel.

So the influence of hydrogenation of the steel on its elongation (A) has appeared to be slightly beneficial, but the influence on the reduction of area (Z) has appeared to be neutral or slightly detrimental. Analogous results have been obtained by Domzalicki et al [7] for an ordinary strength steel at cathodic potential –0.8 V (SCE) without bacterias. In the present Authors opinion parameter A is more important from practical point of view because every static or quasistatic fracture is due to exceeding of critical ability of steel to elongation in certain conditions rather than the ability of the reduction of area.

For notched specimens hydrogenation has not influenced R_m values and has caused a marked increase of elongation A (by 25% for A steel and by 33% for AH32 steel) although A-values for notched specimens are not representative, since they have been measured on the same gage length (40 mm) as for smooth specimens, while true plastic strains were concentrated very locally – in the notch root. Fracture appearance is also indicated in Table 1. All smooth specimens of both steels and the notched specimens of the higher strength steel AH32 fractured in a ductile mode but the notched specimens of steel A exhibited a mixed mode of fracture: ductile and brittle, and the hydrogenated specimens fracture surfaces are less brittle (average 15% brittleness) than as-received ones (25%).

Charpy V impact testing results are listed in Table II for individual specimens as well as averaged values for specimens grouped according to the same steel grade, testing temperature and preconditioning (as received or hydrogenated). Averaged values of Charpy V impact toughness energy (KV) are plotted in Fig. 3 and averaged values of percent ductility (fibrosity) of fracture surface are plotted in Fig. 4 versus the testing temperature. Both the Charpy fracture energy (KV) and the fracture appearance show that the hydrogenated steels behave less brittle than as-received ones. For ordinary strength steel A this beneficial effect of hydrogenation seems to be

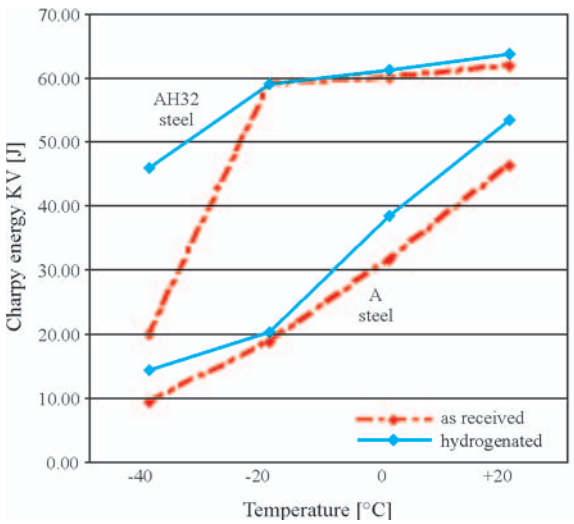

Fig. 3. *Diagrams of Charpy V impact energy versus the testing temperature for both steels.(an ordinary strength A steel and a higher strength AH32 steel) in both an as-received and a hydrogenated conditions*

Table 2.

test temperature °C	hydrogenation	steel	specification no.	fibrosity %		KV J	
20	no	A	1	86.87	82.1	43	46.3
			2	85.90		50	
			3	73.59		46	
		AH32	4	100	100	61	62
			5	100		64	
			6	100		61	
	yes	A	7	91.5	91.5	55	53.3
			8	97.45		53	
			9	85.43		52	
		AH32	10	100	100	63	63.7
			11	100		63	
			12	100		65	
0	no	A	13	27.92	41.1	26	31.7
			14	39.72		32	
			15	55.62		37	
		AH32	16	100	100	60	60
			17	100		60	
			18	100		60	
	yes	A	19	62,36	63.6	36	38.3
			20	66.73		44	
			21	61.74		35	
		AH32	22	100	100	61	61.3
			23	100		62	
			24	100		61	
-20	no	A	25	28.23	18.4	-	18.8
			25’	12.0		19.5	
			26	24.65		17	
			27	8.86		20	
		AH32	28	84.55	90.3	56	59
			29	90.31		58	
			30	96.00		63	
	yes	A	31	16.77	23	17	20.3
			32	17.1		17	
			33	34.98		27	
		AH32	34	96.43	93.5	56	59
			35	92.5		61	
			36	91.4		60	
-40	no	A	37	10.4	10.3	8.5	9.3
			38	10.2		10	
		AH32	39	42.5	39.2	18	20
			40	33.83		22	
	yes	A	41	16.5	8.8	17	14.5
			42	1		12	
		AH32	43	79.62	77.8	52	46
			44	75.92		40	

approximately independent of temperature judging by KV values, while reaches a maximum at a transition temperature judging by fracture appearance. For the higher strength steel AH32 the beneficial effect of hydrogenation increases as temperature decreases, but the specimens have not been tested in temperatures below -40°C which seems to be close to ductile-brittle transition temperature, therefore the maximum beneficial effect of hydrogen can be at a temperature close to a transition one as it was for the ordinary strength steel.

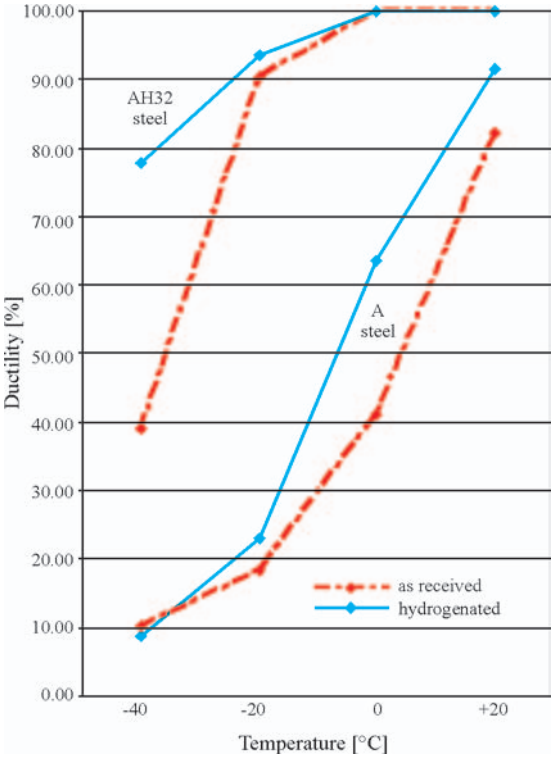

Fig. 4. *Diagrams of percent fibrous (ductile) appearance versus the testing temperature for both steels.(an ordinary strength A steel and a higher strength AH32 steel) in both an as-received and a hydrogenated conditions*

Fracture energy (KV) at any temperature can be considered as a sum of the energy absorbed to initiate fracture (KV_i) and the energy to cause it to extent or propagate (KV_p)[18]:

$$KV = KV_i + KV_p \tag{1}$$

Newhouse [16] has stated that the crack initiation energy KV_i is relatively constant throughout the ductile-brittle transition range of temperatures, while the crack propagation energy KV_p varies with temperature. Although the independence of KV_i on temperature is questioned sometimes [17], Newhouse' approach has been applied for the present analysis. The propagation energy is equal to energy absorbed by the cleavage (brittle) portion of fracture (KV_{pc}) plus that absorbed by the fibrous (ductile) portion (KV_{pf}):

$$KV_p = KV_{pc} + KV_{pf} \tag{2}$$

It has been shown [16] "that an insignificant portion of the total energy measured in the Charpy impact test is absorbed in the brittle portion of the fracture and that almost all is due to fracture initiation, fibrous tearing and lip formation". The fracture propagation energy can be assumed as proportional to fibrous portion of the fracture surface [16, 17] thus in the transition range of temperature:

$$KV = KV_i + kx \tag{3}$$

where: x is the percent of fibrous (ductile) fracture, and k is a constant.

Diagrams KV versus x are presented in Figs 5-8. Following Newhouse approach, each point in these diagrams represents values KV and x for an individual specimen. Equations (3) evaluated by the least square method as well as the correlation coefficients R^2 values are shown in the figures. Following values of fracture initiation energy KV_i have been obtained:

- 10.5 for as received A steel
- 9.6 for hydrogenated A steel
- -5.6 for as received AH32 steel
- -7.4 for hydrogenated AH32 steel

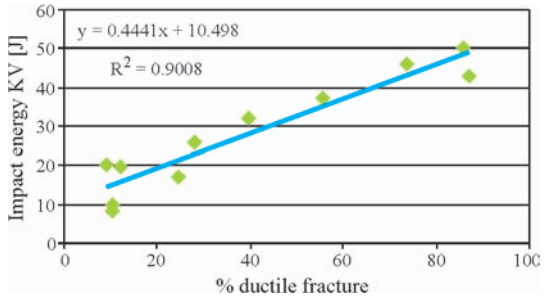

Fig. 5. Relation between Charpy V energy and percent of ductile (fibrous) fracture appearance for as received A steel

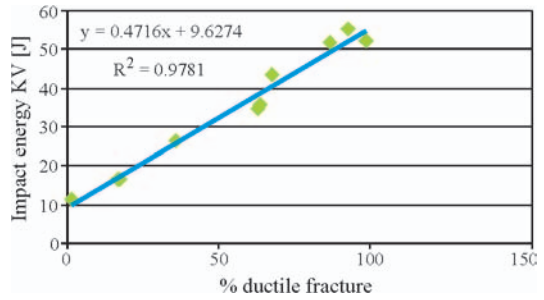

Fig. 6. Relation between Charpy V energy and percent of ductile (fibrous) fracture appearance for hydrogenated A steel

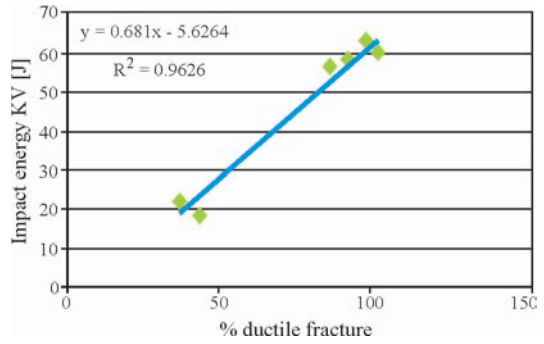

Fig. 7. Relation between Charpy V energy and percent of ductile (fibrous) fracture appearance for as received AH32 steel

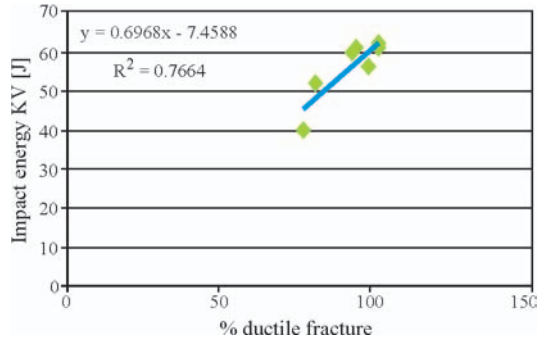

Fig. 8. Relation between Charpy V energy and percent of ductile (fibrous) fracture appearance for hydrogenated AH32 steel

Hydrogenation caused the reduction of the crack initiation energy for A steel (by 8%) and for AH32 steel, but both values for the second steel are below zero. Newhouse reported such results as occasional ones and attributed them to "error in measurement of fracture appearance, particularly at low fibrosity levels" In the present tested temperatures range the overwhelming majority of specimens of the AH32 steel exhibited relatively high fibrosity levels with only two specimens with medium fibrosity, therefore the values of KV_i have been evaluated by far extrapolation of the curve based on data for relatively high fibrosity levels to the nil ductility level with an inevitable error. It has appeared that hydrogen reduced the crack propagation energy for steel A only slightly and beneficial effect of hydrogenation on Charpy impact energy concerns mainly the crack propagation energy. Indeed, the Newhouse approach has appeared not to be successful in the present case of AH32 steel, but one can risk an opinion that energy KV_i for the steel is presumably lower than for steel A.

For present specimens of reduced thickness 7.5 mm the minimum Charpy energy required by the rules of the Classification Societies is equal to 5/6 of the energy for full thickness 10 mm specimens and the energy required for the present A and AH32 steels equals 22.5J and 25.8J respectively. The transition temperature, at which the Charpy energy drops below its required value, for A steel equals -14°C for as-received and -18°C for cathodically hydrogenated specimens, while for AH32 steel the temperature is -36°C and below (probably well below) -40°C for as-received and hydrogenated steel respectively.

Charpy fracture appearance is preferred to Charpy energy KV as a fracture resistance indicator because of its more direct physical significance [18]. It is also more independent of specimen thickness thinner than 10 mm and notch orientation, while Charpy energy is sensitive to both [18]. Newhouse [16] and Sumpter et al [18] have considered fracture appearance transition temperature (FATT) corresponding to 50% ductile fracture as a very meaningful parameter. FATT for the present A steel equals +4°C for as-received and –7°C for hydrogenated conditions, while for AH32 steel FATT equals –37 for as-received and well below -40°C for hydrogenated conditions.

Although air temperature may fall as low as -15°C without the sea becoming frozen, it is very likely under those conditions that extensive icing of the decks would limit the steel temperature to not much below the freezing point of seawater (-2°C)[18]. Temperature 0°C covers most of practical interest. There is an opinion [18] that criterion of less than 70% of cleavage fracture (more than 30% fibrosity) at 0°C ensure a satisfactory level of resistance to cleavage fracture initiation of ship structures at the same temperature [18]. The present A steel in as-received condition is on the edge of this criterion (one of the specimens does not satisfy the criterion), while hydrogenation has shifted the steel into a safety region far from the edge. What is more, hydrogenation of the steel has enabled to fulfill a criterion of minimum 50% fibrosity at 0°C that should ensure a Robertson crack arrest temperature below 0°C [18] (this criterion concerns minimum 50% fibrosity at 0°C, while the above mentioned FATT concerns on an average 50% fibrousity at any temperature). For arrest of very long cracks in ship structures a 100% fibrous fracture appearance at 0°C is considered desirable [18] and the present A steel has not satisfied the criterion. The present AH32 steel in both conditions satisfies all the above criteria: minimum 30% and minimum 50% and 100% fibrosity with a large margin of safety.

Thus the present test results are qualitatively similar to preliminary test results [1, 2]. The beneficial effect of hydrogen is not easy to explain. There are, however, some regularities

in the results that could be taken into account in a formulation of a hypothesis:

- ⇨ Continuous decrease of a detrimental effect of hydrogen on mechanical properties of steels with increase of the steels deformation rate has been reported by numerous investigators, so it has temporarily been hypothesized [1, 2] that a beneficial effect of hydrogen can appear for very high deformation rates as in Charpy test. This working hypothesis is, however, inconsistent with numerous Charpy tests data for steels and only the present Authors investigations results support this hypothesis.
- ⇨ In every case of notched specimens the beneficial effect of hydrogenation is more evident than for smooth ones, e.g. a marked increase of elongation A and decrease of fracture appearance brittleness for hydrogenated specimens in tensile testing The notched specimens were hydrogenated in unstressed condition thus locally increased hydrogen concentration due to stress concentration at the notch root had not been reached before testing. The relation between the presence of notch and hydrogenation effect can be, however, considered as the effect of strain rate too, since in static tensile testing the deformation rate in notch root is always higher than the rate in plane specimen, but lower than for Charpy V specimen in impact test.
- ⇨ The present hydrogenation conditions (the applied potential and near-neutral electrolyte without any promoter of hydrogenation) were not so strong as in numerous studies on hydrogen effects on steels properties. Cathodic deposits visible on the specimens surfaces could additionally reduce the hydrogenation intensity. Therefore hydrogen concentration in the present tests could not be as strong as in other tests. Extensive investigations of numerous steels after high-temperature hydrogenation [12] have also exhibited evidently beneficial effect of hydrogenation on mechanical properties of the steels on condition that hydrogen pressure, temperature and hydrogenation duration were small enough to avoid hydrogen-induced corrosion (mainly: decarburization) and hydrogen concentration was not very high, i.e. moderate. In the present investigations the moderate concentration means the value of concentration reached at a potential about –1.05 V, while in SSRT realized by Domzalicki *et al* [7] it was another value reached at -0.8 V. So the value of concentration denoted above as "moderate" depends on the strain rate, but perhaps on hydrogenation conditions too – in the present tests the cathodic potential was applied before the testing and some, but not large, degree of desorption of hydrogen from subsurface layer of steel can be expected in spite of short time distance between the end of hydrogenation procedure and the end of a test, while in Domzalicki *et al* investigations the appropriate cathodic potential was applied during testing and desorption was impossible.

Some published test results seem to be inconsistent with the above regularities. For example numerous data [19] show a marked reduction of critical values of the stress intensity factor (K_Q, K_{IC} or $K_{Iρ}$) in spite of the fact that the values have been evaluated by testing of notched and usually pre-cracked specimens. On the other hand a diagram [19] show that for a steel containing low hydrogen concentrations an increase of the concentration causes a significant decrease of K_Q at a lower deformation rate and does not influence K_Q at a higher deformation rate. It cannot be excluded that, in fact, a combination of the three above conditions should be satisfied jointly for the beneficial effect of hydrogen to occur, i.e.:

- deformation rate is high enough
- notch is sharp enough if specimens have been cathodically protected in unstressed conditions
- hydrogen concentration is moderate

CONCLUSIONS

Static tensile testing of notched and smooth specimens and Charpy V impact testing have been carried out. An ordinary strength ship steel grade A and a higher strength steel grade AH32 in as received (not hydrogenated) and hydrogenated by cathodic protection (zinc) in salt water have been tested. The following conclusions have been drawn:

- ❍ Hydrogenation of steels have slightly increased yield strength (R_e) and elongation after the fracture (A) of both steels, it has not influenced ultimate tensile strength (R_m) of the both steels and reduction or area (Z) of the ordinary strength steel, while it has reduced Z for the higher strength steel. Notched specimens of the ordinary strength steel have exhibited a mixed mode fracture and the hydrogenated specimens have exhibited less brittle fracture appearance than as-received specimens. Thus the influence of hydrogenation on static tensile testing properties for the ordinary strength steel has been slightly less detrimental or even more beneficial than for the higher strength steel.

- ❍ Charpy V impact testing has shown that hydrogenation of both steels increased Charpy energy and percent fibrousity of fracture and shifted down ductile-brittle transition temperatures both energy-based and fracture-appearance-based (FATT) ones. It is mainly due to the effect of hydrogenation on the fracture propagation energy. In ship service temperature 0°C is very important. The tested steels in as received and in hydrogenated conditions have satisfied minimum 30% of fibrousity at 0°C criterion (that ensures satisfactory crack initiation resistance at this temperature), although the ordinary strength steel tested without hydrogenation has been on the edge of this criterion. Hydrogenation of the ordinary strength steel have also enabled to satisfy the minimum 50% of fibrousity criterion that ensures a Robertson crack arrest temperature below 0°C. A 100% of fibrousity criterion for arrest of very long cracks is satisfied only for the higher strength steel in the both conditions.

- ❍ A common current practice to evaluate mechanical properties of ship steels by testing the specimens that have not been hydrogenated leads to conservative results. A case of notched steels hydrogenated in stressed conditions have to be, however, recognized in future.

- ❍ The present ordinary strength steel A has satisfied the Classification Societies requirements for B steel, while the higher strength steel AH32 satisfied the requirements for DH40 steel.

- ❍ The present author hypothesize that the following conditions are necessary for beneficial effect of hydrogenation on mechanical properties of steels to occur:

  - ◆ hydrogen concentration is moderate;
  - ◆ notch is sharp enough (valid presumably for specimens hydrogenated in unstressed conditions only);
  - ◆ deformation rate is fast enough.

BIBLIOGRAPHY

1. M. Jakubowski: *Causes of the crack in the bottom plating of m/s „Beskid”*, An expert opinion (unpublished) (in Polish), Gdansk University of Technology, Gdansk 2003
2. M. Jakubowski: *Could local buckling of bottom plating of a small tanker be an immediate reason of crack in the structure?* (in Polish), Proc. 21-th Symposium on Fatigue and Fracture of Materials and Structures, Bydgoszcz-Pieczyska, May 23-26, 2006, pp. 139-147
3. D. Le Friant, B. Bayle, C. Adam, Th. Magnin: *Stress corrosion cracking of X52 pipeline steel in deoxygenated dilute aqueous solution*, Proc. Int. Conf. on Environmental Degradation of Engineering Materials, 19-23 Sept. 1999, Gdansk-Jurata, Poland, Vol. I, pp. 168-173
4. E. Lunarska, D, Samatowicz, E. Sitko: *Hydrogen embrittlement of 30HGSNA aircraft steel in Cl^- containing environments*, Proc. Int. Conf. on Environmental Degradation of Engineering Materials, 19-23 Sept. 1999, Gdansk-Jurata, Poland, Vol. I, pp. 334-339
5. K. Pokhodnya, V.I. Shvachko, S.M. Stepanyuk: *Experimental modeling of cold cracking of structural steels and welds*, Proc. Int. Conf. on Environmental Degradation of Engineering Materials, 19-23 Sept. 1999, Gdansk-Jurata, Poland, Vol. I, pp. 351-356
6. A. Zieliński, P. Domżalicki: *Hydrogen degradation of high-strength low-alloyed steels*, J. of Materials Processing Technology, 2003, Vol. 133, pp.230-235
7. P. Domżalicki, E. Łunarska, D. Kwiatkowska, H. Wichary, J. Birn: *Effect of cathodic polarization in microorganisms-containing seawater on mechanical properties of steels* (in Polish), Ochrona przed korozją, 2004, No. 12, pp. 338-340
8. M. Śmiałowski: *Hydrogen in steels, publishers* (in Polish). WNT, Warsaw 1961
9. G.V. Karpenko, *Strength of steels in corrosive environment, publishers* (in Russian). Mashgiz, Moscow-Kiev 1963
10. L.S. Moroz, B.B. Chechulin: *Hydrogen embrittlement of metals* (in Russian), Publishers: Metallurgia, Moscow 1967
11. E. Lunarska: *Effect of hydrogen on the iron plasticity* (in Polish), Scientific Bulletins of the Stanislaw Staszic University of Mining and Technology, No. 997, series: Metallurgy and Foundry Practice, Bulletin 101,(monography), Kraków 1984
12. Yu. I. Archakov: *Hydrogen corrosion of steels* (in Russian), publishers.: Metallurgia, Moscow 1985
13. J. Juraszek, J. Nowak, Z. Jurasz: *Effect of corrosion on mechanical properties of ship hull plate steels*, Proc. Int. Conf. on Environmental Degradation of Engineering Materials, 19-23 Sept. 1999, Gdansk-Jurata, Poland, Vol. II, pp.73-76
14. J. Toribio, V. Kharin: *Load dynamics effects on crack-tip hydrogen accumulation in metals*, Proc. Int. Conf. on Environmental Degradation of Engineering Materials, 19-23 Sept. 1999, Gdansk-Jurata, Poland, Vol. I, pp. 399-404
15. G.V. Karpenko: *Serviceability of structural materials in aggressive environments* (in Russian), publishers: Naukova Dumka, Kiev 1985
16. D.L. Newhouse: *Relationship between Charpy impact energy, fracture appearance and test temperature in alloy steels*. Welding Journal, 1963, no. 3, pp. 105s-114s
17. M. Szkodo, Z. Zaczek: *Application of D.L. Newhouse method in estimation of the energy to initiate fracture in quenched and tempered 18G2A steel* (in Polish). Scientific Bulletins of Gdansk University of Technology, No. 425, Series: Mechanics, No. LV, pp.11-20
18. J.D.G. Sumpter, J. Bird, J.D. Clarke, A.J. Caudrey: *Fracture toughness of ship steels*, The Transactions of The Royal Institution of Naval Architects, Vol. 131, 1988, pp.169-177
19. S.E. Kovchyk, E.M. Morozov: *Fracture Mechanics and material strength* (in Russian), Vol. 3, Publishers: Naukova Dumka, Kiev 1988

NOMENCLATURE

- A – elongation (after fracture in tensile testing)
- D_H – hydrogen diffusion coefficient
- KV – Charpy-V impact energy
- KV_i – energy to cause the crack initiation
- KV_p – energy to cause the crack propagation
- KV_{pc} – impact energy absorbed by the cleavage (brittle) portion of fracture
- KV_{pf} – impact energy absorbed by the fibrous (ductile) portion of fracture
- R_e – yield strength
- R_m – ultimate tensile strength
- t – time of hydrogen diffusion
- x – percent of fibrous (brittle) fracture
- $X_{0.5}$ – distance of diffusion at which the hydrogen concentration equals $0.5C_0$ (where C_0 is hydrogen concentration in the surface layer of steel)
- Z – reduction of area (in tensile testing)

ABBREVIATIONS

FATT – fracture appearance transition temperature
SSRT – slow strain rate test

CONTACT WITH THE AUTHOR
Assoc. Prof. Marek Jakubowski
Faculty of Ocean Engineering
and Ship Technology
Gdansk University of Technology
Narutowicza 11/12
80-952 Gdansk, POLAND
e-mail : marjak@pg.gda.pl

POLISH MARITIME RESEARCH 1(55) 2008 Vol 15; pp. 72-79
DOI: 10.2478/v10012-007-0055-4

Visual identification of underwater objects using a ROV-type vehicle: "Graf Zeppelin" wreck investigation

Commander Adam Olejnik, PhD.
Polish Naval Academy

ABSTRACT

The article presents a method of visual identification of underwater objects using a remotely controlled underwater ROV-type vehicle. The method was developed in the Department of Diving Technology and Underwater Activities, Polish Naval Academy, and was positively verified when identifying wrecks of such vessels as "General von Steuben", "Fryderyk Engels" and "Graf Zeppelin". The article gives a description of the method, illustrated by samples of its use for investigating the wreck of "Graf Zeppelin".

Key words: the wreck of "Graf Zeppelin" as an example of visual identification of underwater objects

INTRODUCTION

The present-day hydrographic survey equipment offers vast opportunities to investigate various underwater objects, which may even include early detection of the leakage of oil derivatives from tanks situated at the sea bottom [5]. The recording instrumentation and computer software which assist nowadays a hydrographer in his/her work are really impressive, among other opportunities they offer three-dimensional visualisation, in the post-processing phase, of the collected measurement data. But despite those facilities and high technical potential, hundred-percent identification of an underwater object still sometimes needs its visual observation. It can be done in a number of ways, out of which hyperbaric methods (with human diving teams), or those making use of unmanned underwater vehicles are most frequently used. As for the hyperbaric methods, diving reconnaissance of objects situated at depths exceeding 50 m H_2O may be difficult. A serious difficulty in this case is not only the hydrostatic pressure itself, but also rather a human being with his/her "imperfections". The air, a natural breathing medium, can only be used in diving to the depths not exceeding 50 meters. Deeper underwater activities require a breathing gas with lower specific gravity and different percent share of the oxygen than in the air. Indeed, numerous technologies were developed to allow divers to do their work even as deep as below 300 – 450 meters, but these activities are very time-consuming, and, first of all, still extremely expensive. Therefore in identification activities, in which very fast mobilisation or the research team is sometimes required, in particular at depth exceeding 50 meters, unmanned underwater vehicles, most frequently of ROV type (Remotely Operated Vehicle), have been used. This device makes it possible to conduct remote observation of an underwater situation in a close zone of its activity. The range of data collected by the vehicle is only limited by parameters and type of the deck equipment installed on it. Among other instruments it may include a TV camera, a sonar, instruments for measuring hydrological parameters of the water, etc. A big advantage of the ROV is its relatively high mobility and ability to work long hours at high depths, sometimes in extremely difficult conditions. It is essential from the point of view of identification of underwater objects that the examined object can be observed in real time using a remote TV system. The recorded data are transmitted using a so-called control cable (stay cable). It not only secures transmission of the data collected by ROV deck equipment to the operator's station, but is also used for passing commands given by the vehicle operator to steer the motion of the vehicle and the operation of the deck equipment. The above advantages are the reason why the ROV vehicles are so useful, and are most frequently used in underwater work worldwide. Among other reasons, that is why the Laboratory of Unmanned Underwater Vehicles was established in the Department of Diving Technology and Underwater Activities (ZTNiPP), Polish Naval Academy. At present, its basic equipment is "Super Achille", a ROV-type vehicle, made by Comex Pro, France, complemented by the underwater navigation system with the USBL Scout ultra short base, produced by Sonardyne Ltd., United Kingdom, (Fig. 1). The Laboratory has obtained the accreditation of Benhtos Inc, (present name: Teledyne Benthos), USA, and Comex Pro for service and repairs of underwater vehicles produces by these companies. Moreover, as parts of Laboratory's activity, the vehicle repair technology was worked out, along with the methodology of ROV-aided assessment of the technical state of underwater objects, and the methodology of ROV-aided search and identification of underwater objects. These research

activities were implemented on commission by the Polish Navy, the Ministry of Justice (within the framework of preliminary proceedings in criminal cases, for instance, for Public Prosecutor's Offices in Olsztyn, Mysliborz, and Warsaw), the "Petrobaltic" Oil and Gas Exploration - Production Joint Stock company (evaluation of the technical state of the B3-4BRe bore-hole installation), and the Polish Navy Hydrographic Office. At present, activities are conducted in the Laboratory, which are oriented on developing a system of real-time three-dimensional visualisation and dimensioning of underwater objects with the aid of a low-cost construction of a small-size ROV-type vehicle. The article presents a methodology, developed in ZTNiPP, of ROV-aided visual wreck identification, complemented by sample results collected during investigations of the wreck of "Graf Zeppelin".

VISUAL WRECK IDENTIFICATION USING A ROV-TYPE VEHICLE

A detected underwater objects which can create a threat for navigation should be immediately reported to national hydrographic services [2]. In local conditions it means that each newly detected underwater object, which reveals the above features, is reported to the Polish Navy Hydrographic Office.

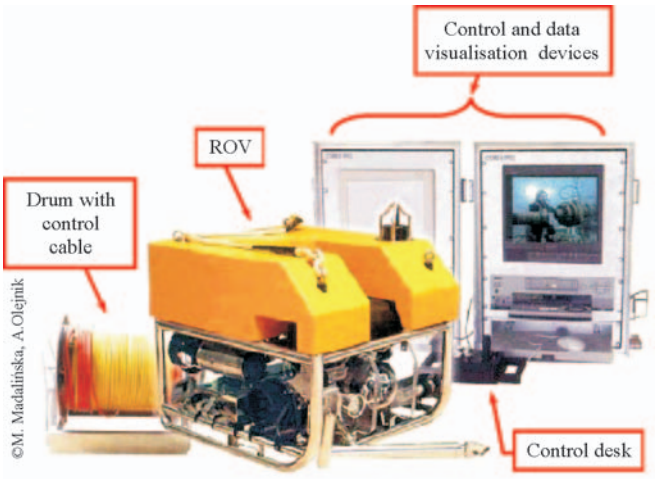

Fig. 1. *ROV-type vehicle „Super Achille" with basic equipment*

This way in July 2006, ORP "Arctowski" was ordered to check the position and dimensions of a large-size underwater object detected by the research ship "St. Barbara". The investigation team was complemented by research workers from the Department of Diving Technology and Underwater Activities, Polish Naval Academy, with ROV as the research equipment (Fig. 1). The task to be done by the investigation team was to take underwater photos of the object and do its visual identification. Usually operations of this type, when conducted with the aid of an underwater vehicle, include the following stages:

- ⇨ preparing the mission of the vehicle,
- ⇨ conducting the operating mission of the vehicle,
- ⇨ processing and analysing the collected data.

Preparing the ROV mission

This stage is executed before the exit to the region of wreck location. It basically consists in collecting relevant historical material, including photos, pictures, cross-sections, and basic technical data of the hypothetical object (for instance: length, width, number of shaft lines, positions and dimensions of the superstructure, masts, and cargo hatches). Moreover, all data are analysed which were collected during earlier hydrographic measurements.

Based on the above material and its analysis, a method of wreck inspection (vehicle trajectory) is worked out. The adopted method should provide opportunities for collecting the maximum possible volume of camera-recorded data, including characteristic constructional elements of the examined wreck. This stage is very important in the ROV operation, as the collected material should make the basis for wreck identification. At the same time the analysis of the information collected during hydrographic measurements in the past should result in working out the strategy of vehicle approach to the wreck, and selecting a relevant configuration of the vehicle - control cable arrangement. These issues will be discussed in detail in the section describing the operating mission of the vehicle.

ROV operating mission

The operating mission of the vehicle is prepared based on all information collected so far, and the data recorded during the hydrographic measurements [6]. Firstly, we select a configuration of the control cable - vehicle system, and then we select for the ROV a method how to approach the wreck. The configuration of the control cable - vehicle system depends on the depth at which the wreck is located [3,7]. When the examined object is at the depth ranging between 20 and 40 meters, the most convenient way is to use a floating cable as a stay cable to avoid trimming. We should remember, however, to avoid situations in which the floating stay cable, of a considerable length, floats freely in the depths of water behind the vehicle. In this case the operator cannot control its shaping, which can provoke hooking of the cable to the wreck construction, or cable damage. If it happens, we can swim along the cable until we reach the point of hooking and then analyse the situation on-site. Sometimes a sufficient remedy to free the vehicle is to do some simple manoeuvres. When this fails, we should drive the vehicle to the surface over the wreck structure, as far as the cable permits. Most frequently in these situations, a loop formed around a mast, for instance, will rise over its construction and free the vehicle. In extreme cases, a diving team is to be involved to free the vehicle. In such a case we loosen the cable to the maximum on the drum and drive the vehicle to the surface, to the minimum possible depth (preferably to the non-decompression zone). When the divers start diving, the ROV supply is to be switched off to allow the diver safely approach the vehicle and disconnect the control cable [8]. Then the cable can be pulled out by winding it onto the drum. In an extreme case when the cable cannot be pulled out, we take the risk to lose the cable but we still can get back the vehicle, the most expensive system component. At higher depths, ranging between 40 and 120 meters, a useful method is to use a combined stay cable, consisting of the floating segment and the non-floating segment. This configuration of the control cable - vehicle system is shown in Fig. 2. This solution reminds a traditional method of circular search in diving techniques. The non-floating cable segment, directed vertically down to the depth at which the wreck is situated, is mounted to the loaded descending line, while the floating segment plays a role of the distance line.

The operating mission of the vehicle at depths exceeding 120 meters can be most safely conducted using a so-called underwater garage. The underwater garage is a structure reminding a metal cage with a cable drum. When inside this cage, the vehicle is safely transported from the deck of the base craft (understood as the vessel/ship from which the vehicle is

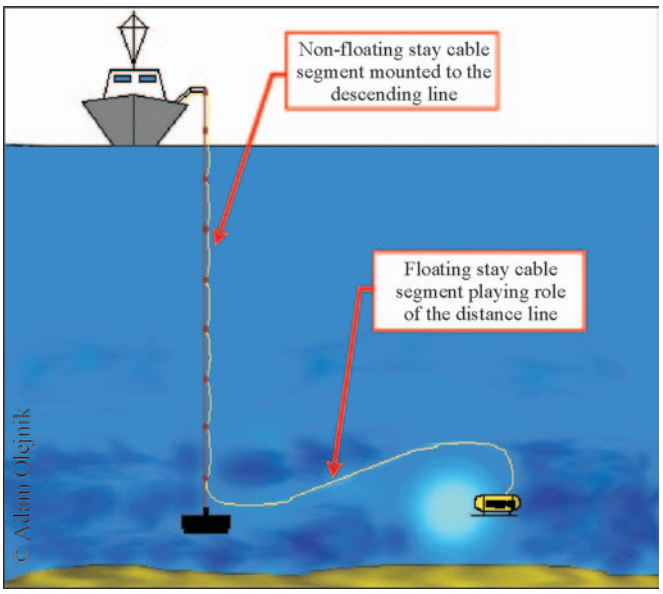

Fig. 2. *The control cable - vehicle arrangement for depths ranging between 40 and 120 meters [8]*

operated) to the level of wreck location. And only when it reaches this level, the vehicle leaves the garage and starts its operating mission, which first of all consists in safe approach to the wreck. After selecting the control cable - vehicle arrangement we can start submerge the vessel in the water. In this case, however, when there is no access to the underwater garage, it is advisable to do first the reconnaissance of the possible ROV approach trajectory to the bottom. Among other factors, its necessity results from the fact that sonar visualisation usually does not take into account nets nor cables/ropes surrounding the wreck. The trajectory of vehicle approach to the bottom in the area or close vicinity of the examined object can be recognised using an underwater TV camera lowered vertically down to the bottom. Using this camera, the situation along the vehicle submersion trajectory can be visualised, which facilitates assessing the type and scale of possible threats. Even if, for various reasons, the camera is damaged or lost, this loss is incomparably less expensive than possible loss of the vehicle. When submerging, the vehicle can crash into protruding construction elements of the examined object (masts, smokestacks), or get immobilised when the vehicle propulsion system gets entangled in parts of the nets surrounding the wreck, in particular in fishing areas. Sometimes lack of this reconnaissance may lead to an accident. A situation of this type took place when identifying the wreck of "Goya" using a small-size ROV vehicle named "Gnom" [6]. After its propellers had got entangled in the nets the vehicle was totally immobilised. An attempt to free it by a team of divers ended with their death.

The reconnaissance is done immediately after the base vessel is anchored. It is noteworthy that the position of base vessel anchorage is usually a compromise between its safety and operating abilities of the underwater vehicle. It happens very rarely that the captain of the ship from which the vehicle is operated agrees to anchor directly over the wreck. In all other cases, taking into account ship safety we should select the anchoring position in such a way as to provide opportunities for the vehicle to approach the examined object from the direction opposite to that defined by its masts and/or smokestacks. After recognising the trajectory of vehicle submersion, the operation can start. When the vehicle reaches the bottom of the sea, it should be directed towards the examined object. The way in which the vehicle approaches the examined object depends on its deck equipment and abilities of the used homing systems. Wreck approaching over a so-called oval wreckage field cannot be used in the Baltic Sea, as this phenomenon occurs at much higher depths than those recorded in this water region [1, 8]. The oval wreckage filed is created when the ship sinks and all heavy constructional elements fall down almost vertically, while the lighter parts are convected by underwater currents and drop slower. As a consequence, when the distance to the bottom is sufficiently large, these light elements are spread over a relatively large area. On the Baltic Sea small wreckage fields can be observed in the vicinity of wrecks, or characteristic bottom material corrugation resulting from the impact of the sinking ship into the bottom [5]. All this is the effect of a relatively low depth, on average, of the water region, in which the sinking ship is sometimes longer than the depth at which is sinks.

In case of the simplest control cable-vehicle arrangement the ROV is directed towards the wreck using indications of the deck sonar mounted on the vehicle.

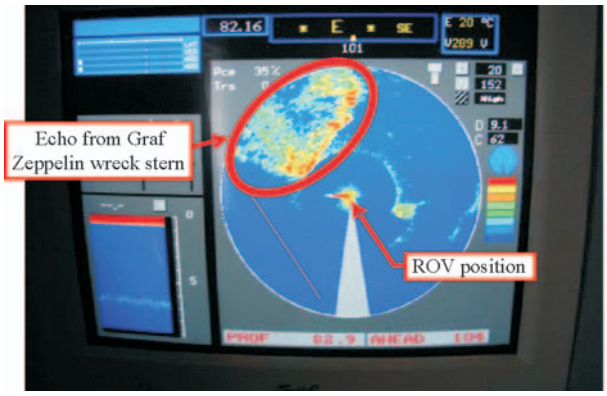

Fig. 3. *ROV service desk in operation: sonar screen. Echo from the stern of the examined underwater object and vehicle position with respect to it are clearly visible (photo: S. Lipiński)*

When submerging the vehicle we stop it at a distance of about 1,5 meters from the bottom surface and do the sonar reconnaissance around the vehicle (Fig. 3). The above task is quite easy if the vehicle is equipped with an all-round sonar, as in this case it will be able to visualise the situation within the angle of 360° in the vicinity of the vehicle. By recording the strongest and the weakest echo on the sonar we obtain the information on the course and distance of the wreck from the current position of the vehicle. When the ROV does not have such a sonar, the water region should be scanned in parts to collect this information. Keeping it at one place, we rotate the vehicle several times by 90° and analyse the sonar screen. Homing the vehicle to the wreck can be made easier by the use of an underwater navigation system, which allows the information on the current underwater position of the ROV vehicle with respect to the wreck position to be recorded. The underwater navigation system makes use of the network of acoustic transponders. Depending on the positions of the transponders and the distance between them, three types of systems can be named:

- with a long base line (LBL),
- with a short base line (SBL),
- with an ultra short base line (USBL).

In ZTNiPP the Scout-type USBL system is used, basic components of which are shown in the figure below.

The USBL system makes use of a hydroacoustic transponder, mounted on the ROV, and the head with a series of transmitters and receivers. The vehicle position is calculated from a series of measurements consisting in determining the distance between the head and the transponder. A converter mounted on the ROV transmits the signal to the head, which, among other things,

measures the time between the signal transmission and the reception of the return signal. The measured time, along with the known speed of sound, make the basis for calculating the distance from a given transponder. A collection of results of these measurements, combined with the geographic position of the transmitting/receiving head, known from the DGPS receiver and treated as the vehicle position, are displayed on the monitor screen of the underwater navigation system (Figs. 4 and 5).

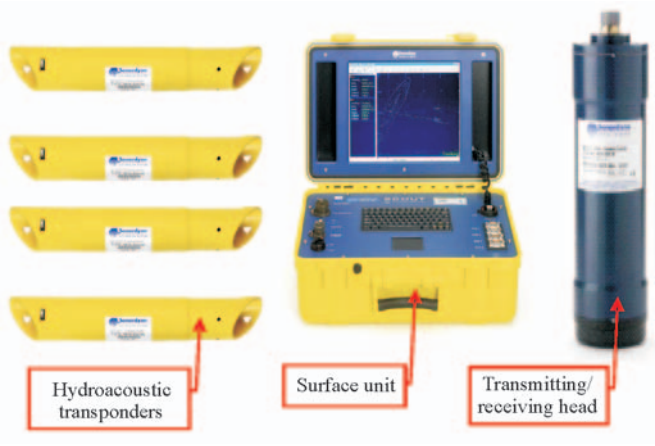

Fig. 4. *Producer's set of the USBL Scout system*

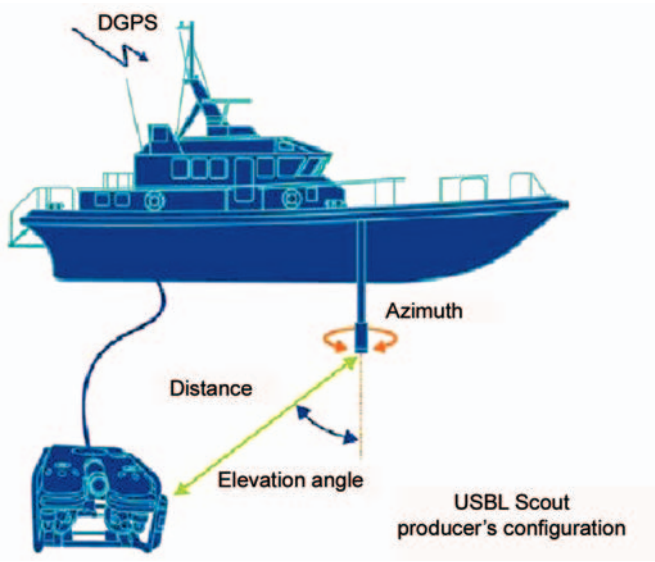

Fig. 5. *Principle of USBL system operation [11]*

Since ZTNiPP operates from various base ships, sometimes also on inland water regions, it turned out necessary to work out and produce a design which would allow the research team to become independent of watercraft type, in order to make full use of the owned USBL system. For this purpose a special measuring buoy was built (Fig. 6). The buoy consists of a mast and displacement floats. On its underwater part the transmitting/ receiving head of the USBL Scout system is mounted, while on the top of the mast the DGPS receiver is installed to read geographic coordinates of the buoy position. The assembly of the DGPS receiver and the USBL Scout head on one mast (in one axis) eliminates the need for measuring the distance and relative positions of these two devices, along with storing these data in the memory of the USBL system.

The last stage of the operating mission of the vehicle is covering the planned trajectory within the wreck structure. Each time the route should be started from the ship's side and from the bottom level. This procedure allows avoiding any damages, which could possibly result from a collision

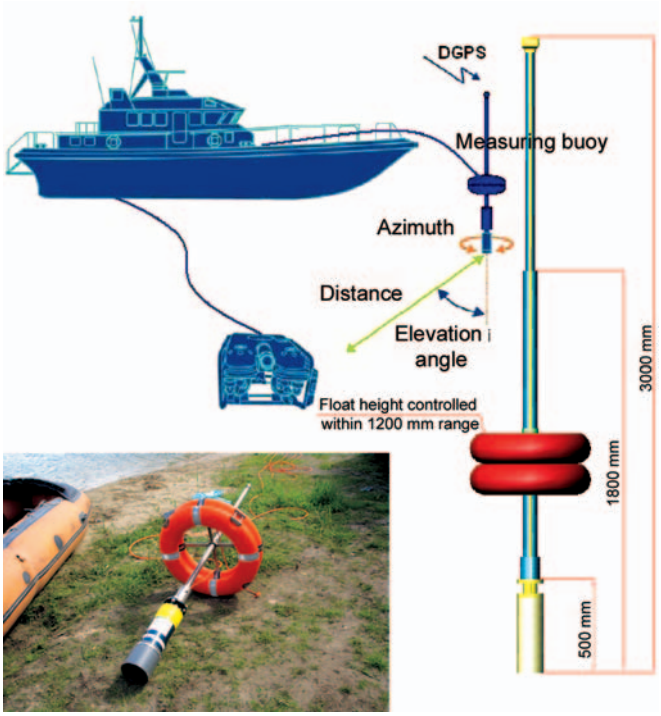

Fig. 6. *USBL Scout system configuration, worked out in ZTNiPP and making use of the measuring buoy*

with the wreck structure due to small space visualised by the camera mounted on the vehicle and insufficient, as a rule, information on the real structure of the wreck. In cases of any identification research, it is most likely the first time for years or even decades when the wreck is observed within a visible band. That is why the reconnaissance is to be started from the bottom level, and the vehicle is to be directed along the ship's side toward the surface, to the level of the main deck. When in there, the vehicle should move in parallel to the ship's side and search for characteristic constructional elements. The passing trajectory over the wreck should provide opportunities for filming most representative material, based on which wreck identification and verification could be done. Each recorded detail (shape of the superstructure, number and distribution of portholes, number of davits, position and size of holds, positions of navigation lamps, number of shaft lines, supporting bearings, etc.) will increase chances for positive verification. An ideal solution is reading the name of the ship written on its side of stern, but it happens rather rarely and refers to wrecks which do not stay long on the bottom. In case of older objects this is less likely due to intensive hull covering with a growth. When the wreck of the "Graf Zeppelin" aircraft carrier was identified, a number of vehicle dives were done from the deck of ORP „Arctowski" to the depth of about 90 meters. During these dives the vehicle covered the trajectory shown in Fig. 7. As a result, about 3,5-hour material was recorded on the film and then used for comparison with the historical material. The next figure presents selected film frames extracted from the above video material.

Processing and analysing of the collected data

When the operating mission of the vehicle ends, we can proceed to processing and analysing the collected data. This is a so-called post-processing stage, in which we make use of all data collected so far on the examined object, and compare them with the archival material. The best way in this case is to use relevant computer software to extract individual frames from the film and process them digitally. If, during the

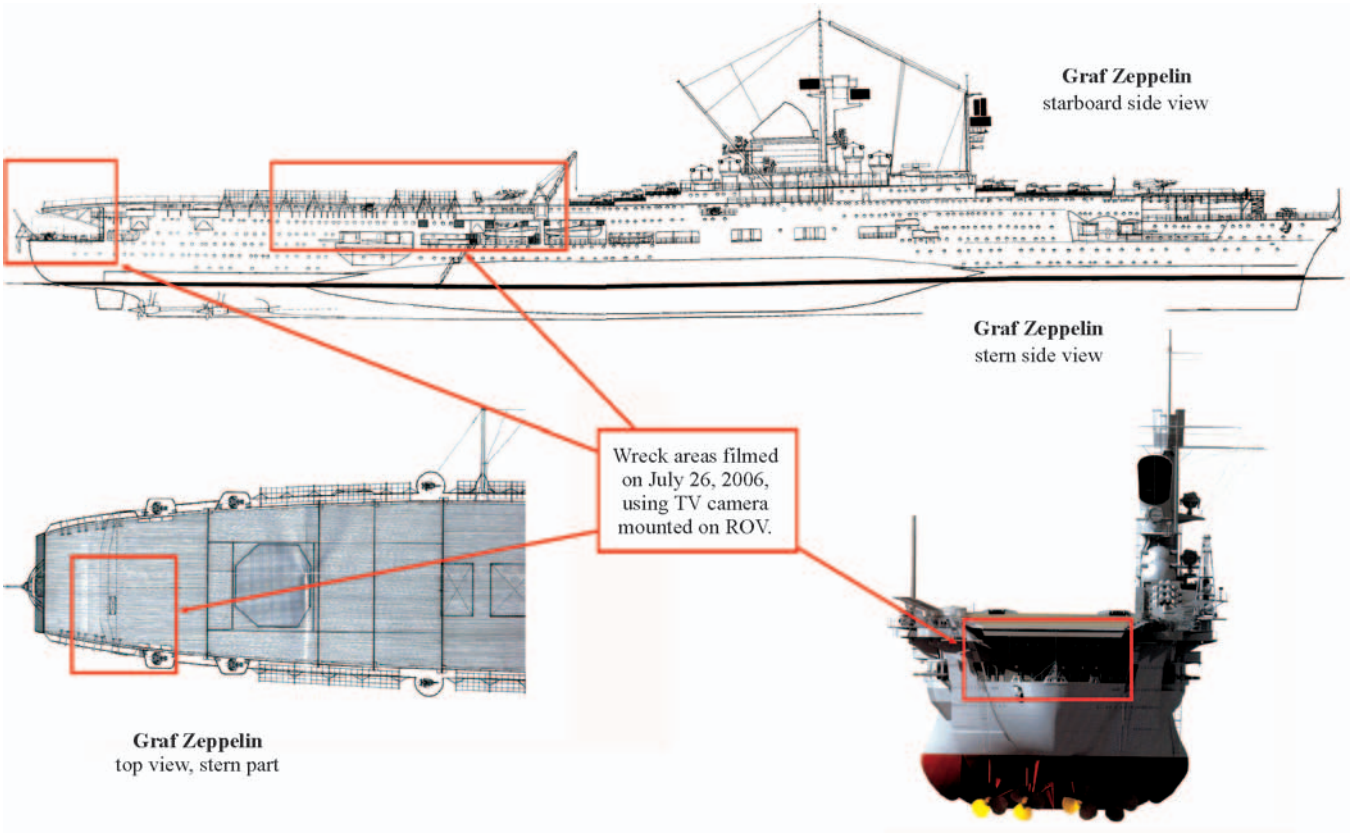

Fig. 7. ROV trajectory during identification of the "Graf Zeppelin" wreck [4, 9]

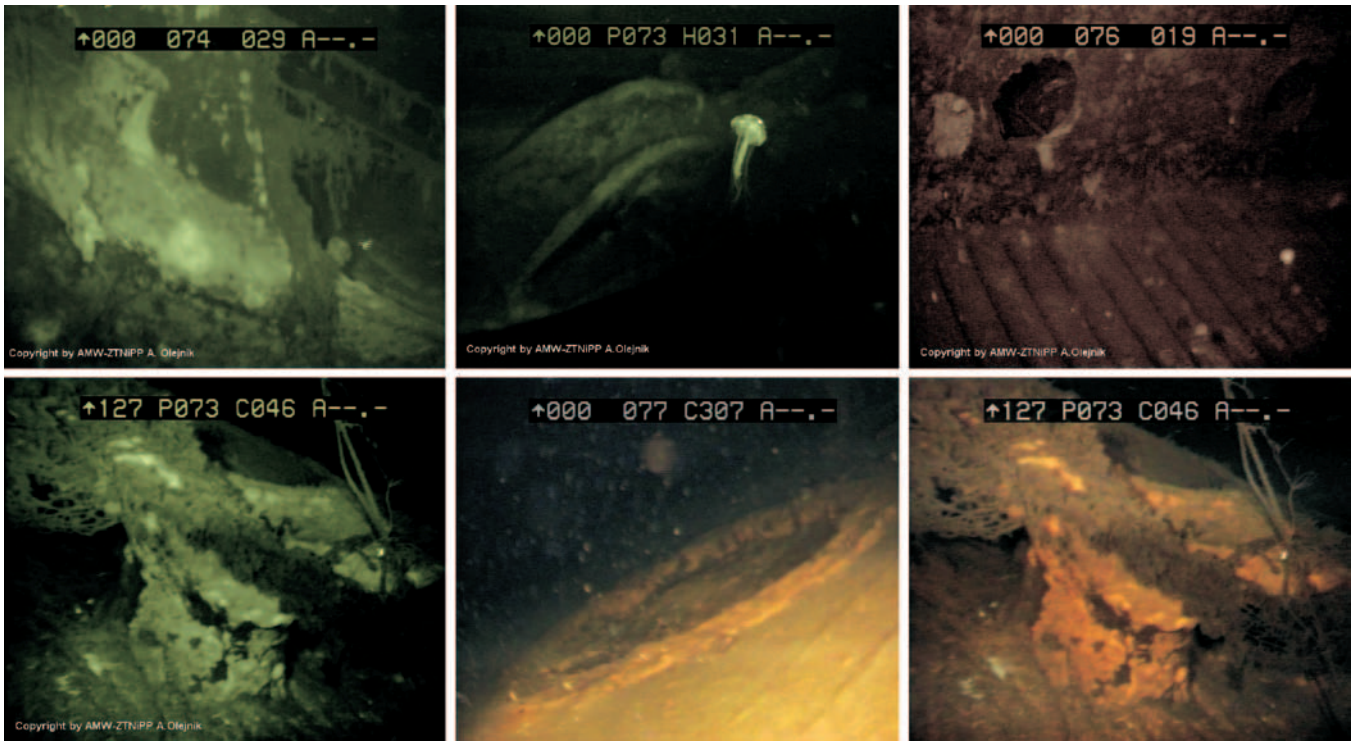

Fig. 8. Selected photos presenting wreck of "Graf Zeppelin". Photos were recorded using ROV [author's investigations]

operating mission, we did not store a digital version of the film recorded by the TV camera mounted on the vehicle, the first step after completing the mission is to copy the film to a digital carrier. Then the entire material is checked, frame-by-frame, looking for pictures which can be compared with the archival material. If we find such a frame, we extract it from the film as a separate photo file, magnify it and compare with the magnified part of a photo of drawing of the ship before its sinking. As for the "Graf Zeppelin" wreck, the comparison material was taken from a cyclic publication "Encyclopaedia of battleships" published by the AJ-Press Publishing House in Gdansk, volume 42 of which, worked out by S. Breyer, was devoted to this ship and included a series of detailed drawings and visualisations of the 3D construction of the ship. Authors of the drawings were S. Breyer, J. Jackiewicz, K. Kania, M. Skwiot and K. Żurek [4]. The drawings were made based on shipyard plans, photos and other historical documents on the "Graf Zeppelin". Having collected all the comparison

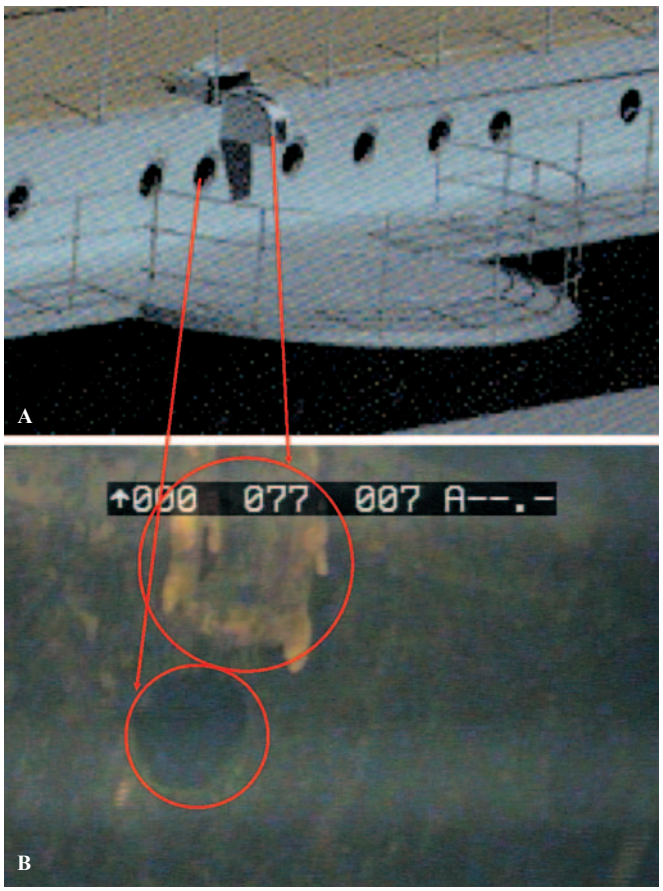

Fig. 9. Comparing material collected using ROV (B) with that presented in Breyer's publication (A): visible clear correspondence between two constructional elements with respect to their shapes and relative positions [4,9].

material, the ship identification is done by comparing the selected film frames with relevant material presenting the ship before sinking. The more details can be matched, the higher is the probability of wreck identification. A collective analysis of the abovementioned drawings, photos and film frames, taking into account the order of filming of particular wreck elements and logical succession of appearance of fragments in accordance with the source material allows a conclusion to be made that in all probability the wreck filmed on July 26, 2006, is the German aircraft carrier "Graf Zeppelin". The figures below present selected fragments from the document entitled "Analysis of the film material recorded using the ROV vehicle during the inspection of the underwater object Graf Zeppelin", prepared for the Navy Hydrographic Office as a report from the identification activities.

SUMMARY

The above-presented method of visual identification of underwater objects was developed as a result of realisation of various orders for research services. Author's personal experience gained in the past was used for its preparation, along with the information obtained during various trainings in the field of: underwater navigation (Sonardyne Sea Trials Center, Plymouth, United Kingdom), use of unmanned vehicles in underwater work technologies (Lerici International Winter School on Marine Technologies, Lerici, Italy) and operation of ROV vehicles (Comex Pro, Marseille, France). The method was positively verified during search and verification works, commissioned by the Polish Navy Sea Rescue Command Centre (search for Su-22, Baltic Sea), identifying wrecks of "Fryderyk Engels", "Steuben", and "Graf Zeppelin" (commissioned by: Polish Navy Hydrographic Office) and numerous activities on inland water regions, for instance search for the body of

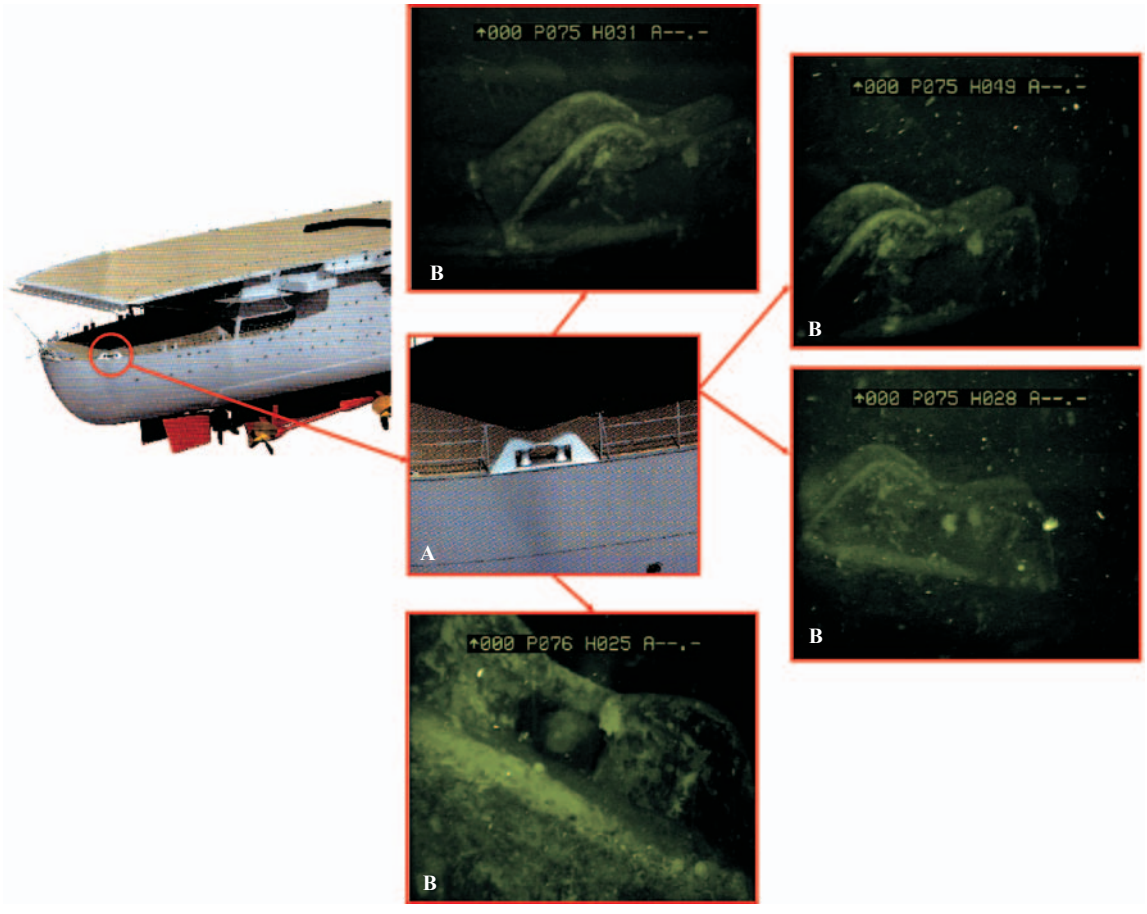

Fig. 10. Comparing material collected using ROV (B) with that presented in Breyer's publication (A) [4,9]

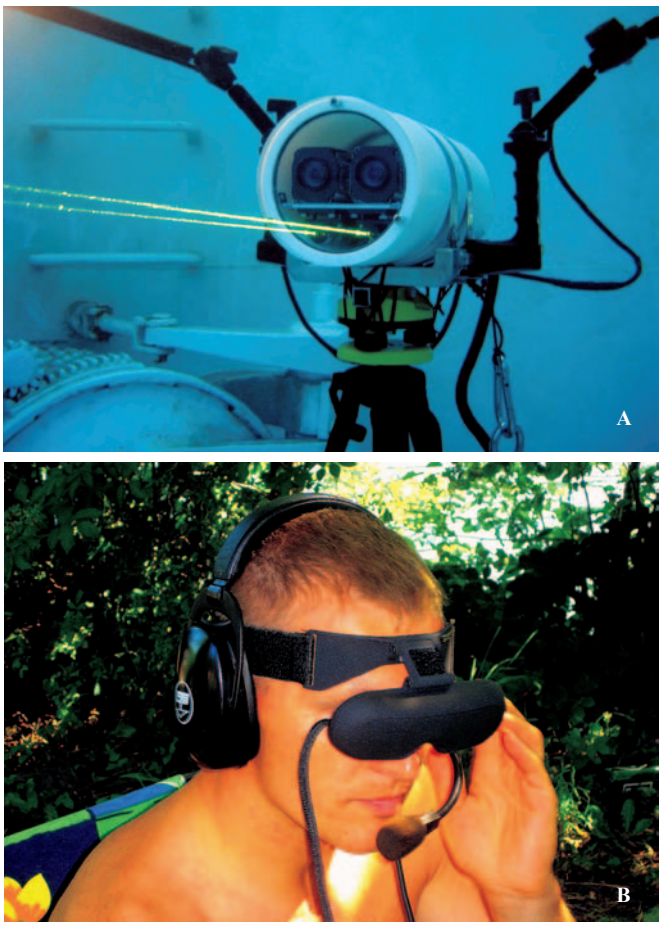

Fig. 11. *System of three-dimensional visualisation of underwater objects: A – underwater part of the system during basin tests, two-camera system of picture acquisition in DVD quality, laser subsystem for placing background points to the frame to allow its scaling and dimensioning, B – element of surface part of the system – subsystem for head-located visualisation, operator is equipped with special goggles and receives a non-compressed picture from two cameras, to each eye separately [13].*

a diver in Lake "Ciecz" (commissioned by: PSP Headquarters of the Poviat of Świebodzin). It is noteworthy that during the identification of the "Steuben" wreck, for instance, these activities were conducted after supposed wreck discovery by the National Geographic team operating from a German vessel "Fritz Reuter". However wreck characteristics indicated by them, along with the general technical state, strongly suggested that their identification was incorrect and that was another object. After some time National Geographic finally admitted that the first team to discover the "Steuben" wreck was that of Polish Navy, in particular the Polish Navy Hydrographic Security Unit (dZH MW), that carried on all hydrographic work[1] [10,12]. Within the framework of these activities, Polish Naval Academy (more precisely: the Department of Diving Technology and Underwater Activities) was responsible for minor part connected with visual identification of the wreck, done using ROV. The above cooperation and experience gained when applying the developed identification methodology made it possible to formulate a conclusion that the proposed methodology, complemented with a wide variety of present-day hydrographic methods, provides wide opportunities for full identification of an underwater object without the presence of a diving team. A practical depth limit to which the above method can be used is only defined by the length of the vehicle control cable. Indeed, the method is not ideal and has its drawbacks. For instance it does not allow dimensioning of the filmed objects and comparing these dimensions with historical data, which would possibly lead to more precise and unique identification. This drawback is connected with the use of a common TV standard, i.e. single-screen visualisation. This visualisation method loses perspective in the picture, with resultant inability to recognise general shapes of the observed objects and their relative positions in space. That is why in the ZTNiPP Unmanned Vehicle Laboratory, activities are in progress over a system of stereoscopic real-time visualisation of underwater objects, with their simultaneous dimensioning and scaling, done using computer aided photogrammetric methods. The effect of remote three-dimensional real-time visualisation was obtained using a two-camera picture acquisition system and special goggles with liquid-crystal screens (Fig. 11) [13].

The prototype, which has been built so far, is under preliminary tests. Further work will be oriented on improving the present design and determining its metrological characteristics. As a final goal, its is intended to be a visual system mounted on the ROV-type vehicle, design assumptions of which have already been worked out. Moreover, a demonstration model of the vehicle has was built and preliminary tests were conducted on depths down to 16 meters in laboratory and real conditions (Figs. 12 and 13).

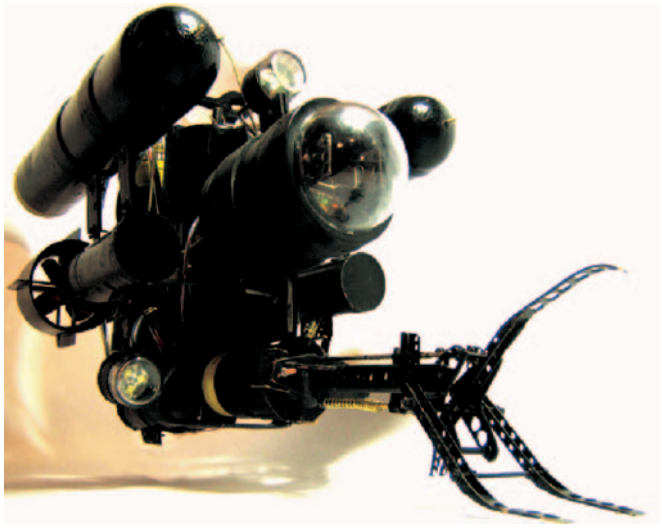

Fig. 12. *Mini ROV "Gammarus": developed and built construction*

Fig. 13. *Mini ROV "Gammarus" in underwater position*

[1] Discovered by ORP „Arctowski", verified by ORP „Heweliusz" (both vessels belong to Polish Navy Hydrographic Security Department)

Acknowledgements

The author thanks the AJ-Press publishing house, Gdansk, for their agreement to use "Graf Zeppelin" drawings published as: **Siegfried Breyer: "Graf Zeppelin" ISBN 83-7237-156-3; Gdańsk 2004,** in the series entitled „Encyclopaedia of Battleships" Volume 42. Moreover, the author thanks the crews of ORP „Heweliusz"[2] and „Arctowski"[3] for their cooperation and assistance during the research work.

BIBLIOGRAPHY

1. Ballard R. D.: "Quests", Bellona Publishers, Warszawa 2000, (in Polish)
2. Beczek D. Grządziel A., Banaszak M., Kłosiński A., Olejnik A.: "Examining the wreck of the aircraft carrier "Graf Zeppelin" using present-day hydroacoustic and visual hydrographic means"; Proceedings of the 15-th International Scientific and Technical Conference on "The Role of Navigation in Support of Human Activity on the Sea" Naval Academy, Gdynia 2006 (in Polish)
3. Bell Ch., Bayliss M., Warburton R. "Handbook for ROV pilot/ technicians" Oilfield Publications Inc. USA, 2006
4. Breyer S. "Graf Zeppelin" Encyclopaedia of Battleships (42), AJ – Press Publishing House, Gdańsk 2004 (in Polish)
5. Dyrcz Cz., Grabiec D., Olejnik A.: "Identifying the "Engels" wreck – sample use of the potential of present-day hydrographic equipment for examining wrecks and sea impurities" Marine Conference on "Aspects of surface water and underwater safety, and flights over the sea" Gdynia 2004 (in Polish)
6. Grabiec D., Olejnik A. "Search and identification of underwater objects" in: "Wrecks of Baltic Sea – manual for divers" collective work, edit. St. Poleszak, Series: Books for Divers, Gdynia 2005, (in Polish)
7. Last G., Williams P. "An introduction to ROV operations" Oilfield Publications Inc. USA 2006
8. Olejnik A. "Methodology of search for underwater objects in seal and inland conditions with the use of unmanned vehicles" Polish Hyperbaric Research, 2005 (in Polish)
9. Olejnik A. "Analysing photo material collected by ROV during inspection of the underwater object "Graf Zeppelin", Naval Academy, Gdynia 2006 (in Polish)
10. Pomian I. "Sensation in the depths of Baltic Sea" National Geographic, No. 7 (2004), (in Polish)
11. Collective work: "USBL Scout - Operation manual" Sonardyne Ltd. WB 2005
12. Collective work: "Steuben. Last big discovery in Baltic Sea?" Diving Magazine, No. 8 (2004) (in Polish)
13. Collective work, edit.: A.Olejnik "System of three-dimensional visualisation of underwater objects, Stage II. Building and tests of the system" Statute work directed by „Narval", Polish Naval Academy, Gdynia 2006, (in Polish).

CONTACT WITH THE AUTHOR
Commander Adam Olejnik, PhD.
Institute of Ship Construction and Operation
Department of Diving Technology
and Underwater Activities
Polish Naval University
Śmidowicza 69
81-103 Gdynia POLAND
e-mail: aolej@wp.pl

[2] Captain: Commander Marek Czarnecki (in years 2002 – 2007), at present Commander Grzegorz Kokosiński
[3] Captain: Commander Dariusz Beczek (in years 2003 – 2007), at present Commander Artur Grządziel

Photo: Cezary Spigarski

POLISH MARITIME RESEARCH 1(55) 2008 Vol 15; pp. 80-85
DOI: 10.2478/v10012-007-0056-3

Classification of the underwater diving equipment

Ryszard Kłos,
Polish Naval Academy

ABSTRACT

In this paper was presented, innovative in preparation of the diving apparatuses classification method, depend on three criteria: the kind of the breathing gas, the operational depth range of the diving apparatus, and the principle of operation. The breathing gas used is the most important criterion. The other basic classification criteria follow from the first one; therefore it should be treated as the one criterion. Such approach to the problem has never been presented before, however it seems to be correct method of the diving apparatuses division.

Keywords: diving apparatus, classification, underwater diving equipment

INTRODUCTION - CHARACTERISTICS OF THE DIVING EQUIPMENT

Traditionally the diving equipment can be divided into the heavy (classic) and light-weight equipment. [2, 3, 6, 7, 8, 9, 10, 11, 12].Classification of the diving equipment according to this criterion is the diving technique based.

The similar to August Siebe's construction, that has been patented in 1836, can be recognised as the heavy diving equipment. The diving equipment has been still developed and improved. However, simultaneously to the new types of the diving equipment the traditional Siebe's constructions are being used in actual diving operations. For these reasons sometimes it seems that the Siebe's constructions were not improved (**Photo 1**). Of course, this diving equipment evolved towards the helmet systems equipped with the diving regulators, however there are also the improved diving equipment with the free flow of the breathing gas. The improved diving systems DM 200/2 (**Photo 2**) and AH-3 are presented below (**Photo 3**).

The features of the heavy diving equipment are presented in Table 1. At assumption that classification criteria, presented

Photo 1a. *The present diving helmet Siebe-Gorman (an advertising materials)*

Photo 1b. *The diving equipment with helmet UWS-50m (the own photography)*

Photo 1c. *The diving helmet UWS-50m (the own photography)*

Photo 2. *The diving equipment type DM 200/2 (the own photography)*

Photo 3. *The diver in the diving equipment type AH-3 (the own photography)*

in Table 1, distinguishing the heavy diving equipment are sufficient it should be recognised that the Henry Fleuss's oxygen diving apparatus (1879) was the independent version of the heavy diving equipment as dive consisted in displacement on the bottom of the especially loaded diver (**Photo 4**). Change in diving methods has led to further development of the oxygen apparatuses and their transformation into light diving equipment.

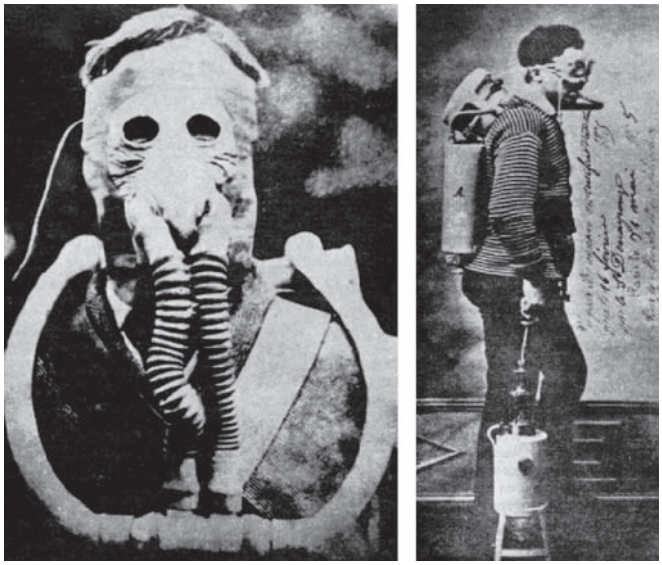

Photo 4. *Henry Fleuss apparatus [4]*

It is generally considered that commander Jaques Ive Cousteau is inventor of the diving apparatus used for free diving (air open-circuit self-contained underwater diving apparatus SCUBA) called Aqua-Lung (1940) – **Photo 5**. It is well known that the prototype such apparatus has been designed earlier. In 1860 Benoit Rouquayrol and August Denayroze have constructed similar apparatus

(**Photo 6**). However, Coustau's gear has caused real landmark and has led to development of free diving. [11, 8].

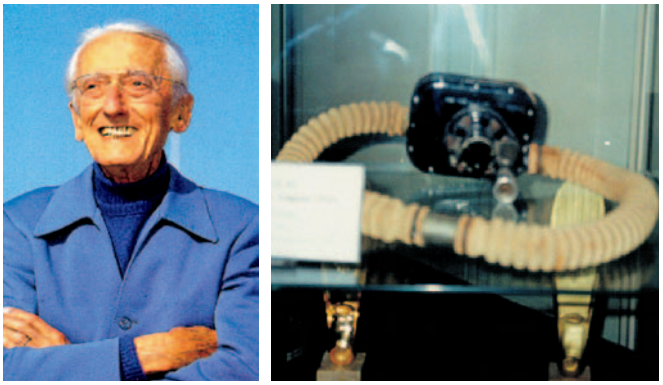

Photo 5. *Jaques Ive Cousteau (left) [5]. Cousteau's diving reulator (right) (the own photography, courtesy La Spirotechnique I.C. Nicea)*

Table 1. *Characteristics of the heavy-weight diving equipment*

The heavy-weight (classic) diving equipment	
During normal work the equipped diver has high negative buoyancy. It is possible to change buoyancy, however it is only used to change the diver's work plane or while descending (ascending).	
Disadvantages:	-The diver can perform work only at the fixed plane such as the trap, the diving platform, the bottom, decks of the sunken vessel etc. -The diver's mobility is limited. Moving of the diver according to the work planes needs to employ a large force.
Advantages:	-The diver's position is stabile. It gives the possibility to perform the heavy work without large effort to keep the diver's position.

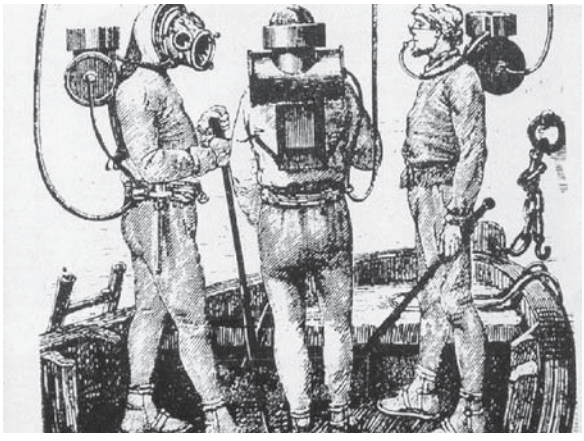

Photo. 6. *Rouquayrol's apparatus [1]*

Paul Bert's physiological research (**Photo 7**) and Elihu Thomson's theoretical works have contributed to the first experimental mixed-gas diving performed in 1924. In 1940 experiments resulted in development of the independent oxygen-nitrogen (nitrox) diving apparatus (**Photo 8**) proposed by Lambertsen.

Photo 7. *Paul BERT [4]*

Photo 8. *Lambertsen diving apparatus [11]*

However, the first diving apparatus type DM 40 (**Photo 9**) was elaborated and manufactured by Dräger in 1915. However, many historians accept that Lambertsen's gear [11] has begun real development of the diving apparatuses. Despite of the breathing gas used, the characteristic features of the diving apparatuses are as follows (**Table 2**).

Photo 9. *The diving apparatus DM 40 manufactured by Dräger 1915 (the own photography, courtesy Dräger AG Lübeck)*

At present, the differences between the heavy and light-weight diving equipment are covered up as dependently upon the additional equipment chosen, the basic equipment can function as the classic or light-weight diving equipment.

Table 2. The features of the light-weight diving equipment

The light-weight diving equipment	
During normal work the equipped diver has neutral buoyancy that can be adjusted within the certain range.	
Disadvantages:	The diver under water is almost weightless. Even if the diver is supported under water by the immovable elements, weightless makes the diver's work (drilling the holes, surface cleaning, shooting pegs, welding etc.) difficult.
Advantages:	Compared to heavy-weight diving equipment, the light-weight one enables relatively long distance diving without the significant effort and free displacement in all directions at depth or reminding at the given place at the depth. This feature enables to make underwater inspection of the technical state of the large underwater objects, sweeping at the depth etc.

METHODS

Generally (here) the diving equipment is defined as follows: it is the technical equipment that enables the man safety descent, staying at the depth and ascent. There are some tendencies to extend the above definition by normobaric dives (see further). In the definition accepted it is essential that the diving equipment enable the man to perform the direct work at the depth. As it follows from above the water environment exerts the pressure on the diver's equipment that is directly transferred on the man.

This feature distinguishes the diving equipment from among the other kinds of the submersibles, for example: atmosphering diving suits (normobaric diving suits, one atmosphere diving suits – **Photo 10**), or manned underwater vehicles (**Photo 11**) that enable normobaric dives. Descent and ascend to water environment should be safety, therefore the diving equipment requires from the diver except operating skills, special health qualifications and training.

Photo 10. *Armored suits:* ***a)*** *Newsuit (the own photography, courtesy Drägerwerk AG Germany)*

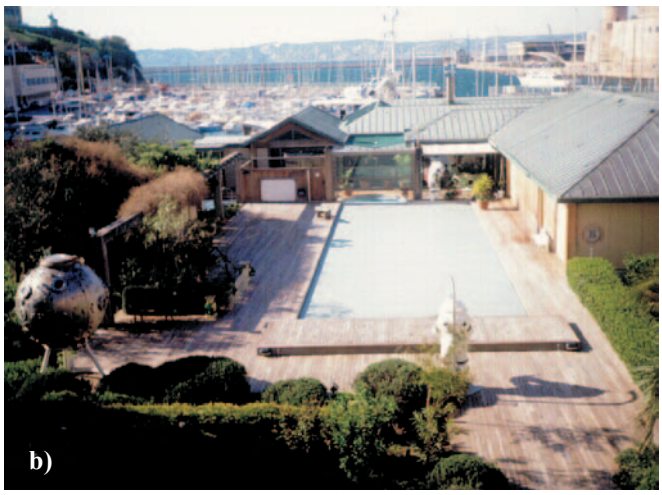

Photo 10. *Armored suits:* ***b)*** *Russian armored suits in the villa of COMEX-President, Marsylia (the own photography, courtesy H. Delauze)*

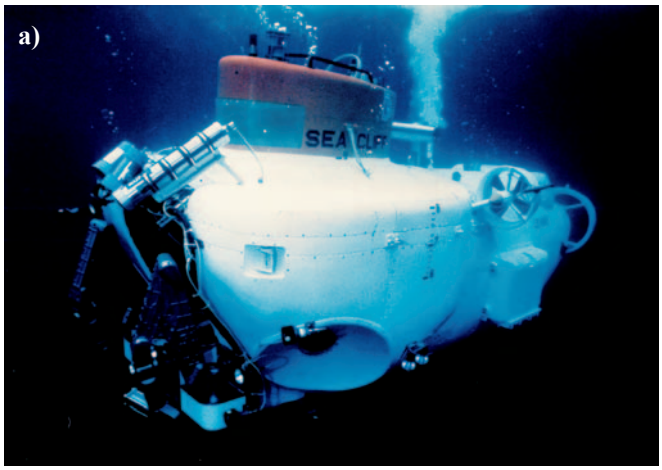

Photo 11. *The underwater vessels - scientific vessels:* ***a)*** *the general view of the underwater vessel SeaCliff,* ***b)*** *the historical underwater vessel of Comex*

THE DIVING APPARATUSES AND THEIR CLASSIFICATION

Except the traditional classification for the heavy and light-weight diving equipment there are many other classification criteria. Most divisions that have been presented in the literature are based on the diving apparatus constructional criteria [for example [2, 7, 9]. In this paper the new classification will be presented that seems to be more accurate and useful. Further,

Photo 11. *The underwater vessels - the rescue vessels:* ***c)*** *the view of DSRV Mystic cockpit (the own photography, courtesy Deep Submergence Unit San Diego),* ***d)*** *the general view of DSRV Mystic (the advertising photography, courtesy Deep Submergence Unit San Diego),* ***e)*** *the general view of the underwater vessel for rescue of the submersible crews (the own photography, courtesy HMS Belos Sweden), f) manned underwater robot produced in UK (the own photography, courtesy HMS Belos Sweden)*

Table 3. *Classification of the underwater diving apparatuses*

Specification		**Classification of the underwater diving apparatuses**									
1.breathing species		air		oxygen	mixed gases (most often: nitrox, helioks, trimix ,hydrox, hydreliox, neox)						
2.depth range		0÷50 mH_2O		up to 6 mH_2O	0÷200 mH_2O				most often deeper than 200 mH_2O		
3. Principle of work	a) group	of the open gas circuit		closed gas circuit	semi-closed gas circuit				closed gas circuit		
	b) sub-group				premix		preparing the breathing gas during diving process				
	c)type	self-contained	hose supply	self-contained	self-contained	hose supply	self-contained	hose supply	small circulation	increased circulation	high circulation
4. Examples	Haux [**1968, 1982**]	PA-38/3600	PL-70	LAR V	-	FGG III	SM III	SM III-S	Elektrolung	-	GAK-600
	Polish construc-tions	PR-27	UAN-82	-	APW-6M	GAN-87	APW-3	-	-	-	-
	the other examples	AGA MkII	KMB-10	COBRA	ACSC	Sealab III (Fink Rig)	SIVA+	-	Mk-15/16	DOLPHIN 7	CCBS
5. Remarks		not recommended to the underwater works	recommended to the underwater works at the shallow and mean depths	military diving	mostly used for the diving works performed beyond the saturation zone (or the bail-out apparatuses during saturation) and for the operational diving at the large depths (standard approximately 150m H_2O)				military diving at the large depths	apparatuses used to underwater works during saturation diving	
WARNING! The diving apparatuses with the chemical preparing and complementation of the breathing gas are not taken into account here											

we will deal with the diving apparatuses as the part of the diving equipment.

The diving apparatuses are defined as the part of the diving equipment that is responsible for supplying the diver the compressed breathing gas. The gas pressure is adequate to the diving depth. The breathing medium can be stored outside the apparatus and supplied by the suitable hose, the gasholders containing the breathing medium can be the integrate part of the diving apparatus or it can be obtained (or complemented) in chemical reaction.

To classify the diving apparatuses for the tasks assumed, the following criteria are the most convenient:

- ⇨ the kind of the breathing gas,
- ⇨ the operational depth range of the diving apparatus,
- ⇨ principle of operation.

The diving apparatus with chemical preparation or complementation of the breathing gas are not discussed here. Classification of the diving apparatuses according to the above criteria is presented in Table 3. The presented here classification of the diving apparatuses used for underwater work enables gathering, systematising and analysing of those construction development trends.

Although the presented here classification is not excellent, it is the most complete classification that has been met in the professional literature. It has practically confirmed it usability at the diving apparatuses' data systemising and analysis.

DISCUSSION AND CONCLUSIONS

- ❍ Development trends of the diving apparatuses and analysis of the development directions have shown in Europe and in the world the great interest in the semi - closed circuit diving apparatuses. It was several years before the great marked for these products has been opened (recreational diving use and beginning of the technical diving).
- ❍ It was innovative in preparation of the diving apparatuses classification to use three criteria: the kind of the breathing gas, the operational depth range of the diving apparatus, and the principle of operation. The breathing gas used is the most important criterion. The other basic classification criteria follow from the first one; therefore it should be treated as the one criterion. Such approach to the problem has never been presented before, however it seems to be the most correct method of the diving apparatuses division.

Acknowledgement

This research was financially supported by the Polish Scientific Research Committee № 0 T00A 072 18: The mathematical models of UBA ventilation with partial regeneration of the breathing medium.

BIBLIOGRAPHY

1. Bachrach A.J., Desiderati B.M., Matzen M.M.: *A pictorial history of diving*. Best Publishing Co. 1988
2. Clarke D.W.: The history of breathing apparatus and current state of the art ‡z:‡ *Lung and physiology and divers breathing apparatus*. Proceedings from the International Workshop Ballater, Scotland, 1÷4 Nov. 1991: Department of Biomedical Sciences Marshal College Aberdeen 1992
3. Diving Manual: Ministry of Defence (Navy), B.R.2805 (Army Code No 61231) March 1982
4. Gussman J.: *Człowiek zdobywa głębiny*. Wydawnictwo Morskie Gdańsk 1984
5. Mer & Océan - *Spécial Cousteau* 1997
6. Prace podwodne: Wydawnictwo Morskie Gdańsk 1971
7. Przylipiak M., Torbus J.: *Sprzęt i prace nurkowe-poradnik*. WMON Warszawa 1981
8. Rawlis J.: *The history of commercial, military and sport diving*. Trans. IMarE 101(1989)161÷170
9. *The five methods for professional diving*. Komunikat Drägerwerk AG Lübeck (Oct.1987)
10. *The underwater handbook*. Pr. zbiorowa pod red. C.W.Shilling, M.F.Werts, N.R.Schandelmeier: Plenum Press New York and London
11. *US Navy diving manual*. Best Publishing Co. Carson California 1980
12. *US Navy diving manual (revision 3)*. The Direction of Commander, Naval Sea Systems Command 1993

CONTACT WITH THE AUTHOR
Ryszard Kłos, D. Sc., Eng.
Department of Diving Technology
and Underwater Activities
Polish Naval Academy
Śmidowicza 69
81-103 Gdynia POLAND
e-mail: skrzyn@wp.pl

Photo: C. Spigarski

The Ship Handling Research and Training Centre at Ilawa is owned by the Foundation for Safety of Navigation and Environment Protection, which is a joint venture between the Gdynia Maritime University, the Gdansk University of Technology and the City of Ilawa.

Two main fields of activity of the Foundation are:

- Training on ship handling. Since 1980 more than 2500 ship masters and pilots from 35 countries were trained at Iława Centre. The Foundation for Safety of Navigation and Environment Protection, being non-profit organisation is reinvesting all spare funds in new facilities and each year to the existing facilities new models and new training areas were added. Existing training models each year are also modernised, that's why at present the Centre represents a modern facility perfectly capable to perform training on ship handling of shipmasters, pilots and tug masters.

- Research on ship's manoeuvrability. Many experimental and theoretical research programmes covering different problems of manoeuvrability (including human effect, harbour and waterway design) are successfully realised at the Centre.

The Foundation possesses ISO 9001 quality certificate.

Why training on ship handling?

The safe handling of ships depends on many factors - on ship's manoeuvring characteristics, human factor (operator experience and skill, his behaviour in stressed situation, etc.), actual environmental conditions, and degree of water area restriction.

Results of analysis of CRG (collisions, rammings and groundings) casualties show that in one third of all the human error is involved, and the same amount of CRG casualties is attributed to the poor controllability of ships. Training on ship handling is largely recommended by IMO as one of the most effective method for improving the safety at sea. The goal of the above training is to gain theoretical and practical knowledge on ship handling in a wide number of different situations met in practice at sea.

For further information please contact:
The Foundation for Safety of Navigation and Environment Protection

Head office:
36, Chrzanowskiego street
80-278 GDAŃSK, POLAND
tel./fax: +48 (0) 58 341 59 19

Ship Handling Centre:
14-200 IŁAWA-KAMIONKA, POLAND
tel./fax: +48 (0) 89 648 74 90
e-mail: office@ilawashiphandling.com.pl
e-mail: office@portilawa.com